Histamine H_3 receptor antagonists in combination with monoamine oxidase B and adenosine A_1/A_{2A} receptor ligands as multi-target approach for the treatment of Parkinson's disease

Dissertation

zur Erlangung des Doktorgrades

der Naturwissenschaften

vorgelegt beim Fachbereich

Pharmazeutische und Medizinische Chemie

der Heinrich-Heine-Universität

in Düsseldorf

von Anna Affini

aus Mantua

Düsseldorf 2019

Dekan	Univ.-Prof. Dr. Martin Mauve
1. Gutachter	Univ.-Prof. Dr. Dr. h. c. H. Stark
2. Gutachter	Univ.-Prof. Dr. H. Gohlke
Tag der Disputation	31.01.2019

Acknowledgements

This investigation was supervised by Pr. Dr. Dr. h. c. Holger Stark and carried out at the Institute of Pharmaceutical and Medicinal Chemistry (Heinrich-Heine Düsseldorf University).

I'd like to thank Prof. Dr. Dr. h. c. Holger Stark for "taking the risk" to let me, a passionate Italian, enter in his research group and give me the opportunity to start a PhD in Germany. I still have multiple versions of my first poster with which I reached a new level of precision in scientific work. For these skills and our deeply scientific discussions I want to say thank you. Coming from a background of organic chemistry, he gave me all the time the support to go in a completely new field. I look back on an exciting project that I will keep in mind as a good memory.

I would like to thank all colleagues, especially Steffi for the good time spend together during the writing of our publications and Stephan for the help and friendship. I wish that one day I will sit again together with Lars, Natalie and Antonino to hear radio DJ.

I would like to thank my group of girlfriends "Le Nonne", which are like a four-leaf clover; hard to find and lucky to have. Cri was my partner in the library and, as I promised you, we will go one day there just to read a newspaper. Katha is "just" a special person, who entered in my life also to take care about me. Alessia is the friend that all the time is walking beside me.

I want also to thank my Italian group of friends "Dusseldorf girls". Time passed, we are older, but those are that kind of relationships that you will never find again. They are just authentic and impossible to substitute.

My Guru, that helped me all the time to find the right way, is my big brother. His passion, energy and optimistic thinking positively influenced all the big decisions of my life. Un grande grazie va alla mia famiglia e alle mie grandi nonne. So quanto per voi sia stato difficile vedermi andar via di casa, ma avete fatto un grande gesto d' amore lasciandomi libera di fare le mie scelte e di costruire passo dopo passo la mia famiglia. Voi mi avete insegnato a mettere prima l'amore di tutto il resto e forse per questo non mi sono mai sentita sola.

The last sentence of my Master thesis was: thanks to a piece of Erasmus that I brought home, Jimbo, that I hope will be with me in the next phase of my life. Six years have been passed and I conclude my PhD thesis as follow: grow old with me, let us share what we see and on the best it could be, just you and I.

Contents

Abbreviations

3-MT	3-Methoxytyramine
5-HT	Serotonin
5NT	5-Nucleotidase
6-OHDA	6-Hydroxydopamine
AC	Adenylyl cyclase
ACh	Acetylcholine
AChE	Acetylcholinesterase
AD	Alzheimer's disease
ADA	Adenosine deaminase
ADK	Adenosine kinase
ADP	Adenosine diphosphate
ADRs	Adenosine receptors
AHCY	S-Adenosyl homocysteine hydrolase
AIMs	Abnormal involuntary movements
Akt	Serine/threonine protein kinase
ALDH	Aldehyde dehydrogenase
ALO	Axial, limb and orolingual
ALS	Amyotrophic lateral sclerosis
ARs	Adenosine receptors
ATP	Adenosine triphosphate
BBB	Blood-brain barrier
BuChE	Butyrylcholinesterase
Calc	Calculated
cAMP	Cyclic adenosine monophosphate
$CDCl_3$	Deuterated chloroform
CHO	Chinese hamster ovary
CI	Confidence interval
CNS	Central nervous system
COMT	Catechol-*O*-methyltransferase
CYP450	Cytochrome P450 enzyme system
DA	Dopamine
DAT	Dopamine transporter
DCE	1,2-Dichloroethane
DEAD	Diethyl azodicarboxylate
DMF	*N*,*N*-Dimethylformamide
DMSO	Dimethyl sulfoxide
DOPAC	3,4-Dihydroxyphenylacetic acid
DR	Dopamine receptor
DTLs	Dual-targeting ligands

E	Enzyme
EDS	Excessive daytime sleepiness
EEG	Electroencephalogram
EMA	European medicines agency
ENTs	Equilibrative nucleoside transporters
ESI-(HR)MS	Electronspray ionization (high resolution) mass spectrometry
FAD	Flavin adenine dinucleotide
FDA	Food and Drug Administration
GABA	Y-Aminobutyric acid
Glu	Glutamate
GPCRs	G-protein-coupled receptors
GP_e	Globus pallidus external
GP_i	Globus pallidus internal
GSH	Glutathione
GSK-3β	Glycogen synthase kinase 3β
HA	Heavy atom
HB	Hydrogen bond
HDC	Histidine decarboxylase
HEK	Human embryonic kidney
HNMT	Histamine N-methyltransferase
HPLC	High performance liquid chromatography
*h*R	Human receptor
HR	Histamine receptor
HVA	Homovanillic acid
IUPAC	International Union of Pure and Applied Chemistry
L	Ligand
LE	Ligand efficacy
LELP	Ligand efficiency dependent lipophilicity
LID	L-DOPA induced dyskinesia
MAOs	Monoamine oxidases
MAPK	Mitogen-activated protein kinase
MPTP	1-Methyl-4-phenyl-1,2,3,6-tetrahydropyridine
MSNs	Medium spiny neurons
MTLs	Multi-targeting ligands
MW	Molecular weight
n.c.	No conversion
NADH	Nicotinamide adenine dinucleotide
NE	Norepinephrine
NMR	Nuclear magnetic resonance
NMDA	*N*-Methyl-D-aspartate
NOESY	Nuclear Overhauser effect spectroscopy

NREM	Nonrapid-eye-movement
NT5E	Ecto-5′-nucleotidase
OE	Omission errors
OSA	Obstructive sleep apnea
ox	Oxidized
PD	Parkinson's disease
PEA	Phenethylamine
PI3K	Phosphoinositide 3-kinase
PKA	Protein kinase A
PLA_2	Phospholipase A_2
PSAs	Polar surface areas
r.t.	Room temperature
RA	Reductive amination
red	Reduced
REM	Rapid-eye-movement
RFU	Relative fluorescence units
ROS	Reactive oxygen species
SAH	S-Adenosylhomocysteine
SD	Standard deviation
Sf	*Spodoptera frugiperdia*
SI	Selectivity index
SN_{pc}	Substantia nigra pars compacta
SN_{pr}	Substantia nigra pars reticulta
SSRI	Serotonin reuptake inhibitors
STN	Subthalamic nucleus
THF	Tetrahydrofuran
TLC	Thin layer chromatography
TMN	Tuberomammillary nucleus
VLPO	Ventrolateral preotic neurons
y	Year

1 Multiple targeting in PD therapeutics

The clinical diagnosis of Parkinson's disease (PD) is primarily based on motor features. While conventional dopaminergic approaches have improved the quality of life of PD patients by mainly reducing tremors, bradykinesia and rigidity, they may cause (mainly by long term L-DOPA treatment) dyskinesia and motor fluctuations and poorly treat non-motor symptoms such as sleep behavior disorders and dementia, which are mainly induced by degeneration of non-dopaminergic systems.[1–4] Recognizing the need to treat both motor and non-motor symptoms and the fact that PD is a highly complex and multifactorial dysregulation, led to the development of ligands that act on multiple targets.[5–7]

Considering this multiple targeting approach and keeping in mind that PD starts to develop when there is a progressive loss of dopaminergic neurons in the central nervous system (CNS),[8] four different targets, the histamine H_3 receptor (H_3R), the monoamine oxidase B (MAO B) and the A_1 and A_{2A} adenosine receptors (A_1R and $A_{2A}R$, respectively) were considered for the development of dual and multi-targeting ligands (DTLs and MTLs, respectively).

1.1 Parkinson´s disease

Parkinson's disease is the second most common neurodegenerative disorder after Alzheimer's disease (AD) affecting 1.5 % of the global population older than 65 years.[1,8]

PD patients lose the ability to control voluntary movements because of profound changes in the functional organization of the basal ganglia, which includes the caudate nucleus, the putamen, the globus pallidus internal (GP_i) and external (GP_e), the subthalamic nucleus (STN) and the substantia nigra pars compacta (SN_{pc}) and substantia nigra pars reticulata (SN_{pr}) (Figure 1).[9–11]

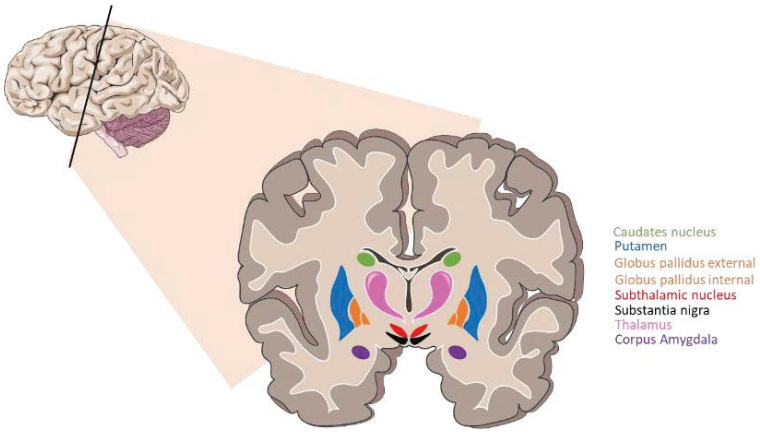

Figure 1. Coronal section of the basal ganglia and its main components.

The basal ganglia circuit is a functional interposition between the cortex and the thalamus, where its primary function is to process the signals coming from the cortex to modulate movement execution.[12] When the prefrontal cortex sends a glutaminergic signal to the putamen to start an action, two pathways are activated: the direct way, which allows the movement to start and the indirect way that avoids unwanted movements.[13]

In the cortico-basal ganglia circuit (Figure 2) dopaminergic neurons, predominantly found in the SN_{pc}, release dopamine (DA), which heads over the striatum, where it binds dopamine D_1 receptor (D_1R) on excitatory neurons (direct pathway) or dopamine D_2 receptor (D_2R) on inhibitory neurons (indirect pathway).[14,15]

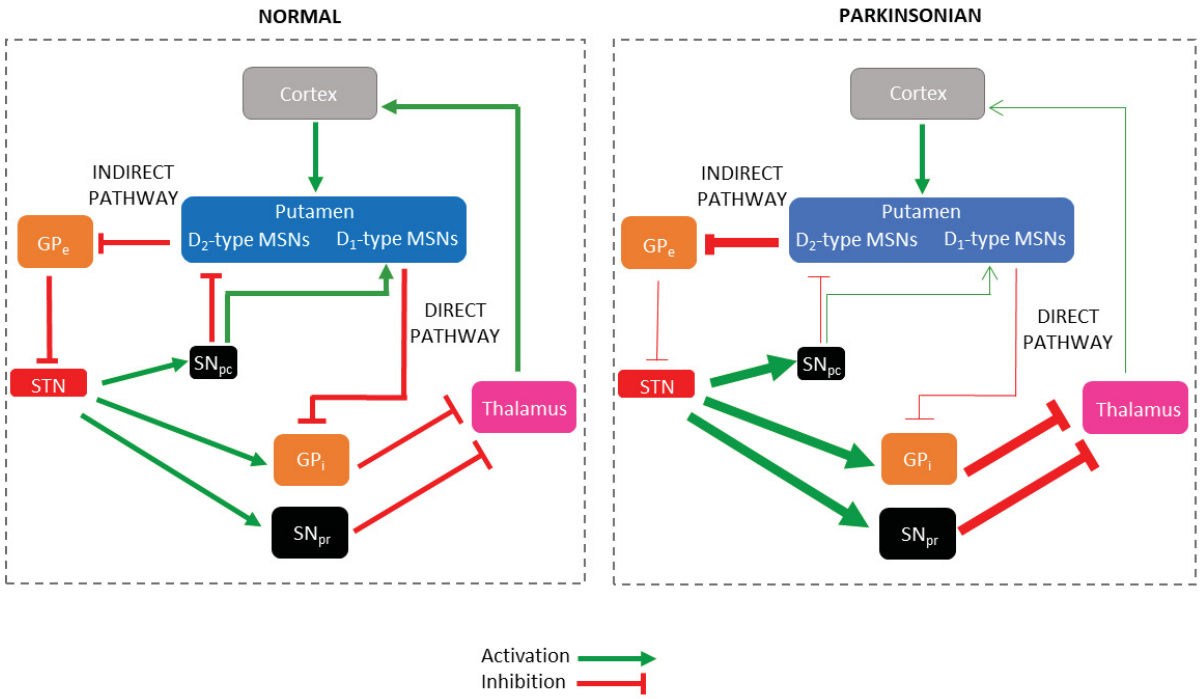

Figure 2. Basal ganglia circuit in normal and parkinsonian states.[15]

DA, dopamine; GABA, γ-aminobutyric acid; Glu, glutamate, GP_e, globus pallidus externus; GP_i, globus pallidus internus; MSNs, medium spiny neurons; SN_{pc}, substantia nigra pars compacta; SN_{pr}, substantia nigra pars reticulata; STN, subthalamic nucleus.

When DA binds at D_1Rs, the inhibition on GP_i GABAergic neurons reduces the inhibition on thalamus, and the initiation of the movement occurs. In the indirect pathway, the inhibition on GP_e GABAergic neurons promotes the activity of glutaminergic subthalamic neurons maintaining an excitatory stimulus on SN_{pr} and GP_i (Figure 2).[16] This, in turn, results in thalamic inhibition and the transmission of motor neuron signals to the cerebral cortex is hindered avoiding an excessive excitation of the cerebral cortex.

In PD patients motor symptoms start to occur when there is a loss of dopaminergic neurons (about 50 %, although some reviews proposed up to 70 %) in the SN_{pc}.[15,17,18] Compared to the normal state, DA depletion results in reduced stimulation of the direct pathway and enhancement of the indirect one, leading in both cases to an increased GABAergic tone on the thalamus. A lower amount of motor neuron signals reach the cerebral cortex, and the initiation of the movement is blocked.[19]

The lack of DA causes the primary motor symptoms of the disorders where bradykinesia, rigidity and resting tremor are the main motor features present in PD patients.[8] To manage these motor symptoms, dopamine agonists (i.e. pramipexole) and mainly L-DOPA, which is the gold-standard treatment for PD patients,[2,20] are used. Catechol-*O*-methyltransferase (COMT) inhibitors (entacapone or tolcapone) and MAO B antagonists (selegiline or rasagiline) might be also added to inhibit the breakdown of L-DOPA and DA.[21] MAO B inhibitors are also used as mono-therapy before moving to L-DOPA and DA agonists in the early stages of the disease, where motor symptoms are mild.

However, after several years of treatment, especially with L-DOPA, initiation of motor complications such as motor fluctuation (alteration between the period in which the patient experiences a good response to medication ("on period") and the period where the benefits received with the medication wear off and PD symptoms reemerge ("off-period")) and dyskinesia (involuntary, non-rhythmic choreo-dystonic movements) arise (Table 1).[22]

When motor symptoms in advanced-PD patients are not relief by medications, deep brain stimulations of the subthalamic nucleus or internal part of the globus pallidus, as well as surgical lesions of the thalamus (thalamotomy) or the globus pallidus (pallidotomy) are the two most commonly surgical treatments.[23] Current therapeutic developments in PD include also the generation of mature, authentic ventral midbrain DA neurons by differentiate pluripotent stem cells as well as gene therapy as disease-modifying treatment for PD.[24]

Along with motor symptoms, non-motor symptoms (i.e. sleep behaviour disorders, cognitive impairment, depression and anxiety) arising mainly from neurodegeneration in non-dopaminergic systems, have a significant impact on the quality of life for PD patients (Table 1).[3,4,8,25] Mainly, adenosine receptors (ARs), serotoninergic, histaminic, glutamatergic, adrenergic pathways are considered for dopamine-related motor and non-motor complications.[26–28]

Table 1. Main motor and non-motor features of PD patients.[8]

	Occurrence	Frequency of symptoms (%)
Primary motor symptoms		
Bradykinesia	At diagnosis	100
Rigidity	At diagnosis or later	90
Tremor	At diagnosis or later	70
	Occurrence	Frequency of symptoms (%)
Early non-motor symptoms		
Fatigue	May precede diagnosis	~ 60
sleep behavior disorders (EDS)	May precede diagnosis	~ 30
Constipation	May precede diagnosis	~ 30
Depression	May precede diagnosis	~ 25
Motor symptoms with L-DOPA therapy		
Dyskinesia	3-5y	~ 35 by 4-6 y; >85 by ≥ 9-15 y
Motor fluctuation	3-5y	~ 40 by 4-6 y; ~70 by ≥ 9-15 y
Late symptoms		
Treatment-resistant axial symptoms	5-10 y after symptoms onset	
Freezing/postural instability/falls		~ 90 by 15 y
Dysphagia		~ 50 by 15 y
Psychiatric disturbances	5-10 y after symptoms onset	
Anxiety		~ 55
Autonomic disturbances	5-10 y after symptoms onset	
Urinary urgency		~ 35
Sialorrhea		~ 30
Sexual dysfunction		~ 20
Postural light-headedness		~ 15
Cognitive impairment	Likelihood increases with time since symptom onset	
Mild cognitive impairment		~ 50 by 5 y
Dementia		> 80 by 20 y

DA, dopamine; y, year.

Evidently, PD is characterized by a complex etiological pathway where dopaminergic and non-dopaminergic systems are involved (Figure 3).[1,29] The use of antagonists at H_3R, MAO B and at ARs is described more in details to understand their potential therapeutically application in the treatment of PD-related motor and non-motor symptoms.

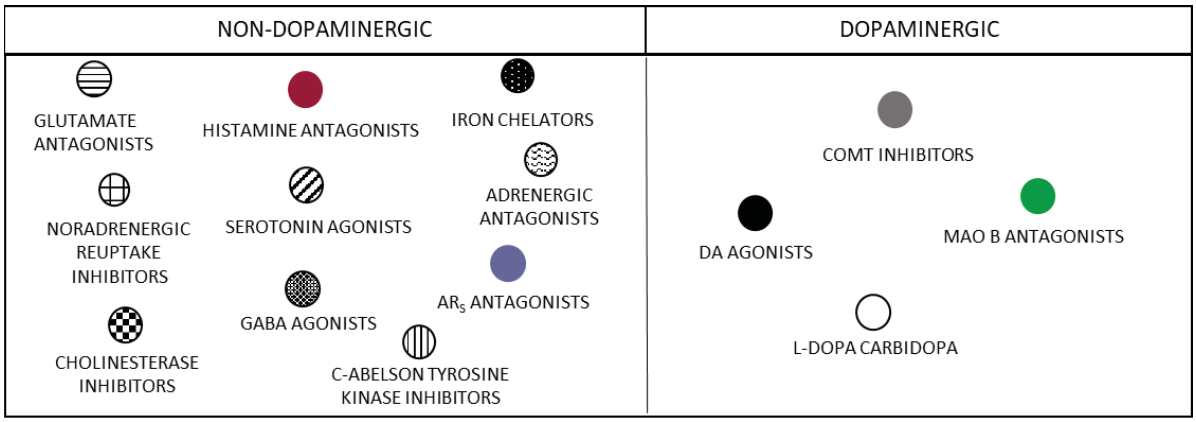

Figure 3. Dopaminergic and non-dopaminergic approaches for the treatment of PD.[1,27]

1.2 Histamine H_3 receptor

The biogenic amine histamine is an important chemical messenger and neurotransmitter.[30] Histamine is synthetised in situ from L-histidine, which reach the cerebrospinal fluid pool and the cytoplasm of neurons though L-amino acid transporters (Figure 4).

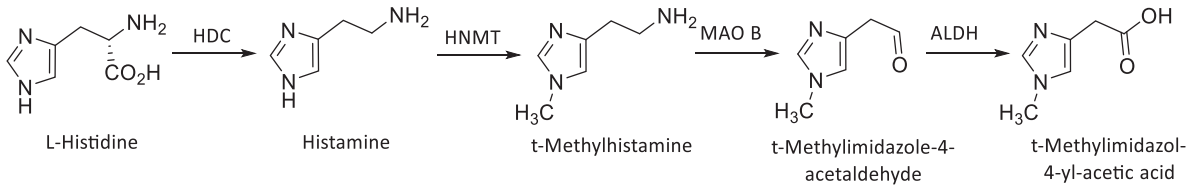

Figure 4. Histamine synthesis and central metabolism.[31]

ALDH, aldehyde dehydrogenase; HDC, histidine decarboxylase; HNMT, histamine t-methyltransferase; MAO B, monoamine oxidase B.

Decarboxylation of L-histidine is performed by the enzyme histidine decarboxylase (HDC). Once synthetised, histamine is stored in vesicles, and upon depolarisation of the histamine neuron, the release of histamine in the synaptic cleft occurs.[30,32] However, the histamine N-methyltransferase (HNMT) terminates in the extracellular space the central action of histamine by methylation of the imidazole ring to give t-methylhistamine which is then oxidised by the enzyme MAO B to t-methylimidazole-4-acetaldehyde. The latter compound is then converted by the enzyme aldehyde dehydrogenase (ALDH) to t-methylimidazole-4-yl-acetic acid.

Histamine activates four G protein-coupled receptor (GPCR) subtypes (H_1R-H_4R). The H_3R was discovered in 1983 by Arrang and co-workers.[33] A Johnson & Johnson team lead by Tim Lovenberg made substantial efforts to expand the knowledge on the molecular structures of the H_3R. The cloning of the hH_3R cDNA in 1999 and the constitutive activity of H_3R were some of the most

important discoveries.[34,35] Besides that, the identification of the genomic organization of the H_3R gene led to the discovery of several H_3R isoforms from alternative splicing of the human gene as well as several rodents.[36,37]

The H_3R is expressed in the CNS and in the peripheral tissues (i.e. airways and cardiovascular system, gastrointestinal tract).[38] In the CNS, the H_3R are mainly located on histaminergic neurons, which are originated in the tuberomammillary nucleus (TMN) and extensively spread to different brain areas (i.e. cerebral cortex, hippocampus, amygdala, nucleus accumbens, globus pallidus, striatum, and hypothalamus).[39–42] The neuronal H_3R was first described as a presynaptic autoreceptor, which controls the synthesis of histamine and its release via a negative feedback process. A few years later, it was found that the H_3R was also involved in the modulation of the release of other neurotransmitters as heteroreceptor (Figure 5) (i.e. acetylcholine (ACh), DA, Y-Aminobutyric acid (GABA), Glu, serotonin (5-HT) and norepinephrine (NE).[33,43–46]

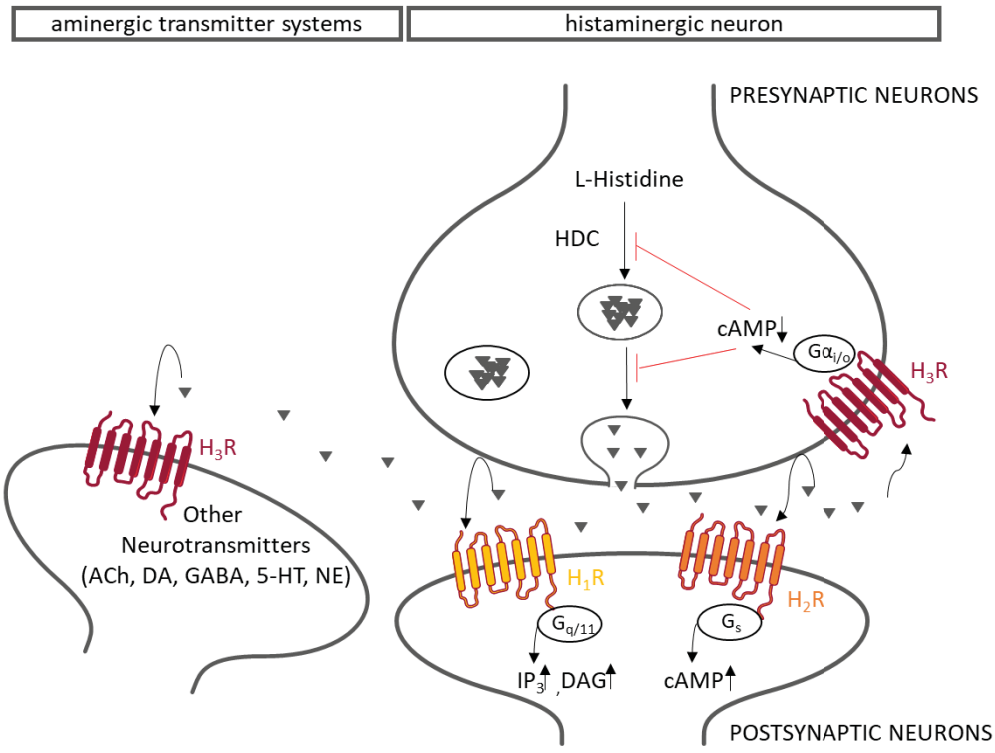

Figure 5. Neuronal H_3R auto and heteroreceptor on histamine neurons and on co-localized neurons.[49]

ACh, acetylcholine; cAMP, cyclic adenosine monophosphate; DA, dopamine; DAG, diacetyl glycerol; GABA, γ-aminobutyric acid; HDC, histidine decarboxylase; 5-HT, 5-hydroxytryptamine; IP_3, inositol triphosphate; NE, norephedrine.

The existence of H_3R/D_1R as well as H_3R/D_2R heteromerization led to novel functional entities, which are also involved in keeping a certain neurotransmitter balance (cf. Chapter 1.2.1).[47,48] The interneuron cross-talk seems to be an important factor in H_3R signaling. The cross-linkage between

the H_3R and the major neurotransmitter systems, demonstrates the central role of the H_3R in many CNS-related disorders like PD, sleep-wake disorders and cognitive impairments, where most of these processes include the activation of postsynaptically located H_1R and H_2R and their downstream signaling.[49,50,51]

The H_3R influences different intracellular pathways (Figure 6).[49,52]

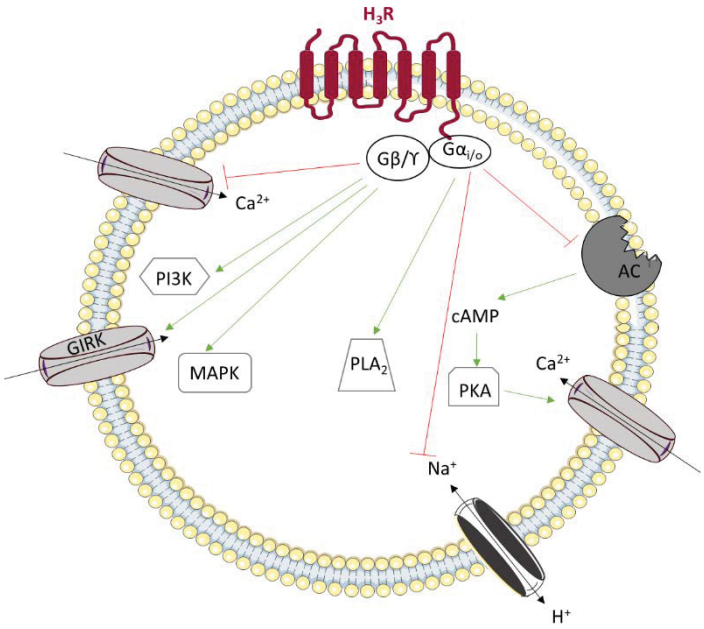

Figure 6. H_3R-associated $G\alpha_{i/o}$ and Gβ/Y downstream signalling.[30,52]

AC, adenylyl cyclase; cAMP, cyclic adenosine 3, 5-monophosphate; GIRK, G protein-coupled inwardly-rectifying potassium channel; MAPK, mitogen-activated protein kinase; PI3K, phosphoinositide 3-kinase; PKA, protein kinase A; PLA_2, phospholipase A_2. Red line, inactivation; green arrow, activation.

Most notably the H_3R, through its coupling to $G\alpha_{i/o}$, on the one hand inhibits adenylyl cyclase (AC) and Na^+/H^+ exchanger activity and on the other hand activates phospholipase A_2 (PLA_2). Inhibition of AC by H_3R decreases cyclic adenosine monophosphate (cAMP) formation. Thus, there is a reduction of protein kinase A (PKA) activity, which is involved in gene expression, behaviour and synaptic plasticity. The Na^+/H^+ exchanger is essential for the restauration of intracellular physiological pH after ischemia-induced acidosis.[53] Stimulation of PLA_2, enhances the release of arachidonic acid and other metabolites that are substrates of other lipids (i.e. 4-hydroxynonenal) which induce neuronal apoptosis and are associated with the progression of AD, PD or ischemia.

The Gβ/Y subunit activates the mitogen-activated protein kinase (MAPK) pathway, which influences cellular growth, differentiation and survival as well as memory processes. The activation of other

mechanisms such as the binding to activated receptors of β-arrestins as well as the crosstalk with growth factor receptors could also contribute to MAPK activation.[53,54]

Also, phosphoinositide 3-kinase (PI3K) and G protein-coupled inwardly-rectifying potassium channel (GIRK) are activated by the Gβ/Y subunit. Modulation of serine/threonine protein kinase and glycogen synthase kinase-3β (Akt and GSK-3β respectively) through PI3K effects mainly neuronal migration and protection against neuronal apoptosis, whereas activation of GIRK modulates neurotransmitters release. Regulation of the intracellular calcium concentration appears to result from the inhibitor action of Gβ/Y subunit or from $G\alpha_{i/o}$ subunit-mediated PKA inhibition.

1.2.1 H_3R antagonists/inverse agonists

The design of H_3R antagonists/inverse agonists, started at the beginning of the eighties. Thioperamide was discovered in 1987, and later potent compounds such as ciproxifan, clobenpropit and FUB-407 were synthetised (Figure 7).[51,55,56]

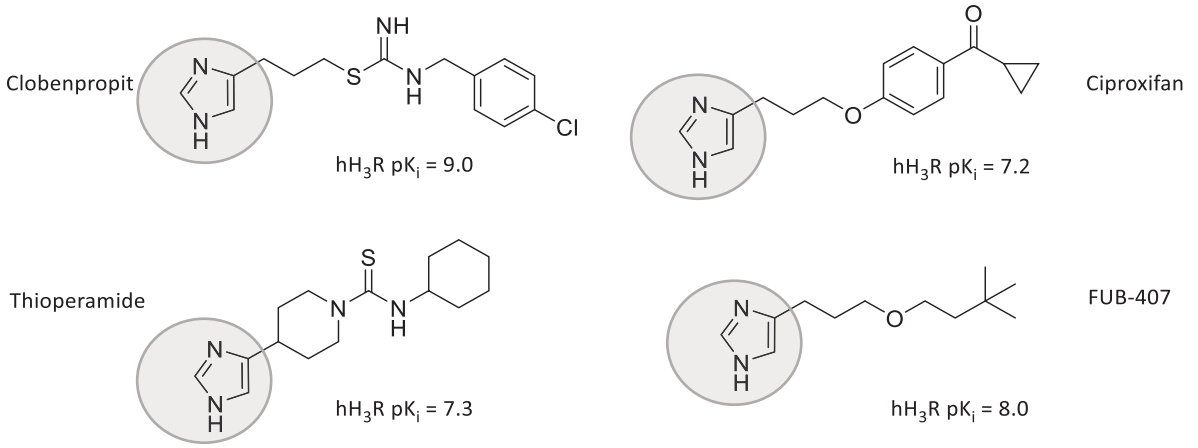

Figure 7. Imidazole-based H_3R antagonists/inverse agonists.[46]

The replacement of the imidazole moiety by other N-containing aromatic heterocycles led to the discovery of potent non-imidazole H_3R antagonists.[51,57,58] A variety of H_3R antagonists/inverse agonists entered clinical trials for the treatment mainly of centrally occurring diseases, such as cognition, sleep-wake and neurodegenerative disorders.[30,31,49,50]

Regarding PD, the histaminergic system may improve motor symptoms by influencing the dopaminergic pathway.[59] Striatal H_3Rs are co-localized postsynaptically with D_1Rs and D_2Rs in the GABAergic neurons and form with both dopamine receptors heteromers.[47,59] Notably, when the antagonist/inverse agonist thioperamide was co-administration with the D_1R agonist SKF-38393 or

the D_2R agonist quinpirole an improvement of the locomotor activity in reserpinized mice was obtained, showing the existence of antagonist H_3R/D_1R or H_3R/D_2R receptor interactions.[47] The use of H_3R antagonists as an adjuvant to dopamine receptor agonists in PD might then have a positive impact on motor symptoms but the benefit of such a therapeutic approach remains to be investigated.

Histaminergic modulation plays also an important role on sleep and wake disorders.[60] In the sleep-wake cycle, the activity of the histaminergic neurons is absent during paradoxical or rapid-eye-movement (REM), increases during slow-wave or nonrapid-eye-movement (NREM) and has the maximal frequency (≤10 Hz) during the waking period.[61,62] To explain the role of histamine in sleep and wakefulness, Williams et al in 2014 demonstrated,[63] by using an optogenetic approach, that histamine indirectly inhibits the ventrolateral preoptic neurons (VLPO), through the activation of GABAergic interneurons, which also reciprocally disinhibit histaminergic neurons to favor the wake state.[59] The inhibition of the H_3 autoreceptors increases the concentration of the "waking amine" in the synaptic cleft and promotes wakefulness *via* postsynaptically located histamine H_1 receptors (H_1Rs).

To date, pitolisant, the former BF2.649, is the only H_3R antagonist/inverse agonist on the drug market, approved by the European Medicines Agency (EMA) for the treatment of narcolepsy with and without cataplexy. Pitolisant is also in late clinical trial stages for cognitive impairment associated with schizophrenia as well as for the treatment of excessive daytime sleepiness (EDS) in PD patients, (clinicaltrials.gov) (Figure 8).[30]

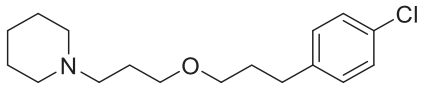

pitolisant (BF2.649)
$hH_3R\ pK_i = 8.06$

Figure 8. Chemical structures and H_3R affinity of pitolisant (BF2.649).[46]

Being the sleep behavior disorder one of the early non-motor symptom affecting PD patients (frequency of about 30%, Table 1), the use of H_3R inverse agonists/antagonists is a promising therapeutic approach for fighting EDS accompanying movement disorders in PD.

While the use of H_3R ligands for wake promotion in PD still needs to be established, inhibitors at the enzyme MAO B have been studied extensively and several drugs (i.e. rasagiline, safinamide) entered the drug market as dopaminergic therapies for the treatment of motor symptoms in PD patients.

1.3 Monoaminoxidases

In 1928, Mary Bernheim discovered the enzyme tyramine oxidase, which was later renamed as monoamine oxidase. After 40 years, the existence of MAO A and MAO B isoenzymes was established.[64,65]

Monoamine oxidases (MAOs) are mitochondrial flavin-dependent enzymes present in human brain and several tissues in different concentrations. MAO B is the predominant form in the human brain, whereas in mice brain the ratio between the two isoforms is 1: 1 (Table 2).[66]

Table 2. Distribution of MAO A and MAO B in brain of different species.

		Brain					
		Human	Monkey	Guinea pig	Cat	Rat	Mouse
Distribution (%)	MAO A	20	25	20	25	55	50
	MAO B	80	75	80	75	45	50

In humans, MAO A is predominantly found in adrenergic, catecholaminergic and dopaminergic neurons and metabolizes mainly serotonin, DA (K_m= 212±33 μM) and norepinephrine, whereas the human MAO B is mainly expressed in serotonergic neurons as well as in glial cells and participates in DA degradation (K_m= 229±33 μM).[67–70]

Figure 9 shows the products of MAOs catalyzed oxidative deamination of DA, which is selected as an example of monoamine neurotransmitters.[71] After the binding of the amine to the active site of the MAOs-FADox complex, the oxidized FAD cofactor is reduced and an enzyme-bound imine complex is formed (Figure 9A).[72] The FAD is then reoxidize by the action of the electron acceptor oxygen and hydrogen peroxide is generated. After that, the MAOs-FADox-Imine complex dissociates, liberating the imine. The hydrolysis of the imine, in a non-enzymatic process, yields the aldehyde product, which can be further oxidized by aldehyde dehydrogenase (ALDH) into 3,4-dihydroxyphenylacetil acid (DOPAC).[73,74] One of the by-products of MAO-catalysed reactions is hydrogen peroxide, which may be involved in neurodegeneration, neuronal apoptosis and in the reduction of neurogenesis and neuroplasticity.[73]

Furthermore, hydrogen peroxide may be converted to the cytotoxic hydroxyl radical in the presence of transition metal ions such as Fe^{2+} and Cu^{+} producing reactive hydroxyl radical.[75] Therefore, inhibition of MAOs became one of the possible key therapy to reduce oxidative stress and to set the monoaminergic tone in diseases involving monoamine neurotransmitters.[70,71,76]

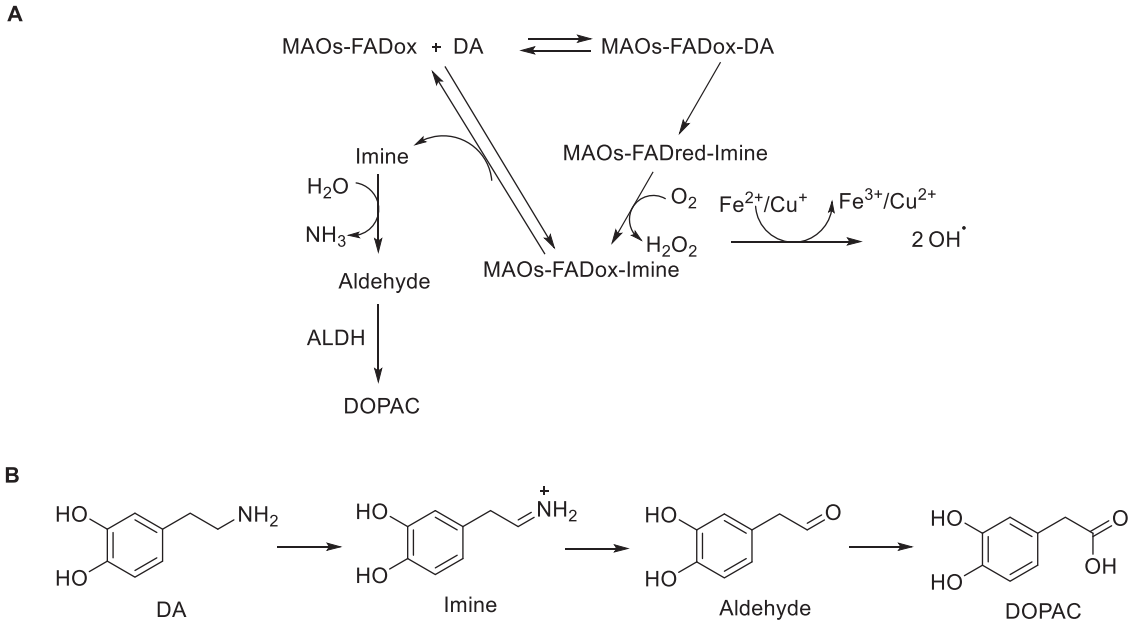

Figure 9. A, scheme for the overall oxidative deamination reactions of DA catalyzed by MAOs; B, reaction products of DA oxidative deamination.

ALDH, aldehyde dehydrogenase; DA, dopamine; DOPAC, 3,4-dihydroxyphenylacetic acid; FAD, flavin adenine dinucleotide.

1.3.1 MAOs inhibitors

The discovery that some non-selective MAO inhibitors such as iproniazid and phenelzine could have antidepressant effects raised the interest in this chemical class of compounds.[77] However, the hydrazine-based MAO inhibitors caused several issues such as liver toxicity, haemorrhage and in some cases death.[71] Moreover, another side effect is the so-called "cheese reaction" occurring in patients consuming fermented food and drinks rich in tyramine and sympathomimetic amines. Studies of Finberg et al. clearly demonstrated that the selective irreversible inhibition of MAO A by at least 80 %, is the consequence of the cheese reaction. The lack of MAO A-mediated metabolism results in hypertensive crises caused by the release of NE, which promotes vessels to constrict and consequently an increase in the blood pressure.[78,79] To overcome this issue, selective reversible MAO A (i.e. moclobemide) as well as selective reversible (i.e. safinamide) and irreversible MAO B (i.e. selegiline and rasagiline) inhibitors have been developed (Figure 10). [65,80]

The use of MAO-A inhibitors in PD has received little attention although also the enzyme MAO A metabolizes DA. A major reason is the occurrence of hypertensives crisis when MAO A inhibitors act with an irreversible mode. However, selective MAO A (i.e. moclobemide) and non-selective MAOs (i.e. phenelzine) inhibitors are used mainly in the treatment of depression, due to the primary task of human MAO A in serotonin metabolism.[66,80]

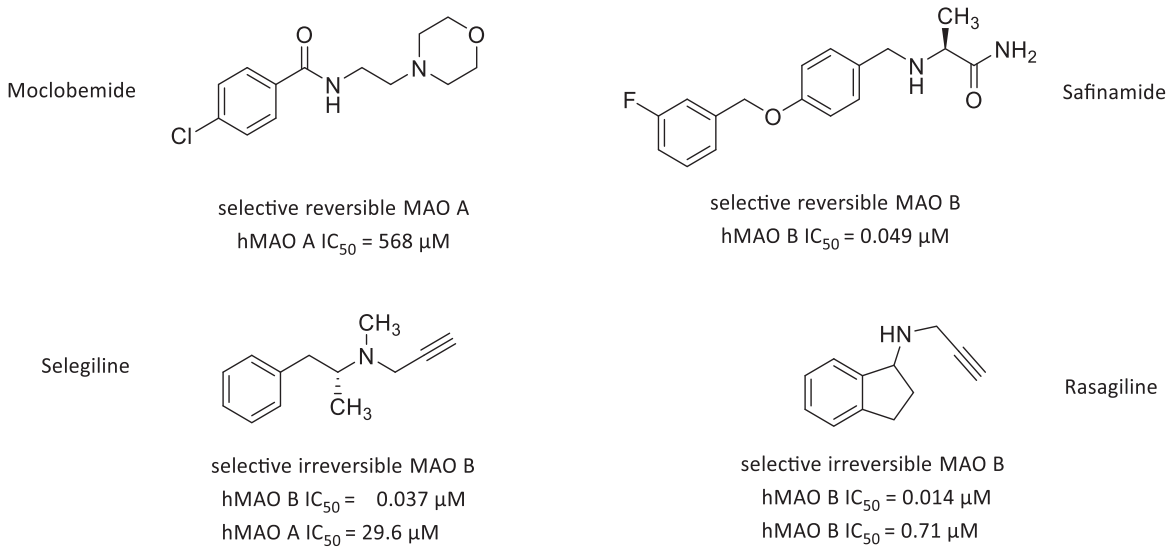

Figure 10. Structure of selective MAO A and MAO B inhibitors.[67,81]

In contrast, selective MAO B inhibitors are used for the treatment of PD since they play a key role in the degradation of DA in the human brain by mainly inhibiting the oxidation of DA into DOPAC. The latter species can then be transformed by catechol-O-methyltransferase (COMT) into homovanillic acid (HVA), a reaction product also obtained, inside the dopaminergic neurons, by the action of MAO B on 3-methoxytyramine (3-MT) (Figure 11).[76]

Selegiline (*L*-Deprenyl) was the first synthesized selective irreversible inhibitor of MAO-B approved for the treatment of PD.[66] After its discovery, several other potent MAO B reversible and irreversible inhibitors have been developed.[82] Rasagiline, which binds covalently to the enzyme MAO B, was approved in 2009 by the US Food and Drug Administration (FDA) as initial monotherapy in early PD and it can be used as adjunct therapy to L-DOPA in moderate-to-advanced disease.[83] Additionally, rasagiline showed neuroprotective activity *in vitro* and several *in vivo* studies using animal model of ischemia,[84] 1-methyl-4-phenyl-1,2,3,6-tetrahydropyridine (MPTP)[85] and 6-hydroxydopamine (6-OHDA)-induced models of PD.[86] The inhibition of MAO B reduces the production of the by-product hydrogen peroxide which can cause mitochondrial death and apoptosis.[87,88]

Safinamide is the only approved reversible MAO B inhibitor by the U.S. FDA as an add-on therapy to L-DOPA/carbidopa in mid-to late-stage PD patients experiencing "off" periods.

Besides the use of MAO B inhibitors for the treatment of PD, also A_1R and mainly $A_{2A}R$ antagonists have received attention as non-dopaminergic PD therapy due mostly to the $A_{2A}R/D_2R$ and A_1R/D_1R heteromers formation.

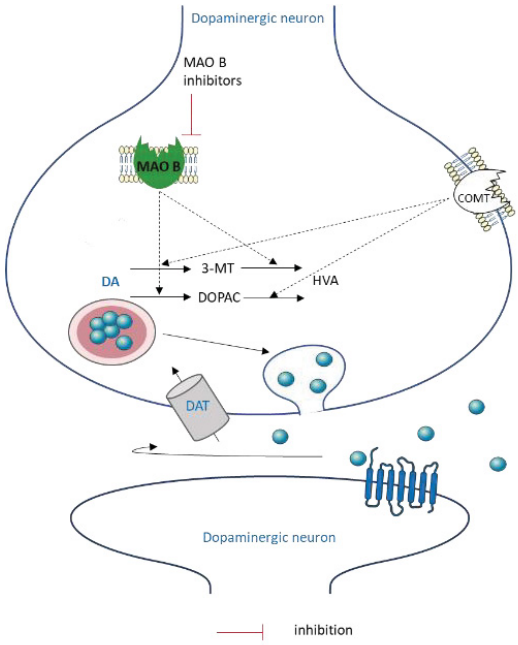

Figure 11. Role of MAO-B inhibitors on dopamine neurons.

COMT, catechol-*O*-methyltransferase; DA, dopamine; DAT, dopamine transporter; DOPAC, 3,4-dihydroxyphenylacetic acid; HVA, homovanillic acid; MAO B, monoamine oxidase; 3-MT, 3-methoxytyramine.

1.4 Adenosine receptors

Distinct from aminergic G-coupled receptors, the ARs are a class of purinergic GPCRs with adenosine as endogenous purine ligand.[89,90] Adenosine is produced primarily from the metabolism of adenosine triphosphate (ATP).[91] While adenosine kinase (ADK), adenosine deaminase (ADA) and S-adenosyl homocysteine hydrolase (AHCY) are the enzymes responsible for the removal of cellular adenosine, the enzymes ecto-5'-nucleotidase (5'-NT) and cytosolic 5'-nucleotidase (cN-I) are involved in the formation of intracellular and extracellular adenosine (Figure 12).[90–92]

The cloning and characterization of four different AR subtypes was described in 1990s.[93] The ARs namely adenosine A_1, A_{2A}, A_{2B} and A_3 receptors, belong to the GPCRs family and show either $G_{i/o}$ - (A_1Rs, A_3Rs) or G_s-coupling ($A_{2A}R$, $A_{2B}R$) behaviour.[89,90,94]

Due to the different G-protein-couplings, the ARs have different effects on cAMP production. A_1R and A_3R inhibit AC and consequently the production of cAMP, whereas A_{2A} and A_{2B} adenosine receptors promote cAMP production (Figure 12).[95]

ARs also possess a different affinity for adenosine.[93] A_3R and $A_{2B}R$, are not activated under normal conditions due to low affinity for adenosine (adenosine concentration in the range of 10^{-6} to 10^{-5} M), while the A_1R and $A_{2A}R$ occupancy in the brain requires a lower adenosine concentration (in the range of 10^{-7} M)[97] and are activated by physiological extracellular levels of adenosine.

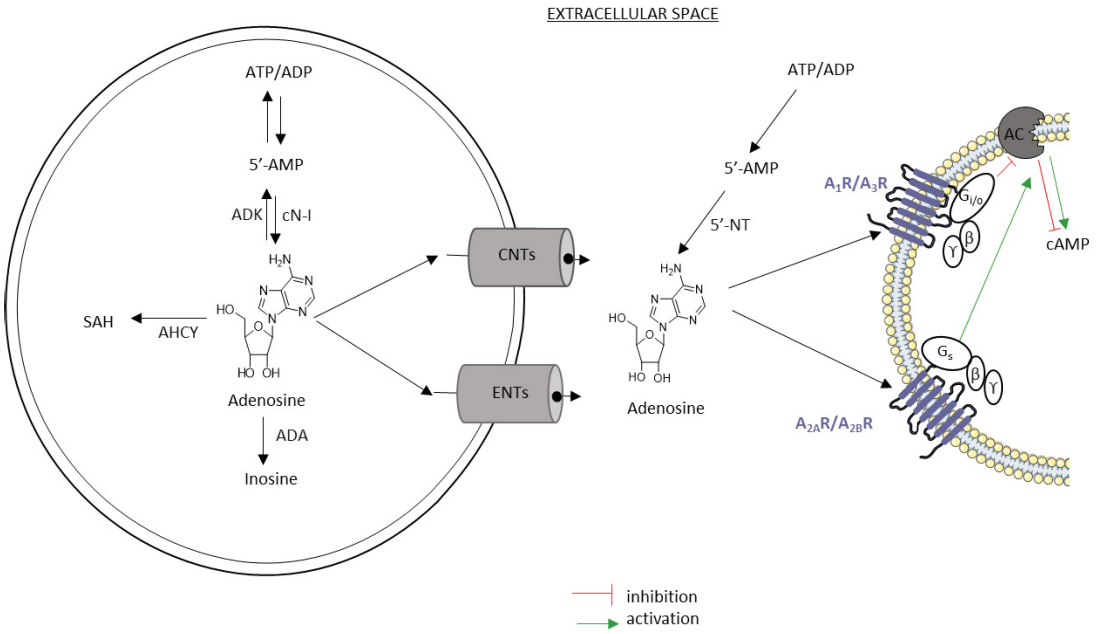

Figure 12. Sources and metabolism of intracellular and extracellular adenosine and main molecular signal pathway of AR_s. [91,96]

AC, adenylyl cyclase; ADA, adenosine deaminase; ADK, adenosine kinase; ADP, adenosine diphosphate; AHCY, S-adenosyl homocysteine hydrolase; 5'-AMP, the 5'-adenosine monophosphate; cAMP, cyclic adenosine monophosphate; ATP, adenosine triphosphate; CNTs, concentrative nucleoside transporters; ENTs, equilibrative nucleoside transporters; 5'-NT, ecto-5'-nucleotidase; cN-I, 5'-nucleotidase; SAH, S-adenosylhomocysteine.

Within the CNS, the A_1R and $A_{2A}R$ are highly expressed in neurons and glial cells such as astrocytes and microglia.[91,98] The A_1Rs are present in the hippocampus, cerebellum, thalamus, striatum and the cortex, while the $A_{2A}Rs$ have a more restricted localisation and are mainly in the striatum.[89,99–102] In the periphery, A_1Rs are located primarily in the heart, whereas the $A_{2A}Rs$ are mainly in the vasculature.[103] The other two adenosine subtype receptors, $A_{2B}Rs$ and A_3Rs, are instead mostly localized in peripheral tissue (gastrointestinal tract, bladder, lung and mast cells), although low levels of these AR subtypes can also be found in cortical and subcortical brain regions as well as in glial cells.[104–107]

1.4.1 A_1R and $A_{2A}R$ antagonists

After the discovery of the non-selective A_1R and $A_{2A}R$ antagonists caffeine and theophylline, different studies have been performed to improve the affinity and selectivity through the adenosine receptors.[92,93]

Regarding PD, the $A_{2A}R$ have been found to be key players in motor control due to their ability to modulate the D2-like pathway.[104,108] Within the striatum, the $A_{2A}R$ are mainly present post-synaptically in the dendritic spine of the striatopallidal GABAergic neurons and in dopamine efferent as well as pre-synaptically in glutaminergic synapses.[109] The striatal GABAergic neurons express high level of D_2R. At the intramembrane level, antagonistic interactions between D_2R and $A_{2A}R$ occur. The heteromers formation between the latter receptor subtypes influences the signaling mediated by D_2R, which is potentiated by $A_{2A}R$ antagonists.[16,104,109–112] The different G-coupling of $A_{2A}R$ (G_s) and D_2R (G_i) may explain these different functional interactions as the AC, which influence cAMP and PKA levels, is activated or inhibited, respectively (Figure 13).[111,113]

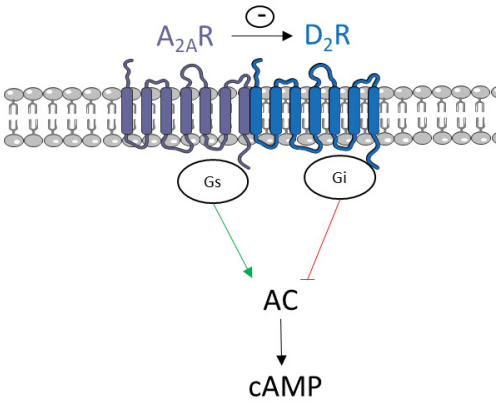

Figure 13. Schematic representation of functional interactions in striatopallidal neurons of $A_{2A}R$ (blue-violet) with D_2R (blue), displaying antagonistic properties.[104,114,115]

AC, adenylyl cyclase; cAMP, cyclic adenosine monophosphate; G_i-inhibitory G-proteins; G_s-stimulatory G-proteins; green arrow, stimulation; red arrow, inhibition.

Selective $A_{2A}R$ antagonists showed beneficial effects in several rodents and non-human primates model of PD, where the symptoms were induced by administration of MPTP in the basal ganglia or by injection of 6-OHDA into the forebrain.[97,104,116,110,117] Notably, $A_{2A}R$ antagonists counteract D_2R-mediated motor impairment in rodent and primate (i.e. catalepsy and hyperlocomotion) induced by the dopamine receptor antagonist haloperidol or the monoamine-depleting agent reserpine.[113,118,119] These results, showing normalization of motor function in animal models of DA dysregulation, suggest a close interaction between $A_{2A}R$ and D_2R.[120]

Approximately 35% of PD patients have a likelihood of developing dyskinesia after 3-5 years of treatment with L-DOPA and more than 85% of patients can develop this motor symptoms after treatment of 9 years. The induction of dyskinesia involves complex pathophysiological changes.[121] Compared to the normal state (cf. Figure 2, Chapter 1.1), chronic L-DOPA treatment results in an overstimulation of D_1Rs and D_2Rs, leading to a decreased GABAergic tone on the thalamus.[121] A higher amount of motor neuron signals reach the cerebral cortex, and involuntary, non-rhythmic choreo-dystonic movements arise.

Also, as PD progresses, changes in glutaminergic receptors (including *N*-methyl-D-aspartate (NMDA)) within the striatum as well as variations in the glutaminergic neurotransmitter systems are in part responsible for the initiation of dyskinesia.[121,122] Amantadine extended-release, acting as an antagonist at the NMDA receptor, is the first medication approved by the US FDA for the treatment of L-DOPA-induced dyskinesia (LID).

A_{2A}R antagonists may be beneficial for reducing dyskinesia in long-term L-DOPA treatment and may have neuroprotective effects. Different studies have shown their ability to attenuate MPTP and 6-OHDA toxicity and minimize glutamate release-induced excitotoxicity.[113,123–125]

The efficiency of A_{2A}R antagonists on LID was investigated in 6-OHDA-lesioned rats scoring abnormal involuntary movements (AIMs) as well as in parkinsonian MPTP-treated primates.[114,126] A_{2A}R antagonists did not cause dyskinesia when administrated alone in both rodents and primate. Also, co-administration with an optimal dose of L-DOPA did not exacerbate the severity of AIMs induced by L-DOPA.[127–129] The effect of sub-threshold dose of L-DOPA in combination with A_{2A}R antagonists was also evaluated. In both animal models of dyskinesia, findings showed that this combination might be beneficial to improve motor activity with a concomitant reduction of the incidence of LID in PD.[97,116,130] However, discrepancies remain across studies on effectiveness treating LID by using A_{2A}R antagonists.[116]

Few A_{2A}R antagonists (i.e. preladenant, istradefylline or tozadenant, Figure 14) are in clinical trials for the treatment of motor symptoms in PD patients.[131] Summarizing the main findings concerning clinical trial studies, it has been found that A_{2A}R antagonists have therapeutic potential in reducing the wearing-off period observed in PD patients.[104]

So far, only istradefylline (KW-6002), received drug approval in Japan in 2013 for clinical uses as an adjunct treatment with optimal doses of L-DOPA to reduce the "off time" in PD patients experiencing motor fluctuations.[132,133] Instead, the US FDA has requested further clinical

investigations due to controversial results obtained in clinical phase II and III on the effectiveness of istradefylline on "wearing-off" phenomena in PD patients.[131]

Preladenant was tested in several phases III trials as a possible drug for patients with advanced PD.[134,135] This studies lasted until 2013 when the US FDA issued a non-approval letter due to the need of other efficacy data. Recently, it has been reported that the co-administration of preladenant in combination with eltoprazine, a serotonin agonist, might be a promising approach to treat dyskinesia without worsening anti-parkinsonian effects of L-DOPA.[18,104]

The $A_{2A}R$ antagonist tozadenant (SYN115) was also showing promising effects on off-period in PD patients.[131,132] However, due to some side-effects such as the risk of inducing agranulocytosis, the development of this drug was discontinued in 2017.[104]

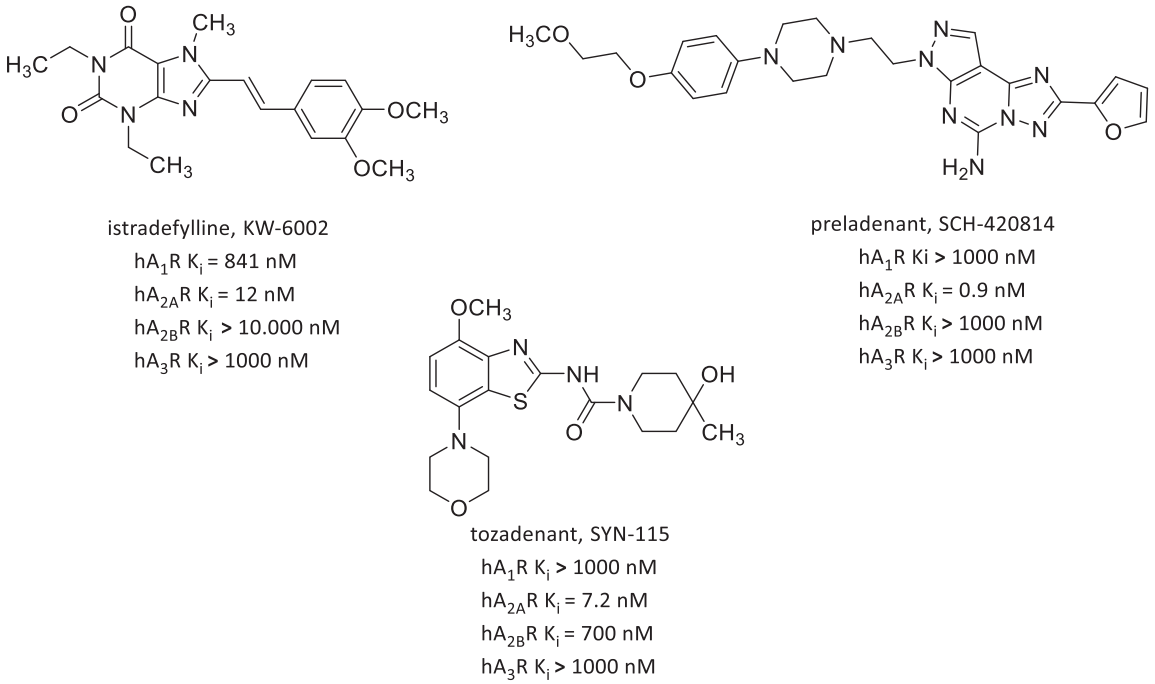

Figure 14. Selective $A_{2A}R$ antagonists.[93,136]

Besides selective $A_{2A}R$ ligands, dual $A_1R/A_{2A}R$ antagonists have entered clinical trials for the treatment of PD (Figure 15).[137–139] Into the striatum, A_1Rs are localised pre-synaptically on dopaminergic and glutaminergic afferents, where they inhibit DA and glutamate release.[120] The striatal glutaminergic neurons express high levels of D_1Rs and the heteromerization of D_1R with A_1R influences the signaling mediated by D_1R in the basal ganglia circuit. A_1R agonists decrease the binding of DA to D_1R, and reduce the D_1R-induced cAMP production, while A_1R antagonists activate D_1R increasing cAMP level.[137]

Caffeine, which has low affinity at A_1R and $A_{2A}R$, potentiates the anti-parkinsonian effect of L-DOPA. In addition, ST1535 and the discontinued vipadenant (BIIB014), also showing affinity at $A_{2B}R$, have been developed in phase I and phase II clinical trials as antiparkinsonian drug, respectively.[140,141] However, since selective A_1R antagonists (i.e. DPCPX) do not show motor improvement in PD models,[142–144] $A_{2A}R$ appears to be most extensively involved in the control of motor behavior but a general contribution of A_1R inhibition on PD motor symptoms is still conceivable, even if distinct AR contributions has to be further elucidated.

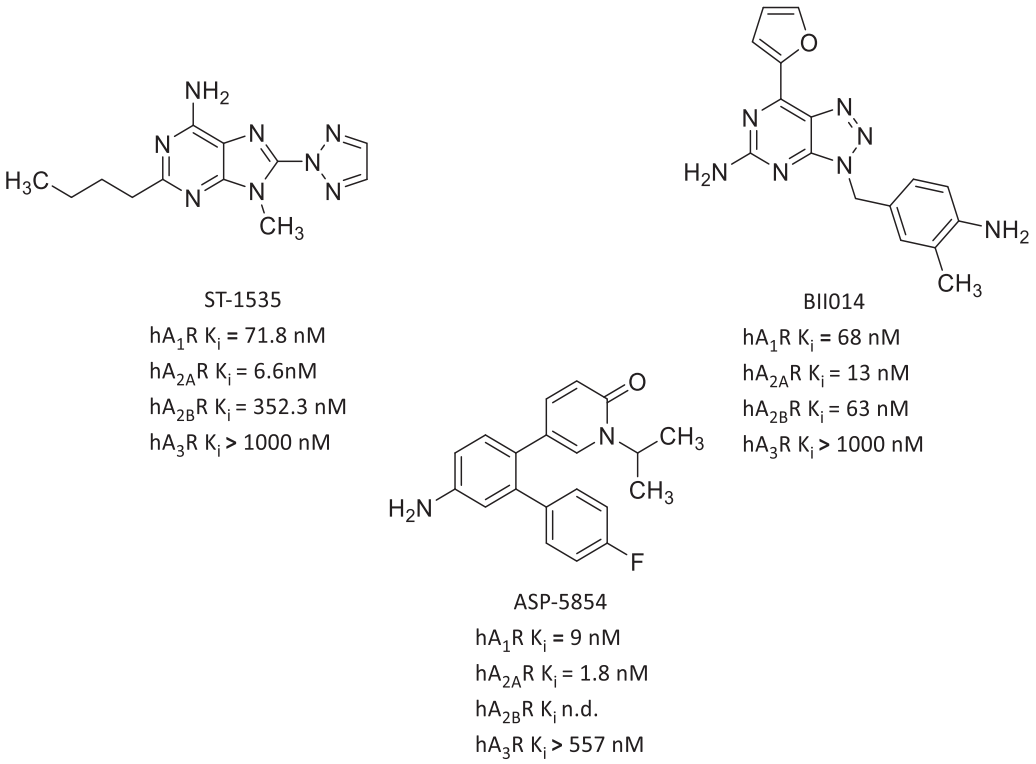

Figure 15. Dual $A_1R/A_{2A}R$ antagonists for the treatment of PD. n.d. not determined.[93,136]

Concerning non-motor symptoms affecting PD patients, it has been recently reported that the selective $A_{2A}R$ antagonist istradefylline improves day-time sleepiness in PD patients.[145–147]

Moreover, it has been found in preclinical studies that the blockade of A_1R may have positive effects on cognitive functions, due to its localisation in brain areas such as the hippocampus and limbic system.[148–150] As an example, the monocyclic non-xanthine derivate ASP-5854 ,showing good affinity in the nanomolar range for both A_1 and A_{2A} receptors, could promote mobility in several preclinical models of PD (Figure 15).[151,152] Additionally, ASP-5854 enhanced cognitive function through A_1R antagonism in models of cognition obtained by blocking the cholinergic receptors with scopolamine.[140,148] Taken together, these results have suggested that antagonizing the A_1R and $A_{2A}R$

simultaneously might effectively improve motor symptoms, with concomitant improvements of some non-motor complications such as cognitive and sleep impairments.

1.5 Development of MTLs with the H_3R pharmacophore for the treatment of PD

H_3R, MAO B and ARs are all targets for the treatment of PD and several clinical trials are ongoing to develop new medications able to avoid side effects of L-DOPA therapy, mainly motor fluctuation and LID, but also to treat non-motor symptoms that influence negatively the daily life of PD patients (i.e. sleep-wake disorders, dementia, depression). Most of the described drugs in clinical trials show high selectivity at a specific target, whereas a few (i.e. safinamide) treat PD symptoms by interacting simultaneously with multiple targets.[6,153,154] In the last decades, a great effort has been brought to design MTLs since they show several advantages compared to single target drugs. Some of the advantages might be potential synergistic efficacy by simultaneous target modulation as well as unified pharmacokinetic profile avoiding separate drug evaluation and drug regimen alignment prior to co-application.[153,155–161] Within the multi-targeting approach, numerous H_3R ligands are described, showing additional affinity to GPCRs, ion channels, transporters or even enzymes.[162–164]

Although ligands combining H_3R affinity with enzyme modulation were already investigated, just a handful of lead structures are described.[162] For example, Apelt et al. developed dual targeting H_3R/histamine methyltransferase (HMT) ligands, by the structural combination of the H_3R pharmacophore with the 4-aminoquinoline group as a key element for HMT inhibition (Figure 16, MTL1 and MTL2).[165] Other potent MTLs show H_3R antagonism along with acetylcholin- and butyrylcholinesterase (AChE/BuChE) inhibition, probably of interest for the treatment of AD.[164,166,167] Recently, contilisant combining affinity at H_3R, MAOs and cholinesterase *in vitro*, demonstrated a precognitive effect in mice.[163,168] In contrast, different types of GPCRs such as DA, histamine and melatonin-receptor subtypes showing H_3R antagonism have received more attention for the development of MTLs (Figure 16, MTL4 and MTL5).[162] However, MTLs able to modulate H_3R and to antagonize A_1R and $A_{2A}R$ have never been designated for the treatment of PD. Therefore, the combination of histamine on the one hand with MAO B and, on the other hand, with A_1 and A_{2A} adenosine receptors is an innovative and potentially therapeutic approach for the treatment of PD patients (Figure 17). In both combinations, the blockade of H_3R by inverse agonists/antagonists elevates neurotransmitters in the CNS and may improve cognition function and daytime sleepiness in PD patients.[59]

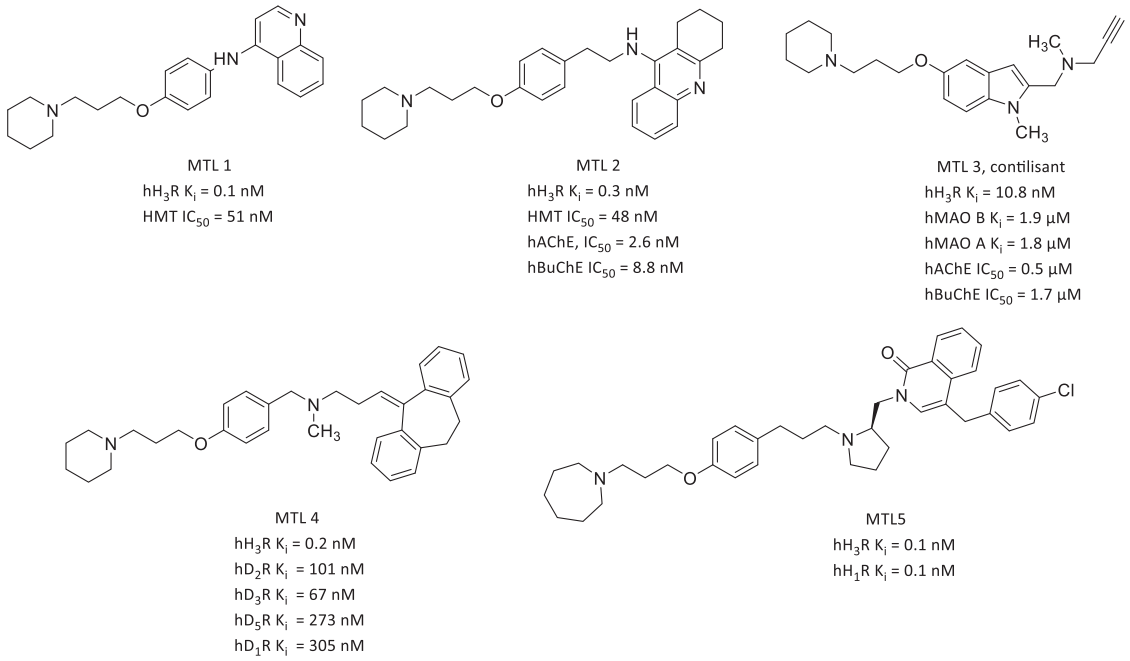

Figure 16. Structural and biological activities of some MTLs antagonizing H_3R as well as enzymes or other GPCRs.[162,163]

The co-localization of MAO B with H_3R, e.g. in the substantia nigra, a region predominantly affected by the loss of dopaminergic neurons in PD patients, might allow a convenient approach improving DA deficiency in PD therapy and neuroprotective activity.[169,170] Whereas, multi-targeting H_3R ligands with additional A_1R and $A_{2A}R$ binding properties might have therapeutic efficacy on motor symptoms primarily through the blockage at $A_{2A}R$, and also improve cognitive functions by antagonising A_1R.[120,148]

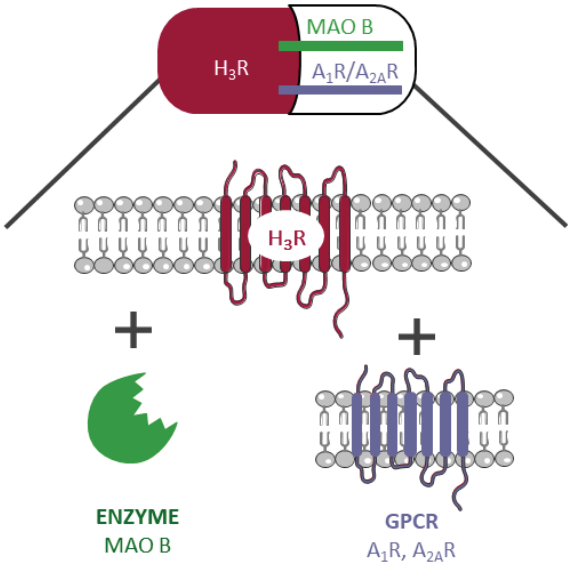

Figure 17. DTLs (H_3R/MAO B) and MTLs (H_3R/A_1R/$A_{2A}R$) with the H_3R pharmacophore for the treatment of PD.[162]

The H_3R antagonist pharmacophore is well accepted, and it contains an aliphatic heterocycle (as replacement of the former imidazole) linked by an alkyl spacer to a central aromatic core (Figure 18).[171] These elements, belonging to the western part of the molecule, are essential for receptor interactions through ionic (Asp114) and π-π interactions (Tyr115 and Trp371). The eastern molecule part allows a great diversity among H_3R antagonists since the central core might be substituted by a variety of moieties (i.e. polar, lipophilic, basic, acid and lipophilic elements).[45]

UCL2190, showing the described H_3R pharmacophore, was used as reference compound for the synthesis of both classes of ligands.[168]

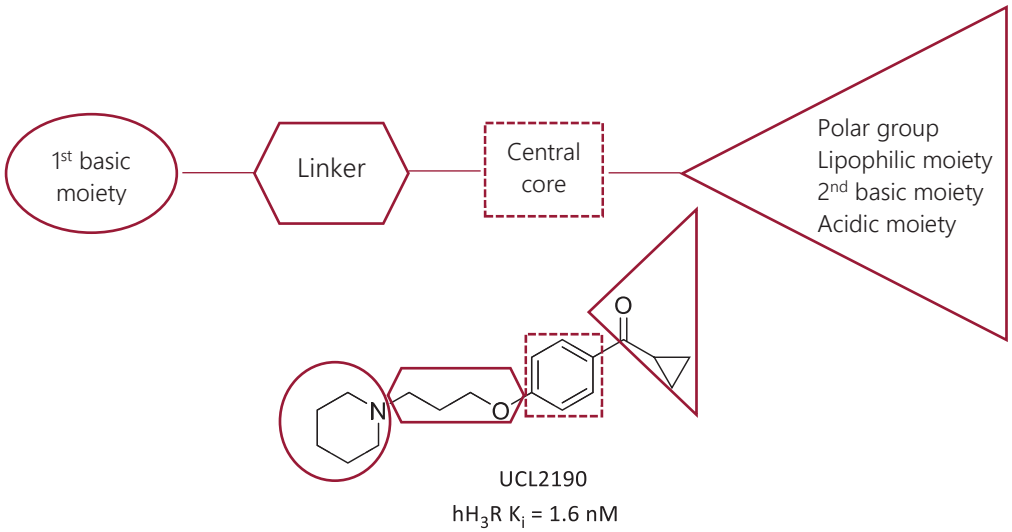

Figure 18. H_3R antagonist/inverse agonist blueprint showed for reference structure UCL219 ([^{125}I]iodoproxyfan replacement studies)[172] taken as lead structure for the synthesis of dual and multipotent targeting ligands.

To obtain the desired H_3R/MAO B DTLs, the potent MAO B inhibitors, **I**, which may be considered as the cyclic analogues of UCL2190, and **II**, were selected as reference ligands (Figure 19). These indanones showed highly selective and reversible inhibition properties in nanomolar concentration ranges for MAO B.[169,170] To expand the SAR on MAO B ligands-containing H_3R pharmacophore, the selective MAO B inhibitor rasagiline (described in chapter 1.3.1) was selected as reference compound for the synthesis of irreversible DTLs.

Distinct from traditional xanthine-based AR antagonists such as caffeine or istradefylline, a central tricyclic arylidenopyrimidine core motif was found to be a suitable pharmacophore for $A_1R/A_{2A}R$ antagonists, demonstrating nanomolar receptor affinity and functional efficacy.[123,173] In the last decade, promising heterocyclyl substituted arylidenopyrimidine $A_1R/A_{2A}R$ antagonists such as JNJ-40255293 were developed,[123] showing therapeutic potential in multiple preclinical models of PD (Figure 19).[120,148,174]

Thus, to synthetize $H_3R/A_1R/A_{2A}R$ MTLs, the cyclic amine propyloxy-linked phenyl H_3R pharmacophore was merged into the arylindenopyrimidine core of the dual $A_1R/A_{2A}R$ antagonists JNJ-40255293.

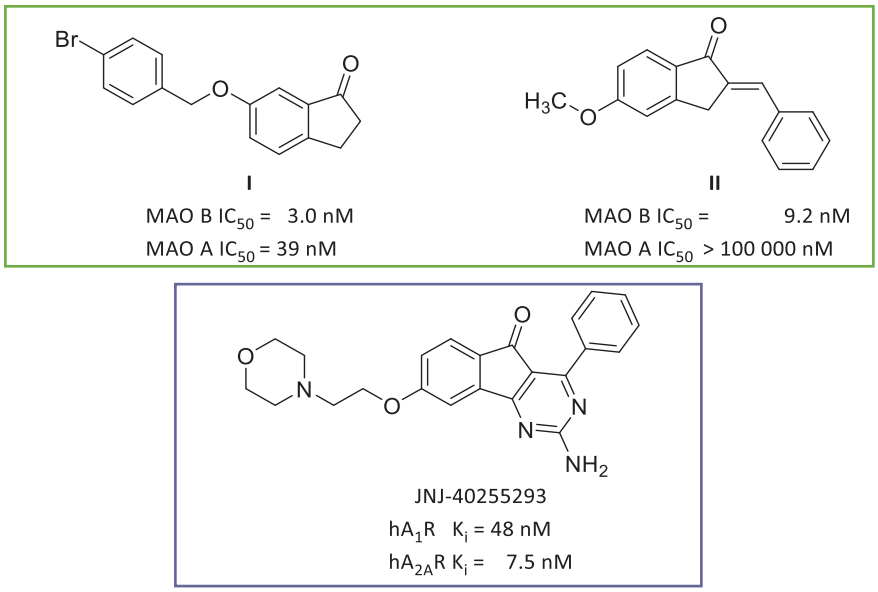

Figure 19. Reversible indanone inhibitors (**I** and **II**) as well as $A_1R/A_{2A}R$ antagonist JNJ-40255293 as lead structures for the synthesis of dual H_3R/MAO B and multipotent $H_3R/A_1R/A_{2A}R$ ligands, respectively.

1.6 Objective

The aim of my thesis was the design and pharmacological characterization of novel hybrid receptor ligands for the treatment of movement disorders with an enlarged therapeutic efficacy on accompanying non-motor symptoms in PD.

At the beginning of my investigation, pitolisant was progressing in phase III for excessive daytime sleepiness in PD patients.[30] Safinamide, a reversible MAO B inhibitor, was approved as an add-on to levodopa or in combination with other PD medications in mid- to late stage PD patients with motor fluctuations.[175] Also, indanone derivatives (i.e. **I** and **II**, Figure 19) were introduced as promising MAO B inhibitors for the treatment of PD.[170,176]

Moreover, JNJ-40255293 was found to be an adenosine $A_1R/A_{2A}R$ antagonist with efficacy in many animal models of PD. [120,148]

Recognizing CNS diseases, such as PD as highly complex and multifactorial dysregulations, forced researchers to come up with more approaches for medicinal therapy.[168] Challenging the "one-drug one-target" paradigm, showing mostly inadequate therapeutical efficacy, the development of MTLs became prominent over the last decades.[160,161] Due to the fact that multi-targeting drugs promise

several improvements compared to highly selective drugs, great effort has been brought to the design of such ligands for treatment of neurological diseases.[168]

With its broad therapeutical potential, H_3Rs gained increasing interest in multi-targeting drug design.[162] Since the H_3R pharmacophore was already combined with other pharmacophore elements for the treatment of neurodegenerative disease,[162] the H_3R receptor was chosen as one of the target for the synthesis of two classes of MTLs.

To obtain the desired MTLs, high H_3R affinity was introduced in compounds that were also potent ligands at the enzyme MAO B or at the A_1 and A_{2A} adenosine receptors, keeping in mind drug-likeness properties. Particularly, a pyrrolidino-/piperidino(alkyloxy)phenyl motif, which is a common H_3R antagonist/inverse agonist pharmacophore as presented by UCL2190,[177] was chosen to be introduced into (benzylidene)-indanones (i.e. **I** and **II**) and rasagiine to develop reversible and irreversible DTLs, respectively. Besides that, the H_3R pharmacophore was also merged to the arylindenopyrimidine core of the reference A_1R/A_{2A}R antagonist JNJ-40255293 to synthetize for the first time H_3R/A_1R/A_{2A}R MTLs.

As proof-of-concept study, based on comprehensive *in vitro* receptor binding characterization, most promising H_3R/A_1R/A_{2A}R MTLs were chosen for initial *in vivo* examination in preclinical rodent PD and sleep models.

2 Standard reactions and chemical approaches

To improve selectivity, affinity and other important parameters for optimal drug-target interactions, reference compounds (*cf.* Chapter 1.5), were modified or combined to generate molecules having enhanced biological properties. The synthesis of the dual H_3R/MAO B and the multipotent $H_3R/A_1R/A_{2A}R$ ligands is described separately in the chemical section as well as in results and discussions. Some of the synthetized materials used for the synthesis of dual H_3R/MAO B ligands has also been used for the synthesis of $H_3R/A_1R/A_{2A}R$ antagonists. In this chapter, the most frequently used reactions and the critical and challenging synthesis steps are reported. The synthesis of H_3R/MAO B indanone derivatives was performed in Madrid during a short termed scientific mission (STSM) supported by the EU COST action CM1103.

2.1 Synthesis of H_3R/MAO B inhibitors

2.1.1 1-(ω-Chloroalkyl)piperidine or pyrrolidine precursors

The H_3R pharmacophore for the synthesis of inverse agonist/antagonist ligands includes a basic N-containing heterocycle connected by an alkyl linker to an aromatic core. The synthesis of this H_3R framework started with the alkylation of piperidine or pyrrolidine with 2-chloroethan-1-ol or 3-chloropropan-1-ol (Scheme 1).[58,178,179] This synthesis step was carried out under basic conditions and in the presence of potassium iodide, which generates a better leaving group in Finkelstein exchange reaction.[180] The products were purified by distillation and good yields were obtained (67%-78%). Considering the boiling points of the reactants, piperidine or pyrrolidine were used in excess to facilitate the separation of the products. Chlorination of the alcohols, **P1-P3**, with an excess of thionyl chloride led to the chloride precursors **P4-P6**, which were obtained in quantitative yields.

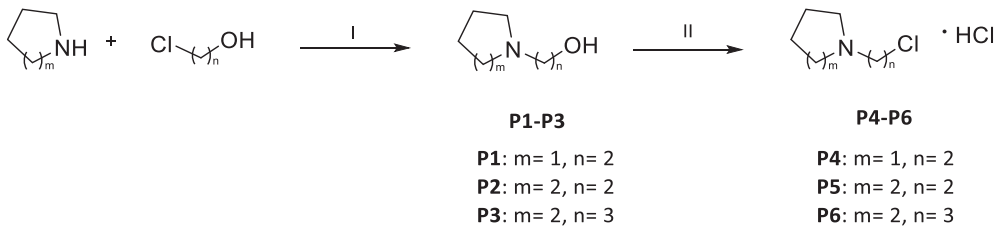

Scheme 1. General procedure for the synthesis of precursor compounds **P1-P6**.

Reagents and conditions: (I) K_2CO_3, KI, acetone, reflux, 24-72 h; (II) $SOCl_2$, toluene, N_2, 0 °C→60 °C, 3h.

2.1.2 1-(ω-Phenoxyalkyl)piperidine or pyrrolidine derivatives

Compound **P3** and the chlorides **P4-P6** were the starting material for the synthesis of phenoxy-alkyl derivatives. UCL2190 was obtained via a nucleophilic aromatic substitution of **P3** and cyclopropyl 4-fluorophenyl methanone in a one-pot procedure under basic conditions (Scheme 2, reaction step I, yield= 62%).[57,181]

In an ether synthesis according to Williamson, the first series of DTLs (**1a-e**) was synthetized in good yields (72%-85%) by attachment of the 1-(chloroalkyl)piperidine or pyrrolidine H_3R structural elements to the 5 or 6-position of hydroxy indanone derivatives (Scheme 2, reaction step II). Additionally, the *para*-substituted benzaldehyde was prepared in the same manner by attaching **P6** to 4-hydroxy-benzaldehyde (yield= 82%).

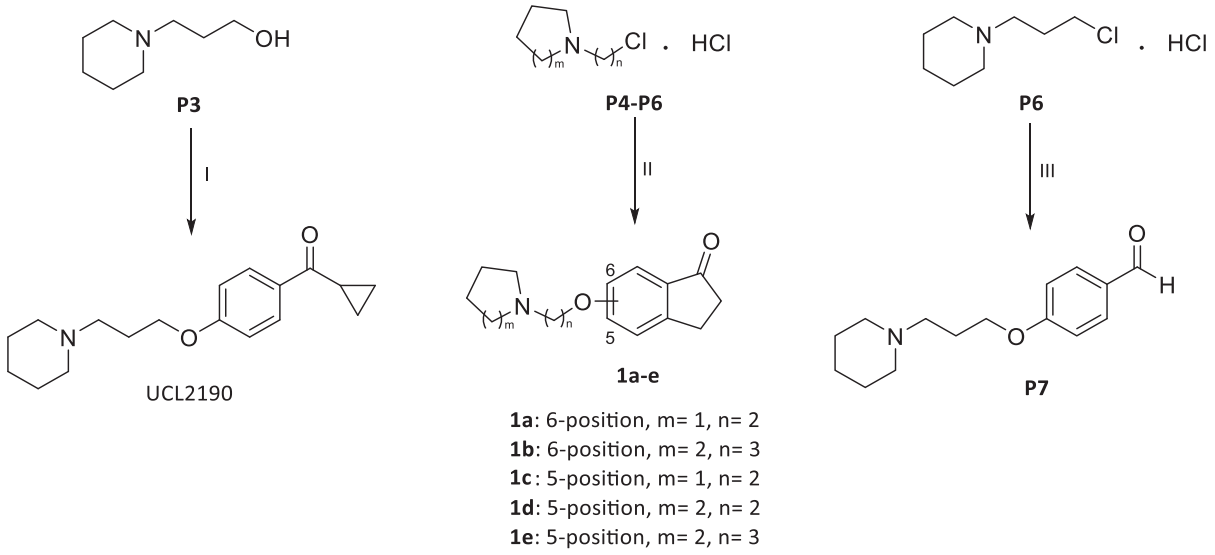

Scheme 2. Synthesis of UCL-2190, 1-indanone derivatives and **P7**.

Reagents and conditions: (I) a. NaH, acetonitrile, N_2, r.t, 3h b. cyclopropyl 4-fluorophenyl methanone, reflux, 24h; (II) 5- or 6-hydroxy-indan-1-on, K_2CO_3, KI, acetone, reflux, 15-24 h; (III) 4-hydroxybenzaldehyde, K_2CO_3, KI, acetone, reflux, 15 h.

2.1.3 2-Benzylidene-1-indanone derivatives

Several 2-benzylidene-1-indanone derivatives were synthesized with the aim to generate ligands with dual activity towards both H_3R and MAO B. These targets were obtained via aldol condensation under basic conditions (Scheme 3).[182] Compounds **1b**, **1d** and **1e**, having a piperidine as heterocycle, were combined with benzaldehyde to give series **2a-c** with good yield (80%-90%), whereas **P7** was connected with substituted indanone derivatives to give series **3a-f** (yields > 80%). The final products, showing low solubility in polar solvents, were re-crystallized in ethanol.

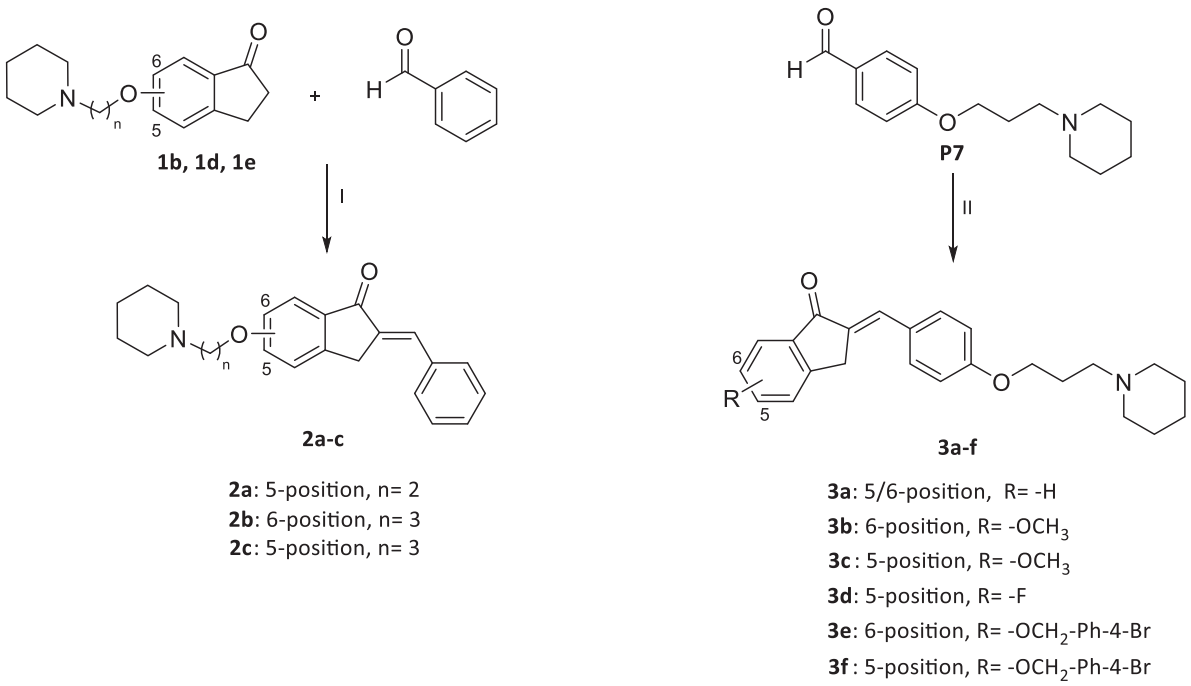

Scheme 3. Synthetic route for the preparation of 2-benzylidene-1-indanone derivatives 2a-c and 3a-f.

Reagents and conditions: Compounds 2a-c: I) NaOH, ethanol, r.t., 10 min-3 h; compounds 3a-f: II) corresponding indanone, NaOH, ethanol, r.t., 10 min-3 h.

2.1.3.1 Structural analysis of 2-benzylidene-1-indanone derivatives: ESI-MS study and 2D ^{1}H-NMR.

From structural point of view, dual 2-benzylidene-1-indanone ligands are Michael acceptor systems. As electrophilic compounds, Michael acceptors may be toxic due to their ability to form covalent bonds with endogenous proteins, DNA of biological organisms and critical peptides such as glutathione, which on the contrary act as nucleophiles.[183–186] Therefore, these compounds might have a risk factor for *in vivo* studies, during the drug development process. To test if this class of compounds may react with endogenous proteins, one of the synthetized benzylideneindanone derivative, 3d (4 µg mL^{-1}) was incubated over 3 days with an excess of acetylcysteine (20 mg mL^{-1}), which was chosen to mimic the cysteine residue of glutathione in proteins. The reaction was monitored by ESI-MS and the pH was adjusted to 7.2 using diluted sodium hydroxide solution (0.01 M). Only the molecular signal of 3d ([M+H]$^{+}$ signal at m/z= 380.2) was found, suggesting that biochemical formation of adducts with proteins are unlikely for the 2-benzylidene-1-indanone derivatives (Figure 20).

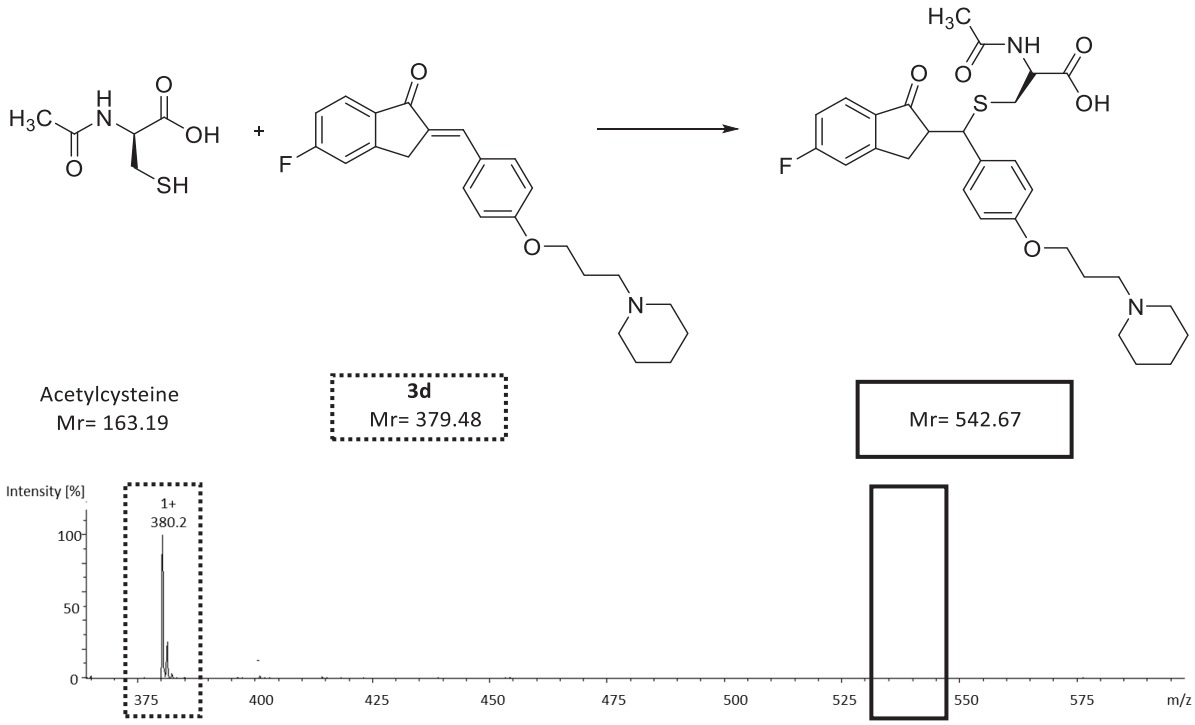

Figure 20. Suggested adduct formation and exemplified ESI-MS of a mixture of compound **3d** and acetylcysteine.

In addition, NOESY 2D ^{1}H-NMR were performed for the best final compounds to evaluate the stereochemistry of the double bound (Figure 21). Exemplified, the spectra of one H_3R/MAO B ligand, **3f**, is shown in figure 21. The *E* conformation is confirmed by the non-spatial proximity of the vinylic hydrogen (ph_{ind}-3*H)* and Ph^{1}-C*H*. This finding is consistent with the configuration of reported indanone aldol condensation products.[176,187,188]

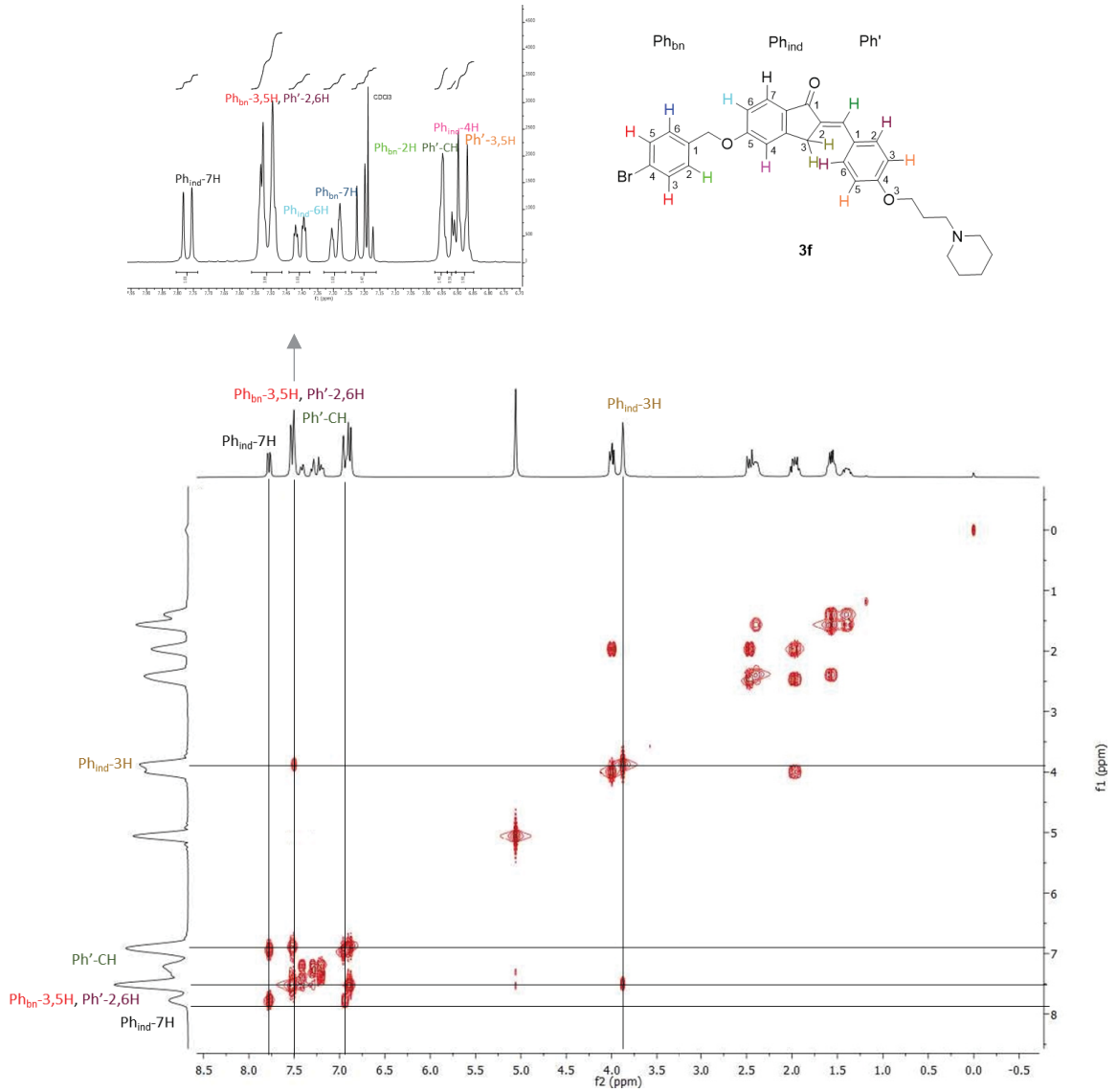

Figure 21. ^{1}H-NMR (aromatic region) and 2D ^{1}H-NMR (NOESY) spectra of compound **3f**.

2.1.4 Synthesis of indenamine derivatives

The reductive amination (RA) of aldehydes or ketones is a convenient method to design different types of amines. In the first reaction step, the nucleophilic attack of the amine to the carbonyl compound generates the intermediate carbinolamine, which dehydrates to form an imine or an iminium ion. The latter compounds are then reduced to the corresponding amine (Scheme 4).[189] When the reductive agent is added at the beginning of the reaction a direct RA occurs, whereas an indirect/stepwise RA takes place when the reductive agent is introduced after the formation of the imine (from primary amine and aldehyde or ketone) or iminium ion (from secondary amine and aldehyde or ketone) followed by reduction in a separate step.[190]

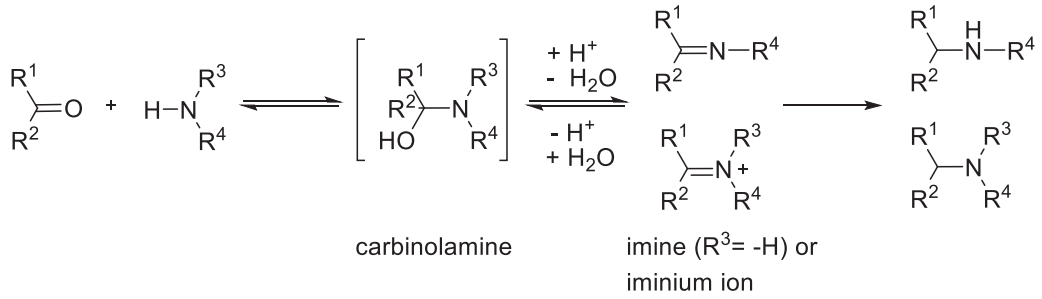

Scheme 4. Reaction mechanism of the reductive amination. R^1, R^3 = -H or alkyl; R^2, R^4 = alkyl or aryl.

In our study, the RA was performed to convert the indanone ketone moiety of compound **1e** to a propargyl amine group, by using the mild ($NaBH(OAc)_3$) as reductive agent. Sodium triacetoxyborohydride was selected as reductive amination reagent because of its mild reducing property, attributed to the steric and electron-withdrawing effects of the three acetoxy groups, which stabilize the boron-hydrogen bonds.[190] In addition, this hydride reductive agent was used for the reductive amination of the ketone function of 1-indanone for the synthesis of rasagiline.[191]

At first, direct reductive aminations were carried out. A mixture of **1e** and the amine (1-1.5 eq) was stirred with 1.2 eq of $NaBH(OAc)_3$ under a nitrogen atmosphere at room temperature. Different solvents were used (THF, MeOH and DCE) and, in some reactions, acetic acid (1.5-3 eq) was added to the reaction mixture. The results in scheme 5 show that the RA of the cyclic ketone was unsuccessful, since no product was formed even after 3 days. The unreacted ketone was recovered unchanged as determined by ^{1}H-NMR analysis of the crude product.

The synthesis of rasagiline was achieved by direct RA of 1-indanone with propargylamine and $NaBH(OAc)_3$. Therefore, the presence in compound **1e** of the basic piperidine(propyloxy) H_3R pharmacophore influences the reduction amination of the ketone moiety.

Indirect RA involving imine formation, followed by reduction with $NaBH(OAc)_3$ was performed. To shift the equilibrium towards the product, dehydrating agents such as molecular sieves, magnesium sulfate or azeotropic removal of water (i.e. with a Dean Stark water separator) were used. The amine reacted slowly with the carbonyl moiety to give the imine derivative (not isolated, determined by ESI-MS). The latter derivative was treated with $NaBH(OAc)_3$ but after three days unreacted ketone (compound **1e**) was still present and no product was formed (Scheme 5).

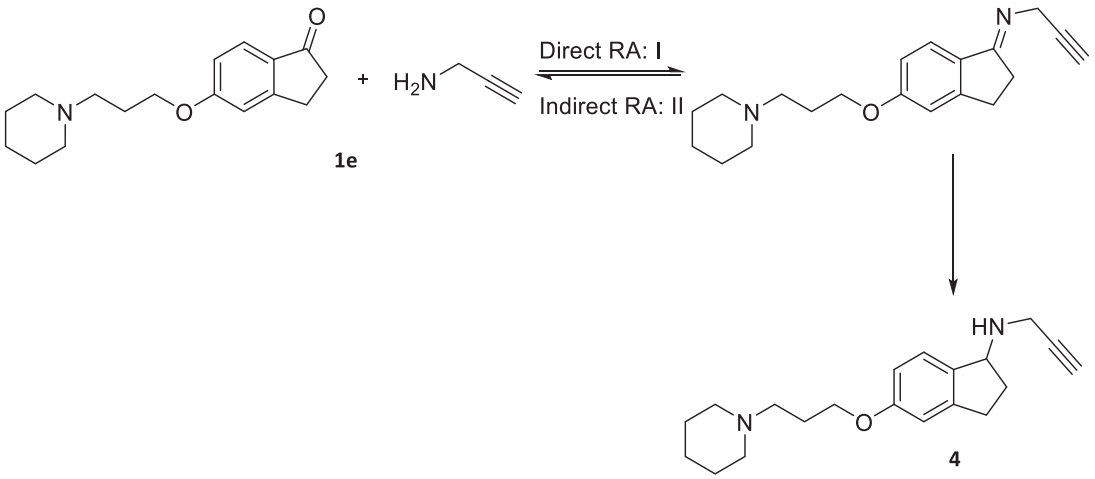

Entry reaction	Eq. amine	Eq. acetic acid	Solvent	Dehydrating agent	Yield **4** (%)
Direct RA (I)					
1	1	0	THF		n.c.
2	1.5	0	THF		n.c.
3	1.5	1.5	THF		n.c.
4	1.5	1.5	MeOH		n.c.
5	1.5	3	MeOH		n.c.
6	1.5	3	DCE		n.c.
7	1	3	DCE		n.c.
Indirect RA (II)					
8	1.5	1.5	DCE	molecular sieves	n.c.
9	1.5	1.5	THF	molecular sieves	n.c.
10	0.5	1.5	MeOH	molecular sieves	n.c.
11	1.5	1.5	MeOH	molecular sieves	n.c.
13	1.5	1.5	MeOH	magnesium sulfate	n.c.
14	1.5	1.5	Toluene	Dean-Stark apparatus	n.c.

n.c.: no conversion; RA: reductive amination

Scheme 5. Direct and indirect amination of compound **1e** (1 eq.) under various reaction conditions with $NaBH(OAc)_3$ (1.2 eq.) as reductive agent.

Reagents and conditions: direct RA: I) $NaBH(OAc)_3$, acetic acid, corresponding solvent, N_2, r.t., 3-72 h; indirect RA: II) a. acetic acid, corresponding solvent, N_2, r.t., 24-72 h; b. $NaBH(OAc)_3$, corresponding solvent, N_2, r.t., 5-24 h.

Substitution of $NaBH(OAc)_3$ with $NaBH_4$ led to the synthesis of the corresponding alcohol derivative as major reaction product (as determined by ESI-MS of the reaction mixture).

Since product **4** was not synthetized by performing the direct/indirect reductive amination, a new synthesis pathway was carried out.

The propargyl derivative ladostigil, was synthetized from the corresponding 6-hydroxy-1-amino-indan.[192] Therefore, attempts to synthetize this key intermediate, showing, in our case, the phenol moiety in 5-position, were performed (Scheme 6, black box).

At first, compound **P9** was prepared by conversion of the 5-methoxy-1-indanone to the oxime (yield = 57%, Scheme 6, reaction step IV) and subsequent reduction with 10% Pd/C (yield = 61%) or via one-step reductive amination with the reductive agent $NaCNBH_3$ (yield = 67%, Scheme 6, reaction step V).

Attempts to demethylate **P9** either with $AlCl_3$ or HBr/HOAc (reaction step I and III, respectively led to its degradation (large number of unidentified compounds). Likewise, reductive amination, with $NaCNBH_3$ of 5-hydroxy-1-indanone (**P10**) resulted in a compound lacking the amino-indan ^{1}H-NMR characteristics (Scheme 6, reaction step II).

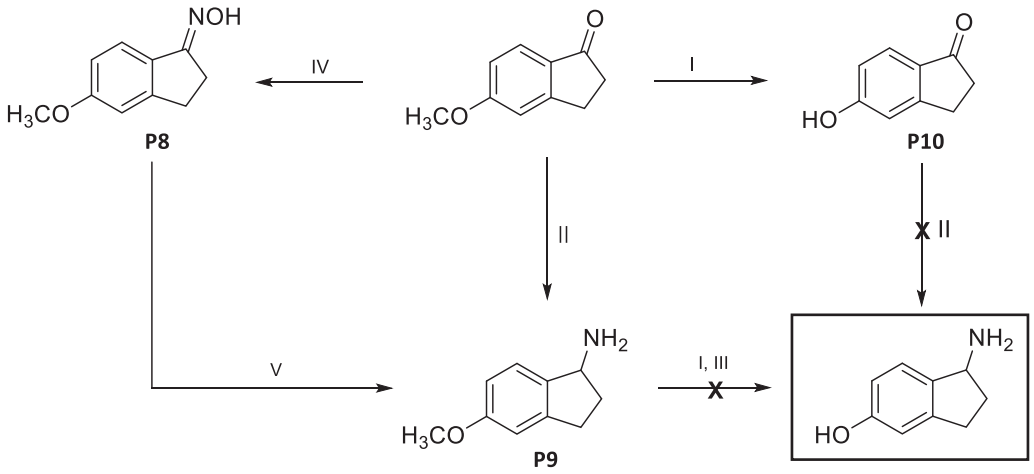

Scheme 6. Synthesis route for the synthesis of 5-hydroxy-1-amino-indan.

Reagents and conditions: (I) $AlCl_3$, toluene, reflux, 3 h; (II) $NaCNBH_3$, NH_4OAc, ethanol, 130 °C, 3 min, MW; (III) HBr/OHAc, 110 °C, 18 h; (IV) NH_2OH HCl, NaOAc, ethanol/water, reflux, 3h; (V) Pd/C (wt. 10 %), methanol, 50 °C, 18 h.

The instability of the 5-hydroxy-1-amino-indan, which might forms under heating the corresponding quinone methide intermediate after elimination of the amine, might explain these unsuccessful results.[192] To overcome this issue, compound **1e** bearing in 5-position a piperidine-propyloxy group instead of a hydroxy moiety was used to synthesize the 1-amino-indan derivative **P12**. The carbonyl group of compound **1e** was converted to the corresponding amine (**P12**) either by conversion of **1e** to oxime (**P11**) and subsequent reduction (Scheme 7, reaction step II and III) or via a one-step reductive amination (Scheme 7, reaction step IV). Afterward, the primary amine of compound **P12**

was transformed in the corresponding propargyl amine derivative, compound **4**, by nucleophilic substitution with propargyl bromide in DMF (47%).

The protection of the amine with an excess of di-*tert*-butyl decarbonate was performed to avoid double-alkylation. However, the use of the unprotected amine was preferred due to more convenient purification steps.

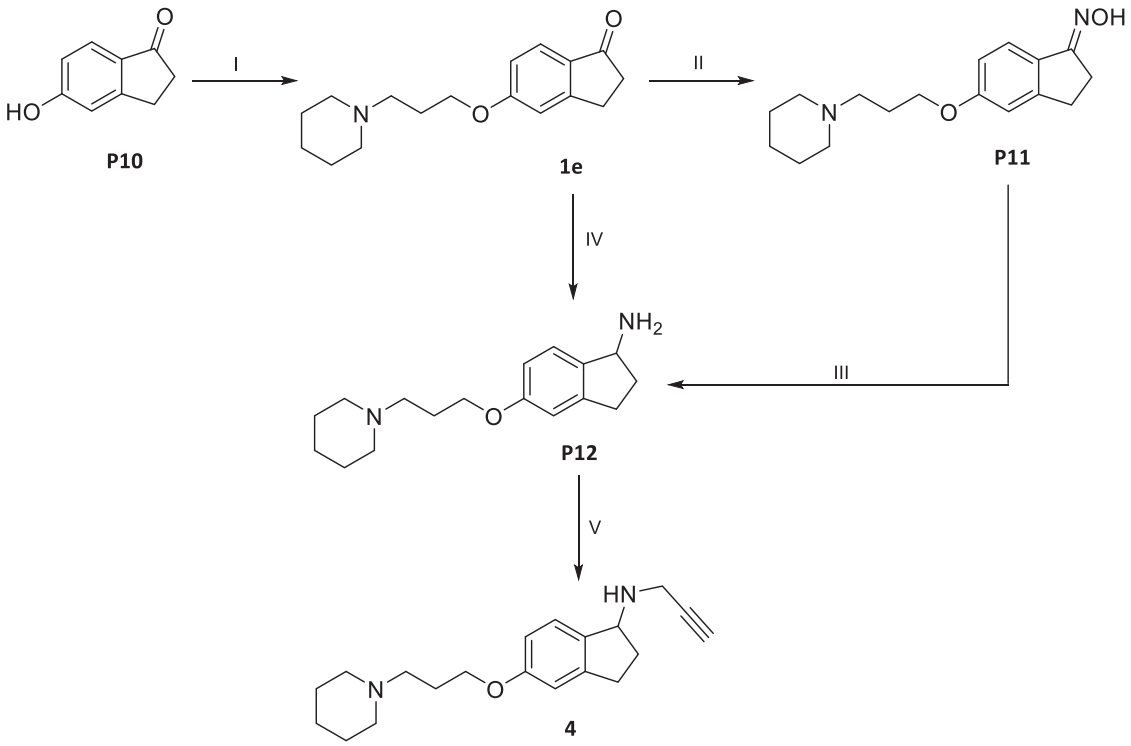

Scheme 7. Synthesis of the propargyl amine derivatives **4**.

Reagents and conditions: (I) 1-(3-chloropropyl)piperidine hydrochloride, K_2CO_3, KI, acetone, reflux, 24 h; (II) NH_2OH HCl, NaOAc, ethanol/water, reflux, 3h; (III) Pd/C (wt. 10 %), methanol, acetic acid, 50 °C, 18 h; (IV) NH_4OAc, $NaCNBH_3$, ethanol, 130 °C, 3 min, MW; (V) propargyl bromide, K_2CO_3, dimethylformamide, 30 °C, 4h.

The hydrogenation of the ketoxime **P11** (step III) was successful when performed at 50 °C with a catalytic amount of acetic acid (yield = 45%). Whereas, the reductive amination of compound **1e** (step IV) was performed by using $NaCNBH_3$ as the reductive agent and NH_4OAc as the ammonia source.[193] The conversion of the reactant in the corresponding amine was not achieved either at room temperature or at reflux, while compounds **P12** was obtained in microwave heating (MW), by using ethanol as a solvent (Table 3). Below 110 °C no significant conversion occurred, and the reactant could be recovered. At 130 °C the amine was obtained after 3 minutes (47 % yield). Longer reaction times (5, 10 minutes) gave a much lower yields (< 10 %, entry 5 and 6, Table 3), mainly due to the formation of the dialkylated by-product, which was characterized in ^{1}H-NMR and in ESI-MS (not isolated).

Table 3. Conventional and microwave heating for the synthesis of compound **P12** by reductive amination of compound **1e**.

Entry reaction	Temperature (°C)	Time	Yield **P12** (%)
Conventional thermal conditions			
1	25	8-48 h	n.c.
2	80	18-48 h	< 5
Microwave heating			
3	110	3 min	< 5
4	130	3 min	47
5	130	5 min	< 10
6	130	10 min	< 10

n.c: no conversion

Since the reductive amination of the ketone moiety with $NaCNBH_3$ under microwave condition was successful, step IV (reaction conditions: $NaCNBH_3$, ethanol, 130 °C, 3 min, MW) was performed also by using propargyl amine as amino source but no conversion was achieved.

2.2 Synthesis of $H_3R/A_1R/A_{2A}R$ ligands

2.2.1 Synthesis of arylindenopyrimidine derivatives

The synthesis of arylindenopyrimidine derivatives was performed by following two reaction pathways. For compounds **5-6**, the H_3R pharmacophore was introduced in the first synthesis step at the 5 or 6-position of the corresponding hydroxy indanones, whereas for compounds **7-10**, the H_3R pharmacophore was added either in 7 (as R^7) or 8-position (as R^8) of the arylindenopyrimidine scaffold and in 4'-position (as $R^{4'}$) of the phenyl group.

The synthesis of compounds **5** and **6** started with the alkylation of 5- or 6-hydroxy-1-indanone with 1-(3-chloropropyl)piperidine by Williamson ether reaction (Scheme 8). Same procedure described in chapter 2.1.3 was used to convert, via aldol condensation, compounds **1b** and **1e** into the corresponding 2-benzylidene-1-indanone derivatives, **2b-2c**, with yields higher than 80%. The latter compounds were then treated with the free base guanidine, to obtain the corresponding arylindenopyrimidine compounds, **5-6**.[120]

Since unreacted reagent was still present after also three days, yields higher than 55% could have not obtained.

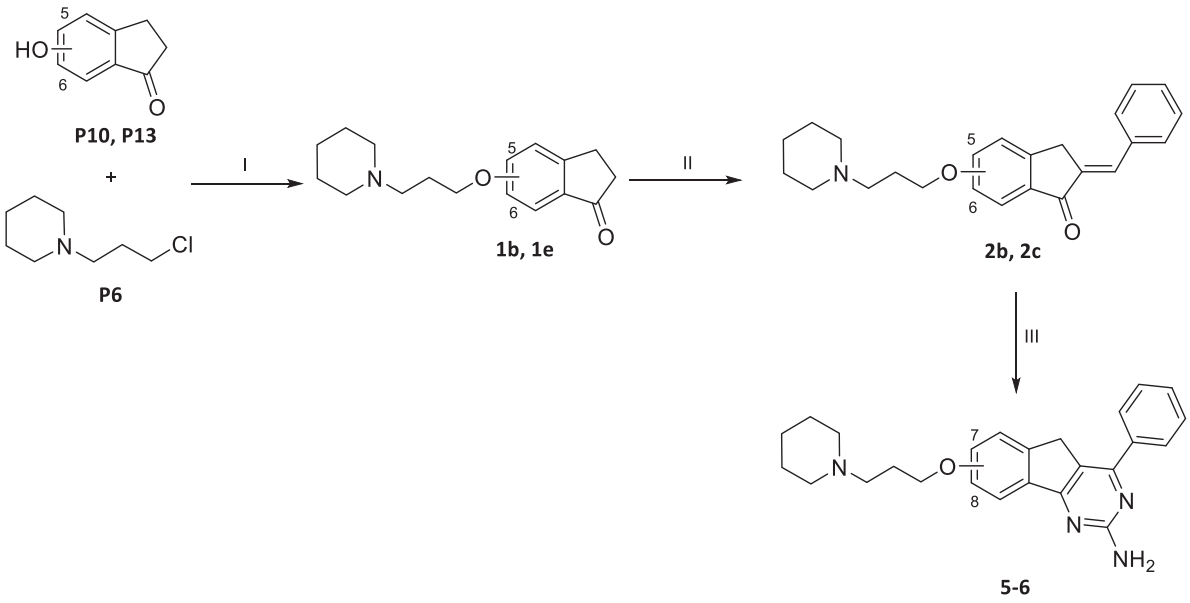

Scheme 8. Synthesis of the arylindenopyrimidine compounds 5 (7-position) and 6 (8-position).

Reagents and conditions: (I) K_2CO_3, KI, acetone, reflux, 24 h; (II) benzaldehyde, NaOH, ethanol, r.t., 15 min; (III) guanidine hydrochloride, NaOH, ethanol, N_2, reflux, 20 h.

The synthesis of compounds 7-10 started with the protection of 5- and 6-hydroxy-1-indanones with the commercially available benzyl bromide to obtain compounds P14-P15 (Scheme 9).[194] Aldol condensation of the latter compounds or 1-indanone, with benzaldehyde or 4-(benzyloxy)benzaldehyde was then performed to obtain the corresponding 2-benzylidene-1-indanone derivatives, P16-19, in good yields (80-90%).[168] The obtained aldehydes reacted with guanidine to form benzyl ether pyrimidine intermediates, which were used without further purifications. The crude materials were dissolved in ethanol and treated with Pd/C under hydrogen to cleave the benzyloxy group. The key intermediates P20-P23 were obtained with a yield ranging from 72 and 85 %.[195] Afterwards, Williamson ether reactions were performed between the phenol derivatives and 1-(3-chloropropyl)piperidine (P6) or pyrrolidine (P24), to give after a short reaction time (4h) compounds 7-10.[120] Although two more synthesis steps had to be performed compared to the synthesis of derivatives 5 and 6, the purification of the crude products via column chromatography gave the desired end products (7-10) in better yields (52%-55%) compared to compounds 5-6 (< 45%).

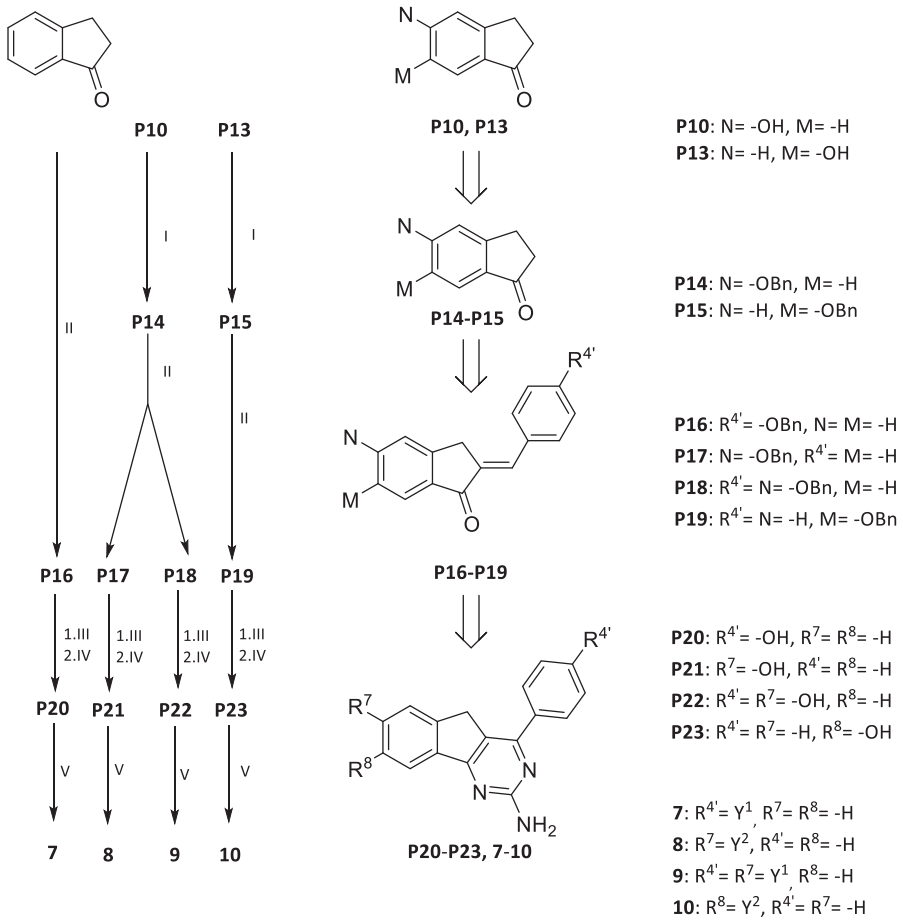

Scheme 9. Synthesis of the arylindenopyrimidine compounds **7-10**.

Reagents and conditions: (I) Benzyl bromide, K_2CO_3, dimethylformamide, r.t., 15 h; (II) Corresponding benzaldehyde, NaOH, ethanol, r.t., 30 min; (III) Guanidine hydrochloride, NaOH, ethanol or methanol, N_2, reflux, 18-24 h; (IV) Pd/C (wt. 10 %), ethanol, H_2, r.t., 18 h; (V) 1-(3-chloropropyl)piperidine (**P6**) or 1-(3-chloropropyl)pyrrolidine (**P24**), K_2CO_3, dimethylformamide, N_2, 80 °C, 4 h; Bn= benzyl; Y^1= 1-(3-oxypropyl)piperidine ; Y^2=1-(3-oxypropyl)pyrrolidine.

The synthesis of compound **P21** was also performed by using a methoxy group instead of the benzyl ether moiety as protective group for the hydroxy indanone (Scheme 10).

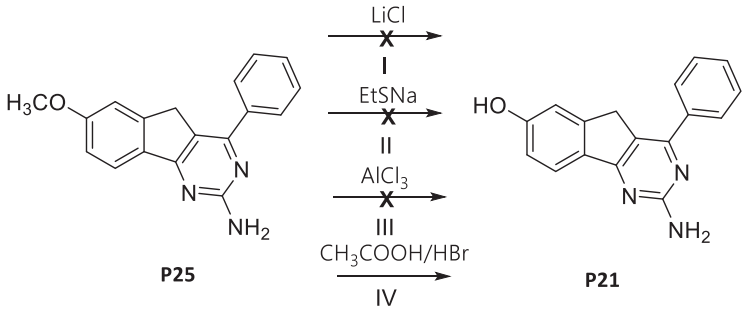

Scheme 10. Demethylation approach for 7-methoxy arylindenopyrimidine **P25**.

Reagents and conditions: (I) N_2, DMF, reflux, 24h; (II) N_2, ethanol, reflux, 24h; (III) N_2, toluene, reflux, 3h; (IV) N_2, reflux, 18h.

Therefore, 6-methoxy-1-indanone was used as starting material for the synthesis of 6-methoxy-2-benzylidene-1-indanone (cf. Chapter 2.1.3 for general procedure). The ring closure of the latter compound with guanidine gave products **P25** (Scheme 10).[120] Attempts to deprotect the methoxy pyrimidine intermediate using aluminum chloride, lithium chloride as well as sodium ethoxide were unsuccessful.[196,197] However, a mixture of acetic and hydrobromidric acid was effective in removing the methoxy group, but was not as efficient as the palladium-catalyzed hydrogenation of the benzyl moiety (yield < 15%).[198]

For the synthesis of compounds **5-10**, working under nitrogen atmosphere was necessary to avoid the oxidation of the methylene group in 5-position of the arylindenopyrimidine scaffold. When a mixture of both compounds (non-oxidized and oxidized derivatives) was obtained, purification via chromatography or crystallization failed due to the very similar physical properties of the compounds. The presence of the oxidized form was confirmed by ESI-MS and by ^{1}H-NMR.

2.2.2 Oxidation of the 5-position of the arylindenopyrimidine derivatives

Compounds **5-10**, were oxidized to the corresponding ketones, **11-16**, by passing air through the solution (Scheme 11).[120]

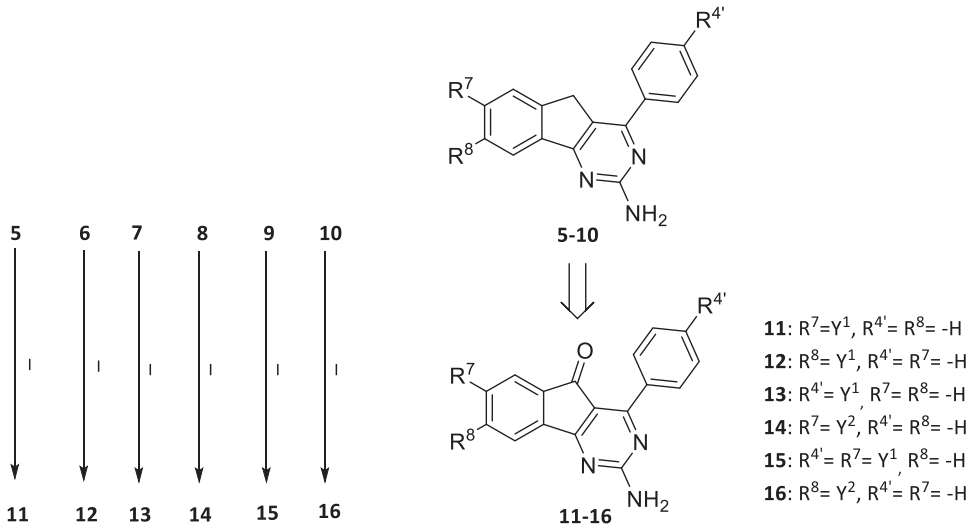

Scheme 11. Synthesis of $H_3R/A_1AR/A_{2A}AR$ ligands via oxidation reaction.

Reagents and conditions: (I) NaOH, DMF, O_2, 80 °C, 2h. Y^1= 1-(3-oxypropyl)piperidine ; Y^2=1-(3-oxypropyl)pyrrolidine.

A carbanion-based (Scheme 12, A) or a radical (Scheme 12, B) mechanism may take place for the oxidation of the methylene group in 5-position of the arylindenopyrimidine scaffold. The isolation of the desired end products, **11-16**, was achieved after purification with column chromatography (yields ranging from 62 % to 79 %).

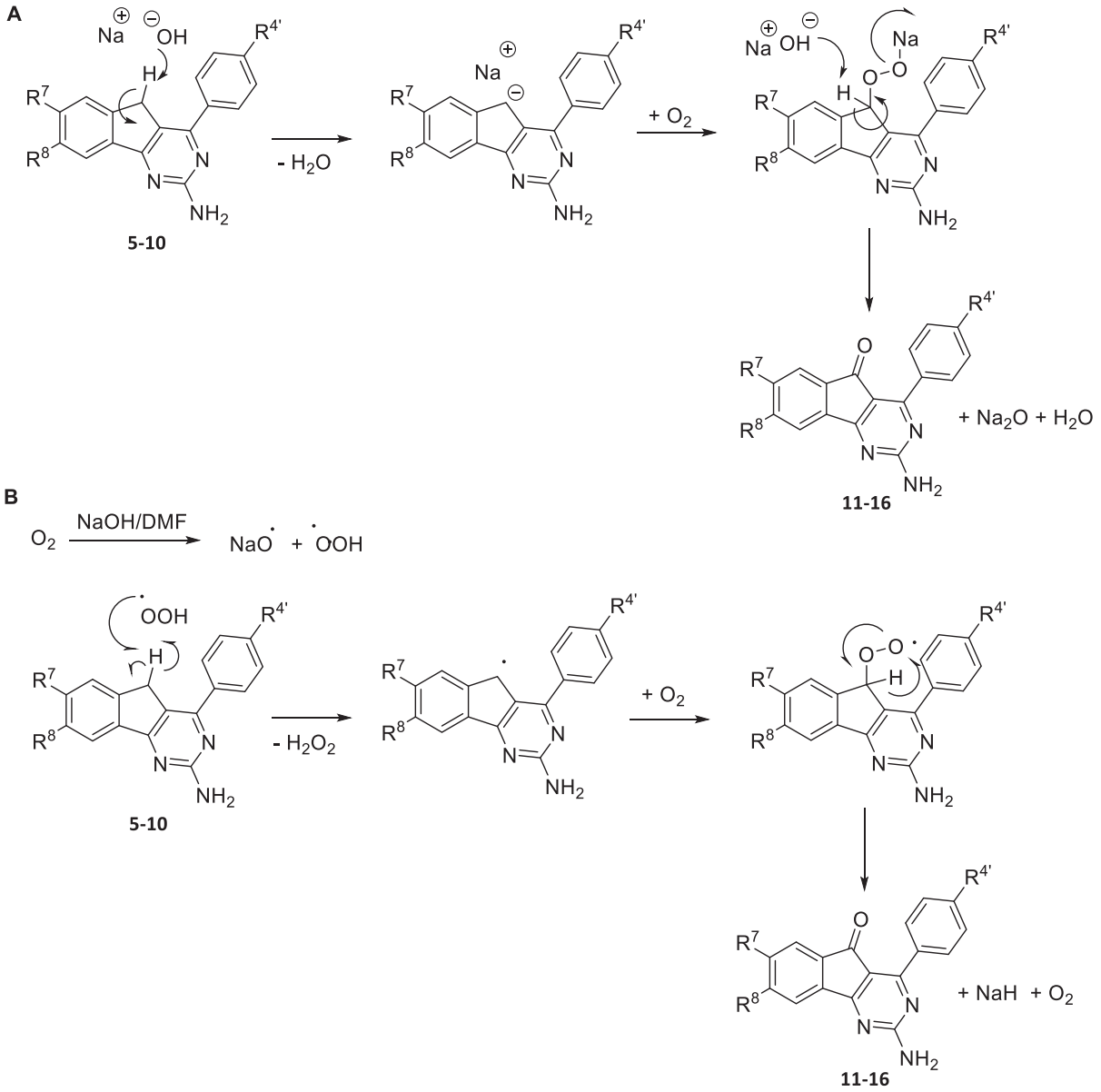

Scheme 12. Mechanisms of action for the oxidation in DMF of compounds 5-10.

2.2.3 Structural analysis of compound 6 and its oxidized form

All final arylindenopyrimidine compounds were converted in the corresponding oxidized derivatives. Compound **6** (Figure 22A) and its oxidized derivative **12** (Figure 22B) are compared in ^{1}H-NMR spectra as example for the classes of compounds. In both structures, the aliphatic protons of the H_3R fragment are high field shifted (low chemical shift). Also, the two protons (prop-1''*H*$_2$), having in the vicinity the electronegative oxygen, were the less shielded and showed a triplet signal around 4 ppm due to the coupling with the adjacent protons (prop-2''*H*$_2$). If oxidation took place, a downfield shift was observed for the signal of pyrimidine-N*H*$_2$ ($\Delta\delta$ = 1.24 ppm) and Aip-6,7,9*H* ($\Delta\delta$ < 0.14 ppm)

probably because of the electron delocalization between the pyrimidine and the carbonyl group, which lead to a magnetic deshielding of the protons.

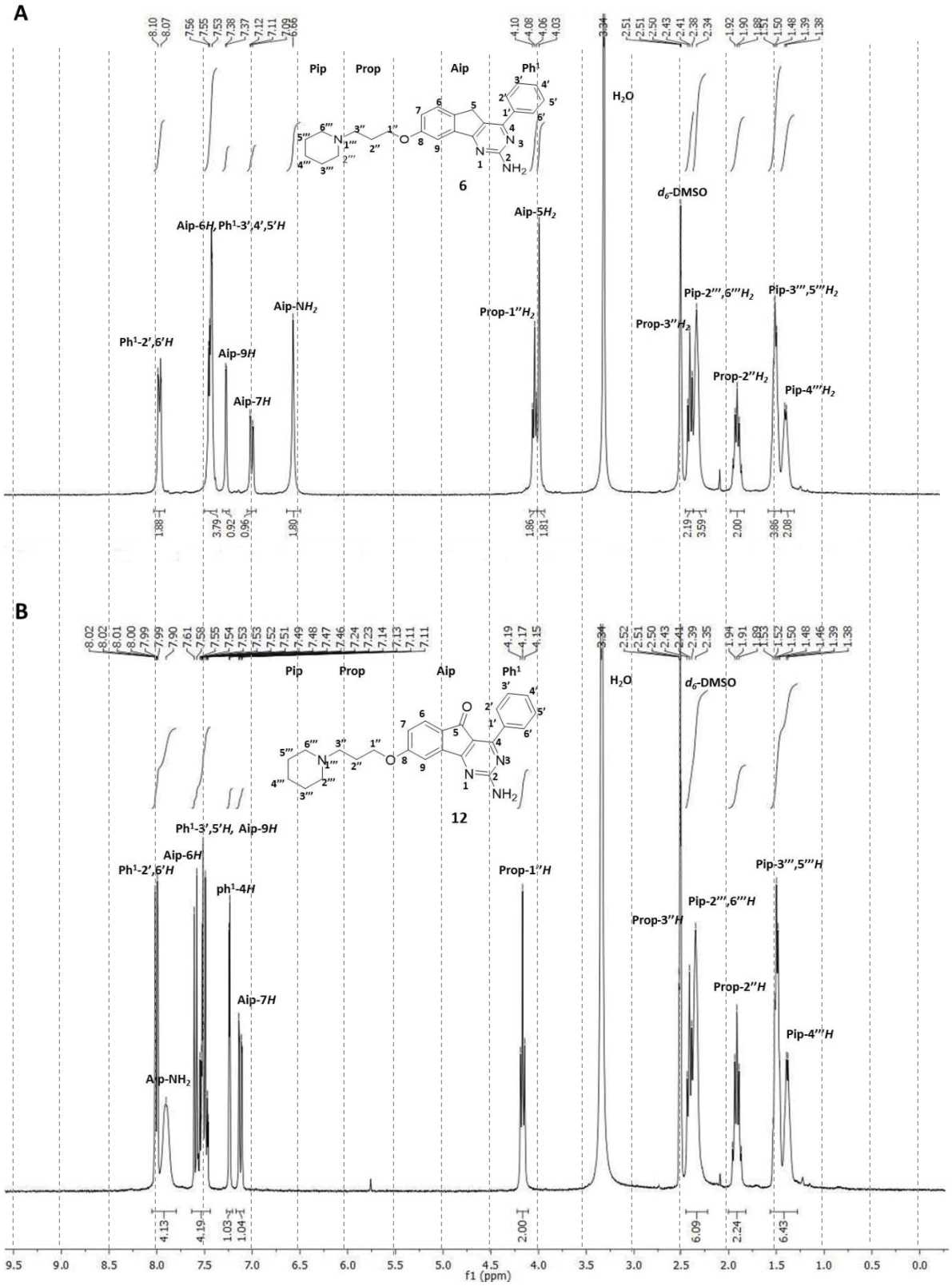

Figure 22. [1]H-NMR spectra of compound 6 (A) and its oxidized derivative 12 (B).

Conditions: [d_6] DMSO, 300 MHz. Abbreviations: Aip, arylindenopyrimidine; Ph, phenyl; Prop, propane; Pip, piperidine.

In addition, the characteristic singlet of the two protons in 5-position of the arylindenopyrimidine scaffold (**6**) named aip-5*H* disappeared from the spectra of the oxidized compound **12** (no signal at 4.03 ppm).

2.2.4 Fluorescence properties of the synthetized arylindenopyrimidine derivatives

The use of fluorescent ligands for the detection and localization of the *h*H_3R has already been described. For example, the fluorescent chalcone ligands facilitate visualization of human *h*H_3R on *h*H_3R–HEK cells.[178] Bodilisant was also described as a bright green fluorescent *h*H_3R ligand used for the localization and detection of *h*H_3R in *h*H_3R overexpressing HEK-293 cells and native human brain tissues.[199]

Therefore, compounds **5**-**16** were investigated as possible fluorescent elements for labelling the histamine H_3 and the adenosine A_1 and A_{2A} receptors to generate novel fluorescent pharmaceutical tools.

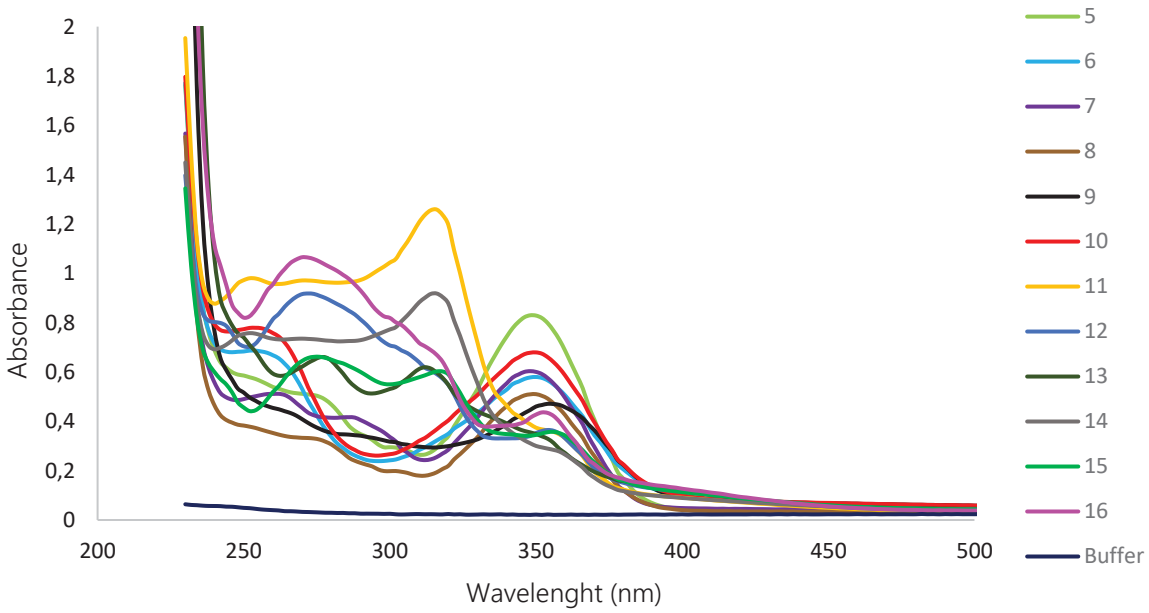

Figure 23. Absorbance spectra of final compounds **5**-**16**.

Compd 100 µM, Buffer (12.5 mM $MgCl_2$, 100 mM NaCl, and 75 mM Tris/HCl, pH 7.4).

Fluorescence properties of the substituted arylindenopyrimidines may arise from the extended conjugation prevalent in them. Except for compounds **11**-**14** and **16**, the maximum excitation wavelength was about 350 nm for all the other synthetized ligands (Figure 23).

Compounds showing a methylene group in 5-position of the arylindenopyrimidine scaffold, **5-10**, have shown an emission peak at 400 nm (Figure 24A).

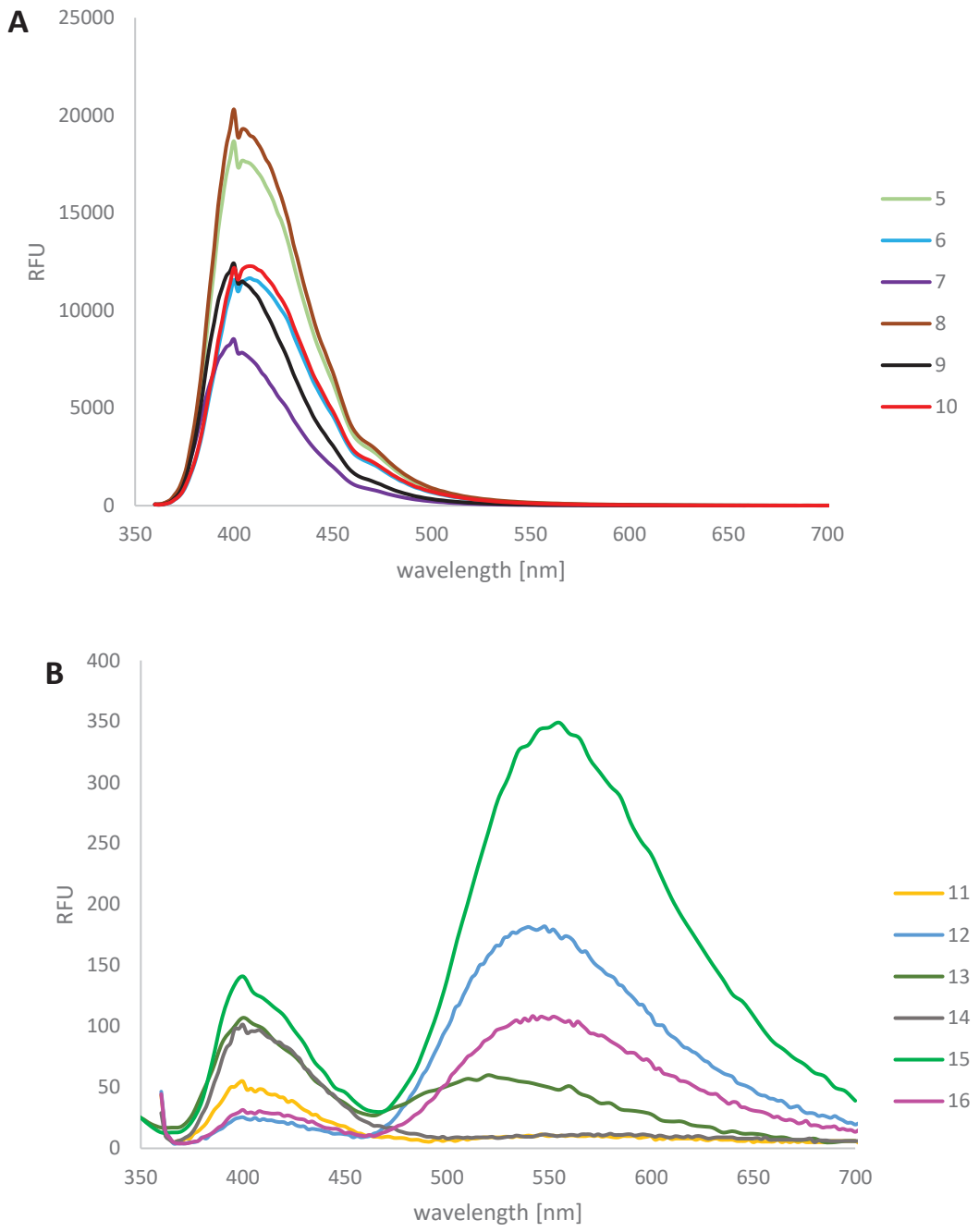

Figure 24. Emission spectra for non-oxidized (A) and oxidized (B) synthetized ligands.

Compd 100 µM; buffer (12.5 mM $MgCl_2$, 100 mM NaCl, and 75 mM Tris/HCl, pH 7.4); λ_{ex} = 316 nm.

The oxidation of these ligands led to the synthesis of derivatives having different emission spectra. When the H_3R pharmacophore was introduced in 7- or 4'-position of the oxidized scaffold (compounds **11**, **13** and **14**) one emission peak at 400 nm was detected after excitation at 316 nm

(Figure 24B). In contrast, the substitution of the H_3R moiety in 8-position or in both 4'- and 7-position of the oxidized arylindenopyrimidine moiety led to a bathochromic shift of the fluorescence transition. Two emission peaks, one at 546 nm and one, less intensive, at 398 nm were obtained (compounds **12**, **15** and **16**) (Figure 24B).

The emission spectra obtained for the latter compounds confirmed the results reported for some 8-substituted indenopyrimidine derivatives, whose fluorescence properties were used to gain insight into the binding properties of these ligands with quadruplex and duplex DNAs.[200]

In conclusion, most of the compounds showed fluorescence absorption and emission wavelengths mainly between 300 and 500 nm, respectively. Although three of the oxidized compounds (**12**, **15**, **16**) showed fluorescence emission maxima higher than 500 nm and high Stokes shifts (for all compounds $\lambda_{em} - \lambda_{abs} = 200$ nm), which is important for avoiding measurements artefacts (Figure 24 B), the fluorescence intensities were too low (< 400 relative fluorescence unit (RFU)) and fluorescence visualization of the three targets may be difficult.

3 Pharmacological assays

The initial characterization of the ligand's biological activity started with the determination of its affinity at the molecular targets. In the next step, some off-target activities were also investigated to establish the selectivity profile. In our study, ligand-receptor binding experiments and substrate-enzyme kinetic reactions were performed for GPCRs and MAO enzymes, respectively.[201] Subsequently, *in vivo* testing of $H_3R/A_1R/A_{2A}R$ derivatives were performed.

The determination of the binding affinities at the different histamine and dopamine receptors was carried out in our work group by Johannes Stephan Schwed, Stefanie Hagenow, Annika Frank and Kathrin Grau. The evaluation of MAOs inhibition was performed by Stefanie Hagenow, whereas the co-operation with Prof. Dr. Christa E. Müller and co-workers (Bonn University, Department of Pharmaceutical Chemistry, Bonn, Germany) determined the binding affinities at the various adenosine receptors. Regarding the *in vivo* testing, the antidyskinetic effect of the selected $H_3R/A_1R/A_{2A}R$ substances was determined in cooperation with Dr. Gregory Porras and Dr. Elsa Pioli from the working group of Prof. Erwan Bézard at the Bordeaux University, Department of Neurodegenerative diseases, Bordeaux, France. Sleep-wake EEG studies were performed by Dr. Jan-Scheng Lin and coworkers (Faculty of medicine, Neuroscience Research Center Lyon, France).

3.1 *In vitro* affinity

According to T. Kenakin, the affinity of a ligand is a measure of how tightly the test substance binds to its biological target[202] and, as stated in IUPAC, for pharmacological receptors it can be thought of as the frequency with which the drug, when brought into the proximity of a receptor by diffusion, will reside at a position of minimum free energy within the force field of that receptor.[203,204]

The test substance's affinity at the receptors was evaluated by determination of the IC_{50} and calculation of the K_i values, whereas the inhibitory potency of the enzymes was established by IC_{50} determination. The IC_{50} value is the concentration of test substance needed to displace 50% of specifically bound labelled ligand or substrate and can be directly determined from the concentration-response curve. Afterwards, the Cheng-Prusoff equation can be used to determine dissociation binding constants for the test substances (Equation 1 and 2).

$$K_i = \frac{IC_{50}}{1 + \frac{[L]}{K_d}} \quad (1) \qquad K_i = \frac{IC_{50}}{1 + \frac{[S]}{K_m}} \quad (2)$$

Equation 1 and 2. CHENG-PRUSOFF equation for receptor (1) or enzyme (2).[205]

IC_{50} = half-maximal binding concentration of test unlabelled ligand or inhibitor; K_i = inhibitory constant of unlabelled ligand or inhibitor; [L] and K_d describe the concentration and equilibrium binding constant of the labelled ligand; [S] and K_m describe the concentration and Michaelis-Menten constant of the substrate.

Table 4 shows a summary of the test models used for displacement assays on different receptors for compounds **1-16**. Tritium labelled radioligands were used as reference ligands to be quantified by liquid scintillation counting.

Table 4. Displacement assay systems used for affinity and selectivity determination at GPCRs.

Receptor construct	Cells	Radioligand	Reference compounds	Reference
Histamine				
hH_1R	CHO	[^{3}H]Pyrilamine	Chlorpheniramine	[206]
hH_3R	HEK-293	[^{3}H]N_α-Methyl-histamine	Pitolisant	[207–210]
hH_4R + $G\alpha_{i/o}$ + $G\beta_1\gamma_2$	Sf9	[^{3}H]Histamine	JNJ-7777120	[204,207,211]
Dopamine				
hD_1R	HEK-293	[^{3}H]SCH23390	Fluphenazin	[212]
hD_5R	HEK-293	[^{3}H]SCH23390	Fluphenazin	[212]
$hD_{2s}R$	CHO	[^{3}H]Spiperon	Haloperidol	[213]
hD_3R	CHO	[^{3}H]Spiperon	Haloperidol	[213]
Adenosine				
hA_1R	CHO	[^{3}H]CCPA	2-Chloroadenosine	[214]
$hA_{2A}R$	CHO	[^{3}H]MSX-2	5′-(*N*-Ethylcarboxamido)adenosine	[215]
hA_3R	CHO	[^{3}H]PSB-11	(*R*)-N^6-Phenylisopropyladenosine	[216]
$hA_{2B}R$	CHO	[^{3}H]ZM-241385	8-Cyclopentyl-1,3-dipropylxanthine	[217]

Briefly, the cell membranes (i.e. Sf9, CHO-K1, HEK-293) expressing the respective human receptor were isolated. Membrane preparations were incubated with a defined amount of radioligand and an increasing concentration of the test substance. The resulting complex between the radioligand and the receptor was separated by filtration and radioactivity was measured by scintillation counting.[218,219]

For assaying potential monoamine oxidase MAO A and MAO B inhibition, compounds of series **1** and **2** as well as derivatives **3a**-**3c** were included in one pot-screening for both isoforms predominantly using a continuous spectrophotometric method as described previously, whereas for compounds **3d**, **3e**, **3f** and **4** a discontinuous fluorimetric assay was used. The IC_{50} curves were determined in the discontinuous fluorimetric assay, which allows higher assay sensitivity as well as time and costs savings.[67,220]

In both methods, the recombinant membrane-bound MAO A and MAO B were incubated with a defined amount of substrate and an increasing concentration of the test substance. The MAO A and MAO B catalytic activities were measured by using the MAO A/B mixed substrate kynuramine and measuring the MAO-catalyzed formation of 4-hydroxyquinoline, which forms after MAO-catalyzed amination and subsequent ring closure.

Using fluorescence spectrophotometry, the formation of 6-hydroxyquinoline (λ_{ex}=320 nm, λ_{em}= 405 nm) can be readily measured in the presence of the test substance since the 1-indanone derivatives do not emit measurable fluorescence under these assay conditions.

Using a continuous spectrometric method, enzyme activity was measured by spectrophotometrical observation of 4-hydroxyquinoline (λ_{em}= 320 nm) formation over time.

3.2 *In vivo* activity

In vivo activity of compounds **6**, **10** and **12** was evaluated in the 6-OHDA-lesioned rat model of LID. Figure 25 shows the experimental design used for tested MTLs in 6-OHDA-lesionated rats model of LID.

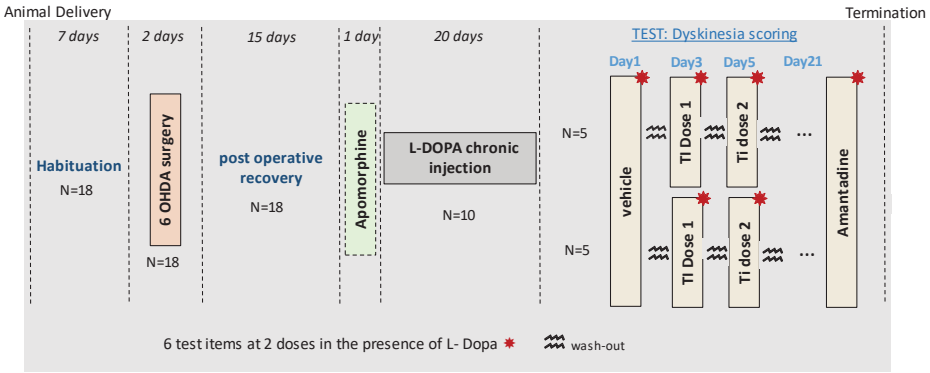

Figure 25. Experimental design for 6-OHDA-lesioned rat model of LID. Dose 1: 0.1 mg/kg; dose 2: 1 mg/kg; L-DOPA: 6 mg/kg; amantadine: 40 mg/kg; TI: test item; N: number of experiments; wash-out period: 48 h.

To produce neurodegeneration of midbrain dopaminergic neurons in the pars compacta of the substantia nigra, rats received a unilateral 6-OHDA injection in the medial forebrain by stereotactic delivery. Shortly, 6-OHDA is transported via the dopamine transporter inside the dopaminergic neurons.[221,222] Degeneration starts with the development of reactive oxygen species causing mainly reduction of total glutathione and impairment of complex I and IV of the electron transport chain, leading to mitochondrial respiration inhibition and oxidative stress.[223]

The loss of DA neurons in the injection side produces an imbalance in DA activity in the two sides of the brain causing asymmetry in motor behavior, that can be increased by DA agonists. Therefore, to assess the extent of the lesion, the DA agonist apomorphine was administrated at two weeks post-lesion and contralateral rotations (opposite to the lesion side) were measured.

Animals showing more than 6 full body turns/min contralateral to the lesion side were treated with L-DOPA for other three weeks to have a stable level of abnormal involuntary movements (AIMs). Rat AIMs were divided into four groups, based on stereotypic behavior: Axial AIMs (dystonic postures or choreiform twisting of the neck and upper body towards the contralateral side), limb AIMs (abnormal movements of the forelimb contralateral to the lesion), orolingual AIMs (jaw movements and contralateral tongue protrusion) and locomotive AIMs (increased locomotion contraversive to the lesion) (Figure 26).[127,224,225]

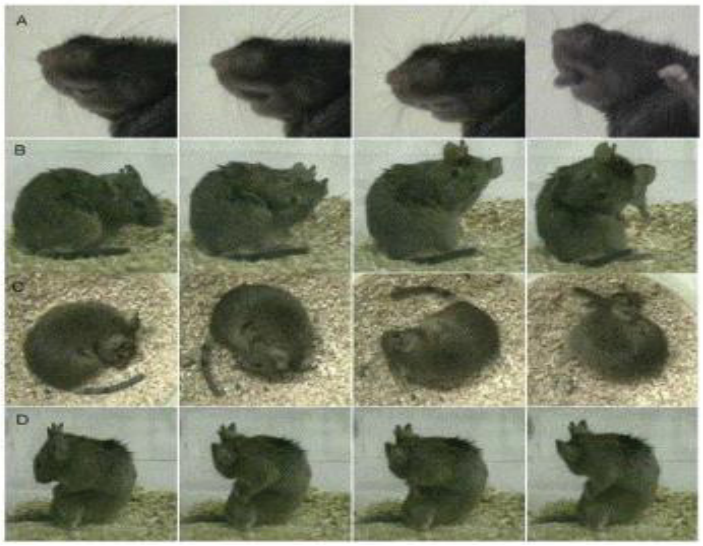

Figure 26. Rats showing the four sub-types AIMs.[226] A: orolingual AIMs; B: limb AIMs; C: locomotive AIMs; D: axial AIMs.

After that, L-DOPA alone or in combination either with the reference amantadine or selected $H_3R/A_1R/A_{2A}R$ ligands was administrated per injection (p.i.) over a period of 120 min.

Sleep-wake studies in mice were performed with compound **12**. Neocortical and hippocampal electroencephalograms (EEGs), neck muscle activity [electromyogram (EMG)], and heart rate [electrocardiogram (EKG)] were recorded. During the experiments the effect of compound **12** on sleep–waking cycles, consisting of W (wakefulness), slow– wave sleep (SWS), and paradoxical [or rapid eye movement (REM)] sleep (PS) were evaluated.[62]

4 Design of dual targeting ligands at H_3R/MAO B

In our study, H_3R inverse agonists/antagonists and MAO B inhibitors were combined for the synthesis of one of the first dual H_3R/MAO B combination.

The well-established piperidine- or pyrrolidine(alkyloxy)phenyl H_3R pharmacophore was attached to already described (2-benzylidene-)indanone MAO B inhibitor scaffolds at different positions (Figure 27).

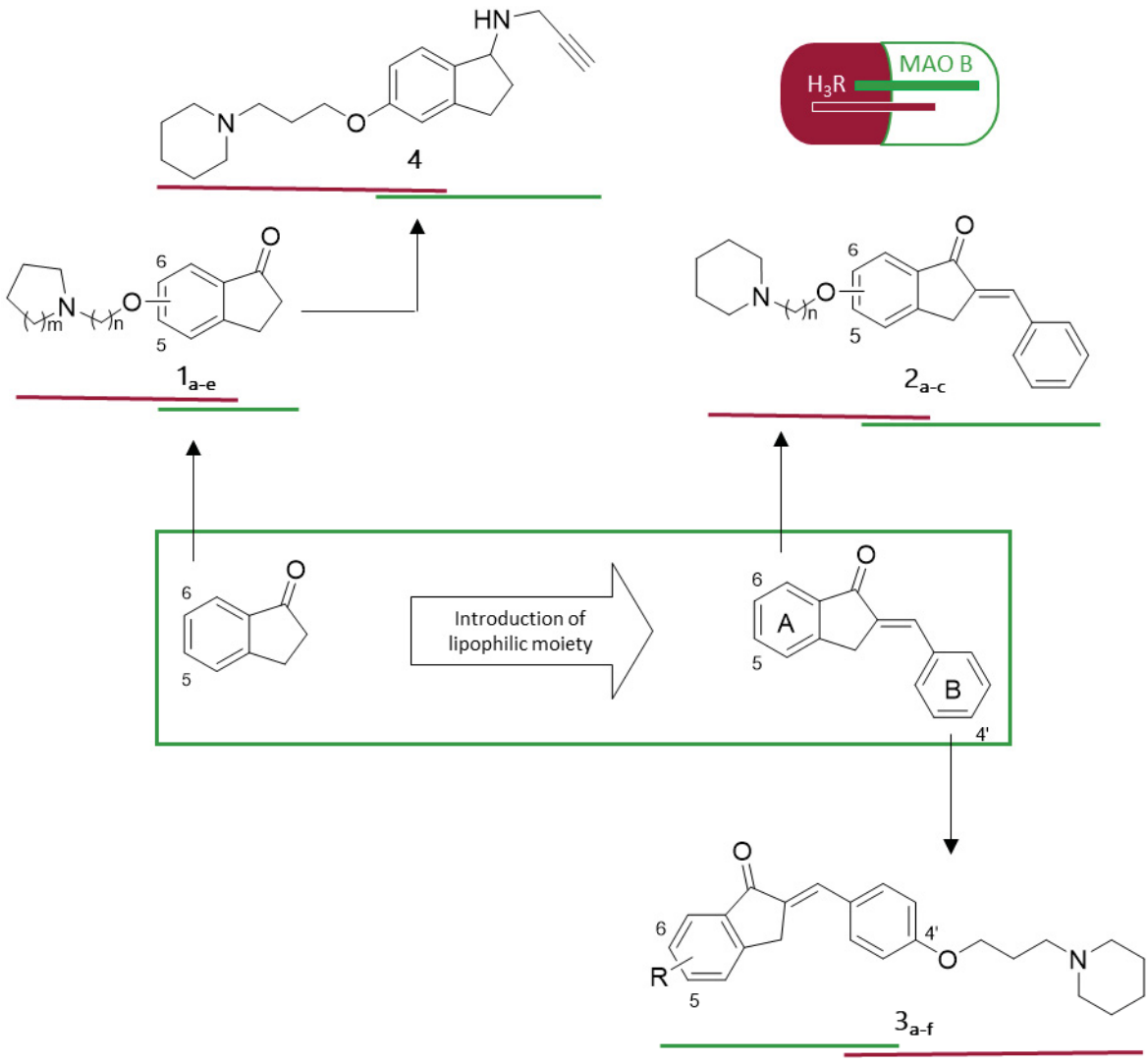

Figure 27. Development concept of dual H_3R/MAO B ligands.

Considering a set of 1-indanone compounds, where product **I** was one of the most potent reversible MAO B inhibitors (chapter 1.5), the first series of H_3R/MAO B DTLs was synthesized by attachment

of the H_3R motif to the 5- or 6-position of an indanone core structure. Variations in the alkyl chain length between the aromatic core and the amine as well as in the size of the aliphatic heterocycle (piperidino or pyrrolidino group) were performed to synthetize compounds **1a-e**. The reductive amination of compound **1e** led also to the synthesis of derivative **4**, bearing a propargylamine group as the potent MAO B inhibitor rasagiline.

A second series of compounds was obtained by introduction of a lipophilic moiety, linking a benzylidene fragment to the central 1-indanone core (**2a-c**). This pharmacophore was already successful for several MAO B inhibitors, where the best and most MAO B selective compound was **II** (chapter 1.5). Within this series (**2a-c**), the H_3R pharmacophore was introduced either in 5- or 6-position.

Additionally, a third class of compounds (**3a-f**) was received by connecting the H_3R pharmacophore to the benzylidene ring B at the 4´-position, while ring A was substituted in 5- and 6-position (Figure 27).

4.1 Pharmacological characterization of novel indanone derivatives

Recently, moderate MAO A and MAO B inhibition of the highly potent H_3R antagonist ciproxifan was discovered (MAO B, IC_{50} = 2.1 µM; MAO A, IC_{50} = 11 µM).[67]

The imidazole moiety may cause drawbacks; thus, the five-member ring was replaced with the *N*-containing heterocycle piperidine, preserving the general accepted aminoalkyloxypropyl H_3R pharmacophore (UCL2190). The latter compound was synthetized in our laboratory and comparing its biological activity to that of ciproxifan, UCL2190 showed 30-fold higher hH_3R affinity (K_i = 11 nM), and a better selectivity profile (MAO B, IC_{50} =3.9 µM; no activity at MAO A (IC_{50} > 50 µM)). Therefore, UCL2190 was used as lead structure for the synthesis of dual H_3R/MAO B ligands.

Designed H_3R/MAO B DTLs were evaluated for *in vitro* binding affinities in radioligand depletion studies as described previously by using hH_3R.[168,207] Additionally, the synthetized ligands were included in one-point screenings for both isoforms to assess potential MAO a and MAO B inhibition. These studies were performed using a continuous spectrophotometric method except for compounds **3d-3f**, where a discontinuous fluorimetric assay was used.

Within the first class of 1-indanone derivatives (**1a-e**) a great loss of hH_3R affinity compared to UCL2190 was found, most probably due to the lack of a lipophilic group in the eastern part of the molecule. For these compounds only slight hH_3R affinity was obtained, while compound **1e** showed highest affinity with a hH_3R K_i value of 159 nM (Table 5).

Table 5. H_3R and MAO B screening data for the synthesis of DTLs **1a-e.**

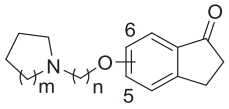

Compound	Pos.	n	m	K_i [nM] [95% CI] hH_3R[a]	% Inhibition at 10 µM[b] [±SD] MAO A	MAO B
1a	6	2	1	6118 [3129, 11963]	21.9 [±11.9]	46.0 [±12.9]
1b	6	3	2	304 [122, 758]	12.1 [±9.4]	71.9 [±4.3]
1c	5	2	1	345 [103, 1148]	37.2 [±9.3]	24.7 [±10.5]
1d	5	2	2	205 [81, 520]	23.8 [±15.1]	34.6 [±13.9]
1e	5	3	2	159 [37, 678]	8.5 [±2.9]	34.5 [±9.0]

[a] H_3R screening: [^{3}H] N^{α}-Methylhistamine binding assay, K_i values for the hH_3R are given as mean within the 95% confidence interval (CI).
[b] MAO_s inhibition was calculated as percentages related to control at a test concentration of 10 µM and given as mean ± SD, spectrophotometric MAO_s screening using kynuramine as substrate.

Variations of linker lengths (ethyl or propyl) and basic moieties (pyrrolidine or piperidine), or either 5- or 6-attachment seems to have a significant impact on hH_3R affinity. A preference of a piperidinepropyl linker compared to pyrrolidinoethyl linker could be seen for 5- and 6-substituted 1-indanones (**1a** vs. **1b** and **1c** vs. **1e**, respectively). Also, 5-substituted derivatives showed better affinity at the hH_3R (**1c** vs. **1a** and **1e** vs. **1b**) For both MAO isoforms most of these compounds exhibited inhibition potency < 50% at 10 µM, while only for compound **1b** moderately inhibition for MAO B of 71.9 ± 4.3% was found. Concerning MAO B inhibition, the substitution in 6-position might be preferred, while the best compound **1b** contains also a piperidinopropyl fragment.

Based on a literature report that 2-benzylidene-1-indanones are MAO B specific-inhibitors showing IC_{50} values lower than 0.1 µM, we decided to investigate these compounds for optimizing the hH_3R and MAO B combination (**2a-c**) (Table 6).[169]

Within this series two compounds showed improved hH_3R affinity, while highest affinity could be shown for **2c** (hH_3R K_i = 3.9 nM). All second series 2-benzylidene-1-indanones did not showed MAO A inhibition at 10 µM, while MAO B inhibition was more promising compared to that of series one (**1a-e**) with 61.5 ± 9.7%, 68.2 ± 12.9% and 81.1 ± 4.5% for **2b**, **2c** and **2a**, respectively. In case of 5-substituted derivatives a propyl instead of ethyl linker led to more than 10-fold higher hH_3R affinity, while MAO B inhibition potency was decreased at the same time (**2a** vs. **2c**).

Table 6. H_3R and MAO B screening data for the synthesis of DTLs **2a-c.**

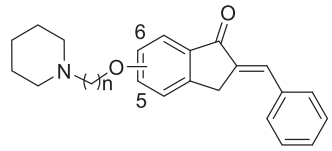

Compound	Pos.	n	K_i [nM] [95% CI] hH_3R[a]	% Inhibition at 10 µM[b] [±SD] MAO A	MAO B
2a	5	2	696 [302, 1605]	19.0 [±7.3]	81.1 [±4.5]
2b	6	3	39 [8.9, 169]	14.1 [±12.5]	61.5 [±9.7]
2c	5	3	3.9 [0.6, 26]	8.9 [±2.2]	68.2 [±12.9]

[a] H_3R screening: [^{3}H] N^{α}-Methylhistamine binding assay, K_i values for the hH_3R are given as mean within the 95% confidence interval (CI); [b] MAO_s inhibition was calculated as percentages related to control at a test concentration of 10 µM and given as mean ± SD, spectrophotometric MAO_s screening using kynuramine as substrate.

Thus, as it could be previously shown, that substitution of the benzylidene moiety in the 4'- position with lipophilic groups (e.g. halogens or alkyl chains) or basic/polar moieties (e.g. tertiary amines) is tolerated by MAO B, in the series three DTLs (**3a-f**) the H_3R pharmacophore was attached in 4'-position of the benzylidene (Table 7).[169]

Derivatives **3a-f** showed high nanomolar hH_3R affinity (K_i = 2.1-33 nM), while highest affinity could be obtained for compound **3a** (K_i = 2.1 nM) and fluoro-substituted derivative **3d** (K_i = 2.2 nM). For MAO B these compounds showed inhibition capability > 60%, while highest, mostly complete inhibition was found for the fluoro-substituted derivative (**3d**: 94 ± 8.7%). In the studies of Nel et al. substitution of the 5-position with a methoxy group revealed the most promising highly selective 2-benzylidene-1-indanone MAO B inhibitor (MAO B IC_{50} = 9.2 nM, selectivity index (SI) > 10 000).[169] In case of the synthetized DTLs, the methoxy-substituted derivatives (**3b** and **3c**) showed about 10-fold lower, but still acceptable hH_3R affinity, while MAO B inhibition potency is slightly increased (**3b**: 67.6 ± 5.7%, **3c**: 71.2 ± 1.5%) compared to non-substituted compound **3a** (61.3 ± 1.5%).

In case of already described MAO inhibitors, introducing a 4-bromophenyl-methyloxy group at the 5- and 6-position of 1-indanones led potent, slightly MAO B preferring inhibition, while introduction at 6-position revealed about 10-fold lower IC_{50} values (MAO B IC_{50} = 3.0 nM, SI = 13) with comparable preference to 5-substituted inhibitors. Same substitution pattern with our dual targeting compounds resulted in potent MAO B inhibition (**3d**: 93.9%, **3e**: 63.7 ± 6.5%, **3f**: 86.8 ± 3.8%) at 10

µM, 2 µM and 5 µM for **3d**, **3e** and **3f**, respectively, where **3d** showed higher hH_3R affinity (K_i = 10 nM) within these three compounds.

Table 7. H_3R and MAO B screening data for the synthesis of DTLs **3a-f**.

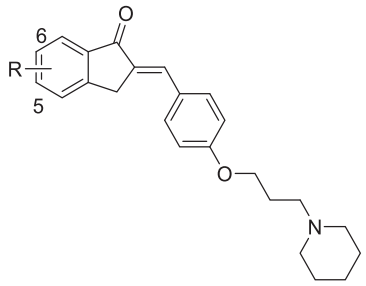

Compound	Pos.	R	K_i [nM] [95% CI] hH_3R[a]	% Inhibition at 10 µM[b] [±SD] MAO A	MAO B
3a		-H	2.1 [0.5, 10]	12.0 [±6.6]	61.3 [±1.5]
3b	6	$-OCH_3$	11 [3.5, 38]	58.3 [±13.6]	67.6 [±5.7]
3c	5	$-OCH_3$	33 [12, 89]	10.5 [±13.5]	71.2 [±1.5]
3d	5	-F	2.2 [0.6, 8.1]	61 [±12.5][c]	93.9 [±8.7][c]
3e	6	$-OCH_2$-Ph-4-Br	32 [13, 81]	38 [±9.4][c]	63.7 [±6.5][c]
3f	5	$-OCH_2$-Ph-4-Br	6.5 [1.5, 29]	40 [±8.6][c]	86.8 [±3.8][c]

[a] H_3R screening: [^{3}H] N^{α}-Methylhistamine binding assay, K_i values for the hH_3R are given as mean within the 95% confidence interval (CI); [b] MAO_s inhibition was calculated as percentages related to control at a test concentration of 10 µM and given as ± SD, spectrophotometric MAO_s screening using kynuramine as substrate. [c] fluorimetric assay with a test concentration of 10, 2 and 5 µM for 3d, 3e and 3f, respectively; ph = phenyl.

Regarding MAO inhibition, substitution of 6-position might result in more balanced MAO inhibition profile as could be shown for methoxy- and 4-bromophenyl-methyloxy-substituted compounds (**3b** vs. **3c** and **3e** vs. **3f**, respectively). Thus, substitution of the 5-position should be favored in case of synthesizing MAO selective dual targeting hH_3R/MAO B ligands.

Compounds **3d**, **3e** and **3f**, showing the highest inhibition at MAO B and K_i values for hH_3R in the low nanomolar range, were further characterized in IC_{50} studies for both isoforms (Table 8).

The IC_{50} values were determined in the discontinuous fluorimetric assay, allowing higher assay sensitivity as well as time and cost saving compared to the continuous spectrophotometric method.

All three compounds showed IC_{50} values in low micromolar to nanomolar concentration ranges, suggesting a general improvement of dual targeting properties compared to UCL2190 but not to safinamide (Table 8).

Table 8. Compared IC_{50} values on MAOs (with and without preincubation) for compounds **3d**, **3e**, **3f** and reference compounds.

Compounds	K_i [nM] [95% CI][a]	Pre-incubation 37°C [min]	IC_{50} [nM] [95% CI] (n)[b]		MAO SI[c]
	hH_3R		MAO A	MAO B	
3d 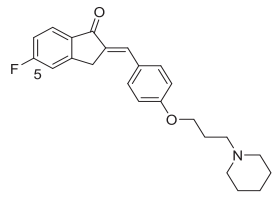	2.2 [0.6, 8.1]	0	9178 [4169, 20207] (4)	1931 [926, 4025] (4)	4.8
		30		541 [362, 807] (5)	
3e 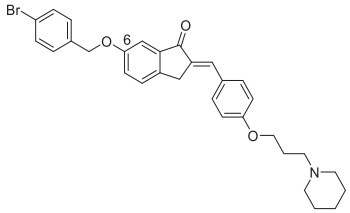	32 [13, 81]	0	5514 [3567, 8522] (7)	1455 [840, 2522] (4)	3.7
		30		232 [70, 769] (5)	
3f 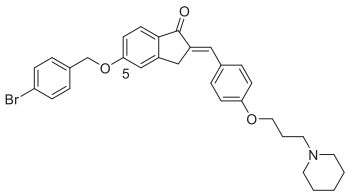	6.5 [1.5, 29]	0	>10 000 (3)	276 [197, 385] (6)	>36
		30		262 [185, 372] (5)	
UCL2190 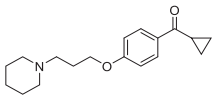	11 [3.5, 33]	0	>50 000 (3)	3884 [1816, 8311] (3)	>12
Safinamide 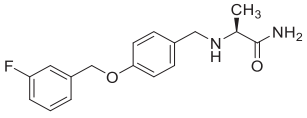		0	>50 000 (4)	53 [20, 141] (4)	>940
		30		21 [13, 33] (4)	

[a] H_3R screening: [^{3}H] N^{α}-Methylhistamine binding assay, K_i values for the hH_3R are given as mean within the 95% confidence interval (CI); [b] IC_{50} values for MAO_s, respectively, are given as mean within the 95% confidence interval (CI) of n independent experiments each performed at least in duplicates, fluorimetric IC_{50} determination (test concentration 10 µM) using kynuramine as substrate; [c] Selectivity index (SI) = IC_{50} (MAO A)/ IC_{50} (MAO B); n = number of experiments.

Both 4-bromophenylmethyloxy-substituted compounds showed best IC_{50} values for MAO B (**3e**: IC_{50} = 1455 nM, **3f**: IC_{50} = 276 nM) within the series and the 5-substituted analogue **3f** revealed much higher preference (SI > 36) for the B isoform (Figure 28).

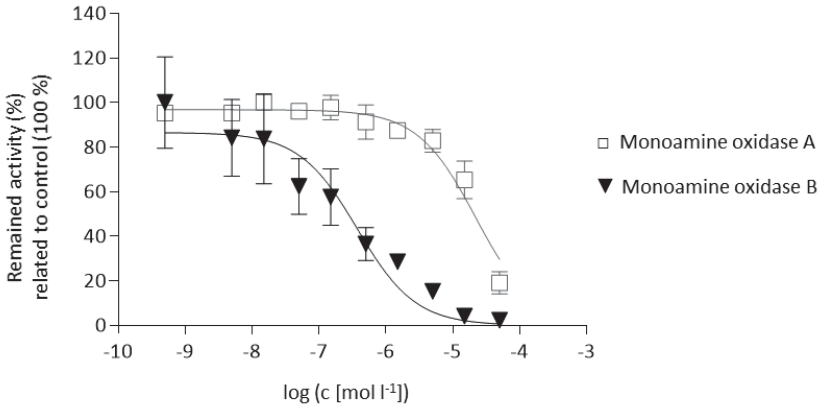

Figure 28. Monoamine oxidase A and B incubation curves of compound **3f**.

Data are given as mean (normalized to control) ± standard deviation (SD) of one representative experiment. n= 2.

The side chain of Phe-208, in MAO A, may restrict the binding of larger inhibitors.[170] In MAO B the residue that corresponds to Phe-208 is Ile-199. In contrast to Phe-208, the side chain of Ile-199 may rotate from the active side cavity, allowing for larger inhibitors to traverse both entrance and substrate cavities.[170] Some larger inhibitors are thus better accommodated in MAO-B than MAO-A leading to specific inhibition of the MAO-B isoform. This analysis may explain the MAO-B specificities of 2-benzylidiene-1-indanone derivatives.[169]

MAO B inhibitors could be classified in reversible or reversible because of the different interactions between the inhibitors and the enzyme. Therefore, to determine the mode and time dependency of inhibition two setups were performed for compounds **3d**, **3e** and **3f**. At first, preincubation experiments (30 min, 37 °C) were performed to elucidate the influence on the IC_{50} values.

Interestingly, within the third series of compounds, only for derivative **3f** the IC_{50} value do not show significant difference to non-preincubated ones (276 nM vs. 262 nM) (Table 8). In contrast, for compounds **3d** and **3e** a 3.5-fold and 6.3-fold shift of IC_{50} from 1931 nM to 541 nM and from 1455 nM to 232 nM respectively, after 30 min incubation was shown, suggesting a slow reversible or tight binding inhibition mode within the test conditions. Tight binding inhibitors which do not form covalent bonds with the active site can behave similar to typical covalent binding "suicide inhibitors" like *L*-Deprenyl in reversibility studies. *In vivo* they might have a safer pharmacological profile with longer duration times than reversible inhibitors, but lacking the suicide inactivation of MAOs. [82,168,228]

The second experiment was performed by adding excess of substrate after incubation of the enzyme with the inhibitors for 0, 30 and 60 min (Figure 29).

Under these conditions, all three 2-benzylidene-1-indanone derivatives revealed a reversible mode of inhibition, as no significant reduction of enzyme activity was seen after even 60 minutes of pre-incubation. Comparable findings were obtained from structural related (*E*)-3-heteroarylidenechroman-4-ones and (*E*)-3-benzylidenechroman-4-ones, confirming the obtained results.[229]

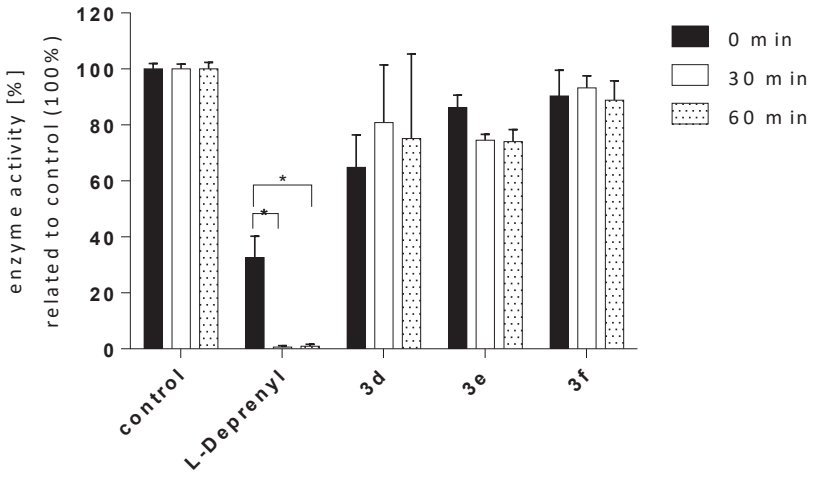

Figure 29. Reversibility of inhibition after preincubation of MAO B and inhibitors for 0, 30 and 60 min, measured under saturated substrate assay conditions.

Data are given as mean (normalized to each control) ± standard deviation (SD) of at least two independent experiments, each performed in duplicates (global fit). *p < 0.001 (ANOVA, multiple comparison).

However, as they do not inactivate the enzyme, reversible MAO inhibitors need higher target affinities to compete with endogenous ligands.

In search for irreversible MAO B ligands, the close structural relationship of first series of H_3R/MAO B ligands (**1a-e**) with propargylamine derivatives such as rasagiline and ladostigil became clear. Thus, compound **1e**, showing best hH_3R K_i value in the nanomolar range, was merged with the rasagiline pharmacophore to develop one propargylamine H_3R/MAO B ligand. Compared to the 1-indanone derivative,**1e**, the hH_3R affinity considerably improved (Table 9). The K_i value in the low nanomolar concentration range was obtained probably due to the presence of a second basic moiety in the eastern part of the molecule. In addition, inhibitory potency at MAO B was also enhanced from 34.5 ± 0.9 % (**1e**) to 92 ± 1.2 % (**4**) without effecting the binding properties toward MAO A.

Table 9. MAOs IC_{50} values for dual H_3R /MAO B ligand **4** and reference compound rasagiline.

Compound	K_i [nM] [95% CI]	IC_{50} [nM] [95% CI] (n)[b]		MAO SI[f]
	hH_3R[a]	MAO A	MAO B	
4 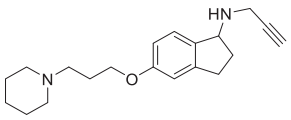	2.5 [1.3, 5.2]	>100000 (3)	1736 [647-4859] (4)	> 50
Rasagiline 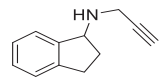		710[c,e] [±93]	14[c,e] [±3.5]	> 50
***L*-Deprenyl** 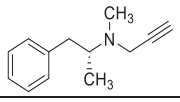		29600[d,e] [±3.9]	37[d,e] [±0.0004]	800

[a] H_3R screening: [^{3}H] N^{α}-Methylhistamine binding assay, K_i values for the hH_3R are given as mean within the 95% confidence interval (CI); [b] IC_{50} values for MAO_s, respectively, are given as mean within the 95% confidence interval (CI) of n independent experiments each performed at least in duplicates, fluorimetric IC_{50} determination (test concentration 10 µM) using kynuramine as substrate; [c] values published in[230]; [d] values published in [67]; [e] IC_{50} values for both isoforms is means ± standard errors of means (s.e.m.); [f] selectivity index (SI) = IC_{50} MAO A/ IC_{50} MAO B.

As compound **4** showed high inhibition at MAO B (92 ± 1.2 %: MAOs inhibition was calculated as percentage related to control at a test concentration of 10 µM and given as mean ± SD, spectrophotometric MAOs screening using kynuramine as a substrate) IC_{50} values for both MAO isoforms were determined. The propargyl amine derivative showed moderate inhibitory potency for MAO B as well as good selectivity profile over MAO A (SI > 58).

The irreversible mode of inhibition was confirmed by dilution experiments under saturated substrate conditions (Figure 30). After 60 minutes a significant reduction of enzyme activity was seen. However, compared to *L*-Deprenyl, a potent irreversible MAO B inhibitor, the binding rate to the enzyme active sites of compound **4** was slower as the reference compound could significantly decrease the enzyme activity after 0 min of preincubation.

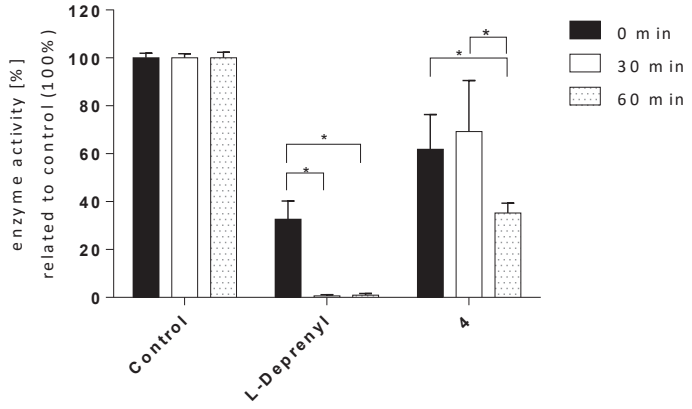

Figure 30. Irreversibility of inhibition after preincubation of MAO B and compound **4** for 0, 30 and 60 min, measured under saturated substrate assay conditions.

Data are given as mean ± standard deviation (SD) of two independent experiments, each performed in duplicates (global fit). *p < 0.001 (ANOVA, multiple comparison).

With the aim of developing CNS drugs, the ability of compounds to cross the blood-brain barrier (BBB) is very important.[231] To cross the BBB, molecules should meet the limiting terms of Lipinski's rules. Lipinski's rule addresses the issue of pharmacokinetics by simplifying it drastically and reducing it to two concepts only: absorption (better absorbed if small) and permeation (better membrane crossing if not too hydrophilic). A poor absorption and permeation is to be expected for substances having the calculated logarithm of the octanol-water partition coefficient, clogP, greater than 5, a molecular weight higher than 500 and more than 5 hydrogen bond donors and 10 hydrogen acceptors. In addition to the molecular properties discussed by Lipinski, the polar surface area, which is defined as sum of surfaces of oxygens, nitrogens and attached hydrogens, were calculated in regard to oral bioavailability.[232,233]

Moreover, to evaluate the quality of drug-target interactions, Kunz et al. introduced the simple but often useful "ligand efficacy" (LE) to relate affinity to heavy atoms (HA). Another parameter is named "ligand efficiency dependent lipophilicity" (LELP), which is determined dividing clogP for LE. For the synthesized ligands, the logP values were calculated with the Marvin Sketch software and proposed acceptable values for lead discovery are LE ≥ 0.3 and -10 < LELP < +10.[227]

BBB permeability properties as well as drug-like physiochemical parameters were calculated for best 2-benzylidene-1-ndanone compounds **3f**, **3e**, **3f** and the propargyl amine derivative **4** (Table 10).

Regarding the reversible ligand **3d**, possessing an electron-withdrawing element, satisfied Lipinski's rules, except for clogP, and showed good LE values for both targets. Substitution of fluoride with the more lipophilic benzylic group, allowed the synthesis of compounds **3e** and **3f**, which showed

improved MAO B affinity but at the cost of LE due to the higher molecular weight (higher than 500 g/mol).[168] While these DTLs can be used as pharmacological tools, further lead optimization is necessary to obtain candidates with promising drug-likeness for both targets simultaneously.

Promising results were obtained for the irreversible ligand **4**, which does not violet Lipinski's rule, as all calculated descriptors and properties were within the expected thresholds. In addition, the combination of low molecular weight and good hH_3R and MAO B affinity, positively influenced the values of LE for both targets, which were found in optimal range. Only the calculated LELP value for MAO B was not as good as the one of rasagiline being slightly out of the optimal range (LELP > 10).

Table 10. Evaluation of Lipinski's rules and metric parameters for best dual H_3R/MAO B ligands.

Comp.	Lipinski's rules					H_3R		MAO B	
	HB donors	HB acceptors	M [g/mol]	clogP[a]	PSA[b] (Å^2)	LE[c]	LELP[d]	LE[c]	LELP[d]
3d	0	3	379.4	6.2	24.5	0.4	11.3	0.3	17.2
3e	0	4	546.5	7.1	24.2	0.3	24.5	0.2	31.4
3f	0	4	546.5	7.1	24.2	0.3	22.4	0.3	27.9
UCL2190	0	3	287.1	3.8	25.3	0.5	7.2	0.4	10.6
Safinamide	1	3	302.3	2.1	52.5			0.5	4.49
4	1	3	312.2	4.8	23.5	0.5	9.3	0.3	13.9
Rasagiline	1	1	171.1	2.5	12.4			0.8	3.1
L-Deprenyl	0	1	187.1	2.7	3.4			0.7	3.8
Rules	≤5	≤10	≤500	≤5	≤140	LE ≥ 3; -10 ≤ LELP ≤ +10			

[a] Calculation with Marvin Sketch; [b] Calculation with Molsoft; [c] hH_3R: LE = pK_i/HA (heavy atoms), [c] MAO B: LE = pIC_{50}/HA; [d] LELP = clogP/LE; HB= hydrogen bond; M= molecular weight; PSA= polar surface area. Green (values in the optimal range), orange (values slightly out of optimal range), red (values out of optimal range).

4.2 Conclusions – dual H_3R/MAO B ligands

The fact, that two targets, the H_3R receptor on the one hand and MAOs on the other hand, are capable of modulating neurotransmitter levels in the CNS encouraged us to design dual-targeting H_3R/MAO ligands as possible approach for treatment of neurological diseases. Exemplified for PD therapy, H_3R/MAO B ligands might show some synergistic effects improving the dopamine deficiency in the substantia nigra. Thus, the design of a novel class of dual targeting H_3R/MAO B ligands by combining pharmacophoric elements already described for both targets was performed. The introduction of the piperidine- or pyrrolidine(alkyloxy)phenyl H_3R pharmacophore to (2-benzylidene)indanones led to the synthesis of three series of compounds. The introduction of the

lipophilic benzylidene group led to the design of most promising 2-benzylidene-1-indanones. The most potent compounds, **3d-3f**, showing low nanomolar affinities at the hH_3R (K_i = 2.2 – 32 nM) and MAO B preferring inhibitory properties (IC_{50} = 276 – 1931 nM), were obtained by attaching the H_3R pharmacophore to the eastern part of the 2-benzylidene-1-indanone, substituted either with the electron-withdrawing halogen fluoride (**3d**) or a bulky, lipophilic element in 6- (**3e**) and 5-position (**3f**), respectively.

This substitution pattern clearly influenced MAO isoform selectivity. The 5-substituted derivative **3f** was the most potent and selective MAO B inhibitor (SI > 36), while 5- and 6-substituted compounds **3d** and **3e**, provided more balanced profile (SI= 4.8 and 3.7, respectively). Reversible mode of inhibition was shown for all three compounds, although compounds **3d** and **3e** may have a slow reversible or tight inhibition mode due to shift of IC_{50} values to nanomolar concentrations in IC_{50} shift experiments. For reversible MAO B inhibitors there is a higher necessity for affinity in nanomolar concentration ranges, since they have to compete with the endogenous ligands.[234] Therefore, regarding describing dual targeting H_3R/MAO B ligands, showing moderate IC_{50} values and low selectivity over MAO A, except for **3e**, this issue has to be address by further improving MAO B inhibitory potency and selectivity over MAO A.

Interestingly, 2-benzylidene-1-indanones similar to our class three compounds, showed inhibitory activity *in vitro* towards cholinesterase, suggesting a potential AChE/BuChE inhibition potency for the synthetized dual targeting H_3R/MAO ligands.[187] Finding some additional AChE/BuChE inhibition properties, however, might be beneficial to design H_3R/MAO B/AChE/BuChE MTLs, were several H_3R/AChE/BuChE MTLs are described and discussed especially for treatment of cognitive impairments or AD. [163,168,187,235]

Searching for candidates with optimal drug-likeness for both targets, compound **3d** showed more promising parameters compared to those of derivatives **3e** and **3f**.

As proof-of-concept, the combination of the G-protein coupled receptor affinity and the enzyme inhibitory potency led to the synthesis of H_3R/MAO B DTLs showing a promising pharmacological profile. However, lower molecular weight and less lipophilic ligands would improve physiochemical properties and drug-likeness.

Considering the structural similarity between first class of 1-indanone derivatives and the irreversible MAO B rasagiline or the more recently discovered ladostigil, the synthesis of a new compound, containing a propargylamine instead of a carbonyl moiety, was performed. A promising dual H_3R/MAO B ligand, compound **4**, which displays hH_3R affinity in the low nanomolar range (K_i = 2.5

nM) and good selectivity profile for MAO B was synthetized. The propargylamine derivative had an irreversible mode of inhibition due to a time-dependent reduction of MAO B activity. Since the enzyme is deactivated, IC_{50} values in the nanomolar range are not needed, overcoming one of the main issues encountered for the design of 2-benzylidene-1-indanone DTLs. Compared to the MTL ladostigil, DTL **4** increased the inhibitory potency at MAO B of almost two orders of magnitude suggesting an improvement of MAO B inhibition when the H_3R pharmacophore is introduced in 5-position.

Comparing to the dual target H_3R/MAO B UCL-2190 or recently discovered contilisant,[163] the synthetized compounds (**1a-e**, **2a-c**, **3a-e** and **4**) show improved inhibition at MAO B with reversible and irreversible binding, having comparable H_3R affinity in the low nanomolar range. This study provided a good starting point for the investigation of dual H_3R/MAO B combination, with a possible extension by other neurological targets, for further optimization and development of potent multitarget drugs for the treatment of PD.

5 Design of multiple target ligands at $H_3R/A_1R/A_{2A}R$

For the synthesis of newly $H_3R/A_1R/A_{2A}R$ ligands, the general accepted aminoalkyloxypropyl H_3R pharmacophore (referred as Y in Figure 31) showed by the piperidine analog of ciproxifan UCL-2190 and from the synthetized (2-benzylidene)-1-indanone H_3R/MAO B DTLs, was introduced into the central tricyclic non-xanthine arylindenopyrimidine core, which was found to be a suitable pharmacophore for $A_1R/A_{2A}R$ antagonists as presented in many heterocyclic substituted arylindenopyrimidine such as JNJ-40255293.[148,173] Both pharmacophores show similar structural elements such as an *N*-containing heterocycle connected by an ether linker to an aromatic core substituted with a lipophilic moiety. For that reason and for the fact that JNJ-40255293 act as an $A_1R/A_{2A}R$ antagonist, other pharmacophores such as the one disclosed by the selective $A_{2A}R$ antagonist xanthine derivative istradefylline (cf. Chapter 1.4.1, Figure 14) as well as the one showed by bicyclic (i.e. ST-1535) and monocyclic (i.e. ASP-5859) non-xanthine derivatives (cf. Chapter 1.4.1, Figure 15) were not selected.

Previous studies were addressing the role of the ketone functionality in 5-position of the arylindenopyrimidine scaffold, showing that its reduction to the corresponding alcohol or its replacement with an amino group (-NH-) as well as with an ethylene moiety ($-CH_2CH_2-$) decreases the affinity at $A_{2A}R$ 100-fold.[173] In contrast, reduction of the ketone to a methylene moiety led to the development of potent 8-substituted $A_1R/A_{2A}R$ antagonists, having K_i values for both receptors in the low nanomolar concentration range. Based on these results twelve $H_3R/A_1R/A_{2A}R$ MTLs were synthetized by introducing the H_3R pharmacophore either in 7- (as R^7) and 8-position (as R^8) of ring A or in 4'-position (as $R^{4'}$) of ring B (Figure 31) in both oxidized (**11-16,** X=-CO) and a non-oxidized/reduced (**5-10,** X= $-CH_2$) tricyclic arylindenopyrimidine moiety.

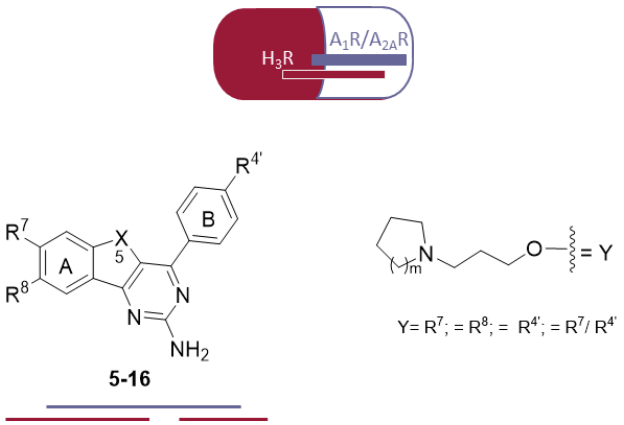

Figure 31. Development of substituted arylindenopyrimidine $H_3R/A_1R/A_{2A}R$ MTLs. m= 1, 2; X= $-CH_2$ (**5-10**), -CO (**11-16**).

5.1 Pharmacological characterization of tricyclic $H_3R/A_1R/A_{2A}R$ ligands

The affinity of the new chemical entities at the corresponding GPCRs targets was evaluated with the aid of radioligand binding assays using human H_3R and recombinant ARs (Table 11).[168,215,216,236]

In both oxidized (X= -CO) and non-oxidized/reduced (X= $-CH_2$) compounds, substitution of the H_3R pharmacophore in 7- and 8-position of ring A (e.g. **5** vs. **6** and **14** vs. **16**) as well as modifications of the *N*-containing heterocycle (e.g. piperidine vs. pyrrolidine, **6** vs. **10** and **12** vs. **16**) slightly influenced the H_3R affinity.

The oxidized derivatives decreased the K_i values at H_3R compared to the non-oxidized/reduced ones (e.g. **12** vs. **6** and **14** vs. **8**). Notably, subnanomolar K_i values for H_3R could be obtained ($0.3 < K_i$ (nM) < 0.6) only when the piperidine(propyloxy) H_3R structural elements was introduced in 4'- and 7-position of the arylindenopyrimidine core.

While the tricyclic adenosine scaffold was well tolerated by the H_3R, the adenosine receptors were more influenced by the 7/8- or 4'-substitutions of the H_3R pharmacophore as well as by the ketone moiety in 5-position of the arylindenopyrimidine core. The synthetized MTLs have shown K_i values at both A_1 and A_{2A} receptors in the low nanomolar concentration ranges ($K_i < 48$ nM) only when the H_3R pharmacophore was substituted in 8-position of the oxidized and non-oxidized arylindenopyrimidine scaffold (cf. **6**, **10**, **12**, **16**), since its attachment in 7-position led to more than 10 or 100-fold decrease of ARs affinity for oxidized and non-oxidized MTLs, respectively (e.g. **16** vs. **14** and **6** vs. **5**). These promising ARs ligands have shown $A_1R/A_{2A}R$ affinity, with a slightly preference for the $A_{2A}R$, but also additional affinity at the $A_{2B}Rs$ (Ki ($A_{2A}R$)/Ki ($A_{2B}R$) = 0.08-0.19), suggesting a similar behavior as that of reference compound JNJ-40255293. So far, the $A_{2B}R$ was investigated as potential therapeutic target for the treatment of chronic lung, vascular disease, renal disease, cancer and diabetes. Therefore, the effect on PD treatment of additional affinity of some of the synthetized compounds at $A_{2B}R$ remains to be evaluated.[237]

Notably, the carbonyl moiety is necessary for ARs binding when the H_3R pharmacophore is introduced in 7-position of ring A, since only oxidized ligands showed high affinities at ARs (e.g. **5** vs. **11** and **8** vs. **14**).

The introduction of the H_3R pharmacophore in 4'-position was less tolerated for not oxidized/reduced MTLs (cf. **7**, **9**).

Table 11. H_3R and $A_1R/A_{2A}R$ screening data (given as K_i values of novel MTLs and reference compounds.

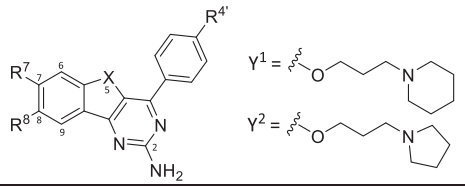

Comp	R^7	R^8	$R^{4'}$	X	hH_3R[a]	hA_1R[b]	$hA_{2A}R$[c]	$hA_{2B}R$[d]	hA_3R[e]
					K_i [nM] $\bar{x}$ [95 % CI]	K_i [nM] $\bar{x}$ ± SD or (% inhibition, $\bar{x}$ ± *SD at 1 μM)*			
5	Y^1	-H	-H	$-CH_2$	2.3 [1.2-4.1]	>1000 [24 ± 6]	>1000 [34 ± 3]	>1000 [34 ± 4]	>1000 [39 ± 4]
6	-H	Y^1	-H	$-CH_2$	4.5 [1.7-12]	18.7 ± 1.3	4.85 ± 0.9	58.1 ± 3.4	231 ± 38
7	-H	-H	Y^1	$-CH_2$	0.49 [0.18-1.34]	2511 ± 454	717 ± 132	>1000 [28 ± 0]	>1000 [24 ± 4]
8	Y^2	-H	-H	$-CH_2$	2.1 [1.1-4.1]	828 ± 166	>1000 [40 ± 7]	>1000 [25 ± 5]	>1000 [35 ±11]
9	Y^1	-H	Y^1	$-CH_2$	0.60 [0.05-7.4]	>1000 [23 ± 6]	941 ± 160	>1000 [13 ± 2]	>1000 [50 ± 5]
10	-H	Y^2	-H	$-CH_2$	11 [0.45-255]	11.5 ± 1.6	7.25 ± 1.53	36.9 ± 8.3	150 ± 10
11	Y^1	-H	-H	-C=O	36 [13-100]	367 ± 77	142 ± 28	114 ± 20	>1000 [12 ± 3]
12	-H	Y^1	-H	-C=O	52 [15-174]	11.2 ± 0.7	4.01 ± 1.0	43.5 ± 16	150 ± 13
13	-H	-H	Y^1	-C=O	0.28 [0.19-0.42]	133 ± 8	35.5 ± 8.9	331 ± 57	>1000 [33 ± 4]
14	Y^2	-H	-H	-C=O	31 [14-69]	129 ± 7	104 ± 18	180 ± 18	846 ± 117
15	Y^1	-H	Y^1	-C=O	0.31 [0.12-0.80]	>1000 [44 ± 3]	203 ± 80	>1000 [15 ± 1]	>1000 [32 ± 8]
16	-H	Y^2	-H	-C=O	27 [3.0-237]	12.6 ± 2.3	6.24 ± 1.93	47.5 ± 3.4	199 ± 9
JNJ-40255293	-H	Morph	-H	-C=O	n.d.	48[g] ± 16	7.5[g] ± 4.9	230[g] ± 92	430[g] ± 150
UCL2190					11	n.d.	n.d.	n.d.	n.d.

K_i values are given as mean either within the 95% confidence interval (CI), or with standard deviation (SD) for hH_3R or hA_xRs, respectively; Data were obtained in radioligand depletion studies (n≥3) each performed at least in duplicates using [a] [^{3}H]*N*$^{\alpha}$-Methylhistamine, [b] [^{3}H]CCPA, [c] [^{3}H]MSX-2, [d] [^{3}H]PSB-603 and [e] [^{3}H]PSB-11 for H_3R and A_1R, $A_{2A}R$, $A_{2B}R$, A_3R, respectively; [g] Values published in Atack at al. 2014, functional activity cAMP assay, EC_{50}; Morph, ethoxymorpholine; n.d. not determined.

Surprisingly, the oxidized representative **15**, having the H_3R pharmacophore in both 4'- and 7-position of ring B and A respectively, was the only synthetized ligand showing increased selectivity over $A_{2A}R$ (K_i ($A_{2A}R$)/K_i (A_1R) < 2), suggesting that other substitutions in 4'-position of ring B may be a promising approach to improve the selectivity over AR subtypes.

Looking for promising MTLs, only compounds showing affinities in low nanomolar concentration for H_3R as well as for A_1R/$A_{2A}R$, were chosen for further evaluations. Non-oxidized derivatives **5** and **8**, having high affinity for H_3R but K_i values for ARs higher than 1000 nM as well as the oxidized ligands **11** and **14** showing moderate *in vitro* affinities for all targets were not further investigated. Also, compounds bearing the H_3R pharmacophore in 4'-position of ring B were not selected as lead structure for further evaluations, due to insufficient ARs affinity. However, the latter compounds, showing excellent H_3R affinities in the subnanomolar concentration range, may be used for comparison with H_3R/A_1R/$A_{2A}R$ MTLs.

Instead, the non-oxidized compounds **6** and **10**, displaying K_i values for H_3R and ARs in the low nanomolar concentration range, and their oxidized forms (**12** and **16**, respectively), which also showed comparable affinities at ARs with slightly decreased K_i values for the H_3R, showed the desired multi-targeting properties (Figure 32).

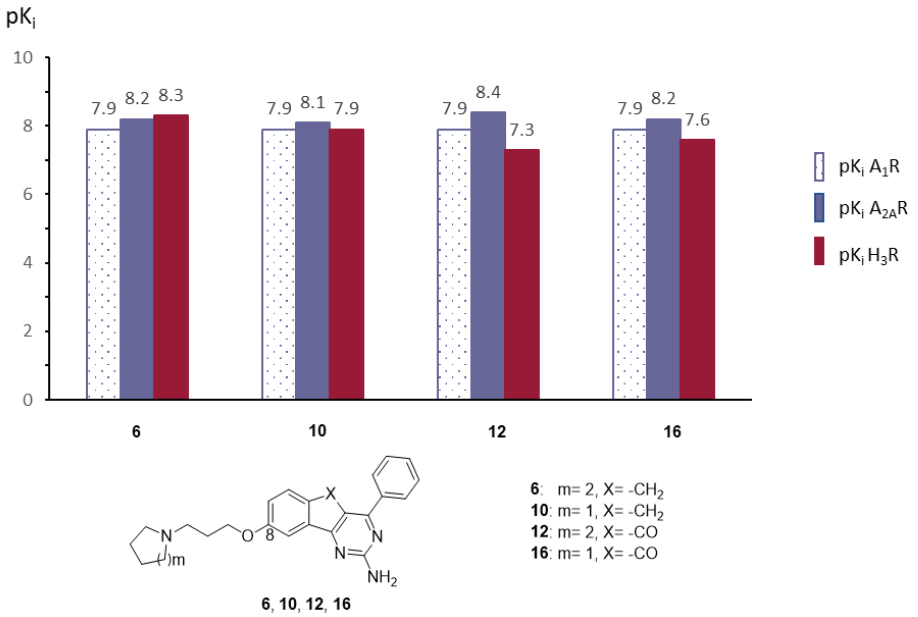

Figure 32. A_1R/$A_{2A}R$ as well as H_3R affinities of non-oxidized/reduced (compounds **6** and **10**) and oxidized (compounds **12** and **16**) MTLs.

To investigate the selectivity profile of newly $H_3R/A_1R/A_{2A}R$ MTLs two compounds, belonging one to non-oxidized and one to oxidized MTLs (derivatives **10** and **12**, respectively), were selected to evaluate off-target affinities (Table 12).

The affinities of the selected MTLs at H_1R and H_4R were determined because of the similar expression pattern in the CNS of hH_1R and hH_3R and the high homology between the hH_4R and hH_3R.[46] MTLs showed low affinity for H_1R, differing two orders of magnitude compared to the K_i values of the H_3R binding, as well as high selectivity for H_3R over H_4R (K_i > 10000).

In vitro binding affinities at dopamine D_1, D_{2s}, D_3 and D_5 receptors as well as at MAO A and MAO B were measured as they are potential targets of PD and therefore may influence the pharmacological results of in *in vivo* experiments.[238,239] The off-target binding data were obtained in radioligand depletion studies for the histamine receptor subtypes and DRs. Concerning MAO A and MAO B, a continuous spectrophotometric method was used for the determination of IC_{50} values or percentages of inhibition.[67]

Table 12. Off-target and selectivity profile of most promising $H_3R/A_1R/A_{2A}R$ MTLs

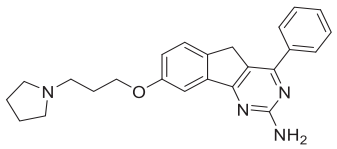

10

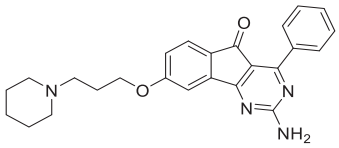

12

Comp	K_i [nM][a] $\bar{x}$ [95 % CI]						IC_{50} [nM][b] *% inhibition at 10 µM ± SD*	
	hH_1R	hH_4R	hD_1R	hD_5R	$hD_{2S}R$	hD_3R	hMAO A	hMAO B
10	>1000	>10 000	>1000	>1000	1246 [697-228]	290 [272-309]	*7.4 ± 12*	>1000 *57 ± 8.6*
12	>1000	>10 000	>1000	>1000	1586 [304-266]	364 [175-759]	*16 ± 3.6*	*50 ± 16*

K_i values are given as mean within the 95% confidence interval (CI), whereas screening data are given as % inhibition mean ± standard deviation (SD); [a] Off-target binding data were obtained in radioligand depletion studies (n=2-4) using [^{3}H] Pyrilamine, [^{3}H] Histamine, [^{3}H] SCH23390 and [^{3}H] Spiperone for hH_1R, hH_4R, D_1R/D_5R and $D_{2S}R/D_3R$, respectively. [b] Spectrophotometric monoamine oxidase inhibition assay using kynuramine as substrate and either seven to ten concentrations (between 10^{-10} M and 10^{-4} M) or 10 µM of test ligand for IC_{50} determinations or one-point screening, respectively.

Compounds **10** and **12** showed low affinity at D_1R and D_2R as well as at D_5R (K_i (nM) > 1000). In contrast, at D_3Rs both MTLs possessed moderate binding capabilities in one to two orders of magnitude higher concentration ranges compared to the desired target receptors.

There is no doubt about involvement of mesolimbic D_3Rs in PD motor symptomology, which are significantly reduced by about 40% in PD patients.[240] Additionally, some prominent dopamine

agonists, i.e. pramipexole, ropinirole or dopamine itself, show a clear D_3R preference over D_2Rs, prompting a therapeutic relevance of D_3Rs. [241] While presented MTLs showed only moderate D_3R binding compared to approved dopamine agonists, a D_3R-mediated influence on *in vivo* activity cannot be ruled out. In the most unfavorable case, as the designed MTLs show rather structural overlap with D_3R antagonists,[242–245] their desired motor-improving capacities might be counteracted via D_3R blockade. Thus, design-out of any D_3R binding is mandatory in the future, when designing $H_3R/A_1R/A_{2A}R$ MTLs using a arylindenopyrimidine core motif. [29,155]

The evaluation of potential MAO A and MAO B inhibition was performed since some of the structural related H_3R/MAO B 2-benzylidene-1-indanone described in chapter 4.1 showed IC_{50} values for MAO B in the nanomolar concentration range. The inhibition of MAO B would add some beneficial effect on the synthetized MTLs since the blockade of MAO B hinders DA degradation, increasing the DA availability in the synaptic cleft. However, both compounds, at a concentration of 10 µM, showed MAOs inhibition lower than 60 % in one-point screening. Also, the calculated IC_{50} value for compound **10** higher than 1000 nM confirmed weak inhibition of MAOs.

As the synthetized compounds were designed for a neurodegenerative disorder, physicochemical properties were also calculated. Based on the values shown in table 13, compounds **10** und **12** do not violate Lipinski's rule, as all calculated descriptors and properties were within the expected threshold, suggesting a good absorption of the synthetized MTLs.[246,247]

Table 13. Evaluation of Lipinski's rules and metric parameters for best $H_3R/A_1R/A_{2A}R$ MTLs.

Comp.	Lipinski's rules					H_3R		A_1R		$A_{2A}R$	
	HB don.	HB acc.	M [g/mol]	clogP[a]	PSA[b] (Å²)	LE[c]	LELP[d]	LE[c]	LELP[d]	LE[c]	LELP[d]
10	2	4	386.5	4.4	52.1	0.4	11.7	0.4	11.4	0.4	11.7
12	2	5	414.2	4.2	64.9	0.3	12.2	0.4	11.3	0.4	11.9
JNJ-40255293	2	6	402.1	3.3	72.8			0.4	8.7	0.3	9.7
UCL2190	0	3	287.1	3.8	25.3	0.5	7.2				
Rules	≤5	≤10	≤500	≤5	≤140	LE ≥ 3-10; -10 ≤ LELP ≤ +10					

[a] Calculation with Marvin Sketch; [b] Calculation with Molsoft; [c] LE = pK_i/HA (heavy atoms); [d] LELP = clogP/LE; HB= hydrogen bond; M= molecular weight; PSA= polar surface area. Don: donator; acc.: acceptor; comp.: compound. Green (values in the optimal range); orange (values slightly out of optimal range); red (values out of optimal range).

In addition, for early evaluation of drug-likeness of compounds **10** and **12**, LE and LELP were calculated for H_3R, A_1R and $A_{2A}R$. The moderate lipophilic MTLs showed favorable LE values (LE ≥ 0.3) but at the cost of LELP, which values were slightly outside the limits.

5.2 $A_{2A}R$ Docking studies

The synthetized MTLs showed best affinity in the low nanomolar concentration ranges for both $A_1R/A_{2A}R$, with a slightly preference for the $A_{2A}R$. Since the $A_{2A}R$ is one of the best characterized GPCRs, also showing a central role compared to the other ARs subtypes in PD treatment, the interaction modes of 8-substituted arylindenopyrimidines with $A_{2A}R$ were investigated in molecular modelling studies. Compound **6**, being one of the most potent synthetized MTLs, was selected as representative compound and docked into the crystal structure of the chimeric protein of $A_{2A}R$-BRIL. A comparison with the $A_{2A}R$ antagonist ZM-241385, having comparable affinity at $A_{2A}R$ (K_i $hA_{2A}R$ = 1.6 nM) with similar structural elements to the selected MTL was conducted (Figure 33).[93,248]

The 3D and 2D images of binding presented in figure 33, showed that the central arylindenopyrimidine ring, which is responsible for the $A_1R/A_{2A}R$ antagonism, could constitute a good alternative as central core, since compound **6** shares with the reference compound ZM241385 several interactions. Within both structure, the primary amine allows hydrogen bonds with the α-amino acid Asn253 and interacts with Glu169. Also, the presence in both $A_{2A}R$ antagonist ligands of an extended π -conjugated system, allows π- π interactions with Ph168. Both ligands demonstrated a similar orientation in the binding pocket, where the phenyl moiety of compound **6** showed the same aromatic interactions with Trp246 as the furan ring in ZM-241385 and the basic 1-(3-oxypropyl)piperidine H_3R pharmacophore occupied the same pocket as the phenol moiety of ZM-241385.

As structural-related tricyclic non-xanthine derivatives substituted in 4' position of the arylindenopyrimidine scaffold with a furan moiety caused mutations in DNA, the phenyl ring was not replaced by a furyl group.[123,173]

Overall, molecular docking studies confirmed *in vitro* affinities by demonstrating, that arylindenopyrimidine-based ligands bearing the H_3R pharmacophore in 8-position such as MTL **6**, fit the $A_{2A}R$ binding pocket.

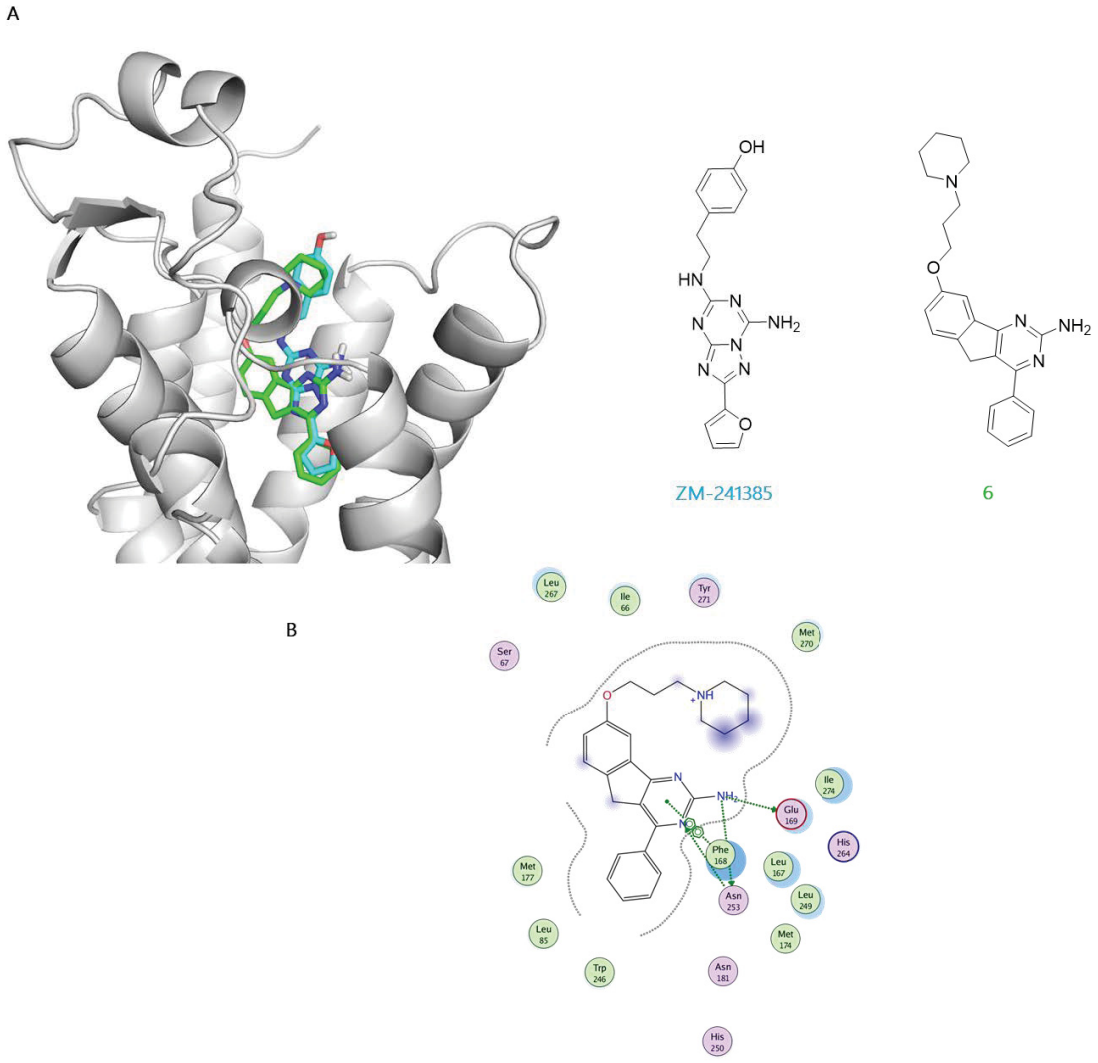

Figure 33. 3D docking model (A) of compound **6** (colored in green, A) and ZM-241385 (colored in cyan, A) with $A_{2A}R$ and 2D schematic diagram of the docking model (B) of compound **6**. For the modelling studies, the structure of $A_{2A}R$ co-crystallized with ZM-241385 (PDB ID: 4EIY) was used.

5.3 *In vivo* studies

Within the small series of oxidized and non-oxidized/reduced arylindenopyrimidine scaffold, some of most potent $H_3R/A_1R/A_{2A}R$ MTLs were chosen for initial *in vivo* examination in preclinical rodent PD and sleep models due to their good *in vitro* affinities for all receptors and their potential to act as CNS agents. Preclinical/clinical trials with compounds targeting the adenosine receptors, mainly $A_{2A}R$, have been shown to affect the expression of LID.[18,116,225] As co-administration of the $A_{2A}R$ antagonists with L-DOPA potentiates the antiparkinsonian activity, the use of $A_{2A}R$ allows the reduction of the effective does of L-DOPA, and thus decreasing the incidence of LID in PD, although not preventing the manifestation of dyskinesia.[127,128,130]

In 2016, it was reported that the selective $A_{2A}R$ antagonist istradefylline, in combination with a sub-threshold dose of L-DOPA attenuate LID without worsening PD disability score in MPTP-treated macaque model of parkinsonian and dyskinetic motor symptoms.[116]

Interestingly, a recent study suggested that blocking both A_1R and $A_{2A}R$ may be beneficial for reducing LID since in animal models of LID, the total AIMs observed for the $A_1R/A_{2A}R$ antagonist caffeine was notably improved compared to those of selected $A_{2A}R$ antagonists such as SCH-412348 and istradefylline.[97,249,250] However, due to the small experimental studies, the efficacy of these $A_1R/A_{2A}R$ antagonists has yet to be confirmed. Thus, to provide further data, a first preclinical evaluation of most potent MTLs, **6**, **10** and **12**, on LID was performed (Figure 34).

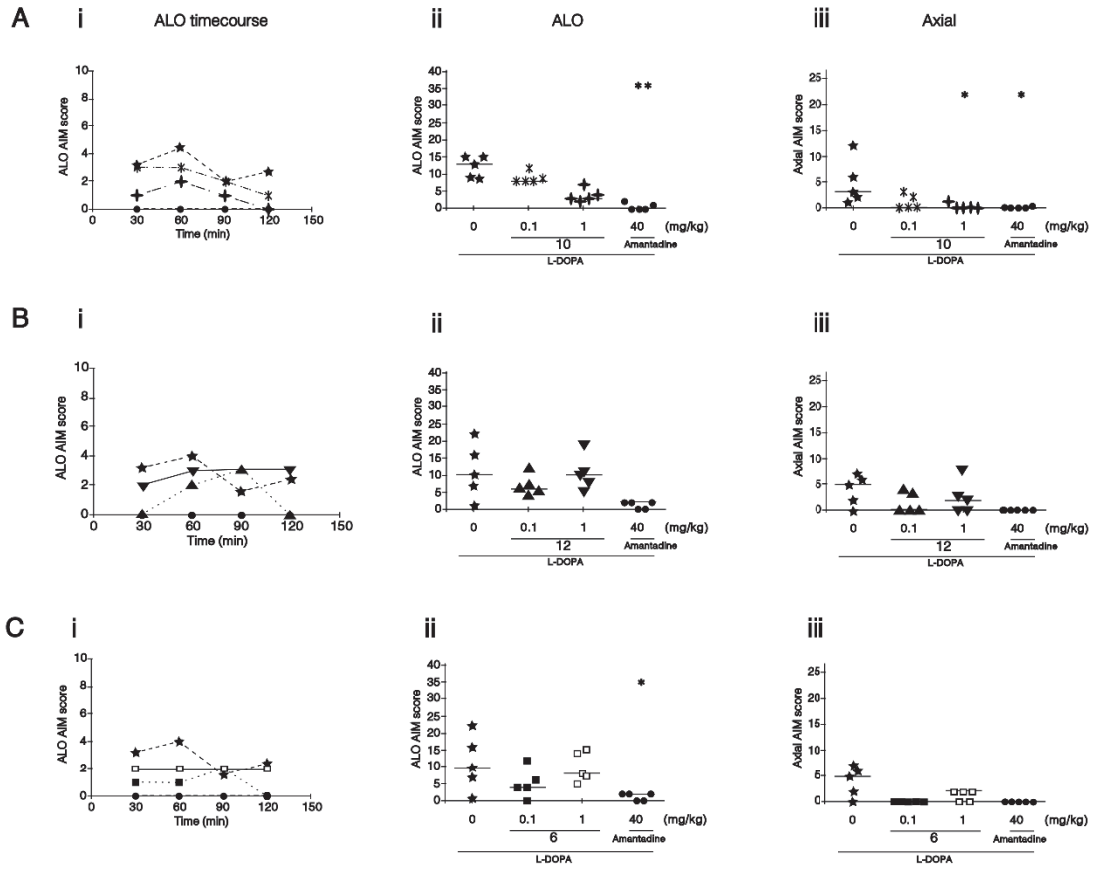

Figure 34. Time-course panels reporting the effect of best MTLs **10** (A), **12** (B), **6** (C) amantadine on either overall axial/limb/orolingual (ALO) or axial AIM scores induced by L-DOPA (6 mg/kg). AIM scores are expressed as individual data and median. Control (★), amantadine (●) 40 mg/kg, L-DOPA + **10** (✳) 0.1 mg/kg, L-DOPA + **10** (✦), L-DOPA + **12** (▲) 0.1 mg/kg, L-DOPA + **12** (▼) 1 mg/kg, L-DOPA + **6** (■) 0.1 mg/kg, L-DOPA + **6** (□) 1 mg/kg. All groups were analyzed by Friedman test followed by Dunn's multiple comparison test; *p < 0.05 and **p < 0.01 *vs* control (0 mg/kg) (n=5).

With such aim, the 6-OHDA rat model of LID was chosen and abnormal involuntary movements were evaluated. MPTP-treated mouse model has some advantages compared to 6-OHDA model

(e.g. no need of type of skilled stereotaxic surgery, bilateral lesion). However, the MPTP model, due mainly to poor lesion reproducibility, is often not chosen to study LID.[251,252]

In this animal model neurodegeneration of dopamine neurons in the nigrostriatal pathway though injection of the toxin 6-OHDA was followed by administration of L-DOPA (6 mg/kg) once a day until AIMs severity stabilization. The effect of each compounds at two doses (0.1 and 1 mg/kg) in the presence of L-DOPA was evaluated on AIMs as previously described.[225]

In figure 34, overall AIM scores for selected MTLs are shown. Compared to AIMs produced by L-DOPA alone (control rats), co-administration of compound **10**, seems to dose-dependently decrease LID (Figure 34, A (ii)) whereas compounds **12** and **6**, tend to decrease LID over the treatment period only when administrated at 0.1 mg/kg (Figure 34, B (ii) and C (ii)). However, significant decrease between the tested compounds and the control ($p < 0.05$) were found only for derivative **10** in axial AIMs at a dose of 1 mg/kg (Figure 34, A (iii)). The lack of significantly effects on the other AIMs sub-types (orolingual and limb AIMs, Figure 35), might explain the non-significant statistical differences in overall AIMs score compared to the reference compound amantadine (Figure 34, A (ii)).

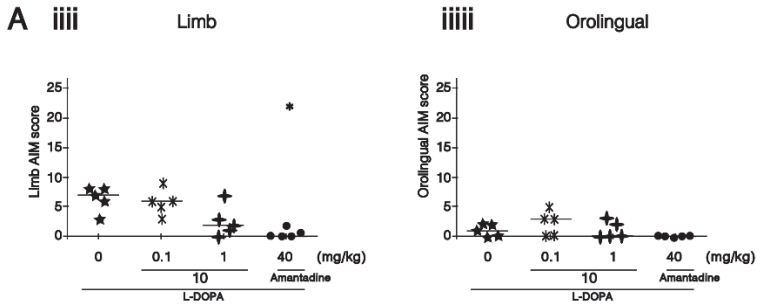

Figure 35. Effect of compound **10** and amantadine on limb (A (iiii)) and orolingual (A (iiiii)) AIM scores induced by L-DOPA (6 mg/kg). AIM scores are expressed as individual data and median. All groups were analyzed by the Friedman test followed by Dunn's multiple comparison test (n= 5). Control (★), amantadine (●) 40 mg/kg, L-DOPA + **10** (✳) 0.1 mg/kg, L-DOPA + **10** (✦). All groups were analyzed by Friedman test followed by Dunn's multiple comparison test; *p < 0.05 and **p < 0.01 *vs* control (0 mg/kg) (n=5).

However, it is worth pointing out that the control for all the experiments tends to vary, and no significant differences even for the positive control amantadine could be demonstrated.

Previous studies suggested also a possible role of D_3R in the development of LID.[253,254] As an example, the D_3R antagonist S33084 in MPTP-treated marmosets reduced LID without exacerbating the L-DOPA action on motor PD symptoms.[255,256] Although compounds **6**, **10** and **12** have moderate affinity at D_3R (in the range from 435 nM to 495 nM) compared to potent D_3R agonists such as pramipexole, the tendency for these MTLs to reduce AIMs might be due also to D_3R antagonism.

Thus, due to the limited validity of the performed study and a possible D_3R antagonism contribution, the observed tendencies, suggesting a slight anti-dyskinetic effect of the tested $H_3R/A_1R/A_{2A}R$ MTLs, should be confirmed by further studies.

In addition to the symptomatic motor symptoms, almost 30% of PD patients suffer from excessive diurnal sleepiness even when the motor symptoms are well controlled.[257]

Notably, the use of H_3R antagonists/inverse agonists such as thioperamide, pitolisant, GSK-189254 and JNJ-520785, improved waking in a wide range of animal models and clinical trials.[258]

Encouraged by these preclinic/clinical results, one of the most potent MTL, compound **12**, showing excellent affinity at H_3R as well as at $A_1R/A_{2A}R$ was tested on sleep-wake electroencephalogram (EEG) studies in mice (Figure 36).

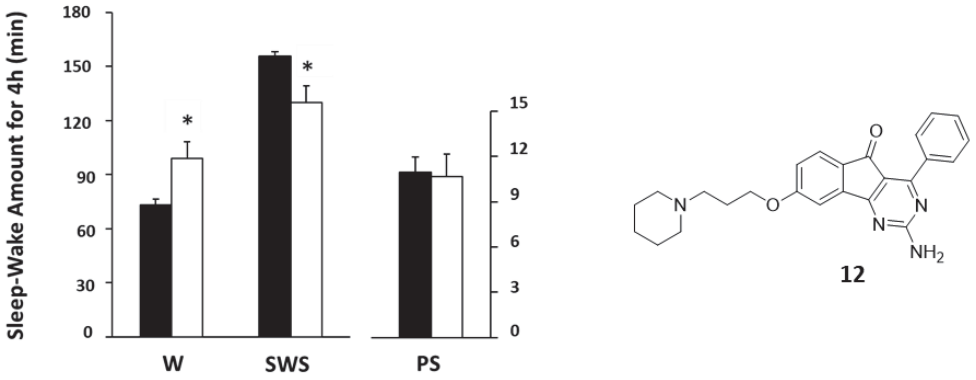

Figure 36. Variation of the sleep-wake cycle following administration of compound **12** (white bar, 2 mg/kg, p.o.). Histogram showing mean time (min) spent in each sleep-wake stage during 4h after compound administration. (*p < 0.05 *vs* control (black bar); Dunnett's t-test after significant ANOVA; n=5).

The sleep-waking cycles, consisting of waking (W), slow-wave sleep (SWS), and paradoxical sleep (PS), was observed. Compound **12** at a dose of 2 mg/kg, p.o., significantly promote waking duration compared to control. The improvement of waking was accompanied by a significant reduction of time spent in SWS and by a slightly insignificant decrease of PS.

Similar changes on sleep-wake cycles were observed for the reference compound JNJ-40255293.

Explicitly, the wake-promoting effect for the $A_1R/A_{2A}R$ antagonist JNJ-40255293, administrated at several doses (0.04 mg/kg, 0.16 mg/kg, 0.63 mg/kg, 2.5 mg/kg and 10 mg/kg, p.o.), was tested on sleep-wake EEG in rats.[148] While low-doses (0.04 mg/kg and 0.16 mg/kg, p.o.) had no significantly effects compared to control, dose-dependently enhancing of the active waking was observed at higher doses, where the minimal effective dose was 0.63 mg/kg.[148]

These results suggest that the additional modulation of $A_1R/A_{2A}R$ by the synthetized MTL **12** positively influence the observed waking obtained by H_3R blockade. A major role for the promotion of wakefulness is played by $A_{2A}R$. Former studies on gene-manipulated mice have shown that the waking effect of the unselected $A_1R/A_{2A}R$ antagonist caffeine was present in A_1R knockout (KO) mice, but not in $A_{2A}R$ KO mice.[141,147,259]

5.4 Conclusions – MTLs at $H_3R/A_1R/A_{2A}R$

In search for new agents for PD therapy, multipotent molecules able to bind selected pharmacological targets involved in the development of the disease were developed. Thus, going a step forward of what has been previously described, new multipotent-arylindenopyrimidine derivatives showing H_3R as well as $A_1R/A_{2A}R$ affinities in the low nanomolar concentration ranges, were described for the first time.

The successful introduction of the H_3R pharmacophore into different positions of the $A_1R/A_{2A}R$ adenosine scaffold was confirmed by (sub)nanomolar affinity at the hH_3R obtained for all synthetized compounds, confirming a high variation tolerability in H_3R ligands when maintaining the general accepted blueprint.

Less tolerance was shown by the ARs. Compounds, bearing the H_3R pharmacophore in 8-position of the oxidized (derivatives **12** and **16**) and non-oxidized/reduced (derivatives **6** and **10**) arylindenopyrimidine moiety, had the desired multi-targeting properties with affinities in low nanomolar concentration ranges for $A_1R/A_{2A}R$ receptors.

The off-target and selectivity profiles of two of the best 8-substituted arylindenopyrimidine MTLs (compound **10** and **12**), were evaluated. *In vitro* affinities at related histamine receptor subtypes showed low affinity at H_1R as well as good to excellent selectivity for H_3Rs over homologous H_4Rs. Negligible affinities were observed for D_1/D_{2s} as well as for D_5 receptors, whereas both MTLs possessed D_3R moderate binding capabilities in one to two orders of magnitude higher concentration ranges compared to the desired target receptors. Due to their localization in the brain and to their involvement in the regulation of motor symptoms affecting PD patients, D_3R are potential therapeutic targets of PD. Thus, further studies need to be done to clarify if the synthetized MTLs act as agonists or antagonists at D_3R.

Remaining the treatment of LID one of the most urgent demand to ameliorate the life of PD patients and affecting selective $A_{2A}R$ antagonists the expression of LID, the effects of MTLs **6**, **10** and **12** in LID

was evaluated in 6-OHDA lesioned rats by scoring AIMs. Observed tendencies and significant reductions in AIMs might point out a slight antiparkinsonian efficacy of H_3R/ADs MTLs **6**, **10** and **12**. The effect of compound **12**, was also evaluated in sleep-wake cycles. The significantly improvement of waking confirm the central role of H_3R antagonists in sleep-wake regulation, with an extension to the $A_1R/A_{2A}R$, which antagonism positively influence the improved-sleep capabilities of compound **12** as shown by the structural related $A_1R/A_{2A}R$ antagonist JNJ-40255293.[148] Although, in comparison to JNJ-40255293, higher effective doses of MTL **12** are needed, since 1 mg/kg p.o. does not result in significant wake-promoting effect. However, these studies prove oral bioavailability of compound **12**, while for example pharmacokinetic properties (i.e. gastrointestinal absorption, blood-brain penetration) should be evaluated as they might explain the differences in effective dosing compared to JNJ-40255293.

Thus, design of $H_3R/A_1R/A_{2A}R$ MTLs, herein described for the first time, may represent an interesting approach for the treatment of motor disorders with accompanying non-motor symptoms such as sleep disruption.

6 Summary

Parkinson's disease (PD) is among the most common neurodegenerative diseases and a major health problem in the ageing society. PD patients suffer from distinct motor abnormalities, exemplified by the cardinal symptoms such as tremor, bradykinesia, rigidity and postural changes. Dopaminergic therapies including L-DOPA are highly effective during the early stages of the treatment but after several years of medications motor fluctuations and dyskinesia start to appear. Motor disorders are commonly associated with non-motor symptoms arising mainly from neurodegeneration in non-dopaminergic systems. Among the most common are depression, sleep behaviour disorders and dementia. Recognizing PD as a highly complex and multifactorial dysregulation where both motor and non-motor symptoms need to be treated, forced researchers to come up with new innovative therapy options such as the design of multi-targeting ligands (MTLs). Within the multi-targeting approach, a great variety of MTLs are described, showing H_3R antagonism combined with other neurotransmitter-regulating targets, i.e. GPCRs, enzymes and ion channels. At the beginning of my investigation just a handful of lead structures combining H_3R affinity with enzyme modulation were described and MTLs able to simultaneously antagonize the H_3R as well as the A_1R and $A_{2A}R$ were still not synthetized. Therefore, the design of H_3R/MAO B DTLs and $H_3R/A_1R/A_{2A}R$ MTLs was performed as potentially innovative therapeutic approach for the treatment of PD motor and non-motor symptoms.

Concerning dual H_3R/MAO B ligands, the H_3R pharmacophore was attached to indanone-related MAO B motifs, leading to the development of three series of H_3R/MAO B DTLs. Among synthesized indanone DTLs, different 5- and 6-substitution patterns of the indanone moiety strongly influenced MAO B inhibition, selectivity and time dependency of inhibition. Compounds bearing the 2-benzylidene-1-indanone core structure showed MAO B preferring inhibition capabilities along with nanomolar hH_3R affinities. Substitution of 5- and 6-position of the 2-benzylidene-1-indanones with lipophilic substituents revealed three promising candidates exhibiting inhibitory potencies for MAO B with IC_{50} values ranging from 1931 nM to 276 nM and high affinities at hH_3R (K_i < 50 nM). Compound **3f** (MAO B IC_{50} = 276 nM, hH_3R K_i = 10 nM) showed highest preference for MAO B over MAO A (SI > 36). Interestingly, IC_{50} determinations after preincubation of enzyme and DTLs revealed also nanomolar MAO B potency for **3f** structural isomer **3e** (MAO B IC_{50} = 232 nM) and F-substituted derivative **3d** (MAO B IC_{50} = 541 nM), suggesting time-dependent inhibition modes.

In search for irreversible MAO B ligands, the close structural relationship of the first series of H_3R/MAO B ligands (**1a-e**) with propargylamine derivatives such as the anti-parkinson drug rasagiline became clear. Notably, the reductive amination of the carbonyl moiety of compound **1e** led to the synthesis of derivative **4**, which showed high affinity at hH_3R in the low nanomolar concentration range (K_i = 2.5 nM). Moderate inhibitory potency for MAO B was determined (IC_{50} = 1736 nM), but since it was found to act as an irreversible ligand, and to have a good selectivity profile over MAO A (MAOs SI > 50), the newly described DTL might be a good starting point for further optimization especially regarding MAO B inhibition potency.

The general accepted aminoalkyloxypropyl H_3R pharmacophore showed by the synthetized (2-benzylidene)-1-indanone H_3R/MAO B DTLs, was introduced into an adenosine antagonist arylindenopyrimidine core for the synthesis of $H_3R/A_1R/A_{2A}R$ MTLs.

The successful introduction of the H_3R pharmacophore into different positions of oxidized (compounds **11-16**) and non-oxidized/reduced (compounds **5-10**) $A_1R/A_{2A}R$ scaffold was confirmed by (sub)nanomolar affinity at hH_3R for all MTLs (0.28 nM < K_i (hH_3R) < 55 nM). Within this series of compounds, those bearing the H_3R pharmacophore in 8-position of the arylindenopyrimidine core (MTLs **6**, **10**, **12**, **16**) showed the most promising multitargeting features with affinities in nanomolar concentration ranges at the desired targets. These most promising ligands showed $A_1R/A_{2A}R$ affinity, with a slightly preference for the $A_{2A}R$, suggesting a similar behavior as reference compound JNJ-40255293. With this innovative *in vitro* profile, two of the most potent compounds **10** (K_i (hH_3R) = 11 nM, K_i (hA_1R) = 12 nM, K_i ($hA_{2A}R$) = 7.3 nM) and **12** (K_i (hH_3R) = 52 nM, K_i (hA_1R) = 11 nM, K_i ($hA_{2A}R$) = 4.0 nM) were chosen for in vivo testing, evaluating either their anti-dyskinetic or wake-promoting efficiency in rodents. Slightly improvement of L-DOPA-induced dyskinesia was observed in rats after co-administrations of **10** (1 mg kg^{-1}, i.p.) with L-DOPA (6 mg kg^{-1}). Furthermore, MTL **12** (2 mg kg^{-1}) was able to increase wakefulness in mice after oral application. However, in comparison to JNJ-40255293, higher effective doses of **12** are needed, since 1 mg/kg p.o. does not result in significant wake-promoting effect. However, these studies prove oral bioavailability of compound **12**, while for example pharmacokinetic properties (i.e. gastrointestinal absorption, blood-brain penetration) should be evaluated as they might explain the differences in effective dosing compared to JNJ-40255293. As proof-of-concept, the combination of the H_3R on the one hand with MAO B and, on the other hand, with A_1 and A_{2A} receptors led to the synthesis of potent MTLs, showing a promising pharmacological profile. Comparing to the dual target H_3R/MAO B UCL-2190 or recently discovered contilisant, the synthetized compounds (**1a-e**, **2a-c**, **3a-e** and **4**) show improved inhibition

at MAO B with reversible and irreversible binding, having comparable H_3R affinity in the low nanomolar range.

Although lead optimization needs to be performed for most promising H_3R/MAO B to improve physiochemical properties and drug-likeness, this study provided an excellent starting point for the investigation of dual H_3R/MAO B combination, for further optimization and development of potent multitarget drugs for the treatment of PD. Also, the most promising designed $H_3R/A_1R/A_{2A}R$ MTLs, herein described for the first time, showing affinities in the low nanomolar concentration ranges at the desired targets as well as a favorable drug-likeness profile, may represent interesting compounds for drug development, especially for the treatment of motor disorders with accompanying non-motor symptoms such as sleep disruption in PD.

7 Zusammenfassung

Die Parkinson-Krankheit gehört zu den häufigsten neurodegenerativen Erkrankungen und ist ein schwerwiegendes Gesundheitsproblem in der alternden Gesellschaft. Parkinson-Patienten leiden an ausgeprägten motorischen Anomalien, wie zum Beispiel den Kardinalsymptomen Muskelzittern, Verlangsamung der Bewegung (Bradykinese), Muskelstarrheit, sowie Haltungsveränderungen. Dopaminerge Therapien, einschließlich L-DOPA sind in den frühen Stadien der Behandlung sehr wirksam, aber nach mehreren Jahren der Medikation beginnen motorische Fluktuationen und Dyskinesien zu erscheinen. Motorische Störungen sind häufig mit nichtmotorischen Symptomen verbunden, die hauptsächlich durch Neurodegeneration in nicht-dopaminergen Systemen entstehen. Zu den häufigsten gehören Depression, Schlafstörungen und Demenz. In Anerkennung der Parkinson-Krankheit als hochkomplexe und multifaktorielle Dysregulation, bei der sowohl motorische als auch nicht-motorische Symptome behandelt werden müssen, sind Forscher gezwungen neue innovative Therapiemöglichkeiten wie der Einsatz von MTLs zu verfolgen. Innerhalb des Multi-Targeting-Ansatzes wird eine große Vielzahl von MTLs beschrieben, die den H_3R-Antagonismus in Kombination mit anderen Neurotransmitter-regulierenden „Targets", d.h. GPCRs, Enzymen und Ionenkanälen, zeigen. Zu Beginn meiner Untersuchung wurde nur eine Handvoll von Leitstrukturen beschrieben, die H_3R-Affinität mit Enzymmodulation kombinieren. MTLs die gleichzeitig H_3R antagonisieren können, sowie A_1R und A_{2A}R wurden noch nicht synthetisiert. Das Design von H_3R/MAO B DTLs und H_3R/ A_1R/A_{2A}R MTLs wurde als potenziell innovativer therapeutischer Ansatz zur Behandlung von motorischen und nichtmotorischen Parkinson-Krankheit-Symptomen durchgeführt.

In Bezug auf duales H_3R/MAO B Liganden wurde der H_3R-Pharmakophor an Indanon-verwandte MAO B-Motive gebunden, was zur Entwicklung von drei Serien von H_3R/MAO B-DTLs führte. Unter den synthetisierten Indanon-DTLs beeinflussen verschiedene 5- und 6-Substitutionsmuster der Indanoneinheit stark die MAO B-Inhibierung, Selektivität und Zeitabhängigkeit der Inhibierung. Verbindungen, die die 2-Benzyliden-1-Indanon-Kernstruktur tragen zeigten, dass MAO B die Inhibierungsfähigkeiten zusammen mit der nanomolaren hH_3R-Affinitäten bevorzugt. Die Substitution der 5- und 6-Position der 2-Benzyliden-1-indanone mit lipophilen Substituenten ergab drei vielversprechende Kandidaten, die Inhibitionspotentiale für MAO B mit IC_{50}-Werten von 1931 nM bis 276 nM und hohen Affinitäten bei hH_3R zeigten (K_i < 50 nM)). Die Verbindung **3f** (MAO B IC_{50} = 276 nM, hH_3R K_i = 10 nM) zeigte die höchste Präferenz für MAO B gegenüber MAO A (SI>

36). Interessanterweise zeigten IC_{50}-Bestimmungen nach Präinkubation von Enzym und DTLs auch nanomolare MAO B-Potenz für **3f**-Strukturisomer **3e** (MAO B IC_{50} = 232 nM) und F-substituiertes Derivat **3d** (MAO B IC_{50} = 541 nM), was auf zeitabhängige Inhibitionsmodi hindeutet.

Auf der Suche nach irreversiblen MAO B-Liganden wurde die enge strukturelle Verwandtschaft der ersten Reihe von H_3R/MAO B-Liganden (**1a-e**) mit Propargylaminderivaten wie dem Anti-Parkinson-Präparat Rasagilin deutlich. Bemerkenswerterweise führte die reduktive Aminierung der Carbonyleinheit der Verbindung **1e** zur Synthese des Derivats **4**, das eine hohe Affinität zu hH_3R im niedrigen nanomolaren Konzentrationsbereich zeigte (K_i = 2.5 nM). Moderate inhibitorische Potenz für MAO B wurde bestimmt (IC_{50} = 1736 nM), da es sich aber als irreversibler Ligand erwies und ein gutes Selektivitätsprofil gegenüber MAO A (MAOs SI> 50) aufweist, könnte das neu beschriebene DTL sein ein guter Ausgangspunkt für weitere Optimierungen, insbesondere hinsichtlich der MAO B-Inhibitionsstärke.

Der allgemein akzeptierte Aminoalkyloxypropyl-H_3R-Pharmakophor, der sich durch die synthetisierten (2-Benzyliden)-1-Indanon-H_3R/MAO B-DTLs gezeigt hat, wurde in einen Adenosin-Antagonisten-Aryllindenopyrimidin-Kern für die Synthese von $H_3R/A_1R/A_{2A}R$-MTLs eingeführt.

Die erfolgreiche Einführung des H_3R-Pharmakophors in verschiedene Positionen von oxidierten (Verbindungen **11-16**) und nicht oxidierten / reduzierten (Verbindungen **5-10**) $A_1R/A_{2A}R$-Gerüst wurde durch (sub)nanomolare Affinität für alle MTLs bestätigt (0.28 nM < K_i (hH_3R) < 55 nM). Innerhalb dieser Reihe von Verbindungen zeigten diejenigen mit dem H_3R-Pharmakophor in 8-Position des Arylindenopyrimidin-Kerns (MTLs **6**, **10**, **12**, **16**) die vielversprechendsten Multitargeting-Merkmale mit Affinitäten in nanomolaren Konzentrationsbereichen bei den gewünschten Zielen. Diese vielversprechendsten Liganden zeigten eine $A_1R/A_{2A}R$-Affinität, mit einer leichten Bevorzugung für das $A_{2A}R$, was ein ähnliches Verhalten wie die Referenzverbindung JNJ-40255293 nahelegt. Mit diesem innovativen In-Vitro-Profil wurden zwei der potentesten Verbindungen **10** (K_i (hH_3R) = 11 nM, K_i (hA_1R) = 12 nM, K_i ($hA_{2A}R$) = 7.3 nM) und **12** (K_i (hH_3R)= 52 nM, K_i (hA_1R) = 11 nM, K_i ($hA_{2A}R$) = 4.0 nM) für In-Vivo-Untersuchungen ausgewählt, wobei entweder ihre anti-dyskinetische oder weckfördernde Wirksamkeit bei Nagern bewertet wurde. Eine leichte Verbesserung der L-DOPA-induzierten Dyskinesie wurde bei Ratten nach gleichzeitiger Verabreichung von **10** (1 mg kg^{-1}, i.p.) mit L-DOPA (6 mg kg^{-1}) beobachtet. Darüber hinaus war MTL **12** (2 mg kg^{-1}) in der Lage, den Wachheitsgrad bei Mäusen nach oraler Applikation zu erhöhen. Obwohl im Vergleich zu JNJ-40255293 höhere wirksame Dosen von **12** benötigt werden, da 1 mg/kg p.o. nicht zu einem signifikanten weckfördernden Effekt führt. Diese Studien beweisen die orale Bioverfügbarkeit von

Verbindung **12**, während beispielsweise pharmakokinetische Eigenschaften (d.h. Gastrointestinale Absorption, Blut-Hirn-Penetration) untersucht werden sollten, da sie die Unterschiede in der wirksamen Dosierung im Vergleich zu JNJ-40255293 erklären könnten.

Als Beweis für das Konzept führte die Kombination des H_3R einerseits mit MAO B und andererseits mit A_1- und A_{2A}-Rezeptoren zur Synthese von potenten MTLs, die ein vielversprechendes pharmakologisches Profil aufweisen.

Im Vergleich zu dem DTL H_3R/MAO B UCL-2190 oder kürzlich entdeckten Contilisant zeigen die synthetisierten Verbindungen (**1a-e**, **2a-c**, **3a-e** und **4**) eine verbesserte Hemmung bei MAO B mit reversibler und irreversibler Bindung, vergleichbar H_3R-Affinität im niedrigen nanomolaren Bereich. Obwohl eine Optimierung des vielversprechenden H_3R/MAO B zur Verbesserung der physikalisch-chemischen Eigenschaften und der Ähnlichkeit der Wirkstoffe durchgeführt werden muss, bot diese Studie einen hervorragenden Ausgangspunkt für die Untersuchung der dualen H_3R/MAO B-Kombination zur weiteren Optimierung und Entwicklung von potenten Multitarget-Wirkstoffen für die Behandlung der Parkinson-Krankheit. Auch die vielversprechendsten entworfenen $H_3R/A_1R/A_{2A}R$ MTLs, hierhin zum ersten Mal beschrieben, zeigen Affinitäten in den niedrigen nanomolaren Konzentrationsbereichen bei den gewünschten Zielen sowie ein günstiges Drug-likeness profil können interessante Verbindungen für die Arzneimittelentwicklung darstellen, insbesonderes für die Behandlung von motorischen Störungen mit begleitenden nichtmotorischen Symptomen wie Schlafstörungen bei der Parkinson-Krankheit.

8 Experimental section

8.1 Chemical experiments

8.1.1 General remarks

Reagents and solvents were commercially obtained from Sigma-Aldrich (Steinheim, Germany), VWR Chemicals (Darmstadt, Germany), Fisher Scientific (Hampton, USA), Alfa Aesar (Haverhill, USA) and Chemsolute (Renningen, Germany), Perkin Elmer Life and Analytical Sciences (Rodgau, Germany) and were used without further purifications (unless stated otherwise). ^{1}H-NMR and ^{13}C-NMR spectra were recorded on a Bruker AMX spectrometer (Bruker, Germany) at 300 and 75 MHz respectively, where $CDCl_3$ or DMSO-d_6 were used as a solvent. Tetramethylsilane was used as standard and chemical shifts are reported in part per million (ppm). Spin multiplicities are given as s (singlet), d (doublet), dd (doublet of doublets), t (triplet), q (quintet) or m (multiplet). Approximate coupling constants (J) in Hertz (Hz). Number and assignment of protons (aip, arylindenopyrimidine; ax, axial; bn, benzyl; cycloprop, cyclopropyl; eth, ethyl; eq, equatorial; ind, indanone; ph, phenyl; prop, propyl; pip, piperidine; pyr, pyrrolidine). Elementary analyses (C, H, N) were measured on a CHN-Rapid (Perkin-Elmer, Rodgau, Germany) and were within 0.4 % of the theoretical values for all final compounds. Electrospray ionization mass spectrometry (ESI-MS) was performed on an amaZon speed (Bruker, Rheinstetten, Germany) in positive polarity. Data are listed as mass number ([M+H$^+$]) and relative intensity (%). High-resolution mass spectra (HRMS) were run in electrospray ionization (ESI) mode. Melting points (m.p., uncorrected) were determined on a M-564 Büchi melting point apparatus (Büchi, Essen, Germany). Preparative column chromatography was performed on silica gel 60 M, 0.04-0.063 mm (Macherey-Nagel, Düren, Germany) and thin-layer chromatography (TLC) was carried out using pre-coated silica gel 60 with fluorescence indicator at UV 254 nm (Macherey-Nagel, Düren, Germany). The microwave oven used was a Biotage Initiator 2.0 (Biotagen, Uppsala, Sweden). The purity determination was measured on an HPLC apparatus (Knauer, Berlin Germany).

8.1.2 General procedures

N-Alkylation (A)[57,179]

An amine, an alkyl halide, potassium carbonate and a catalytic amount of potassium iodide were suspended and refluxed in absolute acetone for 24-72 h. The mixture was allowed to cool at room temperature and the inorganic components were filtered off. The filtrate was concentrated to dryness and the crude product was purified by distillation.

Chlorination of alcohols (B)[57,179]

The respective alcohol was dissolved in toluene and the solution was cooled to 0 °C (ice bath). An excess of thionyl chloride was added dropwise and, once the exothermic reaction had decayed, the mixtures was heated to 60 °C. After 3 h, the solvent and thionyl chloride were distilled off and the crude product was re-crystallized in ethanol.

Williamson ethers synthesis (C)[168,178]

A phenol, an alkyl halide, potassium carbonate or cesium carbonate and catalytic amounts of potassium iodide were reflux for 4-24 h hours, depending on nature of halide and reactivity of the phenol. After cooling the mixture to room temperature, inorganic salts were filtered off. The filtrate was concentrated to dryness and resuspended in dichloromethane. The crude product was taken up in methylene chloride and 2N NaOH solution. The organic phase was then washed with saturated NaCl-solution (brine), dried over magnesium sulfate, and concentrated under vacuum. Crude products were regularly purified with column chromatography on silica gel (methylene chloride: ammoniacal methanol = 9.5: 0.5).

Aldol condensations (D)[168,182]

A water solution of sodium hydroxide was added at room temperature to an ethanolic solution of the appropriately ketone and aldehyde. The formation of a precipitate occurred after different reaction times (from 10 min to 3 h). The solid was filtered off and extracted with dichloromethane and 2N NaOH solution. The crude material was dried over magnesium sulphate and concentrated under vacuum. Column chromatography (methylene chloride: ammoniacal methanol = 9.5: 0.5) was necessary to have pure compounds.

Catalytic hydrogenation of oximes and benzyl ethers (E)[195,260]

Oxime was hydrogenated in an autoclave (10 bar) at 50 °C, using Pd on carbon (10 wt. 10 %), whereas the cleavage of the benzyl ethers group was performed in a batch reactor at room temperature (hydrogen balloons were used). In both cases after 18 h stirring, the catalyst was removed by means of a filtration aid (Celite pad) and the filtrate concentrated under reduced pressure.

Reductive amination of ketones (F)

Method A with $NaBH(OAc)_3$[190,191]

Under nitrogen atmosphere, a primary amine and a ketone were stirred at room temperature in absolute solvent (THF, MeOH, DCE were used). After 2 h, triacetoxyborohydride was added and the mixture was stirred for another 3-48 h. In case of indirect reductive amination, the

triacetoxyborohydride was added after 24h and molecular sieves or magnesium sulfate were used as dehydrating agents for the formation of the imine. In both cases, different amounts of catalyst (acetic acid) and amine were used to optimize the reaction conditions.

Method B: with $NaCNBH_3$[192]

Ammonium acetate and sodium cyanoborohydride were added to a solution of the appropriate indanone in absolute ethanol in microwave vial. The mixture was stirred and heated at 130 °C for 2 min in a microwave reactor. The reaction mixture was concentrated to remove the solvent, treated with 2N NaOH until pH > 10, and extracted with dichloromethane. The organic phase was dried over magnesium sulfate, filtered, and concentrated under reduced pressure to give the crude product, which was purified with column chromatography (methylene chloride: ammoniacal methanol = 9.7: 0.3).

Ring closure of α, β-unsaturated ketones (G)[120,148]

Under argon atmosphere, an ethanolic solution of guanidine hydrochloride was neutralized by addition of sodium hydroxide. After 30 min, sodium chloride was filtered off, and the filtrate was added to a suspension of the appropriate 2-benzylidene-1-indanone derivative in ethanol. The reaction mixture was heated to reflux for 4-24 h. For the final compounds, the crude product was purified by column chromatography (methylene chloride: ammoniacal methanol = 9.7: 0.3) and re-crystallized from methanol or ethanol.

Debenzylation of ethers (H)[198]

Under inert atmosphere, the methoxy-pyrimidine derivative was refluxed in 48 % HBr and acetic acid. After cooling the mixture at room temperature, the crude product was taken up in ethyl acetate and sodium carbonate. The organic phase was then washed with saturated NaCl-solution and water, dried over magnesium sulfate, and concentrated under vacuum. The crude product was used without further purifications.

Oxidation of methylene groups (I)[120,148]

The non-oxidized arylindenopyrimidine derivatives were dissolved in DMF, and powder sodium hydroxide was added. The resulting mixture was heated to 80 °C and air was bubbled through the solution using a steel needle. After 4 h, the mixture was cooled to room temperature, and the crude product was taken up in dichloromethane and sodium carbonate. The organic phase was then washed several times with saturated NaCl-solution and water, dried over magnesium sulfate, and

concentrated to vacuum. The obtained solid was purified by column chromatography (methylene chloride: ammoniacal methanol = 9.5: 0.5) and washed one night in hexane.

Protection of alcohol function (L)[170]

5- or 6-hydroxy-1-indanone, benzyl bromide and potassium carbonate were dissolved in dimethylformamide. After 15 h at room temperature, the mixture was filtered, and the filtrate was diluted with ethyl acetate and washed with water and saturated solution of sodium chloride, dried over sodium sulfate, and concentrate under vacuum. The resulting oil was crystallized in ethyl ether.

8.1.3 1-(ω-Chloroalkyl)piperidine and pyrrolidine precursors

2-(Pyrrolidin-yl)ethan-1-ol (P1)[57,179]

According to procedure **A**, pyrrolidine (20.0 g, 0.3 mol), 2-chloroethan-1-ol (18.7 g, 0.2 mol), potassium carbonate (48.3 g, 0.4 mol) and potassium iodide (3.3 g, 0.02 mol) were stirred in 170 ml of absolute acetone for 24 h at reflux. The resulting yellow oil (22.5 g, 78 % yield) was obtained after distillation (20 mbar, 77 °C).

Chemical formula		$C_6H_{13}NO$
Molecular weight		115.18
^{1}H-NMR (DMSO-d_6)		δ 4.42 (br s, 1H, O*H*), 3.39-3.21 (t, J = 5.6, 2H, eth-1H_2), 2.51-2.36 (m, 4H, pyr-2,5H_2), 1.72-1.61 (m, 4H, Pyr-3,4H_2), 1.60-1.50 (quin, J = 6.5, 2H, eth-2H_2)
^{13}C-NMR (DMSO-d_6)		δ 59.5 (eth-1*C*), 59.3 (eth-2*C*), 56.5 (pyr-2,5*C*), 23.6 (pyr-3,4*C*)
ESI MS [M+H$^+$]	calc	116.10
	found	116.04 (100)

2-(Piperidin-yl)ethan-1-ol (P2)[57,179]

Piperidine (33.2 g, 0.4 mol), 2-chloroethan-1-ol (25.5 g, 0.3 mol), potassium carbonate (66.3 g, 0.5 mol) and potassium iodide (5.3 g, 0.03 mol) were stirred in 230 ml of acetone for 24 h at reflux. Purification was carried out according to procedure **A**. The resulting yellow oil was obtained after distillation (20 mbar, 85 °C).

Chemical formula	$C_7H_{15}NO$
Molecular weight	129.20
^{1}H-NMR (DMSO-d_6)	δ 3.93 (s, 1H, O*H*), 3.55-3.42 (t, J = 5.6, 2H, eth-1H_2), 2.41-2.31 (m, 6H, pip-2,6*H*, eth-2H_2), 1.54-1.39 (m, 4H, pip-3,5H_2)1.36-1.21 (m, 2H, pip-4$H_{eq/ax}$)
^{13}C-NMR (DMSO-d_6)	δ 59.7 (eth-1*C*), 59.3 (eth-2*C*), 57.1 (pip-2,6*C*), 25.9 (pip-3,5*C*), 22.5(pip-4*C*)

ESI MS [M+H$^+$]	calc found	130.12 130.10 (100)

3-(Piperidin-yl)propan-1-ol (P3) [57,179]

According to procedure **A**, piperidine (50.0 g, 0.6 mol), 3-chloropropan-1-ol (46.3 g, 0.5 mol), potassium carbonate (99.5 g, 0.7 mol) and potassium iodide (8.3 g, 0.05 mol) were suspended and refluxed in absolute acetone (300 ml) for 48 h. The purification by distillation (20 mbar, 98 °C) of the crude product resulted in a yellow oil (59.2 g, 67%).

Chemical formula		$C_8H_{17}NO$
Molecular weight		143.23
^{1}H-NMR (DMSO-d_6)		δ 4.42 (s, 1H, O*H*), 3.44-3.23 (t, J = 5.9, 2H, prop-1H_2), 3.38-3.33 (m, 2H, pip-2,6H_{eq}), 3.02-2.95 (m, 2H, prop-3H_2), 2.82-2.78 (m, 2H, pip-2,6H_{ax}), 1.88-1.64 (m, 7H, prop-2H_2, pip-3,5H_2, pip-4H_{eq}), 1.43-1.30 (m, 1H, pip-4H_{ax})
^{13}C-NMR (DMSO-d_6)		δ 57.98 (prop-1*C*), 53.57 (prop-3*C*), 51.95 (pip-2,6*C*), 26.38 (prop-2*C*), 22.27 (pip-3,5*C*), 21.45 (pip-4*C*)
ESI MS [M+H$^+$]	calc found	144.13 144.12 (100)

1-(2-Chloroethyl)pyrrolidine hydrochloride (P4)[57,179]

According to procedure **B**, alcohol **P1** (8.0 g, 0.07 mol), was suspended in toluene (100 ml). and stirred with an excess of thionyl chloride (10.8 ml, 0.2 mol). The crude product was re-crystallized from ethanol (white solid, 9.3 g, quantitative conversion).

Chemical formula		$C_6H_{12}ClN \cdot HCl$
Molecular weight		170.08
^{1}H-NMR (DMSO-d_6)		δ 10.89 (br s, 1H, NH^+), 3.56-3.48 (t, J = 6.2, 2H, eth-1H_2), 2.80-2.64 (m, 2H, pyr-2,5H_{eq}), 2.67-2.51 (m, 2H, eth-2H_2), 2.40-2.35 (m, 2H, pyr-2,5H_{ax}), 2.06-1.79 (m, 4H, pyr-3,4H_2)
^{13}C-NMR (DMSO-d_6)		δ 58.9 (eth-2*C*), 57.7 (pyr-2,5*C*), 42.5 (eth-1*C*), 23.6 (pyr-3,4*C*)
ESI MS [M+H$^+$]	calc found	134.07 134.10 (100)

1-(2-Chloroethyl)piperidine hydrochloride (P5)[57,179]

According to procedure **B**, alcohol **P2** (9.8 g, 0.07 mol), was suspended in toluene (100 ml) and stirred with an excess of thionyl chloride (10.8 ml, 0.2 mol). The crude product was re-crystallized from ethanol (beige solid, 10.3 g, quantitative conversion).

Chemical formula		$C_7H_{14}ClN \cdot HCl$
Molecular weight		184.1
^{1}H-NMR (DMSO-d_6)		δ 11.905 (br s, 1H, N*H*$^+$), 4.16-3.95 (t, J = 6.2, 2H, eth-1H_2), 3.51-3.39 (m, 4H, pip-2,6*H*), 2.81-2.07 (m, 2H, eth-2H_2), 1.91-1.63 (m, 5H, pip-3,5H_2, pip-4H_{eq}), 1.43-1.25 (m, 1H, pip-4H_{ax})
^{13}C-NMR (DMSO-d_6)		δ 59.2 (eth-2*C*), 56.3 (pip-2,6*C*), 42.5 (eth-1*C*), 25.9 (pip-3,5*C*), 24.5 (pip-4*C*)
ESI MS [M+H$^+$]	calc	148.08
	found	148.10 (100)

1-(3- Chloropropyl)piperidine hydrochloride (P6)[57,179]

According to procedure **B**, alcohol **P3** (11.4 g, 0.08 mol), was suspended in toluene (150 ml). and stirred with an excess of thionyl chloride (11.6 ml, 0.2 mol). The crude product was re-crystallized from ethanol (beige solid, 15.8 g, quantitative conversion).

Chemical formula		$C_8H_{16}ClN \cdot HCl$
Molecular weight		198.1
^{1}H-NMR (DMSO-d_6)		δ 10.96 (br s, 1H, N*H*$^+$), 3.74 (t, J = 6.4, 2H, prop-1H_2), 3.44-3.36 (m, 2H, pip-2,6H_{eq}), 3.13-3.02 (m, 2H, prop-3H_2), 2.93-2.75 (m, 2H, pip-2,6H_{ax}), 2.30-2.15 (m, 2H, prop-2H_2), 1.95-1.60 (m, 5H, pip-3,5H_2, pip-4H_{eq}), 1.47-1.25 (m, 1H, pip-4H_{ax})
^{13}C-NMR (DMSO-d_6)		δ 53.56 (prop-3*C*), 51.94 (pip-2,6*C*), 42.50 (prop-3*C*), 26.13 (prop-2*C*), 22.19 (pip-3,5*C*), 21.34 (pip-4*C*)
ESI MS [M+H$^+$]	calc	162.10
	found	162.10 (100)

8.1.4 1-(ω-Phenoxyalkyl)piperidine or pyrrolidine derivatives

4-(3-(Piperidin-1-yl)propoxy)benzaldehyde (P7)[168]

4-Hydroxybenzaldehyde (12.2 g, 0.1 mol), chloride **P6** (9.9 g, 0.05 mol), potassium carbonate (22.1 g, 0.2 mol) and potassium iodate (0.83 g, 0.005 mol) were reflux in absolute acetone (245 ml) for 18 h according to procedure **C**. An orange oil was obtained in a yield of 82% (10.1 g).

Chemical formula	$C_{15}H_{21}NO_2$
Molecular weight	247.34
^{1}H-NMR ($CDCl_3$)	δ 9.86 (s, 1H, CO*H*), 7.89-7.82 (m, 2H, ph-3,7*H*), 7.16-7.07 (m, 2H, 4,6*H*), 4.16-4.06 (t, 2H, J= 6.6 Hz, prop-1*H*), 2.43-2.34 (m, 2H, prop-3*H*), 2.34-2.21 (m, 4H, pip-2,6*H*), 1.95-1.76 (m, 2H, prop-2*H*), 1.55-1.43 (m, 4H, pip-3,5*H*), 1.42-1.30 (m, 2H, pip-4*H*)

ESI MS [M+H⁺]	calc found	248.17 248.20 (100)

Cyclopropyl(4-(3-(piperidin-1-yl)propoxy)phenyl)methanone hydrochloride (UCL-2190)[181]

Under inert atmosphere, alcohol **P3** (0.5 g, 3.1 mmol) was treated at room temperature with an excess of sodium hydride (0.4 g, 20 mmol, 60% suspension mineral oil). After 3h, the freshly prepared ethanolate was heated with cyclopropyl-4-fluorophenyl methanone (0.8 g, 5.1 mol) in acetonitrile for 24 h under reflux. Purification was performed according to procedure **C** and a white solid (0.6 g, 62 %) was obtained after formation of the hydrochloride salt.

Chemical formula		$C_{18}H_{25}NO_2 \cdot HCl$
Molecular weight		323.86
^{1}H-NMR (DMSO-d_6)		δ 10.12 (br s, 1H, N*H*⁺), 7.99-7.90 (m, 2H, ph-3,7*H*), 7.03-6.94 (m, 2H, ph-4,6*H*), 4.21-4.09 (t, 2H, J=5.8, prop-1H_2), 3.62-3.37 (m, 2H, prop-3H_2), 3.29-3.16 (m, 2H, pip-2,6H_{eq}), 3.02-2.81 (m, 2H, pip-2,6H_{ax}), 2.79-2.69 (m, 1H, COC*H*CH$_2$), 2.23-2.10 (m, 2H, prop-2H_2), 2.01-1.30 (m, 6H, pip-3,5H_2, pip-4*H*), 1.14-1.01 (m, 4H, cycloprop-2,3H_2)
^{13}C-NMR (DMSO-d_6)		δ 204.6 (*C*O), 162.4 (ph-5*C*), 129.7 (Ph-3,7*C*), 129.4 (ph-6,4*C*), 128.2 (Ph-2*C*), 73.1 (prop-1*C*), 58.5 (prop-3*C*), 57.1 (pip-2,6*C*) 27.7 (prop-2*C*), 25.9 (pip-3,5*C*), 24.5 (pip-4*C*), 18.1 (CO*C*HCH$_2$), 12.6 (cycloprop-2,3(*C*H$_2$)$_2$)
ESI HRMS [M+H⁺]	calc found	288.1964 288.1958 (100)
Analysis	calc found	C 66.76 %, H 8.09 %, N 4.33 % C 67.06 %, H 8.11 %, N 4.29 %
Melting point		174.6 °C

6-(2-(Pyrrolidin-1-yl)ethoxy)-2,3-dihydro-1*H*-inden-1-one hydrochloride (1a)[168]

Chloride **P4** (0.3 g, 1.8 mmol), 6-hydroxy-indanone (0.2 g, 1.4 mmol), potassium carbonate (0.6 g, 4.6 mmol) and potassium iodide (0.02 g, 0.1 mmol) were suspended in absolute acetone (25 ml) for 24 h. Purification was carried out following procedure **C** and the resulting product was crystallized as hydrochloride from 1,4-dioxane (1.65 g, 76 %).

Chemical formula	$C_{15}H_{19}NO_2 \cdot HCl$
Molecular weight	281.12

^{1}H-NMR (D_2O)		δ 10.23 (br s, 1H, N*H*$^+$), 7.48-7.41 (d, 1H, J= 8.5, ph$_{ind}$-7*H*), 7.31-7.25 (dd, 1H, J = 8.5, ph$_{ind}$-5*H*), 7.13-7.08 (d, 1H, J= 2.5, ph$_{ind}$-4*H*), 4.38-4.25 (t, 2H, J= 5.0, eth-1*H*$_2$), 3.72-3.51 (m, 4H, COC*H*$_2$, COCH$_2$C*H*$_2$), 3.20-3.05 (m, 2H, eth-2*H*$_2$), 3.04-2.92 (m, 2H, pyr-2,5*H*$_{eq}$), 2.70-2.57 (m, 2H, pyr-2,5*H*$_{ax}$), 2.21-1.80 (m, 4H, pyr-3,4*H*$_2$)
^{13}C-NMR (DMSO-*d*$_6$)		δ 206.4 (*C*O), 157.6 (ph$_{ind}$-6*C*), 148.7 (CO*C*ph$_{ind}$-7C), 138.4 (COCH$_2$CH$_2$*C*), 128.4 (ph$_{ind}$-7*C*), 123.9 (ph$_{ind}$-6*C*), 106.4 (ph$_{ind}$-4*C*), 64.3 (prop-1*C*), 54.0 (pyr-2,5*C*), 52.1 (prop-2*C*), 37.2 (CO*C*H$_2$), 25.3 (COCH$_2$*C*H$_2$), 23.0 (pyr-3,4*C*)
ESI HRMS [M+H$^+$]	calc	246.1494
	found	246.1495 (100)
Analysis	calc	C 63.94 %, H 7.15 %, N 4.97 %
	found	C 63.43 %, H 7.06 %, N 4.98 %
Melting point		195.2 °C

6-(3-(Piperidin-1-yl)propoxy)-2,3-dihydro-1*H*-inden-1-one (1b)[168]

Chloride **P6** (1.8 g, 0.01 mol), 6-hydroxy-indanone (2.0 g, 0.01 mol), potassium carbonate (2.9 g, 0.03 mol) and potassium iodide (0.2 g, 0.001 mol) were suspended in absolute acetone (100 ml) for 15 h. Purification was carried out following procedure **C** and resulted in beige solid (2.2 g, 81 %).

Chemical formula		$C_{17}H_{23}NO_2$
Molecular weight		273.37

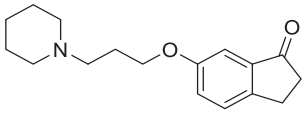

^{1}H-NMR (DMSO-*d*$_6$)		δ 7.64-7.57 (d, 1H, J= 8.7, ph$_{ind}$-7*H*), 7.28-7.21 (dd, 1H, J= 8.4, ph$_{ind}$-5*H*), 7.09-7.04 (m, 1H, J= 2.28, ph$_{ind}$-4*H*), 4.07-3.97 (t, 2H, J= 6.4, prop-1*H*$_2$), 3.06-2.94 (t, 2H, J= 5.3, CO*C*H$_2$), 2.68-2.59 (m, 2H, COCH$_2$*C*H$_2$), 2.42-2.33 (t, 2H, J = 6.9, prop-3*H*$_2$), 2.32-2.20 (m, 4H, pip-2,6*H*), 1.93-1.77 (q, 2H, J = 6.7, prop-2*H*$_2$), 1.56-1.43 (m, 4H, pip-3,5*H*$_2$), 1.42-1.30 (m, 2H, pip-4*H*)
^{13}C-NMR (DMSO-*d*$_6$)		δ 208.7 (*C*O), 160.9 (ph$_{ind}$-6*C*), 150.3 (CO*C*ph$_{ind}$-7C), 140.5 (COCH$_2$CH$_2$*C*), 130.5 (ph$_{ind}$-7*C*), 128.1 (ph$_{ind}$-5*C*), 108.1 (ph$_{ind}$-4*C*), 69.0 (prop-1*C*), 57.7 (prop-3*C*), 56.8 (pip-2,6*C*), 39.3 (CO*C*H$_2$), 28.8 (COCH$_2$*C*H$_2$), 28.2 (pip-3,5*C*), 27.3 (prop-2*C*), 26.8 (pip-4*C*)
ESI HRMS [M+H$^+$]	calc	274.1807
	found	274.1800 (100)
Analysis	calc	C 74.68 %, H 8.48 %, N 5.12 %
	found	C 74.76 %, H 8.68 %, N 5.06 %
Melting point		59.1 °C

5-(2-(Pyrrolidin-1-yl)ethoxy)-2,3-dihydro-1*H*-inden-1-one hydrochloride (1c)[168]

Chloride **P4** (0.3 g, 1.8 mmol), 5-hydroxy-indanone (2.2 g, 1.5 mmol), potassium carbonate (0.6 g, 4.7 mmol) and potassium iodide (0.2 g, 0.2 mmol) were suspended in absolute acetone (40 ml) for 18 h. Purification was carried out following procedure **C** and the resulting product was crystallized as hydrochloride from 1,4-dioxane (0.3 g, 75 %).

Chemical formula		$C_{15}H_{19}NO_2 \cdot HCl$
Molecular weight		281.12
^{1}H-NMR (D_2O)		δ 10.13 (br s, 1H, N*H*$^+$), 7.59-7.53 (d, 1H, J= 8.6, ph$_{ind}$-7*H*), 7.07-7.01 (m, 1H, ph$_{ind}$-4*H*), 6.99-6.91 (dd, 1H, J= 8.6, ph$_{ind}$-6*H*), 4.43-4.33 (t, 2H, J= 5.0, eth-1*H*$_2$), 3.73-3.58 (m, 4H, COC*H*$_2$, COCH$_2$C*H*$_2$), 3.24-3.07 (m, 2H, eth-2*H*$_2$), 3.06-2.98 (m, 2H, pyr-2,5*H*$_{eq}$), 2.67-2.55 (m, 2H, pyr-2,5*H*$_{ax}$), 2.20-1.86 (m, 4H, pyr-3,4*H*$_2$)
^{13}C-NMR (DMSO-*d*$_6$)		δ 204.7 (*C*O), 163.3 (ph$_{ind}$-5*C*), 158.5 (CO*C*ph$_{ind}$-7*C*), 130.8 (COCH$_2$CH$_2$*C*), 125.01(ph$_{ind}$-7*C*), 116.1 (ph$_{ind}$-4*C*), 111.4 (ph$_{ind}$-6*C*), 64.1 (prop-1*C*), 54.1 (pyr-2,5*C*), 52.8 (prop-2*C*), 36.4 (CO*C*H$_2$), 25.8 (COCH$_2$*C*H$_2$), 22.9 (pyr-3,4*C*)
ESI HRMS [M+H$^+$]	calc	246.1494
	found	246.1484 (100)
Analysis	calc	C 63.94 %, H 7.15 %, N 4.97 %
	found	C 63.69 %, H 7.09 %, N 5.03 %
Melting point		193.8 °C

5-(2-(Piperidin-1-yl)ethoxy)-2,3-dihydro-1*H*-inden-1-one hydrochloride (1d)[168]

Chloride **P5** (0.6 g, 4.0 mmol), 5-hydroxy-indanone (0.4 g, 2.7 mmol), potassium carbonate (1.2 g, 8.6 mmol) and potassium iodide (0.04 g, 0.3 mmol) were suspended in absolute acetone (45 ml) for 18 h. Purification was carried out following procedure **C** and the resulting product was crystallized as hydrochloride from 1,4-dioxane (0.6 g, 72 %).

Chemical formula	$C_{16}H_{21}NO_2 \cdot HCl$
Molecular weight	295.80
^{1}H-NMR (D_2O)	δ 10.22 (br s, 1H, N*H*$^+$), 7.51-7.43 (d, 1H, J= 8.6, ph$_{ind}$-7*H*), 7.28-7.21 (m, 1H, ph$_{ind}$-4*H*), 6.96-6.88 (dd, 1H, J=8.5, ph$_{ind}$-6*H*), 4.43-4.31 (t, 2H, J= 5.0, eth-1*H*$_2$), 3.65-3.42 (m, 4H, COC*H*$_2$, COCH$_2$C*H*$_2$), 3.10-2.88 (m, 4H, pip-2,6*H*$_{eq}$, eth-2*H*$_2$), 2.64-2.50 (m, 2H, pip-2,6*H*$_{ax}$), 2.03-1.30 (m, 6H, pip-3,5*H*$_2$, pip-4*H*)
^{13}C-NMR (DMSO-*d*$_6$)	δ 204.7 (*C*O), 163.3 (ph$_{ind}$-5*C*), 158.5 (CO*C*ph$_{ind}$-7*C*), 130.7 (COCH$_2$CH$_2$*C*), 125.1 (ph$_{ind}$-7*C*), 116.1 (ph$_{ind}$-4*C*), 111.4 (ph$_{ind}$-6*C*), 66.1 (prop-1*C*), 54.9 (prop-2*C*), 52.9 (pip-2,6*C*), 36.4 (CO*C*H$_2$), 25.8 (COCH$_2$*C*H$_2$), 22.6 (pip-3,5*C*), 21.5 (pip-4*C*)

ESI HRMS [M+H$^+$]	calc	260.1651
	found	260.1642 (100)
Analysis	calc	C 64.97 %, H 7.50 %, N 4.74 %
	found	C 64.52 %, H 7.55 %, N 4.88 %
Melting point		60.2 °C

5-(3-(Piperidin-1-yl)propoxy)-2,3-dihydro-1*H*-inden-1-one (1e)[168]

Chloride **P6** (0.6 g, 3.2 mmol), 5-hydroxy-indanone (0.4 g, 2.7 mmol), potassium carbonate (1.2 g, 8.6 mmol) and potassium iodide (0.04 g, 0.27 mmol) were suspended in absolute acetone (45 ml) for 24 h. Purification was carried out following procedure **C** and the product was crystallized in a mixture of toluene/ethanol (0.6 g, 85 %).

Chemical formula		$C_{17}H_{23}NO_2$
Molecular weight		273.38
^{1}H-NMR (DMSO-d_6)		δ 7.64-7.57 (d, 1H, J=8.5, ph-7*H*), 7.18-7.11 (m, 1H, ph-4*H*), 7.05-6.96 (dd, 1H, J=8.5, ph-6*H*), 4.24-4.11 (t, 2H, J= 6.4, prop-1H_2), 3.19-3.04 (t, 2H, J= 6.0, COCH_2), 2.76-2.61 (m, 2H, $COCH_2CH_2$), 2.51-2.40 (t, 2H, J= 7.3, prop-3H_2), 2.40-2.28 (m, 4H, pip-2,6*H*), 2.03-1.88 (q, 2H, J= 6.7, prop-2H_2), 1.65-1.51 (m, 4H, pip-3,5H_2), 1.50-1.38 (m, 2H, pip-4*H*)
^{13}C-NMR (DMSO-d_6)		δ 204.6 (*C*O), 164.1 (ph-5*C*), 158.6 (COC ph-7*C*), 130.4 ($COCH_2CH_2C$), 124.9 (ph-7*C*), 115.9 (ph-4*C*), 111.1 (ph-6*C*), 66.3 (prop-1*C*), 53.4 (prop-3*C*), 52.2 (pip-2,6*C*), 36.1 ($COCH_2$), 25.8 ($COCH_2CH_2$), 23.5 (prop-2*C*), 22.7 (pip-3,5*C*), 21.7 (pip-4*C*)
ESI HRMS [M+H$^+$]	calc	274.1807
	found	274.0000 (100)
Analysis	calc	C 74.69 %, H 8.48 %, N 5.12 %
	found	C 74.82 %, H 8.58 %, N 5.01 %
Melting point		192.1 °C

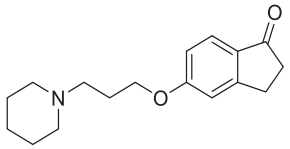

8.1.5 2-Benzylidene-1-indanone derivatives

(*E*)-2-Benzylidene-6-(2-(piperidin-1-yl)ethoxy)-2,3-dihydro-1*H*-inden-1-one (2a)[168]

Indanone **1d** (0.2 g, 0.7 mmol), benzaldehyde (0.08 g, 0.8 mmol) and sodium hydroxide (0.04 g, 0.9 mmol) were dissolved in ethanol (3 ml) and treated according to procedure **D** to give a light-yellow solid (0.2 g, 90 %).

Chemical formula		$C_{23}H_{25}NO_2$
Molecular weight		347.46
^{1}H-NMR (DMSO-d_6)		δ 7.86-7.72 (m, 2H, ph^1-2,6*H*), 7.63-7.41 (m, 5H, ph^1-C*H*, ph$_{ind}$-4,7*H*, ph^1-3,5*H*), 7.37-7.20 (m, 2*H*, ph^1-4*H*, ph$_{ind}$-6*H*),

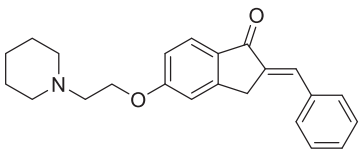

		4.20-4.10 (t, 2H, J= 5.5, eth-1H_2), 4.04 (s, 2H, C=CCH_2), 2.76-2.62 (t, 2H, J= 5.2, eth-2H_2), 2.48-2.32 (m, 4H, pip-2,6*H*), 1.60-1.44 (m, 4H, pip-3,5H_2), 1.43-1.29 (m, 2H, pip-4*H*)
^{13}C-NMR (DMSO-d_6)		δ 193.1 (*C*O), 158.4 (ph_{ind}-5*C*), 142.6 (CO*C*ph_{ind}-7*C*), 138.3 (ph^1-*C*H), 135.8 (C=CCH_2*C*), 134.8 (CO*C*=C), 132.7 (ph^1-1*C*), 130.7 (ph^1-2,6*C*), 129.8 (ph^1-4*C*), 128.9 (ph^1-3,5*C*), 127.5 (ph_{ind}-7*C*), 123.9 (ph_{ind}-4*C*), 106.3 (ph_{ind}-4*C*), 66.0 (prop-1*C*), 57.2 (prop-2*C*), 54.3 (pip-2,6 *C*), 31.2 (C=CCH_2), 25.5 (pip-3,5*C*), 25.9 (pip-4*C*)
ESI HRMS [M+H$^+$]	calc	348.1964
	found	348.1964 (100)
Analysis	calc	C 79.51 %, H 7.25 %, N 4.03 %
	found	C 79.23 %, H 7.17 %, N 3.88 %
Melting point		130.1 °C

(*E*)-2-Benzylidene-6-(3-(piperidin-1-yl)propoxy)-2,3-dihydro-1*H*-inden-1-one (2b)[168]

Indanone **1b** (0.7 g, 2.5 mmol), benzaldehyde (0.3 g, 2.6 mmol) and sodium hydroxide (0.1 g, 3.1 mmol) were dissolved in ethanol (5 ml) and treated according to procedure **D** to give a light-yellow solid (0.7 g, 80 %).

Chemical formula		$C_{24}H_{27}NO_2$
Molecular weight		361.49
^{1}H-NMR (DMSO-d_6)		δ 7.88-7.80 (m, 2H, ph^1-2,6*H*), 7.65-7.47 (m, 5H, ph^1-C*H*, ph_{ind}-5,7*H*, ph^1-3,5*H*), 7.38-7.31 (dd, 1H, J = 8.3, ph^1-4*H*), 7.30-7.27 (d, 1H, J = 2.4, ph_{ind}-4*H*), 4.18-4.10 (t, 2H, J = 6.4, prop-1H_2), 4.09 (s, 2H, C=CCH_2), 2.48-2.40 (t, 2H, J = 7.3, prop-3H_2), 2.40-2.30 (m, 4H, pip-2,6*H*), 1.99-1.87 (q, 2H, J = 6.8, prop-2H_2), 1.61-1.48 (m, 4H, pip-3,5H_2), 1.47-1.35 (m, 2H, pip-4*H*)
^{13}C-NMR (DMSO-d_6)		δ 193.1 (*C*O), 158.5 (ph_{ind}-6*C*), 142.2 (CO*C*ph_{ind}-7C), 138.3 (ph^1-*C*H), 135.8 (C=CCH_2*C*), 134.8 (CO*C*=C), 132.6 (ph^1-1*C*), 130.7 (ph^1-2,6*C*), 129.8 (ph^1-4*C*), 128.9 (ph^1-3,5*C*), 127.5 (ph_{ind}-7*C*), 123.8 (ph_{ind}-5*C*), 106.1 (ph_{ind}-4*C*), 66.4 (prop-1*C*), 55.0 (prop-3*C*), 54.1 (pip-2,6*C*), 31.1 (C=CCH_2), 26.1 (prop-2*C*), 25.5 (pip-3,5*C*), 24.1 (pip-4*C*)
ESI HRMS [M+H$^+$]	calc	362.2120
	found	362.2117 (100)
Analysis	calc	C 79.74 %, H 7.53 %, N 3.87 %
	found	C 79.41 %, H 7.31 %, N 3.78 %
Melting point		119.9 °C

(*E*)-2-Benzylidene-5-(3-(piperidin-1-yl)propoxy)-2,3-dihydro-1*H*-inden-1-one (2c)[168]

Indanone **1e** (0.2 g, 0.8 mmol), benzaldehyde (0.08 g, 0.81 mmol) and sodium hydroxide (0.03 g, 0.9 mmol) were dissolved in ethanol (2.5 ml) and treated according to procedure **D** to give a light-yellow solid (0.2 g, 86 %).

Chemical formula		$C_{24}H_{27}NO_2$
Molecular weight		361.49
^{1}H-NMR (DMSO-d_6)		δ 7.80-7.74 (m, 2H, ph^1-2,6*H*), 7.74-7.41 (m, 5H, ph^1-C*H*, ph$_{ind}$-4,7*H*, ph^1-3,5*H*), 7.19-7.14 (d, 1H, J = 1.9, ph^1-4*H*), 7.06-6.98 (dd, 1H, J = 8.5, ph$_{ind}$-6*H*), 4.18-4.11 (t, 2H, J = 6.4, prop-1*H*$_2$), 4.07 (s, 2H, C=CC*H*$_2$), 2.45-2.35 (t, 2H, J = 6.9, prop-3*H*$_2$), 2.35-2.22 (m, 4H, pip-2,6*H*), 1.98-1.82 (q, 2H, J = 6.7, prop-2*H*$_2$), 1.55-1.45 (m, 4H, pip-3,5*H*$_2$), 1.44-1.31 (m, 2H, pip-4*H*)
^{13}C-NMR (DMSO-d_6)		δ 191.5 (*C*O), 164. (ph$_{ind}$-5*C*), 152.9 (CO*C*ph$_{ind}$-7C), 135.7 (ph^1-*C*H), 135.0 (C=C*C*H$_2$), 131.4 (CO*C*=C), 130.5 (ph^1-2,6C), 130.3 (ph^1-1*C*), 129.5 (ph^1-4*C*), 128.9 (ph^1-3,5*C*), 125.4 (ph$_{ind}$-7*C*), 115.7 (ph$_{ind}$-4*C*), 110.6 (ph$_{ind}$-*6*C), 66.6 (prop-1*C*), 54.9 (prop-3*C*), 54.7 (pip-2,6*C*), 31.9 (C=C*C*H$_2$), 26.1 (pip-3,5*C*), 25.6 (prop-2*C*), 24.1 (pip-4*C*)
ESI HRMS [M+H$^+$]	calc	362.2120
	found	362.2120 (100)
Analysis	calc	C 79.74 %, H 7.53 %, N 3.87 %
	found	C 79.81 %, H 7.33 %, N 3.57 %
Melting point		110.7 °C

(*E*)-2-(4-(3-(Piperidin-1-yl)propoxy)benzylidene)-2,3-dihydro-1*H*-inden-1-one (3a)[168]

1-Indanone (0.5 g, 4.0 mmol), **P7** (1 g, 4.0 mmol) and sodium hydroxide (0.2 g, 5.0 mmol) were dissolved in ethanol (10 ml) and treated according to procedure **D** to give a light-yellow solid (1.1 g, 81 %).

Chemical formula		$C_{24}H_{27}NO_2$
Molecular weight		361.49
^{1}H-NMR (DMSO-d_6)		δ 7.84-7.80 (d, 1H, J = 7.6, ph$_{ind}$-7*H*), 7.61-7.45 (m, 5H, ph^1-2,6*H*, ph$_{ind}$-4,5*H*, ph^1-C*H*), 7.39-7.31 (m, 1*H*, ph$_{ind}$-6*H*), 6.94-6.86 (m, 2H, ph^1-3,5*H*), 4.07-3.98 (t, 2H, J= 6.2, prop-1*H*$_2$), 3.94 (s, 2H, C=CC*H*$_2$), 2.64-2.51 (t, 2H, J= 7.7, prop-3*H*$_2$), 2.51-2.31 (m, 4H, pip-2,6*H*), 2.10-1.96 (q, 2H, J= 6.7, prop-2*H*$_2$), 1.69-1.54 (m, 4H, pip-3,5*H*$_2$), 1.49-1.33 (m, 2H, pip-4*H*)

^{13}C-NMR ($CDCl_3$)		δ 193.1 (*C*O), 158.5 (ph^1-4*C*), 142.5 (CO*C*ph$_{ind}$-7C), 138.4 (ph^1-*C*H), 135.8 (C=C*C*H$_2$*C*), 134.8 (ph^1-2,6*C*), 132.5 (CO*C*=C), 130.7 (ph^1-1*C*), 129.7 (ph$_{ind}$-7*C*), 128.9 (ph$_{ind}$-4*C*), 127.5 (ph$_{ind}$-6*C*), 123.8 (ph$_{ind}$-5*C*), 106.1 (ph^1-3,5*C*), 66.3 (prop-1*C*), 55.0 (prop-3*C*), 54.1 (pip-2,6*C*), 31.2 (C=*C*CH$_2$), 26.2 (prop-2*C*), 25.6 (pip-3,5*C*), 24.1 (pip-4*C*)
ESI HRMS [M+H$^+$]	calc	362.2120
	found	362.2116 (100)
Analysis	calc	C 79.74 %, H 7.53 %, N 3.87 %
	found	C 79.72 %, H 7.82 %, N 3.58 %
Melting point		113.85 °C

(*E*)-6-Methoxy-2-(4-(3-(piperidin-1-yl)propoxy)benzylidene)-2,3-dihydro-1*H*-inden-1-one (3b)[168]

6-Methoxy-1-indanone (0.6 g, 3.7 mmol), **P7** (9.1 g, 3.7 mmol) and sodium hydroxide (0.2 g, 5.0 mmol) were dissolved in ethanol (10 ml) and treated according to procedure **D** to give a light-yellow solid (1.2 g, 86 %).

Chemical formula	$C_{25}H_{29}NO_3$
Molecular weight	391.51

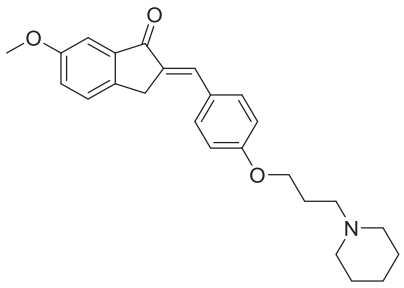

^{1}H-NMR (DMSO-*d*$_6$)		δ 7.79.7.69 (d, 2H, J= 8.6, ph^1-2,6*H*), 7.62-7.55 (d, 1H, J= 8.3, ph$_{ind}$-7*H*), 7.52 (br s, 1*H*, ph^1-C*H*), 7.33-7.19 (d, 2H, J= 8.3, ph^1-3,5*H*), 7.11-7.0 (d, 2H, J = 8.5, ph$_{ind}$-4,5*H*), 4.17-4.03 (t, 2H, J = 6.3, prop-1*H*$_2$), 3.99 (s, 2H, C=CC*H*$_2$), 3.83 (s, 3H, OC*H*$_3$), 2.46-2.34 (t, 2H, J = 6.9, prop-3*H*$_2$), 2.34-2.18 (m, 4H, pip-2,6*H*), 1.97-1.79 (q, 2H, J = 6.6, prop-2*H*$_2$), 1.60-1.43 (m, 4H, pip-3,5*H*$_2$), 1.43-1.25 (m, 2H, pip-*4H*)
^{13}C-NMR (DMSO-*d*$_6$)		δ 193.0 (*C*O), 160.0 (ph^1-4*C*), 159.1 (ph$_{ind}$-6*C*), 142.4 (CO*C*ph$_{ind}$-7C), 138.7 (ph^1-*C*H), 133.2 (C=C*C*H$_2$*C*), 132.7 (ph^1-2,6*C*), 132.7 (CO*C*=C), 127.4 (ph^1-1*C*), 127.3 (ph$_{ind}$-7*C*), 123.1 (ph$_{ind}$-4*C*), 115.0 (ph^1-3,5*C*), 105.5 (ph$_{ind}$-5*C*), 66.2 (prop-1*C*), 55.5 (prop-3*C*), 55.0 (O*C*H$_3$), 54.1 (pip-2,6*C*), 31.2 (C=*C*CH$_2$), 26.2 (prop-2*C*), 25.6 (pip-3,5*C*), 24.1 (pip-4*C*)
ESI HRMS [M+H$^+$]	calc	392.2226
	found	392.2225 (100)
Analysis	calc	C 76.70 %, H 7.47 %, N 3.58 %
	found	C 76.57 %, H 7.47 %, N 3.39 %
Melting point		118.7 °C

(*E*)-5-Methoxy-2-(4-(3-(piperidin-1-yl)propoxy)benzylidene)-2,3-dihydro-1*H*-inden-1-one (3c)[168]

5-Methoxy-1-indanone (0.3 g, 2.0 mmol), **P7** (0.5 g, 2.0 mmol) and sodium hydroxide (0.1 g, 3.0 mmol) were dissolved in ethanol (3 ml) and treated according to procedure **D** to give a light-yellow solid (0.6 g, 81 %).

Chemical formula		$C_{25}H_{29}NO_3$
Molecular weight		391.51

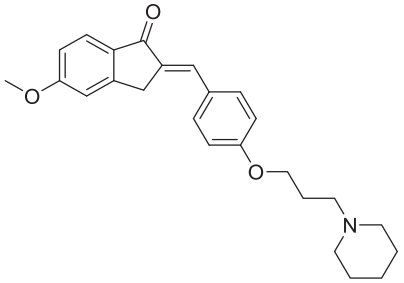

^{1}H-NMR ($CDCl_3$)		δ 7.81-7.42 (d, 1H, J = 8.4, ph_{ind}-7*H*), 7.58-7.47(m, 3H, ph^1-2,6*H*, ph^1-C*H*), 6.95-6.63 (m, 4*H*, ph_{ind}-4*H*, ph_{ind}-6*H*, ph^1-3,5*H*), 4.07-3.97 (t, 2H, J = 6.3, prop-1H_2), 3.88 (s, 2H, C=CCH_2), 3.83 (s, 3H, OCH_3), 2.56-2.47 (t, 2H, J = 7.2, prop-3H_2), 2.46-2.33 (m, 4H, pip-2,6*H*), 2.07-1.94 (q, 2H, J = 7.9, prop-2H_2), 1.68-1.52 (m, 4H, pip-3,5H_2), 1.47-1.34 (m, 2H, pip-4*H*)
^{13}C-NMR (DMSO-d_6)		δ 191.5 (*C*O), 164.7 (ph^1-4*C*), 159.8 (ph_{ind}-5*C*), 152.7 (CO*C*ph_{ind}-7C), 133.0 (ph^1-*C*H), 132.4 (ph^1-2,6*C*), 131.5 (C=CCH_2*C*), 130.7 (CO*C*=C), 127.5 (ph^1-1*C*), 125.2 (ph_{ind}-7*C*), 115.2 (ph_{ind}-4*C*), 114.7 (ph^1-3,5*C*), 110.1 (ph_{ind}-6*C*), 66.1(prop-1*C*), 55.7 (prop-3*C*), 55.0 (OCH_3), 54.1 (pip-2,6*C*), 31.9 (C=*C*CH_2), 26.2 (prop-2*C*), 25.6 (pip-3,5*C*), 24.1 (pip-4*C*)
ESI HRMS [M+H$^+$]	calc	392.2226
	found	392.2222 (100)
Analysis	calc	C 76.70 %, H 7.47 %, N 3.58 %
	found	C 76.52 %, H 7.61 %, N 3.49 %
Melting point		116.6 °C

(*E*)-5-Fluoro-2-(4-(3-(piperidin-1-yl)propoxy)benzylidene)-2,3-dihydro-1*H*-inden-1-one (3d)[168]

5-Fluoro-1-indanone (0.7 g, 4.0 mmol), **P7** (1.1 g, 4.0 mmol) and sodium hydroxide (0.2 g, 6.0 mmol) were dissolved in ethanol (3 ml) and treated according to procedure **D** to give a light-yellow solid (1.2 g, 80 %).

Chemical formula	$C_{24}H_{26}FNO_2$
Molecular weight	379.48

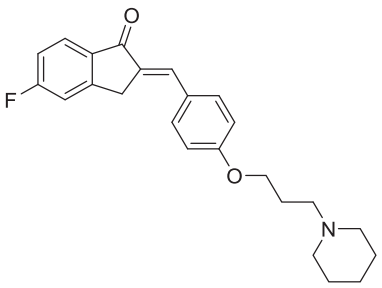

^{1}H-NMR (DMSO-d_6)		δ 7.88-7.79 (m, 1H, ph_{ind}-7*H*), 7.58-7.50 (m, 3H, ph^{1}-2,6*H*, ph^{1}-C*H*), 7.17-7.10 (dd, 1*H*, J = 8.4, ph_{ind}-4*H*), 7.09-6.99 (td, 1H, J = 8.9, ph_{ind}-6*H*), 6.96-6.86 (m, 2H, ph^{1}-3,5*H*), 4.10-3.96 (t, 2H, J = 6.3, prop-1H_2), 3.93 (s, 2H, C=CCH_2), 2.59-2.46 (t, 2H, J = 7.7, prop-3H_2), 2.46-2.28 (m, 4H, pip-2,6*H*), 2.08-1.91 (q, 2H, J = 7.1, prop-2H_2), 1.69-1.51 (m, 4H, pip-3,5H_2), 1.49-1.32 (m, 2H, pip-4*H*)
^{13}C-NMR (DMSO-d_6)		δ 192.6 (*C*O), 165.9 (ph^{1}-4*C*), 160.4 (ph_{ind}-5*C*), 152.3 (CO*C*ph_{ind}-7*C*), 134.7(ph^{1}-*C*H), 133.9 (C=CCH_2*C*), 132.6 (ph^{1}-2,6*C*), 131.8 (CO*C*=C), 127.8 (ph^{1}-1*C*), 126.5 (ph_{ind}-7*C*), 115.6 (ph_{ind}-4*C*), 115.1 (ph^{1}-3,5*C*), 112.8 (ph_{ind}-6*C*), 66.6 (prop-1*C*), 55.8 (prop-3*C*), 54.6 (pip-2,6*C*), 32.4 (C=CCH_2), 26.6 (prop-2*C*), 25.8 (pip-3,5*C*), 24.3 (pip-4*C*)
ESI HRMS [M+H$^+$]	calc	380.2026
	found	380.2017 (100)
Analysis	calc	C 75.96 %, H 6.91 %, N 3.69 %
	found	C 75.90 %, H 6.71 %, N 3.67 %
Melting point		123.2 °C

(*E*)-6-((4-Bromobenzyl)oxy)-2-(4-(3-(piperidin-1-yl)propoxy)benzylidene)-2,3-dihydro-1*H*-inden-1-one (3e)[168]

6-((4-Bromobenzyl)oxy)-2,3-dihydro-1*H*-inden-1-one (0.5 g, 1.1 mmol), **P7** (0.3 g, 1.1 mmol) and sodium hydroxide (0.06 g, 1.5 mmo) were dissolved in ethanol (10 ml) and treated according to procedure **D** to give a yellow solid (0.5 g, 87 %).

Chemical formula	$C_{31}H_{32}BrNO_3$
Molecular weight	546.51

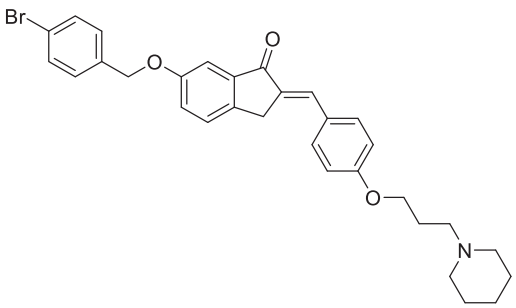

^{1}H-NMR (DMSO-d_6)	δ 7.58-7.51 (m, 3H, ph^{1}-2,6*H*, ph_{ind}-7*H*), 7.47-7.41 (m, 2H, ph_{bn}- 3,5*H*), 7.40-7.35 (d, 1*H*, J = 8.4, ph_{ind}-5*H*), 7.33-7.30 (d, 1H, J = 2.4, ph_{bn}-6*H*), 7.28-7.21 (m, 2H, ph^{1}-C*H*, ph_{bn}-2*H*), 7.19-7.14 (dd, 1H, J = 8.3, ph_{ind}-4*H*), 6.93-6.85 (m, 2H, ph^{1}-3,5*H*), 4.99 (s, 2H, ph_{bn}-CH_2O), 4.09-3.96 (t, 2H, J = 6.2, prop-1H_2), 3.86 (s, 2H, C=CCH_2), 2.65-2.50 (t, 2H, J = 7.7, prop-3H_2), 2.50-2.30 (m, 4H, pip-2,6*H*), 2.13-1.94 (q, 2H, J = 6.9, prop-2H_2), 1.73-1.55 (m, 4H, pip-3,5H_2), 1.49-1.33 (m, 2H, pip-4*H*)
^{13}C-NMR (DMSO-d_6)	δ 194.1 (*C*O), 160.2 (ph^{1}-4*C*), 158.4 (ph_{ind}-6*C*), 142.7 (C=CCH_2*C*), 139.5 (ph^{1}-*C*H), 135.5 (ph_{bn}-1*C*), 133.8 (CO*C*=C), 133.1 (ph_{ind}-7*C*), 132.6 (ph^{1}-2,6*C*), 131.7 (ph_{bn}-3,5*C*), 129.1 (ph_{bn}-2,6*C*), 128.1 (CO*C*ph_{ind}-7*C*), 127.0 (ph^{1}-1*C*), 124.0 (ph_{ind}-

		5*C*), 122.0 (ph^2-4*C*), 114.9 (ph^1-3,5*C*), 104.94 (ph_{ind}-4*C*), 69.5 (prop-1*C*), 66.3 (ph_{bn}-CH_2O), 55.7 (prop-3*C*), 54.1 (pip-2,6*C*), 31.8 (C=CCH_2), 26.1 (prop-2*C*), 25.3 (pip-3,5*C*), 23.9 (pip-4*C*)
ESI HRMS [$M+H^+$]	calc	546.1644
	found	546.1643 (100)
Analysis	calc	C 68.13 %, H 5.90 %, N 2.56 %
	found	C 67.84 %, H 5.80 %, N 2.36 %
Melting point		159.5 °C

(*E*)-5-((4-Bromobenzyl)oxy)-2-(4-(3-(piperidin-1-yl)propoxy)benzylidene)-2,3-dihydro-1*H*-inden-1-one (3f)[168]

5-((4-Bromobenzyl)oxy)-2,3-dihydro-1*H*-inden-1-one (0.3 g, 9.5 mmol), **P7** (0.2 g, 9.5 mmol) and sodium hydroxide (0.05 g, 1.4 mmol) were dissolved in ethanol (10 ml) and treated according to procedure **D** to give a yellow solid (0.4 g, 85 %).

Chemical formula		$C_{31}H_{32}BrNO_3$
Molecular weight		546.51

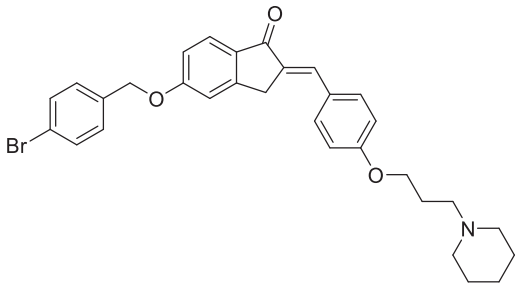

^{1}H-NMR ($CDCl_3$)		δ 7.81-7.74 (d, 1H, J= 8.6, ph_{ind}-7*H*), 7.57-7.47 (m, 4H, ph_{bn}-3,5*H*, ph^1-2,6*H*), 7.44-7.38 (dd, 1*H*, J = 1.3, ph_{ind}-6*H*), 7.33-7.26 (dd, 1H, J = 1.1, ph_{bn}-6*H*), 7.23-7.16 (dd, 1H, J = 7.6, ph_{bn}-2*H*), 6.98 (br s, 1H, ph^1-C*H*), 6.92-6.90 (d, 1H, J= 6.9, ph_{ind}-4*H*), 6.90-6.85 (m, 2H, ph^1-3,5*H*), 5.05 (s, 2H, ph_{bn}-CH_2O), 4.05-3.95 (t, 2H, J = 6.2, prop-1H_2), 3.87 (s, 2H, C=CCH_2), 2.52-2.42 (t, 2H, J = 7.7, prop-3H_2), 2.41-2.30 (m, 4H, pip-2,6*H*), 2.03-1.89 (q, 2H, J = 6.9, prop-2H_2), 1.62-1.51 (m, 4H, pip-3,5H_2), 1.43-1.34 (m, 2H, pip-4*H*)
^{13}C-NMR (DMSO-d_6)		δ 191.5 (*C*O), 163.5 (ph^1-4*C*), 159.8 (ph_{ind}-5*C*), 152.6 (C=CCH_2*C*), 139.2 (ph^1-*C*H), 132.9 (ph_{bn}-1*C*), 132.4 (ph^1-2,6*C*), 131.6 (ph_{bn}-3*C*), 131.0 (ph_{bn}-5*C*), 130.9 (ph_{bn}-2*C*), 130.7 (ph_{bn}-6*C*), 130.3 (*C*OC=C), 127.4 (ph_{ind}-7*C*), 126.7 (*C*O*C*ph_{ind}-7*C*), 125.3 (ph^1-1*C*), 121.7 (ph_{ind}-4*C*), 115.7 (ph_{bn}-4*C*), 114.9 (ph^1-3,5*C*), 111.2 (ph_{ind}-6*C*), 68.7 (prop-1*C*), 66.1 (ph_{bn}-CH_2O), 55.0 (prop-3*C*), 54.0 (pip-2,6*C*), 31.9 (C=CCH_2), 26.2 (prop-2*C*), 25.5 (pip-3,5*C*), 24.1 (pip-4*C*)
ESI HRMS [$M+H^+$]	calc	546.1644
	found	546.1632 (100)
Analysis	calc	C 68.13 %, H 5.90 %, N 2.56 %
	found	C 68.06 %, H 6.11 %, N 2.48 %
Melting point		133.8 °C

8.1.6 Indenamine derivatives

5-Methoxy-2,3-dihydro-1H-inden-1-one oxime (P8)[192]

5-Methoxy-1-indanone (0.5 g, 3.1 mmol) hydroxylamine hydrochloride (0.3 g, 3.3 mmol) and sodium acetate (0.2 g, 3.3 mmol) were reflux for 3h in a mixture of EtOH/H_2O (1/1) to give a white solid (0.3 g, 57 %).

Chemical formula		$C_{10}H_{11}NO_2$
Molecular weight		177.08
^{1}H-NMR (DMSO-d_6)		δ 11.02 (s, 1H, NO*H);* 7.32-7.25 (m, 1H, phi$_{ind}$-7*H*), 6.95-6.84 (m, 2H, ph$_{ind}$-4,6*H*), 3.70 (s, 3H, O*CH*$_3$), 2.99-2.80 (m, 2H, NH_2CHC*H*$_2$), 2.39-2.18 (m, 2H, NH_2CHCH_2C*H*$_2$)
ESI MS [M+H$^+$]	calc	178.09
	found	178.12 (100)

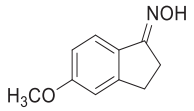

5-Methoxy-2,3-dihydro-1*H*-indene-1-amine (P9)[192]

5-Methoxy-1-indanone (0.1 g, 0.6 mmol) ammonium acetate (0.7 g, 9.0 mmol) and sodium cyanoborohydride (0.05 g, 0.7 mmol) were treated according to procedure **F** (method B) to give a white solid (0.06 g, 67 %).

Chemical formula		$C_{10}H_{13}NO$
Molecular weight		163.22
^{1}H-NMR (DMSO-d_6)		δ 8.77 (s, 2H, NH_2), 7.21-7.20 (m, 1H, phi$_{ind}$-7*H*), 6.69-6.56 (m, 2H, ph$_{ind}$-4,6*H*), 4.15-4.06 (t, 1H, J = 3.9, NH_2C*H*CH_2), 3.84 (s, 3H, O*CH*$_3$), 2.81-2.69 (m, 2H, NH_2CHC*H*$_2$), 2.39-2.18 (m, 1H, NH_2CHCH_2C*H*$_2$)
^{13}*C*-NMR (DMSO-d_6)		δ 155.04 (ph$_{ind}$-5*C*), 140.91 ($NH_2CHCH_2CH_2$*C*), 140.85 (NH_2CH*C*), 123.10 (ph$_{ind}$-7*C*), 111.43 (ph$_{ind}$-4*C*), 109.93 (ph$_{ind}$-6*C*), 55.8 (O*C*H$_3$), 54.01 (NH_2*C*H), 36.25 (NH_2CH*C*H$_2$), 28.77 (NH_2CHCH_2*C*H$_2$)
ESI MS [M+H$^+$]	calc	164.23
	found	164.18 (100)

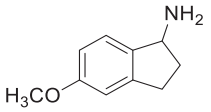

5-Hydroxy-1-indanone (P10)[261]

5-Methoxy-1-indanone (1.2 g, 7.4 mmol) was suspended at room temperature in toluene under nitrogen atmosphere. Aluminium chloride (1.6 g, 14.8 mmol) was added and the mixture was refluxed for 3 h. The crude product was re-crystallized from toluene (white solid, 0.9 g, 96 %).

Chemical formula		$C_9H_8O_2$
Molecular weight		148.05
^{1}H-NMR (DMSO-d_6)		^{1}H-NMR (300 MHz, DMSO-d_6) δ 10.46 (s, 1H, O*H*), 7.51-7.45 (d, 1H, J=8.3, ph$_{ind}$-7*H*), 7.13-7.07 (td, 2H, J=8.0, ph$_{ind}$-4,6*H*), 3.03-2.94 (t, 2H, J=6.2, COC*H*$_2$), 2.60-2.49 (m, 2H, COCH$_2$C*H*$_2$)
ESI MS [M+H$^+$]	calc	149.06
	found	140.10 (100)

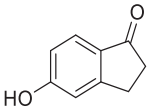

5-(3-(Piperidin-1-yl)propoxy)-2,3-dihydro-1H-inden-1-oxime (P11)[262]

Under inert atmosphere, hydroxylamine hydrochloride (0.1 g, 1.6 mmol) and sodium acetate (0.1 g, 1.7 mmol) were stirred at room temperature in 6 ml of H_2O/MeOH (1: 1). After 30 minutes, product **1e** (0.3 g, 1.1 mmol) was added and the reaction mixture was heated to reflux for 3 h. After cooling the mixture to room temperature, the crude product was taken up in methylene chloride and saturated $NaHCO_3$ solution. The organic phase was then dried over sodium sulfate, and concentrated under vacuum (white solid, 0.2 g, 65 %).

Chemical formula		$C_{17}H_{24}N_2O_2$
Molecular weight		288.39
^{1}H-NMR (DMSO-d_6)		δ 10.48 (s, 1H, NO*H*), 7.22-7.18 (m, 1H, ph$_{ind}$-7*H*), 6.92-6.85 (m, 1H, ph$_{ind}$-6*H*), 6.82-6.76 (m, 1H, ph$_{ind}$-4*H*), 4.10-4.01 (t, 2H, J = 5.8, prop-1*H*), 2.93-2.85 (m, 2H, CNC*H*$_2$), 2.79-2.62 (m, 4H, COCH$_2$C*H*$_2$, prop-3*H*$_2$), 2.43-2.32 (m, 6H, pip-2,6*H*, prop-2*H*$_2$), 1.54-1.33 (m, 6H, pip-3,5*H*, pip-4*H*)
ESI MS [M+H$^+$]	calc	289.40
	found	289.43(100)

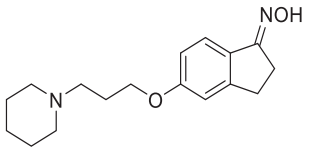

5-(3-(Piperidin-1-yl)propoxy)-2,3-dihydro-1*H*-inden-1-amine (P12)[192,195]

P12 was obtained by following two procedures. According to procedure **E**, compound **P11** (0.1 g, 0.3 mmol) was hydrogenated with 10 % Pd/C and with a catalytic amount of acetic acid to give a white product (0.04 g, 45 %).

According to procedure **F** (method B), the reductive amination of product **1e** (0.6 g, 2.2 mmol), was carried out with ammonium acetate (2.5 g, 32.8 mmol) and sodium cyanoborohydride (0.2 g, 2.6 mmol) in a microwave reactor to give a white solid (0.3 g, 47 %).

Chemical formula	$C_{17}H_{26}N_2O$
Molecular weight	274.41

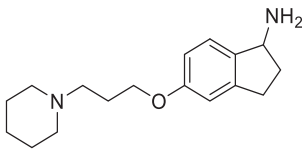

^{1}H-NMR (DMSO-d_6)		δ 7.23-7.15 (m, 1H, ph_{ind}-7*H*), 6.75-6.66 (m, 2H, ph_{ind}-4,6*H*), 4.18-4.06 (t, 1H, J = 4.1, NH_2CHCH_2), 3.99-3.87 (t, 2H, J = 5.6, prop-1*H*), 2.87-2.74 (m, 1H, NH_2CHCH_2), 2.72-2.55 (m, 1H, NH_2CHCH_2), 2.40-2.17 (m, 7H, $NH_2CHCH_2CH_2$, pip-2,6*H*, prop-3*H*), 1.89-1.74 (q, 2H, J = 6.4, prop-2*H*), 1.64-1.43 (m, 5H, pip-3,5*H*, $NH_2CHCH_2CH_2$), 1.42-1.30 (m, 2H, pip-4*H*)
^{13}C-NMR (DMSO-d_6)		δ 158.01 (ph_{ind}-5C), 143.97 ($NH_2CHCH_2CH_2C$), 140.29 (NH_2CHC), 124.10 (ph_{ind}-7C), 112.67 (ph_{ind}-4C), 109.93 (ph_{ind}-6C), 65.91 (prop-1C), 56.12 (prop-3C), 55.02 (NH_2CH), 54.10 (pip-2,6C), 37.27 (NH_2CHCH_2), 29.78 ($NH_2CHCH_2CH_2$), 26.39 (prop-2C), 25.61 (pip-3,5C), 24.15 (pip-4C)
ESI HRMS [M+H$^+$]	calc	275.2123
	found	275.2120 (100)

5-(3-(Piperidin-1-yl)propoxy)-N-(prop-2-yn-1-yl)-2,3-dihydro-1*H*-inden-1-amine hydrochloride (4)[179]

Compound **P12** (0.3 g, 1.1 mmol), a propargyl bromide solution 80 % wt. in toluene (0.1 ml, 1.1 mmol) and potassium carbonate (0.2 g, 1.1 mmol) were treated according to procedure **A** in DMF for 4 h. The crude product was purified by column chromatography (methylene chloride: ammoniacal methanol = 9.7: 0.3) and crystallized as hydrochloride from 1,4-dioxane (0.2 g, 55 %).

Chemical formula		$C_{17}H_{26}N_2O{\cdot}2HCl$
Molecular weight		385.87

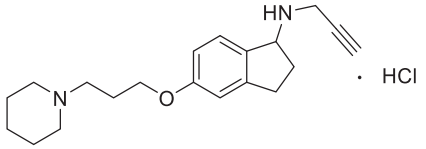

^{1}H-NMR (D_2O)		δ 10.4 (br s, 1H, N*H*$^+$), 7.44-7.36 (m, 1H, ph_{ind}-7*H*), 6.96-6.90 (m, 1H, ph_{ind}-4H), 6.89-6.82 (m, 1H, ph_{ind}-6H), 4.87-4.80 (dd, 1H, J = 4.8, NHC*H*), 4.15-4.04 (t, 2H, J = 5.8, prop-1*H*), 3.88-3.82 (t, 2H, J = 3.9, $NHCH_2C{\equiv}CH$), 3.57-3.44 (m, 2H, prop-3*H*), 3.31-3.18 (m, 2H, $NHCHCH_2$), 3.14-2.99 (m, 1H, $NHCHCH_2CH_2$), 2.99-2.79 (m, 4H, pip-2,6H), 2.61-2.42 (m, 1H, $NHCHCH_2CH_2$), 2.30-2.08 (m, 3H, prop-2*H*, $CH_2C{\equiv}CH$), 1.96-1.32 (m, 6H, pip-3,5*H*, pip-4*H*)
^{13}C-NMR (D_2O)		δ 157.02 (ph_{ind}-5C), 144.95 ($NHCHCH_2CH_2C$), 125.89 (NHCHC), 123.95 (ph_{ind}-7C), 111.21 (ph_{ind}-4C), 108.42 (ph_{ind}-6C), 75.20 ($CH_2C{\equiv}CH$), 70.54 ($CH_2C{\equiv}CH$), 62.74 (prop-1C), 58.82 (prop-3C), 51.77 (NHCH), 50.63 (pip-2,6C), 31.35 ($NHCH_2C{\equiv}CH$), 27.07 ($NHCHCH_2$), 26.11 ($NHCHCH_2CH_2$), 20.71 (prop-2C), 20.13 (pip-3,5C), 18.38 (pip-4C)
ESI HRMS [M+H$^+$]	calc	313.2280
	found	313.2277 (100)
Analysis	calc	C 62.33 %, H 7.85 %, N 7.27 %
	found	C 62.02 %, H 8.07 %, N 7.17 %
Melting point		162 °C

8.1.7 Synthesis of arylindenopyrimidine derivatives

6-Hydroxy-1-indanone (P13)[261]

6-Methoxy-1-indanone (1.2 g, 7.4 mmol) was suspended at room temperature in toluene under nitrogen atmosphere. Aluminium chloride (1.6 g, 14.8 mmol) was added and the mixture was refluxed for 3 h. The crude product was re-crystallized from toluene (white solid, 0.8 g, 95 %).

Chemical formula		$C_9H_8O_2$
Molecular weight		148.05
^{1}H-NMR (DMSO-d_6)		^{1}H-NMR (300 MHz, DMSO-d_6) δ 9.74 (s, 1H, O*H*), 7.41-7.36 (dd, 1H, J=8.3, Ph_{ind}-7*H*), 7.13-7.07 (dd, 1H, J=7.9, ph_{ind}-5*H*), 6.94-6.91 (dd, 1H, J=7.5, ph_{ind}-4*H*), 3.01-2.93 (t, 2H, J=6.2, $COCH_2$), 2.63-2.57 (m, 2H, $COCH_2CH_2$)
ESI MS [M+H$^+$]	calc	149.06
	found	140.12 (100)

5-(Benzyloxy)-2,3-dihydro-1*H*-inden-1-one (P14)[170]

Compound **P10** (1.0 g, 6.7 mmol), benzyl bromide (1.2 g, 7.4 mmol) and potassium carbonate (2.9 g, 21.4 mmol) were dissolved in dimethylformamide and treated according to procedure **L**. The resulting oil was crystallized in ethyl ether (white solid, 1.6 g, 93 %).

Chemical formula		$C_{16}H_{14}O_2$
Molecular weight		238.1
^{1}H-NMR (DMSO-d_6)		^{1}H-NMR (300 MHz, DMSO-d_6) δ 8.11-8.08 (d, 1H, J=8.3, Ph_{ind}-7*H*), 7.48-7.10 (m, 4H, Ph_{bn}-2-6*H*), 6.97-6.93 (dd, 1H, J=7.5, ph_{ind}-4*H*), 6.93-6.89 (dd, 1H, J=7.9, ph_{ind}-6*H)*, 5.14 (s, 2H, ph_{bn}-CH_2O), 3.01-2.93 (t, 2H, J=6.2, $COCH_2$), 2.63-2.57 (m, 2H, $COCH_2CH_2$)
ESI MS [M+H$^+$]	calc	239.11
	found	239.12 (100)

6-(Benzyloxy)-2,3-dihydro-1*H*-inden-1-one (P15)[170]

Compound **P13** (1.0 g, 6.7 mmol), benzyl bromide (1.2 g, 7.4 mmol) and potassium carbonate (2.9 g, 21.4 mmol) were dissolved in dimethylformamide and treated according to procedure **L**. The resulting oil was crystallized in ethyl ether (white solid, 1.6 g, 97 %).

Chemical formula	$C_{16}H_{14}O_2$
Molecular weight	238.1

^{1}H-NMR (DMSO-d_6)		^{1}H-NMR (300 MHz, DMSO-d_6) δ 8.15-8.10 (d, 1H, J=8.3, Ph_{ind}-7*H*), 7.50-7.10 (m, 4H, Ph_{bn}-2-6*H*), 6.95-6.92 (dd, 1H, J=7.5, ph_{ind}-4*H*), 6.90-6.86 (dd, 1H, J=7.9, ph_{ind}-5*H)*, 5.13 (s, 2H, ph_{bn}-CH_2O), 3.02-2.90 (t, 2H, J=6.2, COCH_2), 2.61-2.55 (m, 2H, $COCH_2CH_2$)
ESI MS [M+H$^+$]	calc	239.11
	found	239.14 (100)

(*E*)-2-(4-(Benzyloxy)benzylidene)-2,3-dihydro-1*H*-inden-1-one (P16)[168]

According to procedure **D**, a water solution of sodium hydroxide (0.6 g, 16.9 mmol) was added at room temperature to an ethanolic solution of 1-indanone (1.5 g, 11.3 mmol) and 4-(benzyloxy)benzaldehyde (2.4 g, 11.3 mmol)). A white solid was obtained (3.4 g, 93 %).

Chemical formula		$C_{23}H_{18}O_2$
Molecular weight		326.29

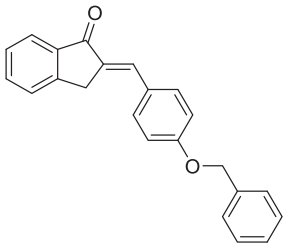

^{1}H-NMR (DMSO-d_6)		^{1}H-NMR (300 MHz, DMSO-d_6) δ 7.81-7.64 (m, 5H, ph'-2,6H, Ph_{ind}-7*H*, Ph_{bn}-2,6H), 7.54-7.31 (m, 7H, Ph_{ind}-4-6H, ph^1-C*H*, Ph_{bn}-3-5*H*), 7.19-7.11 (m, 2H, ph'-3,5H), 5.20 (s, 2H), 4.08 (s, 2H)
ESI MS [M+H$^+$]	calc	327.14
	found	327.21 (100)

(*E*)-2-Benzylidene-5-(benzyloxy)-2,3-dihydro-1*H*-inden-1-one (P17)[168]

According to procedure **D**, a water solution of sodium hydroxide (0.4 g, 9.45 mmol) was added at room temperature to an ethanolic solution of **P14** (1.5 g, 6.3 mmol) and benzaldehyde (0.6 g, 6.3 mmol)). A white solid was obtained (1.9 g, 95 %).

Chemical formula		$C_{23}H_{18}O_2$
Molecular weight		326.29

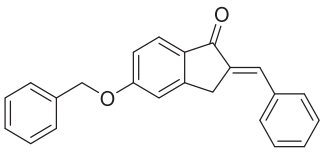

^{1}H-NMR (DMSO-d_6)		^{1}H-NMR (300 MHz, DMSO-d_6) δ 7.79-7.72 (m, 1H, Ph_{ind}-7*H*), 7.61-7.49 (m, 3H, ph'-2,6*H*, ph^1-C*H*), 7.41-7.20 (m, 8H, Ph_{ind}-4,6*H*, Ph_{bn}-2-6*H*, Ph'-4*H*), 6.98-6.88 (m, 2H, Ph'-3,5*H*), 5.07 (s, 2H), 3.88 (s, 2H).
ESI MS [M+H$^+$]	calc	327.14
	found	327.20 (100)

(*E*)-5-(Benzyloxy)-2-(4-(benzyloxy)benzylidene)-2,3-dihydro-1*H*-inden-1-one (P18)[168]

According to procedure **D**, a water solution of sodium hydroxide (0.2 g, 6.3 mmol) was added at room temperature to an ethanolic solution of **P14** (1.0 g, 4.2 mmol) and 4-(benzyloxy)benzaldehyde (0.9 g, 4.2 mmol)). A white solid was obtained (1.6 g, 91 %).

Chemical formula		$C_{30}H_{24}O_3$
Molecular weight		432.17
^{1}H-NMR (DMSO-d_6)		^{1}H-NMR (300 MHz, DMSO-d_6) δ 7.85-7.7.80 (m, 1H, ph_{ind}-7*H*), 7.57-7.32 (m, 15H, ph'-2,6H, Ph_{ind}-4,6H, Ph_{bn}2-6H, $P_{bn'}$-2-6H, ph^1-C*H*), 6.88-6.81 (m, 2H, ph'-3,5H), 5.16 (s, 2H), 5,14 (s, 2H), 3.68 (s, 2H).
ESI MS [M+H$^+$]	calc found	433.17 433.21 (100)

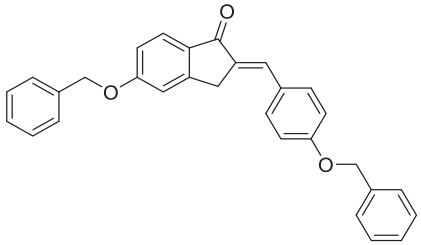

(*E*)-2-Benzylidene-6-(benzyloxy)-2,3-dihydro-1*H*-inden-1-one (P19)[168]

According to procedure **D**, a water solution of sodium hydroxide (0.5 g, 12.6 mmol) was added at room temperature to an ethanolic solution of **P15** (2 g, 8.4 mmol) and benzaldehyde (0.9 g, 8.4 mmol)). A white solid was obtained (2.6 g, 95 %).

Chemical formula		$C_{23}H_{18}O_2$
Molecular weight		326.29
^{1}H-NMR (DMSO-d_6)		^{1}H-NMR (300 MHz, DMSO-d_6) δ 7.82-7.7.75 (m, 2H, ph'-2,6*H*), 7.64-7.28 (m, 12H, Ph_{ind}-4,5,7*H*, Ph_{bn}-2-6*H*, ph^1-C*H*, Ph'-3-5*H*), 5.21 (s, 2H, Ph'-3,5*H*), 4.05 (s, 2H)
ESI MS [M+H$^+$]	calc found	327.14.11 327.19 (100)

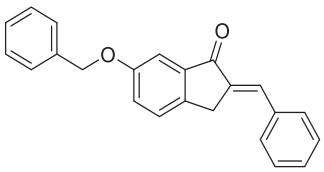

4-(2-Amino-5*H*-indeno[1,2-*d*]pyrimidin-4-yl) phenol (P20)[148,198]

An ethanolic solution of guanidine hydrochloride (2.5 g, 26.1 mmol) was treated with powder NaOH (1.1 g, 26.1 mmol). After 30 min, the free base was added to an ethanolic solution of **P16** (3.4 g, 10.4 mmol) as described in procedure **G** and the reaction mixture was refluxed for 18 h. A white solid was obtained (2.0 g, 54 %) after column chromatography and crystallization in ethanol. The crude material was stirred in EtOH with 10 % Pd/C as described in procedure **E**. A yellow solid was obtained (1.4 g, 90 %).

Chemical formula		$C_{16}H_{14}O_2$
Molecular weight		275.11

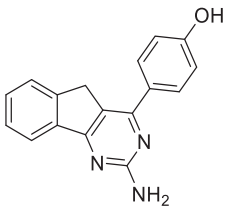

^{1}H-NMR (DMSO-d_6)		^{1}H-NMR (300 MHz, DMSO-d_6) δ 8.06-7.98 (m, 2H, ph^1-2,6*H*), 7.93-7.86 (m, 1H, aip-6*H*), 7.70-7.63 (m, 1H, aip-9*H*), 7.57-7.43 (m, 2H, aip-7,8*H*), 6.96-6.88 (m, 2H, ph^1-3,5*H*), 6.55 (s, 2H, pyrim-NH_2), 4.13 (s, 2H, aip-5*H*)
ESI MS [M+H$^+$]	calc	276.32
	found	276.28 (100)

2-Amino-4-phenyl-5*H*-indeno[1,2-d]pyrimidin-7-ol (P21)[148,198]

An ethanolic solution of guanidine hydrochloride (0.4 g, 4.5 mmol) was treated with powder NaOH (0.2 g, 4.5 mmol). After 30 min, the free base was added to an ethanolic solution of **P17** (0.6 g, 1.8 mmol) as described in procedure **G** and the reaction mixture was refluxed for 18 h. A white solid was obtained (0.7 g, 45 %) after column chromatography and crystallization in ethanol. The crude material was stirred in EtOH with 10 % Pd/C as described in procedure **E**. A yellow solid was obtained (0.8 g, 75 %).

Chemical formula		$C_{17}H_{13}N_3O$
Molecular weight		275.11

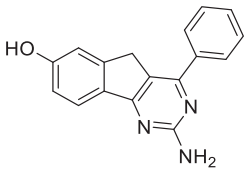

^{1}H-NMR (DMSO-d_6)		^{1}H-NMR (300 MHz, DMSO-d_6) δ 9.98 (s, 1H, O*H*), 8.12-8.02 (m, 2H, ph^1-2,6*H*), 7.76-7.69 (d, 1*H*, J = 7.7, aip-9*H*), 7.60-7.45 (d, 3H, J = 7.13, ph^1-3,4,5*H*), 7.09-7.0 (d, 1H, aip-6*H*), 6.92-6.85 (dd, 1H, J = 6.9, aip-8*H*), 6.53 (s, 2H, pyrim-NH_2), 4.02 (s, 2H, aip-5*H*)
ESI MS [M+H$^+$]	calc	276.32
	found	276.37 (100)

2-Amino-4-(4-hydroxyphenyl)-5*H*-indeno[1,2-*d*]pyrimidin-7-ol (P22)[148,198]

An ethanolic solution of guanidine hydrochloride (0.8 g, 9.2 mmol) was treated with powder NaOH (0.4 g, 9.2 mmol). After 30 min, the free base was added to an ethanolic solution of **P18** (1.6 g, 3.7 mmol) as described in procedure **G** and the reaction mixture was refluxed for 18 h. A white solid was obtained (0.8 g, 45 %) after column chromatography and crystallization in ethanol. The crude material was stirred in EtOH with 10 % Pd/C as described in procedure **E**. A yellow solid was obtained (1.4 g, 81 %).

Chemical formula		$C_{16}H_{14}O_2$
Molecular weight		291.10

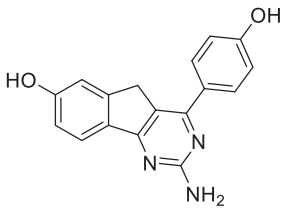

^{1}H-NMR (DMSO-d_6)		^{1}H-NMR (300 MHz, DMSO-d_6) δ 9.98 (s, 1H, O*H*), 9.95 (s, 1H, O*H*), 8.12-8.02 (m, 2H, ph^1-2,6*H*), 7.76-7.69 (d, 1*H*, J = 7.7, aip-9*H*), 7.60-7.45 (d, 2H, J = 7.13, ph^1-3,5*H*), 7.09-7.0 (d, 1H, aip-6*H*), 6.92-6.85 (dd, 1H, J = 6.9, aip-8*H*), 6.53 (s, 2H, pyrim-NH_2), 4.02 (s, 2H, aip-5*H*)
ESI MS [M+H$^+$]	calc	292.11
	found	292.13 (100)

2-Amino-4-(4-hydroxyphenyl)-5*H*-indeno[1,2-*d*]pyrimidin-8-ol (P23)[148,198]

An ethanolic solution of guanidine hydrochloride (1.8 g, 19.7 mmol) was treated with powder NaOH (0.8 g, 19.7 mmol). After 30 min, the free base was added to an ethanolic solution of **P19** (2.6 g, 7.9 mmol) as described in procedure **G** and the reaction mixture was refluxed for 18 h. A white solid was obtained (1.4 g, 52 %) after column chromatography and crystallization in ethanol. The crude material was stirred in EtOH with 10 % Pd/C as described in procedure **E**. A yellow solid was obtained (0.9 g, 81 %).

Chemical formula		$C_{17}H_{13}N_3O$
Molecular weight		275.11

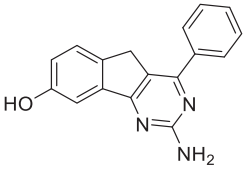

^{1}H-NMR (DMSO-d_6)		^{1}H-NMR (300 MHz, DMSO-d_6) δ 9.71 (s, 1H, O*H*), 8.12-8.02 (m, 2H, ph^1-2,6*H*), 7.59-7.49 (m, 3*H*, ph^1-3,4,5*H*), 7.48-7.41 (d, 1H, J = 7.3, aip-6*H*), 7.32-7.26 (m, 1H, aip-9*H*), 6.99-6.91 (dd, 1H, J = 6.9, aip-7*H*), 6.64 (s, 2H, pyrim-NH_2), 3.98 (s, 2H, aip-5*H*)
ESI MS [M+H$^+$]	calc	276.32
	found	276.35 (100)

1-(3-Chloropropyl)pyrrolidine hydrochloride (P24)[57,179]

Thionyl chloride (1.4 ml, 0.02 mol) was added dropwise to a suspension of alcohol 3-(pyrrolidine-yl)propan-1-ol (1 g, 0.01 mol) in 40 ml of dichloromethane and stirred at room temperature for 3 h, as described in procedure **B**. The crude product was re-crystallized from ethanol and washed several times in diethyl ether (hygroscopic brown solid, 1.4 g, 75 %).

Chemical formula	$C_7H_{14}ClN \cdot HCl$
Molecular weight	184.1

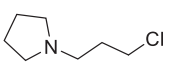

^{1}H-NMR (DMSO-d_6)		δ 11.04 (br s, 1H, NH^+), 3.75 (t, J = 6.4, 2H, prop-1H_2), 3.56-3.43 (m, 2H, pyr-2,5H_{eq}), 3.25-3.14 (m, 2H, prop-3H_2), 3.04-2.87 (m, 2H, pyr-2,5H_{ax}), 2.24-2.09 (quint, J= 6.4, 2H, prop-2H_2), 2.06-1.79 (m, 4H, pyr-3,4H_2)
^{13}C-NMR (DMSO-d_6)		δ 52.76 (prop-3*C*), 51.34 (pyr-2,5*C*), 40.33 (prop-1*C*), 28.09 (prop-2*C*), 22.67 (pyr-3,4*C*)
ESI MS [M+H$^+$]	calc	148.08
	found	148.02 (100)

7-Methoxy-4-phenyl-5*H*-indeno[1,2 *d*]pyrimidin-2-amine (P25)[148,198]

As described in procedure **G,** powder NaOH (0.2 g, 6.0 mmol) was added to an ethanolic solution of guanidine hydrochloride (0.6 g, 6.0 mmol). After 30 min, sodium chloride was filtered off, and the filtrated was added to a suspension of (*E*)-2-benzylidene-5-methoxy-2,3-dihydro-1*H*-inden-1-one (0.3 g, 1.3 mmol) in EtOH. A white solid was obtained (0.3 g, 91 %) without further purification.

Chemical formula		$C_{18}H_{15}N_3O$
Molecular weight		289.34

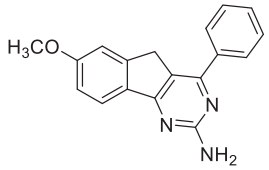

^{1}H-NMR (DMSO-d_6)		8.15-8.09 (m, 2H, ph^1-2,6*H*), 7.80-7.73 (d, 1*H*, J = 7.7, aip-9*H*), 7.56-7.42(d, 3H, J = 7.13, ph^1-3,4,5*H*), 7.11-7.0 (d, 1H, aip-6*H*), 6.95-6.89 (dd, 1H, J = 6.9, aip-8*H*), 6.52 (s, 2H, pyrim-NH_2), 4.02 (s, 2H, aip-5*H*), 3.95 (s, 3H, OCH_3)
ESI MS [M+H$^+$]	calc	290.13
	found	290.11 (100)

4-Phenyl-7-(3-(piperidin-1-yl)propoxy)-5*H*-indeno[1,2-*d*]pyrimidin-2-amine (5)[148]

An ethanolic solution of guanidine hydrochloride (0.4 g, 4.5 mmol) was treated with powder NaOH (0.2 g, 4.5 mmol). After 30 min, the free base was added to an ethanolic solution of **2c** (0.6 g, 1.8 mmol) as described in procedure **G** and the reaction mixture was refluxed for 18 h. A white solid was obtained (0.4 g, 45 %) after column chromatography and crystallization in ethanol.

Chemical formula		$C_{25}H_{28}N_4O$
Molecular weight		400.53

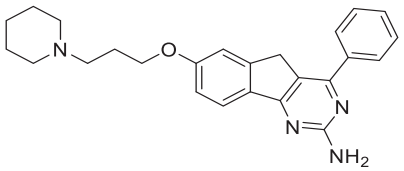

^{1}H-NMR (DMSO-d_6)		δ 8.17-8.08 (dd, 2H, *J* = 8.1, ph^1-2′,6′*H*), 7.90-7.82 (d, 1H, *J* = 7.8, ph^1-4′*H*), 7.66-7.51 (m, 3H, aip-6H, ph^1-3′,5′*H*), 7.31-7.24 (d, 1H, *J* = 7.3, aip-9*H*), 7.15-7.05 (dd, 1H, *J* = 7.1, aip-8*H*), 6.63 (s, 2H, aip-NH_2), 4.20-4.13 (t, 2H, *J* = 6.2, prop-1′′H_2), 4.12 (s, 2H, aip-5H_2), 2.51-2.42 (t, 2H, *J* = 6.9, prop-3′′H_2), 2.41-2.28 (m, 4H, pip-5′′,9′′H_2), 2.02-1.88 (q, 2H, *J* = 5.9, prop-2′′H_2), 1.61-1.49 (m, 4H, pip-6′′,8′′H_2), 1.48-1.37 (m, 2H, pip-7′′H_2)

^{13}C-NMR (DMSO-d_6)		δ 168.9 (aip-4*C*), 163.6 (NCNH$_2$N*C*), 160.9 (aip-2*C*), 158.8 (aip-7*C*), 148.3 (aip-6C*C*), 138.0 (aip-9C*C*), 131.3 (ph^1-1′*C*), 129.5 (aip-9*C*), 128.3 (ph^1-2′,6′*C*), 128.1 (ph^1-3′,5′*C*), 122.2 (ph^1-4′*C*), 118.1 (aip-4C*C*), 114.3 (aip-6*C*), 110.9 (aip-8*C*), 66.2 (prop-1′′*C*), 55.0 (prop-3′′*C*), 54.0 (pip-5′′,9′′*C*), 34.0 (aip-5*C*), 26.2 (prop-2′′*C*), 25.5 (pip-6′′,8′′*C*), 24.1 (pip-7′′*C*)
ESI HRMS [M+2H$^+$]	calc	402.2420
	found	402.2412 (100)
HPLC		96.1 %
Melting point		176.3 °C

4-Phenyl-8-(3-(piperidin-1-yl)propoxy-5*H*-indeno[1,2-*d*]pyrimidin-2-amine (6)[148]

A methanolic solution of guanidine hydrochloride (0.6 g, 7.0 mmol) was treated with powder NaOH (0.3 g, 7.0 mmol). After 30 min, the free base was added to a methanolic solution of **2b** (1 g, 3.0 mmol) as described in procedure **G** and the reaction mixture was refluxed for 21 h. A white solid was obtained (0.6 g, 44 %) after column chromatography and several crystallizations in ethanol.

Chemical formula		$C_{25}H_{28}N_4O$
Molecular weight		400.53
^{1}H-NMR (DMSO-d_6)		δ 8.15-8.03 (m, 2H, ph^1-2′,6′*H*), 7.61-7.47 (m, 4H, aip-9*H*, ph^1-3′,4′,5′*H*), 7.41-7.35 (d, 1H, *J* = 7.4, aip-6*H*), 7.16-7.05 (dd, 1H, *J* = 7.1, aip-7*H*), 6.66 (s, 2H, aip-N*H*$_2$), 4.12-4.05 (t, 2H, *J* = 6.4, prop-1′′*H*$_2$), 4.03 (s, 2H, aip-5*H*$_2$), 2.45-2.38 (t, 2H, *J* = 6.8, prop-3′′*H*$_2$), 2,36-2.25 (m, 4H, pip-5′′,9′′*H*$_2$), 1.97-1.84 (q, 2H, *J* = 5.8, prop-2′′*H*$_2$), 1.57-1.43 (m, 4H, pip-6′′,8′′*H*$_2$), 1.43-1.31 (m, 2H, pip-7′′*H*$_2$)
^{13}C-NMR (DMSO-d_6)		δ 168.9 (aip-4*C*), 163.6 (NCNH$_2$N*C*), 159.6 (NH$_2$-2*C*), 158. (aip-8*C*), 140.1 (aip-9C*C*), 137.9 (ph^1-1′*C*), 137.8 (aip-6C*C*), 129.7 (aip-6*C*), 128.4 (ph^1-2′,6′*C*), 128.2 (ph^1-3′,5′*C*), 126.2 (ph^1-4′*C*), 119.6 (aip-4C*C*), 118.4 (aip-7*C*), 104.9 (aip-9*C*), 66.2 (prop-1′′*C*), 55.1 (prop-3′′*C*), 54.0 (pip-5′′,9′′*C*), 33.3 (aip-5*C*), 26.2 (prop-2′′*C*), 25.6 (pip-6′′,8′′*C*), 24.1 (pip-7′′*C*)
ESI HRMS [M+H$^+$]	calc	401.2341
	found	401.2339 (100)
HPLC		97.1 %
Melting point		142.1 °C

4-(4-(3-(Piperidin-1-yl)propoxy)phenyl)-5*H*-indeno[1,2-*d*]pyrimidin-2-amine (7)[178]

To a solution of **P20** (0.6 g, 2.1 mmol) in 10 ml of DMF, $CsCO_3$ (1.0 g, 3.2 mmol), potassium iodide (0.3 g, 2.1 mmol) and **P6** (0.5 g, 2.5 mmol) were added under inert atmosphere. After 5 h, the crude product was treated according to procedure **C** to give a white solid (0.4 g, 52 %). To remove residue of silicone grease, the final product was washed in hexane for one night.

Chemical formula		$C_{25}H_{28}N_4O$
Molecular weight		400.58

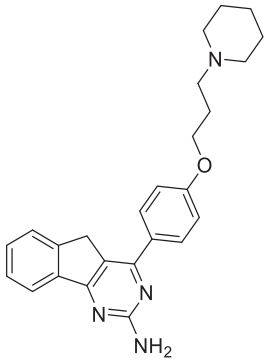

^{1}H-NMR (DMSO-d_6)		δ 8.14-8.05 (m, 2H, ph^1-2′,6′*H*), 7.94-7.87 (d, 1H, *J* = 7.8, ph^1-3′*H*), 7.72-7.64 (d, 1H, *J* = 7.1, ph^1-5′*H*), 7.59-7.44 (m, 2H, aip-6,7*H*), 7.13-7.03 (m, 2H, aip-8,9*H*), 6.60 (s, 2H, aip-NH_2), 4.12 (s, 2H, aip-5H_2), 4.11-4.02 (t, 2H, *J* = 5.9, prop-1′′H_2), 2.44-2.37 (t, 2H, *J* = 6.9, prop-3′′H_2), 2.38-2.23 (m, 4H, pip-5′′,9′′H_2), 1.97-1.82 (q, 2H, *J* = 6.4, 1.9, prop-2′′H_2), 1.58-1.44 (m, 4H, pip-6′′,8′′H_2), 1.43-1.30 (m, 2H, pip-7′′H_2)
^{13}C-NMR (DMSO-d_6)		δ 162.2 (aip-4*C*), 163.5 (NCNH$_2$*C*), 159.9 (aip-2*C*), 159.2 (ph^1-4′*C*), 145.8 (aip-9C*C*), 138.9 (aip-6C*C*), 130.0 (ph^1-2′,6′*C*), 129.8 (ph^1-3′,5′*C*), 127.1 (aip-6*C*), 125.4 (aip-9*C*), 121.0 (ph^1-1′*C*), 117.9 (aip-4C*C*), 114.2 (aip-7,8*C*), 66.0 (prop-1′′*C*), 55.0 (prop-3′′*C*), 53.9 (pip-5′′,9′′*C*), 34.3 (aip-5*C*), 26.0 (prop-2′′*C*), 25.4 (pip-6′′,8′′*C*), 23. (pip-7′′*C*)
ESI HRMS	calc	401.2341
[M+H$^+$]	found	401.2333 (100)
HPLC		97.3 %
Melting point		166.1 °C

4-Phenyl-7-(3-(pyrrolidin-1-yl)propoxy)-5*H*-indeno[1,2-*d*]pyrimidin-2-amine (8)[178]

To a solution of **P21** (0.2 g, 0.9 mmol) in 10 ml of DMF, $CsCO_3$ (0.4 g, 1.4 mmol), potassium iodide (0.1 g, 0.9 mmol) and **P24** (0.2 g, 1.1 mmol) were added under inert atmosphere. After 4 h, the crude product was treated according to procedure **C** to give a white solid (0.2 g, 55 %). To remove residue of silicone grease, the final product was washed in hexane for one night.

Chemical formula		$C_{24}H_{26}N_4O$
Molecular weight		386.50

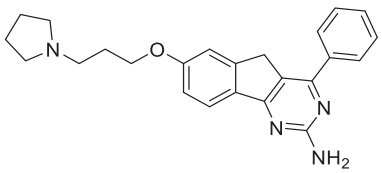

^{1}H-NMR (DMSO-d_6)		δ 8.10-8.02 (m, 2H, ph^1-2′,6′*H*), 7.84-7.77 (d, 1H, *J* = 7.8, ph^1-4′*H*), 7.58-7.45 (m, 3H, aip-6*H*, ph^1-3′,5′*H*), 7.26-7.20 (d, 1H, *J* = 7.2, aip-9*H*), 7.08-7.0 (dd, 1H, *J* = 7.1, aip-8*H*), 6.58 (s, 2H, aip-NH_2), 4.16-4.07 (t, 2H, *J* = 6.3, prop-1′′H_2), 4.01 (s, 2H, aip-5H_2), 2.62-2.53 (t, 2H, *J*= 6.7, prop-3′′H_2), 2.49-2.37 (m, 4H, pyr-5′′,8′′H_2), 1.99-1.85 (q, 2H, *J* = 5.6, prop-2′′H_2), 1.76-1.59 (m, 4H, pyr-6′′,7′′H_2)

^{13}C-NMR (DMSO-d_6)		168.9 (aip-4*C*), 163.6 (NCNH$_2$N*C*), 160.9 (aip-2*C*), 158.8 (aip-7*C*), 148.3 (aip-6C*C*), 138.0 (aip-9C*C*), 131.4 (ph^1-1′*C*), 129.5 (aip-9*C*), 128.3 (ph^1-2′,6′*C*), 128.1 (ph^1-3′,5′*C*), 122.2 (ph^1-4′*C*), 118.1(aip-4C*C*), 114.3 (aip-6*C*), 110.9 (aip-8*C*), 66.1 (prop-1′′*C*), 55.0 (prop-3′′*C*), 54.1 (pyr-5′′,8′′*C*), 34.09(aip-5*C*), 28.09 (prop-2′′*C*), 23.07 (pyr-6′′,7′′*C*)
ESI HRMS [M+H$^+$]	calc	387.2185
	found	387.2177 (100)
HPLC		96.3 %
Melting point		141.6 °C

7-(3-(Piperidin-1-yl)propoxy)-4-(4-(3-(piperidin-1-yl)propoxy)phenyl)-5*H*-indeno[1,2-*d*]pyrimidin-2-amine (9)

To a solution of **P22** (0.6 g, 2.1 mmol) in 10 ml of DMF, $CsCO_3$ (1.0 g, 3.2 mmol), potassium iodide (0.3 g, 2.1 mmol) and **P6** (0.5 g, 2.5 mmol) were added under inert atmosphere. After 5 h, the crude product was treated according to procedure **C** to give a white solid (0.6 g, 52 %). To remove residue of silicone grease, the final product was washed in hexane for one night.[178]

Chemical formula		$C_{33}H_{43}N_5O_2$
Molecular weight		541.74

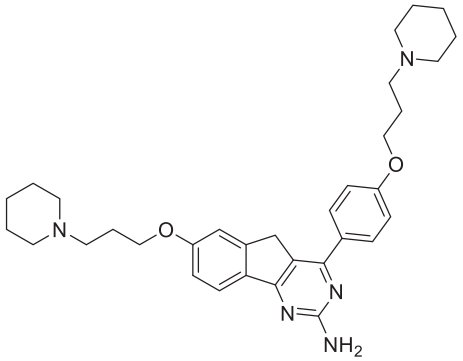

^{1}H-NMR (DMSO-d_6)		δ 8.16-8.05 (m, 2H, ph^1-2′,6′*H*), 7.60-7.51 (m, 1H, ph^1-4′*H*), 7.42-7.32 (d, 1H, *J*= 7.4, aip-6*H*), 7.18-7.03 (m, 4H, ph^1-3′,5′*H*, aip-8,9*H*), 6.58 (s, 2H, aip-N*H$_2$*), 4.18-4.05 (t, 4H, *J* = 6.5, prop/prop^1-1′′H$_2$), 4.03 (s, 2H, aip-5*H$_2$*), 2.48-2.23 (m, 12H, prop/prop^1-3′′*H$_2$*, pip/pip^1-5′′,9′′*H$_2$*), 1.83-1.61 (m, 4H, prop/prop^1-2′′*H$_2$*), 1.44-1.30 (m, 12H, pip/pip^1-6′′,7′′,8′′*H$_2$*)
^{13}C-NMR ($CDCl_3$)		δ 169.7 (aip-4*C*), 163.0 (NCNH$_2$*C*), 160.3 (aip-2*C*), 160.2 (aip-7*C*), 158.7 (ph^1-4′*C*), 140. (aip-6C*C*), 138.1 (aip-9C*C*), 128.5 (ph^1-2′,6′*C*), 129.9 (ph^1-1′*C*), 124.9 (aip-9*C*), 119.0 (aip-8*C*), 114.4 (ph^1-3′,5′*C*), 105.6 (aip-4C*C*), 106.3 (aip-6*C*), 66.6 (prop^1-1′′*C*), 66.3 (prop-1′′*C*), 55.8 (prop^1-3′′*C*), 55.8 (prop-3′′*C*), 54.4 (pip^1-2′,6′*C*), 54.3 (pip-5′′,9′′*C*), 34.1 (aip-5*C*), 26.1 (prop/prop^1-2′′*C*), 25.2 (pip^1-6′′,8′′*C*), 25.2 (pip-6′′,8′′*C*) 23.9 (pip^1-7′′*C*), 23.9 (pip-7′′*C*)
ESI HRMS [M+2H$^+$]	calc	543.3573
	found	543.3574 (100)
HPLC		96.7 %
Melting point		165.3 °C

4-Phenyl-8-(3-(pyrrolidin-1-yl)propoxy)-5*H*-indeno[1,2-*d*]pyrimidin-2-amine (10)[178]

To a solution of **P23** (0.5 g, 1.9 mmol) in 6 ml of DMF, $CsCO_3$ (0.9 g, 2.9 mmol), potassium iodide (0.3 g, 1.9 mmol) and **P24** (0.4 g, 2.3 mmol) were added under inert atmosphere. After 6 h, the crude product was treated according to procedure **C** to give a white solid (0.4 g, 53 %). To remove residue of silicone grease, the final product was washed in hexane for one night.

Chemical formula		$C_{24}H_{26}N_4O_2$
Molecular weight		386.50
^{1}H-NMR (DMSO-d_6)		δ 8.14-8.04 (m, 2H, ph^1-2′,6′*H*), 7.60-7.47 (m, 4H, aip-6*H*, ph^1-3′,4′,5′*H*), 7.42-7.36 (d, 1H, *J* = 7.4, aip-9*H*), 7.14-7.06 (dd, 1H, *J* = 7.1, aip-7*H*), 6.66 (s, 2H, aip-NH_2), 4.16-4.08 (t, 2H, *J* = 6.4, prop-1′′H_2), 4.02 (s, 2H, aip-5H_2), 2.65-2.55 (t, 2H, *J* = 6.8, prop-3′′H_2), 2.55-2.39 (m, 4H, pyr-5′′,8′′H_2), 2.01-1.85 (q, 2H, *J* = 5.9, prop-2′′H_2), 1.75-1.61 (m, 4H, pyr-6′′,7′′H_2)
^{13}C-NMR (DMSO-d_6)		δ 168.9 (aip-4*C*), 163.6 (NCNH_2N*C*), 159.6 (aip-2*C*), 158.2 (aip-8*C*), 140.1 (aip-C9*C*), 138.0 (ph^1-1′*C*), 137.8 (aip-6C*C*), 129.7 (aip-6*C*), 128.4 (ph^1-2′,6′*C*), 128.2 (ph^1-3′,5′*C*), 126.2 (ph^1-4′*C*), 119.6 (aip-4C*C*), 118.4 (aip-7*C*), 104.9 (aip-9*C*), 66.1 (prop-1′′*C*), 53.5 (prop-3′′*C*), 52.1 (pyr-5′′,8′′*C*), 33.3 (aip-5*C*), 28.0 (prop-2′′*C*), 23.0 (pyr-6′′,7′′*C*)
ESI HRMS [M+H$^+$]	calc	387.2185
	found	387.2186 (100)
HPLC		97.3 %
Melting point		140.5 °C

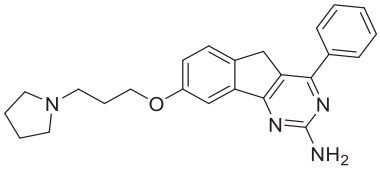

2-Amino-7-(3-(piperidin-1-yl)propoxy)-4-phenyl-5*H*-indeno[1,2-*d*]pyrimidin-6-one (11)[120]

Compound **5** (0.3 g, 0.7 mmol) and sodium hydroxide (0.05 g, 1.0 mmol) were refluxed in 10 ml of DMF for 4 h. The purification was performed as described in procedure **I**. A yellow solid was obtained (0.2 g, 79 %).

Chemical formula	$C_{25}H_{26}N_4O_2$
Molecular weight	414.51
^{1}H-NMR (DMSO-d_6)	δ 8.02-7.96 (m, 2H, ph^1-2′,6′*H*), 7.96 (s, 2H, aip-NH_2), 7.71-7.65 (d, 1H, *J* = 7.7, aip-9H), 7.58-7.45 (m, 3H, aip-6H, ph^1-3′,5′*H*), 7.23-7.16 (dd, 1H, *J* = 7.2, ph^1-4′*H*), 7.16-7.12 (d, 1H, *J* = 7.2, aip-8*H*), 4.18-4.07 (t, 2H, *J* = 6.4, prop-1′′H_2), 2.47-2.25 (m, 6H, prop-3′′H_2, pip-5′′,9′′H_2), 1.96-1.82 (q, 2H, *J* = 5.8, prop-2′′H_2), 1.55-1.44 (m, 4H, pip-6′′,8′′H_2), 1.43-1.31 (m, 2H, pip-7′′H_2)

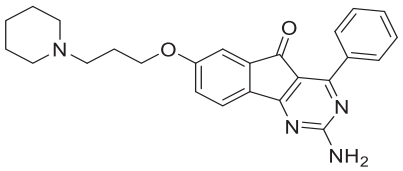

^{13}C-NMR (DMSO-d_6)		δ 187.0 (*C*O), 175.7 (aip-4*C*), 164.9 (NCNH$_2$N*C*), 164.3 (NH$_2$-2*C*), 162.7 (aip-7*C*), 138.7 (aip-6C*C*), 135.7 (aip-C9*C*), 131.3 (ph^1-1′*C*), 130.6 (aip-9*C*), 129.3 (ph^1-2′,6′*C*), 127.6 (ph^1-3′,5′*C*), 122.4 (ph^1-4′*C*), 119.6 (aip-4C*C*), 110.6 (aip-6*C*), 108.8 (aip-8*C*), 66.7 (prop-1′′*C*), 54.8 (prop-3′′*C*), 53.9 (pip-5′′,9′′*C*), 25.9 (prop-2′′*C*), 25.4 (pip-6′′,8′′*C*), 23.9 (pip-7′′*C*); ESI-HRMS *m/z*: calcd for $C_{25}H_{26}N_4O_2$ (MH^+), 415.2134, found 415.2126.
ESI HRMS [M+H$^+$]	calc	415.2134
	found	415.2126 (100)
HPLC		96.5 %
Melting point		182.2 °C

2-Amino-8-(3-(piperidin-1-yl)propoxy)-4-phenyl-5*H*-indeno[1,2-*d*]pyrimidin-5-one (12)[120]

Compound **6** (0.2 g, 0.5 mmol) and sodium hydroxide (0.03 g, 0.7 mol) were refluxed in 6 ml of DMF for 4 h. The purification was performed as described in procedure **I**. A yellow solid was obtained (0.1 g, 74 %).

Chemical formula		$C_{25}H_{26}N_4O_2$
Molecular weight		414.51

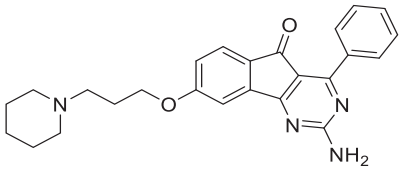

^{1}H-NMR (DMSO-d_6)		δ 8.05-7.97 (m, 2H, ph^1-2,6*H*), 7.96-7.81 (s, 2H, pyrim-N*H*$_2$), 7.62-7.57 (d, 1H, *J* = 7.6, ph-6*H*), 7.57-7.45 (m, 3H, ph-9H, ph^1-3,5*H*), 7.26-7.22 (d, 1H, *J* = 7.2, ph^1-4*H*), 7.16-7.09 (dd, 1H, *J* = 7.1, ph-7*H*), 4.21-4.11 (t, 2H, *J* = 6.4, prop-1*H*$_2$), 2.47-2.38 (t, 2H, *J* = 6.7, prop-3*H*$_2$), 2.37-2.23 (m, 4H, pip-2,6*H*$_2$), 1.98-1.84 (q, 2H, *J* = 5.6, prop-2*H*$_2$), 1.57-1.45 (m, 4H, pip-3,5*H*$_2$), 1.44-1.31 (m, 2H, pip-4*H*$_2$)
^{13}C-NMR (DMSO-d_6)		δ 186.5 (*C*O),174.8 (pyrim-4*C*), 164.8 (NCNH$_2$N*C*), 164.1 (NH$_2$-*C*), 163.6 (ph-8*C*), 142.1 (ph-C9*C*), 135.6 (ph^1-1*C*), 130.6 (C6*C*), 129.5 (ph-6*C*), 128.6 (ph^1-2,6*C*), 127.6 (ph^1-3,5*C*), 125.0 (ph^1-4*C*), 118.3 (pyrim-4C*C*), 111.5 (ph-7*C*), 106.3 (ph-9*C*), 66. (prop-1*C*), 54.8 (prop-3*C*), 54. (pip-2,6*C*), 26.0 (prop-2*C*), 25.5 (pip-5,3*C*), 24.0 (pip-4*C*)
ESI HRMS [M+H$^+$]	calc	415.2134
	found	415.2129 (100)
HPLC		97.0 %
Melting point		176.6 °C

2-Amino-4-(4-(3-(piperidin-1-yl)propoxy)phenyl)-5*H*-indeno[1,2-*d*]pyrimidin-5-one (13)[120]

Compound **7** (0.9 g, 2.0 mmol) and sodium hydroxide (0.1 g, 3.0 mmol) were refluxed in 10 ml of DMF for 3 h. The purification was performed as described in procedure **I**. A yellow solid was obtained (0.8 g, 73 %).

Chemical formula		$C_{25}H_{26}N_4O_2$
Molecular weight		414.51

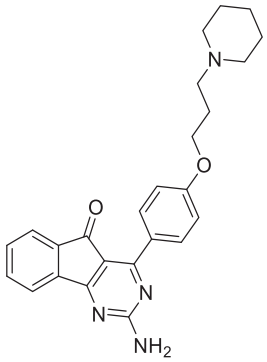

^{1}H-NMR (DMSO-d_6)		δ 8.18-8.08 (m, 2H, ph^1-2′,6′*H*), 7.93 (s, 2H, aip-N*H*$_2$), 7.83-7.61 (m, 4H, aip-6,7H, ph^1-3′,5′), 7.10-7.0 (m, 2H, aip-8,9*H*), 4.18-4.04 (t, 2H, *J* = 6.4, prop-1′′*H*$_2$), 2.48-2.39 (t, 2H, *J* = 5.8, prop-3′′*H*$_2$), 2.38-2.20 (m, 4H, pip-5′′,9′′*H*$_2$), 1.96-1.82 (q, 2H, *J* = 6.0, prop-2′′*H*$_2$), 1.60-1.45 (m, 4H, pip-6′′,8′′*H*$_2$), 1.44-1.32 (m, 2H, pip-7′′*H*$_2$)
^{13}C-NMR (DMSO-d_6)		δ 187.6 (*C*O), 175.8 (aip-4*C*), 164.7 (NCNH$_2$*C*), 164.0 (NH$_2$-2*C*), 161.0 (ph^1-4′*C*), 139.4 (aip-9C*C*), 136.2 (aip-6C*C*), 134.0 (aip-6*C*), 132.8 (aip-9*C*), 131.4 (ph^1-1′*C*), 127.8 (ph^1-2′,6′*C*), 122.9 (aip-4C*C*), 120.7 (aip-8*C*), 113.4 (ph^1-3′,5′*C*), 110.1 (aip-7*C*), 66.1 (prop-1′′*C*), 55.0 (prop-3′′*C*), 54.0 (pip-5′′,9′′*C*), 26.2 (prop-2′′*C*), 25.5 (pip-6′′,8′′*C*), 24.1 (pip-7′′*C*)
ESI HRMS [M+H$^+$]	calc	415.2134
	found	415.2132 (100)
HPLC		96.3 %
Melting point		100.5 °C

2-Amino-7-(3-(pyrrolidin-1-yl)propoxy)-4-phenyl-5*H*-indeno[1,2-*d*]pyrimidin-6-one (14)[120]

Compound **8** (0.1 g, 0.4 mmol) and sodium hydroxide (0.02 g, 0.6 mol) were refluxed in 4 ml of DMF for 4 h. The purification was performed as described in procedure **I**. A yellow solid was obtained (0.12 g, 76 %).

Chemical formula		$C_{24}H_{24}N_4O_2$
Molecular weight		400.48

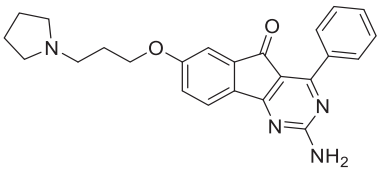

^{1}H-NMR (DMSO-d_6)		δ 8.05-7.96 (m, 2H, ph^1-2′,6′*H*), 7.94 (s, 2H, aip-N*H*$_2$), 7.73-7.64 (d, 1H, J = 7.7, aip-9H), 7.60.7.44 (m, 3H, aip-6H, ph^1-3′,5′*H*), 7.24-7.18 (dd, 1H, J = 7.2, ph^1-4′*H*), 7.18-7.11 (d, 1H, J = 7.2, aip-8*H*), 4.22-4.06 (t, 2H, $_J$ = 6.4, prop-1′′*H*$_2$), 2.64-2.53 (t, 2H, J = 5.3, prop-3′′*H*$_2$), 2.49-2.41 (m, 4H, pyr-5′′,8′′*H*$_2$), 2.01-1.85 (q, 2H, $_J$ = 6.7, prop-2′′*H*$_2$), 1.79-1.58 (m, 4H, pyr-6′′,7′′*H*$_2$)

^{13}C-NMR (DMSO-d_6)		δ 187.0 (*C*O), 175.7 (aip-4*C*), 164.9 (NCNH$_2$N*C*), 164.3 (NH$_2$-2*C*), 162.7 (aip-7*C*), 138.7 (aip-6C*C*), 135.7 (aip-9C*C*), 131.3 (ph^1-1′*C*), 130.6 (aip-9*C*), 129.3 (ph^1-2′,6′*C*), 127.6 (ph^1-3′,5′*C*), 122.5 (ph^1-4′*C*), 119.6 (aip-4C*C*), 110.6 (aip-6*C*), 108.8 (aip-8*C*), 66.6 (prop-1′′*C*), 53.5 (prop-3′′*C*), 51.9 (pyr-5′′,8′′*C*), 27.8 (prop-2′′*C*), 23.0 (pip-6′′,7′′*C*)
ESI HRMS [M+H$^+$]	calc	401.1978
	found	401.1976 (100)
HPLC		97.5 %
Melting point		145.3 °C

2-Amino-7-(3-(piperidin-1-yl)propoxy)-4-(4-(3-(piperidin-1-yl)propoxy)phenyl)-5*H*-indeno[1,2-*d*]pyrimidin-5-one (15)[120]

Compound **9** (0.1 g, 0.2 mmol) and sodium hydroxide (0.01 g, 0.3 mmol) were refluxed in 3 ml of DMF for 3 h. The purification was performed as described in procedure **I**. A yellow solid was obtained (0.06 g, 62 %).

Chemical formula		$C_{33}H_{41}N_5O_3$
Molecular weight		555.72

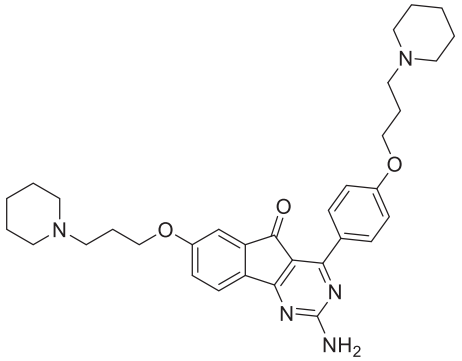

^{1}H-NMR (DMSO-d_6)		δ 8.16-8.06 (m, 2H, ph^1-2′,6′*H*), 7.80 (s, 1H, aip-N*H*$_2$), 7.63-7.55 (d, 1H, *J* = 7.6, aip-9*H*), 7.25-7.19 (d, 1H, *J* = 7.2, aip-6*H*), 7.15-7.07 (dd, 1H, *J* = 7.1, aip-8*H*), 7.06-6.96 (m, 2H, ph^1-3′,5′*H*), 4.24-4.12 (t, 2H, *J* = 6.5, prop^1-1′′*H*$_2$), 4.12-4.00 (t, 2H, *J* = 6.5, prop-1′′*H*$_2$), 2.47-2.38 (m, 4H,prop/prop^1-3′′H$_2$), 2.38-2.17 (m, 8H, pip/pip^1-5′′,9′′*H*$_2$), 2.02-1.81 (m, 4H, prop/prop^1-2′′*H*$_2$), 1.58-1.44 (m, 8H, pip/pip^1-6′′,8′′*H*$_2$), 1.43-1.27 (m, 4H, pip/ pip^1-7*H*′′$_2$)
^{13}C-NMR (DMSO-d_6)		δ 187.0 (*C*O), 174.9 (aip-4*C*), 164.6 (NCNH$_2$*C*), 163.6 (NH$_2$-2*C*), 163.4 (aip-7*C*), 160.9 (ph^1-4′*C*), 142.1 (aip-6C*C*), 131.5 (ph^1-2′,6′*C*), 128.5 (aip-9C*C*), 127.8 (ph^1-1′*C*), 124.9 (aip-9*C*), 118.2 (aip-8*C*), 113.4 (ph^1-3′,5′*C*), 111.0 (aip-4C*C*), 106.2 (aip-6*C*), 67.1 (prop^1-1′′*C*), 66.0 (prop-1′′*C*), 55.0 (prop^1-3′′*C*), 54.8 (prop-3′′*C*), 54.0 (pip/pip^1-5′′,9′′*C*), 26.1 (prop^1-2′′*C*), 25.9 (prop-2′′*C*), 25.4 (pip/pip^1-6′′,8′′*C*), 24. (pip/pip^1-7′′*C*)
ESI HRMS [M+H$^+$]	calc	556.3288
	found	556.3279 (100)
HPLC		97.2 %
Melting point		116.5 °C

2-Amino-8-(3-(pyrrolidin-1-yl)propoxy)-4-phenyl-5*H*-indeno[1,2-*d*]pyrimidin-5-one (16)[120]

Compound **10** (0.2 g, 0.5 mmol) and sodium hydroxide (0.03 g, 0.7 mmol) were refluxed in 4 ml of DMF for 4 h. The purification was performed as described in procedure **I**. A yellow solid was obtained (0.1 g, 75 %).

Chemical formula		$C_{24}H_{24}N_4O_2$
Molecular weight		400.48
^{1}H-NMR (DMSO-d_6)		8.05-7.97 (m, 2H, ph^1-2′,6′*H*), 7.90 (s, 2H, aip-N*H*$_2$), 7.62-7.56 (d, 1H, *J* = 7.6, aip-6*H*), 7.56-7.45 (m, 3H, aip-9H, ph^1-3′,5′*H*), 7.27-7.22 (d, 1H, *J* = 7.2, ph^1-4′*H*), 7.16-7.09 (dd, 1H, *J* = 7.1, aip-7*H*), 4.25-4.11 (t, 2H, *J* = 6.4, prop-1′′*H*$_2$), 2.59-2.51 (t, 2H, *J* = 6.8, prop-3′′*H*$_2$), 2.48-2.38 (m, 4H, pyr-5′′,8′′*H*$_2$), 1.99-1.86 (q, 2H, *J* = 5,8, prop-2′′*H*$_2$), 1.75-1.61 (m, 4H, pyr-6′′,7′′*H*$_2$)
^{13}C-NMR (DMSO-d_6)		δ 186.5 (*C*O), 174.8 (aip-4*C*), 164.8 (NCNH$_2$N*C*), 164. (NH$_2$-2*C*), 163.6 (aip-8*C*), 142.1 (aip-9C*C*), 135.6 (ph^1-1′*C*), 130.6 (aip-6C*C*), 129.5 (aip-6*C*), 128.6 (ph^1-2′,6′*C*), 128.2 (ph^1-3′,5′*C*), 124.9 (ph^1-4′*C*), 118.3 (aip-4C*C*), 111.5 (aip-7*C*), 106.3 (aip-9*C*), 66.8 (prop-1′′*C*), 53.5 (prop-3′′*C*), 52.0 (pyr-5′′,8′′*C*), 29.9 (prop-2′′*C*), 23.0 (pyr-6′′,7′′*C*)
ESI HRMS [M+H$^+$]	calc	401.1978
	found	401.1972 (100)
HPLC		97.1 %
Melting point		144.5 °C

8.2 Pharmacological experiments

8.2.1 hH$_1$R radioligand depletion assay on CHO cell membrane preparation

CHO cells stably expressing the *h*H$_1$R were washed with PBS-buffer (140 mM NaCl, 3 mM KCl, 1.5 mM KH_2PO_4, 8 mM $NaHPO_4$, pH = 7.4), scraped in ice-cold HEPES buffer (20 mM HEPES, 10 mM $MgCl_2$, 100 mM NaCl) and homogenized with sonification.[163] The cell membranes were reduced in pellets, which were homogenized in the HEPES buffer and stored under liquid nitrogen. The cell membranes were thawed, homogenized with sonification at 4 °C and kept in ice-cold binding buffer before starting the experiments. Membranes were incubated, for 120 min at room temperature, with [^{3}H]-pyrilamine and several concentrations of test ligand (between 1 nM and 100 µM) to perform competition binding experiments. Non-specific binding was calculated in the presence of the reference compound chlorpheniramine (10 µM) and the assays were run at least in duplicates. Determination of K_i values was performed as described for the *h*H$_3$R.

8.2.2 hH_3R radioligand depletion assay on HEK-293 cell membrane preparation

Radioligand depletion assay for human histamine H_3 receptor were performed as described previously with the following slight modifications.[168] Briefly, HEK-293 cells stably expressing the human histamine H_3 receptor were washed and harvested in phosphate buffered saline (PBS) solution. They were centrifuged (3 000 xg, 10 min, 4°C) and homogenized with an ULTRA-TURRAX® T 25 digital (IKA, Germany) in ice-cold binding buffer (12.5 mM $MgCl_2$, 100 mM NaCl and 75 mM Tris/HCl, pH 7.4). The cell membrane homogenate was centrifuged two times at 20 000 xg for 20 min (4°C). Crude membranes, using 20 µg per well in a final volume of 0.2 ml binding buffer, were incubated with [^{3}H]-N-α-methylhistamine (2 nM, 78.3 Ci mmol^{-1}) purchased from PerkinElmer (MA, USA) and various concentrations of test compounds. Assays were performed at least in duplicates with at least seven appropriate concentrations of test compounds. The incubation was performed for 90 min at room temperature by continuous shaking using 10 µM Pitolisant for determination of non-specific binding. Radioactivity was determined by liquid scintillation counting. Data were analysed using GraphPad PRISM 6 using implemented non-linear regression fit "one-site competition", where K_i values were calculated according to Cheng-Prusoff equation. Statistical analysis was performed on –log K_i values. Mean values and confidence intervals (95%) were converted to micro- or nanomolar concentrations.

8.2.3 hH_4R radioligand depletion assay on Sf9 cell membrane preparation

Cell membranes expressing *h*H_4R were obtained after infecting Sf-9 cells with baculoviruses containing the *h*H_4R.[163] After centrifugation, the cells were washed in binding buffer (12.5 mM MgCl2, 1 mM EDTA, 75 mM Tris/HCl, pH = 7.4). Membranes were pelleted at 4 °C homogenized in the binding buffer and stored at 80 °C. The cell membranes were thawed, homogenized with sonification at 4 °C and kept in ice-cold binding buffer before starting the experiments. Membranes were incubated with [^{3}H]-histamine and several concentrations of test ligand (between 100 nM and 100 µM) to perform competition binding experiments. Non-specific binding was calculated in the presence of the reference compound JNJ-77771200 (100 µM) and the assays were run at least in duplicates. Determination of K_i values was performed as described for the *h*H_3R.

8.2.4 $hD_{2s}R$ and *h*D_3R radioligand depletion assay on CHO cell membrane preparation

CHO cells stably expressing the hD2sR and hD3R were washed with PBS-buffer. Ice-cold HEPES buffer (10 mM MgCl2, 10 mM CaCl2, 5 mM KCl, 120 mM NaCl, 50 mM Tris, pH = 7.4) was used

before pelleting the cell membrane.[163] The cell membranes were thawed, homogenized with sonification at 4 °C and kept in ice-cold binding buffer before starting the experiments. Membranes were incubated, for 120 min at room temperature, with [3H]-spiperone and several concentrations of test ligand (between 1 nM and 100 μM) to perform competition binding experiments. Non-specific binding was calculated in the presence of the reference compound haloperidol (10 μM) and the assays were run at least in duplicates. Determination of Ki values was performed as described for the hH$_3$R.

8.2.5 Adenosine receptors depletion assay on CHO cell membrane preparation

CHO cell membranes expressing the human receptors (hA$_1$R, hA$_{2A}$R, hA$_{2B}$R, hA$_3$R) were used as previously described by Prof. Muller and co-workers.[263,264,215,217,216] The Cheng-Prusoff equation was used to calculate K_i values from IC_{50} values, determined by the nonlinear curve fitting program Graph Pad Prism 2.01 (GraphPad, SanDiego, CA).

8.2.6 Monoamine oxidases inhibition assays

For assaying potential monoamine oxidase (MAO) A and B inhibition, compounds were included in one-point screening for both isoforms predominantly using a continuous spectrophotometric method as described previously[67] with the exception of **3d-f**, where a discontinuous fluorimetric assay was used.[220] The spectrophotometric one-point measurements were performed in clear, flat-bottom 96 well plates (UV-Star®, No. 655801, greiner bio-one GmbH, Austria), measuring enzyme activity by spectrophotometrical observation of 4-hydroxyquinoline (λ_{max}=316 nm) formation over time as described previously.[67] Initial velocities of substrate conversion (expressed as milli absorption units per minute) were plotted against log inhibitor concentrations and fitted using the implemented non-linear regression "log inhibitor vs. response (three parameters)". For one-point measurements data were calculated as percentage of control (product formation in absence of inhibitor) and expressed as mean ± standard deviation (%) performing at least two independent experiments, each in duplicates. The IC_{50} curves were determined in the discontinuous fluorimetric assay, allowing higher assay sensitivity as well as time and cost savings. MAO inhibition assays were carried out using human recombinant membrane-bound MAO A and MAO B purchased from Sigma-Aldrich (MO, USA). Fluorimetric MAO assays were conducted in a total assay volume of 100 μL (max. 1% DMSO) using black, flat-bottom 96 well plates (No. 655076, greiner bio-one GmbH, Austria), while pipetting was partly automated using a EVO freedom pipetting robot (Tecan Trading AG, Switzerland). IC_{50} values were obtained by measuring enzyme activity (determined as MAO-dependent product

formation) with inhibitor concentrations ranging from 0.001 µM to 100 µM in the presence of 2-fold K_M concentrations of kynuramine (K_M = 30 µM for MAO A and K_M = 20 µM for MAO B). Reactions were started by addition of MAO A (1.25 ng μL^{-1}, 900 units/mL) or MAO B (1.67 ng μL^{-1}, 375 units/mL). Shift of IC_{50} values were also measured after preincubating inhibitors with enzyme (30 min, 37°C), while reactions were started by addition of substrate. For optimal enzyme activity conditions, reactions were performed in pre-warmed potassium phosphate buffer (50 mM, pH = 7.4). After incubation (15 or 20 min, 37°C with and without preincubation IC_{50} setup, respectively) reactions were stopped by manual addition of 35 µL sodium hydroxide (2 N) and enzyme activity was determined by detection of 4-hydroxyquinoline (λ_{Ex}=320±20 nm, λ_{Em}=405±20 nm) using an infinite M1000 Pro microplate reader (Tecan Trading AG, Switzerland). Data were analysed using GraphPad PRISM 6. Enzyme activity, expressed as relative fluorescence units (RFU), were plotted against log inhibitor concentrations and fitted using the implemented non-linear regression "log inhibitor vs. response (three parameters)". Since few compounds do not reach the lower plateau in IC_{50} curves (e.g. poor soluble compounds 3e and 3f), the bottom for non-linear regression was set to zero. Data were obtained from at least three independent experiments, each performed at least in duplicates. Reversibility of inhibition was assayed by preincubation of MAO B (10 ng μL^{-1}) and inhibitors (10x IC_{50}) for 0, 30 and 60 min at 37°C prior to 50x dilution in potassium phosphate buffer to give a final concentration of 0.05xIC_{50} of inhibitor. Remained enzyme activity were measured fluorimetrically as described above under substrate saturating (10xK_M) conditions. Data were calculated as percentage of control (without inhibitor for each time point) and expressed as mean ± standard deviation (%) of at least two independent experiments, each performed in duplicates (global fit).

8.2.7 L-DOPA-induced dyskinesia in 6-OHDA-lesioned rats

To produce neurodegeneration of dopaminergic neurons, rats received a unilateral 6-Hydroxydopamine (6-OHDA) injection in the medial forebrain (MFB) by stereotactic delivery.[225] Buprenorphine (0.05 mg/kg; 0.03 mg/ml) was given as analgesic before and after the surgery. Thirty minutes prior to surgery, male Sprague-Dawley rats received the noradrenaline uptake inhibitor desipramine (25 mg/kg; i.p.) to protect noradrenaline neurons. Each animal was placed in an anesthetic chamber supplied with a continuous flow of oxygen (1.5 l/min) and 5% isoflurane. Following loss of consciousness, animals were placed in a stereotactic frame (Kopf) and (6-OHDA, 5 mg/ml dissolved in sterile 0.1% ascorbic acid) was injected into the right medial forebrain bundle at 0.4 µl/minute over a 10-minute period using a Hamilton 1701N syringe (30Ga/15 mm/PST3)

coupled to an automatic injector UMP-3 linked to Micro-4 controller (WPI). The injection site was located according to the following coordinates relative to bregma: - 2.2 mm rostral, 1.6 mm lateral and 8.5 mm below the skull. Two weeks post-lesion, prior to L-DOPA treatment, rats were injected subcutaneously with 0.05 mg/kg apomorphine (dissolved in 0.9% saline; Sigma) and placed in rotometer bowls, where movements were observed for 15 minutes to assess the extent of the lesion. Animals responding with rotations were included in the subsequent study. After 3 weeks of recovery, animals were primed by administration of 6 mg/kg L-DOPA + 15mg/kg benzerazide (i.p.) once a day until AIMs severity stabilization (up to 21 consecutive days). The effects of the test items at two concentrations (0.1, 1 mg/kg i.p.) in combination with L-DOPA (6 mg/kg, i.p.) were evaluated via AIM scores. Briefly, animals were placed in clear Perspex boxes (22 cm x 34 cm x 20 cm). Each rat was observed for 1 minute at 30-minute intervals following the L-DOPA administration over a 2-hour time period. Four subtypes of AIMs were assessed including axial (A), limb (L) and orolingual (O). The severity of AIMs was scored between 1 and 4 depending on the duration of AIMs throughout the observational minute (1: present less for less than 30 seconds, 2: present for more than 30 seconds, 3: present throughout the minute but suppressed by external stimuli, 4: present throughout the minute but not suppressible by external stimuli). Statistical analysis was performed using Prism 7.0 software (GraphPad Inc., La Jolla, California, USA). Data were analyzed with a parametric one-way repeated measure analysis of variance (ANOVA) followed by Dunnett's multiple comparison test. AIMs data were subjected to a non-parametric one-way analysis of variance (ANOVA) using Friedman's test with repeated measures for the overall treatment comparison, followed by Dunn's multiple comparison test for the pairwise comparisons (versus L-DOPA), where $p < 0.05$ was considered as statistically significant.

8.2.8 Sleep studies in mice

Male adult C57BL/6 mice (28 –35 g at the time of surgery; Harlan, Gannat, France) were used. Under pentobarbital anesthesia (50 mg/kg i.p.), electrodes were implanted to record neocortical and hippocampal electroencephalograms (EEGs), neck muscle activity [electromyogram (EMG)], and heart rate [electrocardiogram (EKG)].[265] For EEG recordings, screw electrodes were fixed in the frontal, parietal, and occipital cortices, and a stainless-steel wire (200 µm diameter, bare except for 0.5 mm at the tip) was implanted in the dorsal hippocampus. For EMG and EKG recordings, two stainless steel wires (250 µm diameter) were inserted in the neck muscles and one in the lateral chest. In addition, a U-shaped plastic plate (18 mm wide, 16 mm long, 5 mm thick) was fixed stereotaxically

to the skull using dental acrylic cement so that the cranium could be painlessly returned to the same stereotaxic position using a semichronic head holder (SA-8; Narishige, Tokyo, Japan). A small hole was drilled in the skull above the posterior hypothalamus and covered by antibiotic cream for the subsequent insertion of microelectrodes. After a recovery period of 1 week, the animals were habituated to the head-restrained position by being placed on a cotton sheet inside a plastic box, painlessly restraining the head with a semichronic head holder and preventing large body movements with a cotton-coated plastic covering. During experiments, the head was covered to reduce visual stimuli. Under these conditions, the mice displayed complete sleep–waking cycles, consisting of W (wakefulness), slow– wave sleep (SWS), and paradoxical [or rapid eye movement (REM)] sleep (PS) during all experiments lasting 6 – 8 h. During experiments, sugared water was regularly given through a fine tube attached to a syringe.

9 References

(1) Meissner, W. G.; Frasier, M.; Gasser, T.; Goetz, C. G.; Lozano, A.; Piccini, P.; Obeso, J. A.; Rascol, O.; Schapira, A.; Voon, V.; Weiner, D. M.; Tison, F.; Bezard, E. Priorities in Parkinson's Disease Research. *Nat. Rev. Drug Discov.* **2011**, *10*, 377–393.

(2) Nagatsu, T.; Sawada, M. L-Dopa Therapy for Parkinson's Disease: Past, Present, and Future. *Parkinsonism Relat. Disord.* **2009**, *15*, S3–S8.

(3) Chaudhuri, K. R.; Healy, D. G.; Schapira, A. H. Non-Motor Symptoms of Parkinson's Disease: Diagnosis and Management. *Lancet Neurol.* **2006**, *5*, 235–245.

(4) Poewe, W. Non-Motor Symptoms in Parkinson's Disease. *Eur. J. Neurol.* **2008**, *15*, 14–20.

(5) Youdim, M. B. H. Why Do We Need Multifunctional Neuroprotective and Neurorestorative Drugs for Parkinson's and Alzheimer's Diseases as Disease Modifying Agents. *Exp. Neurobiol.* **2010**, *19*, 1–14.

(6) Youdim, M. B. H.; Kupershmidt, L.; Amit, T.; Weinreb, O. Promises of Novel Multi-Target Neuroprotective and Neurorestorative Drugs for Parkinson's Disease. *Park. Relat. Disord.* **2014**, *20*, S132–S136.

(7) Youdim, M. B. H. Multi Target Neuroprotective and Neurorestorative Anti-Parkinson and Anti-Alzheimer Drugs Ladostigil and M30 Derived from Rasagiline. *Exp. Neurobiol.* **2013**, *22*, 1.

(8) Connolly, B. S.; Lang, A. E. Pharmacological Treatment of Parkinson Disease. *Jama* **2014**, *311*, 1670.

(9) Alexander, G. E.; Crutcher, M. D. Functional Architecture of Basal Ganglia Circuits: Neural Substrates of Parallel Processing. *Trends Neurosci.* **1990**, *13*, 266–271.

(10) Gerfen, C. R.; Bolam, J. P. The Neuroanatomical Organization of the Basal Ganglia. In *Handbook of Basal Ganglia Structure and Function*; Elsevier Inc., 2010; Vol. 20, pp 3–28.

(11) Blesa, J.; Trigo-Damas, I.; Dileone, M.; Del Rey, N. L. G.; Hernandez, L. F.; Obeso, J. A. Compensatory Mechanisms in Parkinson's Disease: Circuits Adaptations and Role in Disease Modification. *Exp. Neurol.* **2017**, *298*, 148–161.

(12) Blandini, F.; Nappi, G.; Tassorelli, C.; Martignoni, E. Functional Changes of the Basal Ganglia Circuitry in Parkinson's Disease. *Prog. Neurobiol.* **2000**, *62*, 63–88.

(13) Calabresi, P.; Picconi, B.; Tozzi, A.; Ghiglieri, V.; Di Filippo, M. Direct and Indirect Pathways of Basal Ganglia: A Critical Reappraisal. *Nat. Neurosci.* **2014**, *17*, 1022–1030.

(14) Surmeier, D. J.; Day, M.; Gertler, T.; Chan, S.; Shen, W. D1 and D2 Dopamine Receptor Modulation of Glutamatergic Signaling in Striatal Medium Spiny Neurons. In *Handbook of Basal Ganglia Structure and Function*; Elsevier Inc., 2010; Vol. 20, pp 113–132.

(15) Dauer, W.; Przedborski, S. Parkinson's Disease: Mechanisms and Models. *Neuron.* **2003**, *39*, 889–909.

(16) Pollack, A. E. Anatomy, Physiology, and Pharmacology of the Basal Ganglia. *Neurol. Clin.* **2001**, *19*, 523–534.

(17) Mhyre, T. R.; Nw, R.; Boyd, J. T.; Hall, G.; Room, C. Protein Aggregation and Fibrillogenesis in Cerebral and Systemic Amyloid Disease. *Subcell Biochem.* **2012**, *65*, 389–455.

(18) Ko, W. K. D.; Li, Q.; Cheng, L. Y.; Morelli, M.; Carta, M.; Bezard, E. A Preclinical Study on the Combined Effects of Repeated Eltoprazine and Preladenant Treatment for Alleviating L-DOPA-Induced Dyskinesia in Parkinson's Disease. *Eur. J. Pharmacol.* **2017**, *85*, 10–16.

(19) Kreitzer, A. C.; Malenka, R. C. Striatal Plasticity and Basal Ganglia Circuit Function. *Neuron.* **2009**, *60*, 543–554.

(20) Mercuri, N. B.; Bernardi, G. The 'Magic' of L-Dopa: Why Is It the Gold Standard Parkinson's Disease Therapy? *Trends Pharmacol. Sci. Pharmacol. Sci.* **2005**, *26*, 341–344.
(21) Radad, K.; Gille, G.; Rausch, W. D. Short Review on Dopamine Agonists: Insight into Clinical and Research Studies Relevant of Parkinson's Disease. *Pharmacol. Rep.* **2005**, *57*, 701–712.
(22) Thanvi, B. R. Long Term Motor Complications of Levodopa: Clinical Features, Mechanisms, and Management Strategies. *Postgrad. Med. J.* **2004**, *80*, 452–458.
(23) Maiti, P.; Manna, J.; Dunbar, G. L. Current Understanding of the Molecular Mechanisms in Parkinson's Disease: Targets for Potential Treatments. *Transl. Neurodegener.* **2017**, *6*, 28.
(24) Kirkeby, A.; Parmar, M.; Barker, R. A. *Strategies for Bringing Stem Cell-Derived Dopamine Neurons to the Clinic: A European Approach*; Elsevier, 2017; Vol. 230, pp 165-190.
(25) Frucht, S. J. Parkinson Disease: An Update. *Neurologist* **2004**, *10*, 185–194.
(26) Oertel, W.; Schulz, J. B. Current and Experimental Treatments of Parkinson Disease: A Guide for Neuroscientists. *J. Neurochem.* **2016**, *139*, 325–337.
(27) Du, J.-J.; Chen, S.-D. Current Nondopaminergic Therapeutic Options for Motor Symptoms of Parkinson's Disease. *Chin. Med. J.* **2017**, *130*, 1856.
(28) Cacabelos, R. Parkinson's Disease: From Pathogenesis to Pharmacogenomics. *Int. J. Mol. Sci.* **2017**, *18*, 1–28.
(29) Brichta, L.; Greengard, P.; Flajolet, M. Advances in the Pharmacological Treatment of Parkinson's Disease: Targeting Neurotransmitter Systems. *Trends Neurosci.* **2013**, *36*, 543–554.
(30) Sadek, B.; Saad, A.; Sadeq, A.; Jalal, F.; Stark, H. Histamine H3 Receptor as a Potential Target for Cognitive Symptoms in Neuropsychiatric Diseases. *Behav. Brain Res.* **2016**, *312*, 415–430.
(31) Berlin, M.; Boyce, C. W.; de Lera Ruiz, M. Histamine H3 Receptor as a Drug Discovery Target. *J. Med. Chem.* **2010**, *54*, 26–53.
(32) Verdiere, M.; Rose, C.; Schwartz, J. C. Synthesis and Release of Histamine Studied on Slices from Rat Hypothalamus. *Eur. J. Pharmacol.* **1975**, *34*, 157–168.
(33) Arrang, J. M.; Garbarg, M.; Schwartz, J. C. Auto-Inhibition of Brain Histamine Release Mediated by a Novel Class (H3) of Histamine Receptor. *Nature* **1983**, *302*, 832–837.
(34) Lovenberg, T. W.; Roland, B. L.; Wilson, S. J.; Jiang, X.; Pyati, J.; Huvar, A.; Jackson, M. R.; Erlander, M. G. Cloning and Functional Expression of the Human Histamine H3 Receptor. *Mol. Pharmacol.* **1999**, *55*, 1101–1107.
(35) Kenakin, T. The Physiological Significance of Constitutive Receptor Activity. *Trends Pharmacol. Sci.* **2005**, *26*, 603–605.
(36) Cogè, F.; Guènin, S. P.; Auditon, V.; Renouardtry, A.; Beauverger, P.; Macia, C.; Ouvry, C.; Nagel, N.; Rique, H.; Boutin, J. A.; Jean, A.; Galizzi, J. P. Genomic Organization and Characterization of Splice Variants of the Human Histamine H3 Receptor. *Biochem. J.* **2001**, *355*, 279–288.
(37) Wellendorph, P.; Goodman, M. W.; Burstein, E. S.; Nash, N. R.; Brann, M. R.; Weiner, D. M. Molecular Cloning and Pharmacology of Functionally Distinct Isoforms of the Human Histamine H3 receptor. *Neuropharmacology* **2002**, *42*, 929–940.
(38) Bertaccini, G.; Coruzzi, G.; Adami, M.; Pozzoli, C.; Gambarelli, E. Histamine H3 Receptors: An Overview. *Ital. J. Gastroenterol.* **1991**, *23*, 169–189.
(39) Panula, P.; Yang, H.; Costa, E. Histamine-Containing Neurons in the Rat Hypothalamus. *Proc. Nat. Acad. Sci.* **1984**, *81*, 2572–2576.
(40) Pillot, C.; Heron, A.; Cochois, V.; Tardivel-Lacombe, J.; Ligneau, X.; Schwartz, J. C.; Arrang, J. M. A Detailed Mapping of the Histamine H3 Receptor and Its Gene Transcripts in Rat Brain. *Neuroscience* **2002**, *114*, 173–193.

(41) Watanabe, T.; Taguchi, Y.; Shiosaka, S.; Tanaka, J.; Kubota, H.; Terano, Y.; Tohyama, M.; Wada, H. Distribution of the Histaminergic Neuron System in the Central Nervous System of Rats; a Fluorescent Immunohistochemical Analysis with Histidine Decarboxylase as a Marker. *Brain Res.* **1984**, *295*, 13–25.

(42) Pollard, H.; Moreau, J.; Arrang, J. M.; Schwartz, J. C. A Detailed Autoradiographic Mapping of Histamine H3 Receptors in Rat Brain Areas. *Neuroscience* **1993**, *52*, 169–189.

(43) Schlicker, E.; Fink, K.; Detzner, M.; Göthert, M. Histamine Inhibits Dopamine Release in the Mouse Striatum via Presynaptic H3 Receptors. *J. Neural Transm.* **1993**, *93*, 1–10.

(44) Passani, M. B.; Giannoni, P.; Bucherelli, C.; Baldi, E.; Blandina, P. Histamine in the Brain: Beyond Sleep and Memory. *Biochem. Pharmacol.* **2007**, *73*, 1113–1122.

(45) Łażewska, D.; Kieć-Kononowicz, K. New Developments around Histamine H3 Receptor Antagonists/inverse Agonists: A Patent Review. *Expert Opin. Ther. Pat.* **2014**, *24*, 89–111.

(46) Panula, P.; Chazot, P. L.; Cowart, M.; Gutzmer, R.; Leurs, R.; Liu, W. L. S.; Stark, H.; Thurmond, R. L.; Haas, H. L. International Union of Basic and Clinical Pharmacology. XCVIII. Histamine Receptors. *Pharmacol. Rev.* **2015**, *67*, 601–655

(47) Ferrada, C.; Ferré, S.; Casadó, V.; Cortés, A.; Justinova, Z.; Barnes, C.; Canela, E. I.; Goldberg, S. R.; Leurs, R.; Lluis, C.; Franco, R. Interactions between Histamine H3 and Dopamine D2 Receptors and the Implications for Striatal Function. *Neuropharmacology* **2008**, *55*, 190–197.

(48) Ferré, S.; Ciruela, F.; Woods, A. S.; Lluis, C.; Franco, R. Functional Relevance of Neurotransmitter Receptor Heteromers in the Central Nervous System. *Trends Neurosci.* **2007**, *30*, 440–446.

(49) Sander, K.; Kottke, T.; Stark, H. Histamine H3 Receptor Antagonists Go to Clinics. *Biol. Pharm. Bull.* **2008**, *31*, 2163–2181.

(50) Gemkow, M. J.; Davenport, A. J.; Harich, S.; Ellenbroek, B. A.; Cesura, A.; Hallett, D. The Histamine H3 Receptor as a Therapeutic Drug Target for CNS Disorders. *Drug Discov. Today* **2009**, *14*, 509–515.

(51) Schwartz, J. The Histamine H3 Receptor : From Discovery to Clinical Trials with Pitolisant. *Br. J. Pharmacol.* **2011**, *163*, 713–721.

(52) Bongers, G.; Bakker, R. A.; Leurs, R. Molecular Aspects of the Histamine H3 Receptor. **2007**, *73*, 1195–1204.

(53) Nieto-alamilla, G.; Márquez-gómez, R. The Histamine H3 Receptor : Structure , Pharmacology and Function. *Mol. Pharmacol.* **2016**, *90*, 649–673.

(54) Drutel, G.; Peitsaro, N.; Karlstedt, K.; Wieland, K.; Smit, M. J.; Timmerman, H.; Panula, P.; Leurs, R. Identification of Rat H3 Receptor Isoforms with Different Brain Expression and Signaling Properties. *Mol. Pharmacol.* **2001**, *59*, 1–8.

(55) Arrang, J. M.; Garbarg, M.; Lancelo, J. C.; Lecomte, J. M.; Pollard, H.; Robba, M.; Schunack, W.; Schwartz, J. C. Highly Potent and Selective Ligands for Histamine H3-Receptors. *Nature* **1987**, *327*, 117–123.

(56) Ligneau, X.; Lin, J.; Vanni-Mercier, G.; Jouvet, M.; Muir, J. L.; Ganellin, C. R.; Stark, H.; Elz, S.; Schunack, W.; Schwartz, J. Neurochemical and Behavioral Effects of Ciproxifan, a Potent Histamine H3-Receptor Antagonist. *J. Pharmacol. Exp. Ther.* **1998**, *287*, 658–666.

(57) Meier, G.; Apelt, J.; Reichert, U.; Graßmann, S.; Ligneau, X.; Elz, S.; Leurquin, F.; Ganellin, C. R.; Schwartz, J. C.; Schunack, W.; Stark, H. Influence of Imidazole Replacement in Different Structural Classes of Histamine H3-Receptor Antagonists. *Eur. J. Pharm. Sci.* **2001**, *13*, 249–259.

(58) Sadek, B.; Schwed, J. S.; Subramanian, D.; Weizel, L.; Walter, M.; Adem, A.; Stark, H. Non-Imidazole Histamine H3 Receptor Ligands Incorporating Antiepileptic Moieties. *Eur. J. Med. Chem.* **2014**, *77*, 269–279.

(59) Hu, W.; Chen, Z. The Roles of Histamine and Its Receptor Ligands in Central Nervous System Disorders: An Update. *Pharmacol. Ther.* **2017**, *175*, 116–132.

(60) Stevens, D. R.; Eriksson, K. S.; Brown, R. E.; Haas, H. L. The Mechanism of Spontaneous Firing in Histamine Neurons. *Behav. Brain Res.* **2001**, *124*, 105–112.

(61) Georgsson, H.; Murray, B. J. *Sleep Disorders in Parkinson's Disease and Parkinsonian Syndromes*; Elsevier, 2012; pp 330-344.

(62) Lin, J.; Sergeeva, O. A.; Haas, H. L. Histamine H3 Receptors and Sleep-Wake Regulation. *J. Pharmacol. Exp. Ther.* **2011**, *336*, 17–23.

(63) Williams, R. H.; Chee, M. J. S.; Kroeger, D.; Ferrari, L. L.; Maratos-flier, E.; Scammell, T. E.; Arrigoni, E. Optogenetic-Mediated Release of Histamine Reveals Distal and Autoregulatory Mechanisms for Controlling Arousal. *J. Neurosci.* **2014**, *34*, 6023–6029.

(64) Slotkin, T. A. Mary Bernheim and the Discovery of Monoamine Oxidase. *Brain Res. Bull.* **1999**, *50*, 373.

(65) Finberg, J. P. M. Update on the Pharmacology of Selective Inhibitors of MAO-A and MAO-B: Focus on Modulation of CNS Monoamine Neurotransmitter Release. *Pharmacol. Ther.* **2014**, *143*, 133–152.

(66) Youdim, M. B. H.; Riederer, P. F. Monoamine Oxidase A and B Inhibitors in Parkinson's Disease. In *Handbook of Clinical Neurology*; Elsevier B.V., 2007; Vol. 84, pp 93–120.

(67) Hagenow, S.; Stasiak, A.; Ramsay, R. R.; Stark, H. Ciproxifan, a Histamine H3 Receptor Antagonist, Reversibly Inhibits Monoamine Oxidase A and B. *Sci. Rep.* **2017**, *7*, 40541.

(68) Saura, J.; Richards, J. G.; Mahy, N. Differential Age-Related Changes of MAO A and MAO B in Mouse Brain and Peripheral Organs. *Neurobiol. Aging* **1994**, *15*, 399–408.

(69) Westlund, K. N.; Denney, R. M.; Rose, R. M.; Abell, C. W. Localization of Distinct Monoamine Oxidase A and Monoamine Oxidase B Cell Populations in Human Brainstem. *Neuroscience* **1988**, *25*, 439–456.

(70) Youdim, M. B. H.; Edmondson, D.; Tipton, K. F. The Therapeutic Potential of Monoamine Oxidase Inhibitors. *Nat. Rev. Neurosci.* **2006**, *7*, 295–309.

(71) Ramsay, R. R. Molecular Aspects of Monoamine Oxidase B. *Prog. Neuro-Psychopharmacology Biol. Psychiatry* **2016**, *69*, 81–89.

(72) Wang, C. C.; Billett, E.; Borchert, A.; Kuhn, H.; Ufer, C. Monoamine Oxidases in Development. *Cell. Mol. Life Sci.* **2013**, *70*, 599–630.

(73) Edmondson, D. E.; Binda, C.; Wang, J.; Upadhyay, A. K.; Mattevi, A. Molecular and Mechanistic Properties of the Membrane-Bound Mitochondrial Monoamine Oxidases. *Biochemistry* **2009**, *48*, 4220–4230.

(74) Gasparro D. M., Almeida D.R.P., Pisterzi Luca F. , Juhasz J., Viskolcz B., Penkec B., C. I. G. Reaction Profiling of the MAO-B Catalyzed Oxidative Deamination of Amines in Alzheimer's Disease. *J. Mol. Struct.* **2003**, 527–536.

(75) Fišar, Z. Drugs Related to Monoamine Oxidase Activity. *Prog. Neuro-Psychopharmacology Biol. Psychiatry* **2016**, *69*, 112–124.

(76) Bortolato, M.; Chen, K.; Shih, J. C. Monoamine Oxidase Inactivation : From Pathophysiology to Therapeutics. *Adv. Drug Deliv. Rev.* **2008**, *60*, 1527–1533.

(77) Pisani, L.; Catto, M.; Leonetti, F.; Nicolotti, O.; Stefanachi, A.; Campagna, F.; Carotti, A. Targeting Monoamine Oxidases with Multipotent Ligands: An Emerging Strategy in the Search of New Drugs against Neurodegenerative Diseases. *Curr. Med. Chem.* **2011**, *18*, 4568–4587.
(78) Sathyanarayana Rao, T. S.; Yeragani, V. K. Hypertensive Crisis and Cheese. *Indian J. Psychiatry* **2009**, *51*, 65–66.
(79) Wimbiscus, M.; Kostenko, O.; Malone, D. MAO Inhibitors: Risks, Benefits, and Lore. *Cleve. Clin. J. Med.* **2010**, *77*, 859–882.
(80) Entzeroth, M.; Ratty, A. K. Monoamine Oxidase Inhibitors—Revisiting a Therapeutic Principle. *Open J. Depress.* **2017**, *6*, 31–68.
(81) Tzvetkov, N. T.; Hinz, S.; Ku, P.; Gastreich, M.; Mu, C. E. Indazole- and Indole-5-Carboxamides: Selective and Reversible Monoamine Oxidase B Inhibitors with Subnanomolar Potency. *J. Med. Chem.* **2014**, *57*, 6679–6703.
(82) Carradori, S.; Silvestri, R. New Frontiers in Selective Human MAO-B Inhibitors. *J. Med. Chem.* **2015**, *58*, 6717–6732.
(83) Youdim, M. B. H.; Gross, A.; Finberg, J. P. M. Rasagiline [N-Propargyl-1R(+)-Aminoindan], a Selective and Potent Inhibitor of Mitochondrial Monoamine Oxidase B. *Br. J. Pharmacol.* **2001**, *132*, 500–506.
(84) Speiser, Z.; Mayk, A.; Eliash, S.; Cohen, S. Studies with Rasagiline, a MAO-B Inhibitor, in Experimental Focal Ischemia in the Rat. *J. Neural Transm.* **1999**, *106*, 593–606.
(85) Sagi, Y.; Mandel, S.; Amit, T.; Youdim, M. B. H. Activation of Tyrosine Kinase Receptor Signaling Pathway by Rasagiline Facilitates Neurorescue and Restoration of Nigrostriatal Dopamine Neurons in Post-MPTP-Induced Parkinsonism. *Neurobiol. Dis.* **2007**, *25*, 35–44.
(86) Blandini, F.; Armentero, M. T.; Fancellu, R.; Blaugrund, E.; Nappi, G. Neuroprotective Effect of Rasagiline in a Rodent Model of Parkinson's Disease. *Exp. Neurol.* **2004**, *187*, 455–459.
(87) Robakis, D.; Fahn, S. Defining the Role of the Monoamine Oxidase-B Inhibitors for Parkinson's Disease. *CNS Drugs* **2015**, *29*, 433–441.
(88) Riederer, P.; Laux, G. MAO-Inhibitors in Parkinson's Disease. *Exp. Neurobiol.* **2011**, *20*, 1–17.
(89) Burnstock, G. Purinergic Signalling: Therapeutic Developments. *Front. Pharmacol.* **2017**, *8*, 1–55.
(90) Burnstock, G. Purinergic Signalling: From Discovery to Current Developments. *Exp. Physiol.* **2014**, *99*, 16–34.
(91) Masino, S.; Boison, D. Adenosine Metabolismcies, Adenosine Kinase, and Evolution. In *Adenosine: A Key Link between Metabolism and Brain Activity*; Springer, 2013; pp 23–54.
(92) Chen, J. F.; Eltzschig, H. K.; Fredholm, B. B. Adenosine Receptors as Drug Targets — What Are the Challenges. *Nat. Rev. Drug Discov.* **2013**, *12*, 265–286.
(93) Fredholm, B. B.; IJzerman, A. P.; Jacobson, K. A.; Klotz, K. N.; Linden, J.; Mueller, C. E. International Union of Pharmacology. XXV. Nomenclature and Classification of Adenosine Receptors. *Pharmacol. Rev.* **2001**, *53*, 527–552.
(94) Schulte, G.; Fredholm, B. B. Signalling from Adenosine Receptors to Mitogen-Activated Protein Kinases. *Cell. Signal.* **2003**, *15*, 813–827.
(95) Fredholm, B. B.; Chen, J. F.; Cunha, R. A.; Svenningsson, P.; Vaugeois, J. M. Adenosine and Brain Function. *Int. Rev. Neurobiol.* **2005**, *63*, 191–270.
(96) Sheth, S.; Brito, R.; Mukherjea, D.; Rybak, L. P.; Ramkumar, V. Adenosine Receptors: Expression, Function and Regulation. *Int. J. Mol. Sci.* **2014**, *15*, 2024–2052.

(97) Van Waarde, A.; Dierckx, R. A. J.; Zhou, X.; Khanapur, S.; Tsukada, H.; Ishiwata, K.; Luurtsema, G.; Vries, E. F. J. De; Elsinga, P. H. Potential Therapeutic Applications of Adenosine A2A Receptor Ligands and Opportunities for A2A Receptor Imaging. *Med. Res. Rev.* **2017**, 1–53.

(98) Mueller, C. E.; Jacobson, K. A. Recent Developments in Adenosine Receptor Ligands and Their Potential as Novel Drugs. *Natl. Inst. Heal.* **2011**, *1808*, 1290–1308.

(99) Svenningsson, P.; Le Moine, C.; Fisone, G.; Fredholm, B. B. Distribution, Biochemistry and Function of Striatal Adenosine A(2A) Receptors. *Prog. Neurobiol.* **1999**, *59*, 355–396.

(100) Rosin, D. L.; Robeva, A.; Woodard, R. L.; Guyenet, P. G.; Linden, J. Immunohistochemical Localization of Adenosine A2A Receptors in the Rat Central Nervous System. *J. Comp. Neurol.* **1998**, *401*, 163–186.

(101) Svenningsson, P.; Hall, H.; Sedvall, G.; Fredholm, B. B. Distribution of Adenosine Receptors in the Postmortem Human Brain: An Extended Autoradiographic Study. *Synapse* **1997**, *27*, 322–335.

(102) Schiffmann, S. N.; Fisone, G.; Moresco, R.; R.A, C.; Ferrè, S. Adenosine A2A Receptors and Basal Ganglia Physiology. *Prog. Neurobiol.* **2007**, *83*, 277–292.

(103) Schindler, C. W.; Karcz-Kubicha, M.; Thorndike, E. B.; Müller, C. E.; Tella, S. R.; Ferré, S.; Goldberg, S. R. Role of Central and Peripheral Adenosine Receptors in the Cardiovascular Responses to Intraperitoneal Injections of Adenosine A 1 and A 2A Subtype Receptor Agonists. *Br. J. Pharmacol.* **2005**, *144*, 642–650.

(104) Pinna A., Serra M., Morelli M., Simola N. Role of Adenosine A2A Receptors in Motor Control: Relevance to Parkinson's Disease and Dyskinesia. *J. Neural Transm.* **2018**, 125, 1273-1286.

(105) Hammarberg, C.; Schulte, G.; Fredholm, B. B. Evidence for Functional Adenosine A3 Receptors in Microglia Cells. *J. Neurochem.* **2003**, *86*, 1051–1054.

(106) Sachdeva, S., Gupta, M. Adenosine and Its Receptors as Therapeutic Targets: An Overview. *Saudi Pharm. J.* **2013**, 245–253.

(107) Popoli, P.; Pepponi, R. Potential Therapeutic Relevance of Adenosine A 2B and A 2A Receptors in the Central Nervous System. *CNS Neurol. Disord. - Drug Targets* **2012**, *11*, 664–674.

(108) Richardson P.J. The Adenosine A 2A Receptor of the Basal Ganglia. *J. Physiol.* **1997**, *532*, 284–286.

(109) Ferré, S.; Ciruela, F.; Canals, M.; Marcellino, D.; Burgueno, J.; Casadó, V.; Hillion, J.; Torvinen, M.; Fanelli, F.; De Benedetti, P.; Goldberg, S. R.; Bouvier, M.; Fuxe, K.; Agnati, L. F.; Lluis, C.; Franco, R.; Woods, A. Adenosine A2A-Dopamine D2 Receptor-Receptor Heteromers. Targets for Neuro-Psychiatric Disorders. *Park. Relat. Disord.* **2004**, *10*, 265–271.

(110) Armentero, M. T.; Pinna, A.; Ferré, S.; Lanciego, J. L.; Müller, C. E. .; Franco, R. Past, Present and Future of A2A Adenosine Receptor Antagonists in the Therapy of Parkinson's Disease. *Pharmacol. Ther.* **2011**, *132*, 280–299.

(111) Ferré, S.; von Euler, G.; Johansson, B.; Fredholm, B. B.; Fuxe, K. Stimulation of High-Affinity Adenosine A2 Receptors Decreases the Affinity of Dopamine D2 Receptors in Rat Striatal Membranes. *Proc. Natl. Acad. Sci.* **1991**, *88*, 7238–7241.

(112) Fuxe, K.; Marcellino, D.; Genedani, S.; Agnati, L. Adenosine A2A Receptors, Dopamine D2 Receptors and Their Interactions in Parkinson's Disease. *Mov. Disord.* **2007**, *22*, 1990–2017.

(113) Cieslak, M.; Komoszynski, M.; Wojtczak, A. Adenosine A2A Receptors in Parkinson's Disease Treatment. *Purinergic Signal.* **2008**, *4*, 305–312.

(114) Morelli, M.; Di Paolo, T.; Wardas, J.; Calon, F.; Xiao, D.; Schwarzschild, M. A. Role of Adenosine A2A Receptors in Parkinsonian Motor Impairment and L-DOPA-Induced Motor Complications. *Prog. Neurobiol.* **2007**, *83*, 293–309.

(115) Fuxe, K.; Ferre, S.; Canals, M.; Torvinen, M.; Terasmaa, A.; Marcellino, D.; Goldberg, S. R.; Staines, W.; Jacobsen, K. X.; Lluis, C.; Woods, A. S.; Agnati, L. F.; Franco, R. Adenosine A2A and Dopamine D2 Heteromeric Receptor Complexes and Their Function. *J. Mol. Neurosci.* **2005**, *26*, 209–217.

(116) Ko, W. K. D.; Camus, S. M.; Li, Q.; Yang, J.; McGuire, S.; Pioli, E. Y.; Bezard, E. An Evaluation of Istradefylline Treatment on Parkinsonian Motor and Cognitive Deficits in 1-Methyl-4-Phenyl-1,2,3,6-Tetrahydropyridine (MPTP)-Treated Macaque Models. *Neuroph.* **2016**, *110*, 48–58.

(117) Shao, Y.-M.; Ma, X.; Paira, P.; Tan, A.; Herr, D. R.; Lim, K. L.; Ng, C. H.; Venkatesan, G.; Klotz, K.-N.; Federico, S.; Spalluto, G.; Cheong, S. L.; Chen, Y. Z.; Pastorin, G. Discovery of Indolylpiperazinylpyrimidines with Dual-Target Profiles at Adenosine A2A and Dopamine D2 Receptors for Parkinson's Disease Treatment. *PLoS One* **2018**, *13*, 1–27.

(118) Rose, S.; Jackson, M. J.; Smith, L. A.; Stockwell, K.; Johnson, L.; Carminati, P.; Jenner, P. The Novel Adenosine A2A Receptor Antagonist ST1535 Potentiates the Effects of a Threshold Dose of L -DOPA in MPTP Treated Common Marmosets. *Eur. J. Pharmacol.* **2006**, *546*, 82–87.

(119) Hodgson, R. A.; Bedard, P. J.; Varty, G. B.; Kazdoba, T. M.; Di, T.; Grzelak, M. E.; Pond, A. J.; Hadjtahar, A.; Belanger, N.; Gregoire, L.; Dare, A.; Neustadt, B. R.; Stamford, A. W.; Hunter, J. C. Preladenant , a Selective A2A Receptor Antagonist , Is Active in Primate Models of Movement Disorders. *Exp. Neurol.* **2010**, *225*, 384–390.

(120) Shook, B. C.; Rassnick, S.; Wallace, N.; Crooke, J.; Ault, M.; Chakravarty, D.; Barbay, J. K.; Wang, A.; Powell, M. T.; Leonard, K.; Alford, V.; Scannevin, R. H.; Carroll, K.; Lampron, L.; Westover, L.; Lim, H.-K.; Russell, R.; Branum, S.; Wells, K. M.; Damon, S.; Youells, S.; Li, X.; Beauchamp, D. A.; Rhodes, K.; Jackson, P. F. Design and Characterization of Optimized Adenosine A2A/A1 Receptor Antagonists for the Treatment of Parkinson's Disease. *J. Med. Chem.* **2012**, *55*, 1402–1417.

(121) Sharma, V. D.; Lyons, K. E.; Pahwa, R. Amantadine Extended-Release Capsules for Levodopa-Induced Dyskinesia in Patients with Parkinson's Disease. *Ther. Clin. Risk Manag.* **2018**, *14*, 665–673.

(122) Finlay, C.; Duty, S. Therapeutic Potential of Targeting Glutamate Receptors in Parkinson's Disease. *J. Neural Transm.* **2014**, *121*, 861–880.

(123) Shook, B. C.; Jackson, P. F. Adenosine A2A Receptor Antagonists and Parkinson's Disease. *ACS Chem. Neurosci.* **2011**, *2*, 555–567.

(124) Chen, J.; Xu, K.; Petzer, J. P.; Staal, R.; Xu, Y.; Beilstein, M.; Sonsalla, P. K.; Castagnoli, K.; Jr, N. C.; Schwarzschild, M. A. Neuroprotection by Caffeine and A2A Adenosine Receptor Inactivation in a Model of Parkinson's Disease. *J. Neurosci.* **2001**, *21*, 2–7.

(125) Ikeda, K.; Kurokawa, M.; Aoyama, S.; Kuwana, Y. Neuroprotection by Adenosine A2A Receptor Blockade in Experimental Models of Parkinson's Disease. *J. Neurochem.* **2002**, *80*, 262–270.

(126) Morelli, M.; Blandini, F.; Simola, N.; Hauser, R. A. A 2A Receptor Antagonism and Dyskinesia in Parkinson's Disease. *Parkinsons. Dis.* **2012**, *2012*, 1–8.

(127) Lundblad, M.; Andersson, M.; Winkler, C.; Kirik, D.; Wierup, N.; Cenci Nilsson, M. A. Pharmacological Validation of Behavioural Measures of Akinesia and Dyskinesia in a Rat Model of Parkinson's Disease. *Eur. J. Neurosci.* **2002**, *15*, 120–132.

(128) Kanda, T.; Jackson, M. J.; Smith, L. A.; Pearce, R. K. B.; Nakamura, J.; Kase, H.; Kuwana, Y.; Jenner, P. Combined Use of the Adenosine A(2A) Antagonist KW-6002 with L-DOPA or with Selective D1 or D2 Dopamine Agonists Increases Antiparkinsonian Activity but Not Dyskinesia in MPTP-Treated Monkeys. *Exp. Neurol.* **2000**, *162*, 321–327.

(129) Kanda, T.; Jackson, M. J.; Smith, L. A.; Pearce, R. K. B.; Nakamura, J.; Kase, H.; Kuwana, Y.; Jenner, P. Adenosine A(2A) Antagonist: A Novel Antiparkinsonian Agent That Does Not Provoke Dyskinesia in Parkinsonian Monkeys. *Ann. Neurol.* **1998**, *43*, 507–513.

(130) Uchida, S-H., Soshiroda, K., Okita, E., Uchida, M. K., Mori, A., Jenner, P., K. T. The Adenosine A2A Receptor Antagonist, Istradefylline Enhances Anti-Parkinsonian Activity Induced by Combined Treatment with Low Doses of L-DOPA and Dopamine Agonists in MPTP-Treated Common Marmosets. *Eur. J. Pharmacol.* **2015**, *766*, 25–30.

(131) Pinna, A. Adenosine A2A Receptor Antagonists in Parkinson's Disease: Progress in Clinical Trials from the Newly Approved Istradefylline to Drugs in Early Development and Those Already Discontinued. *CNS Drugs* **2014**, *28*, 455–474.

(132) Rascol, O.; Perez-Lloret, S.; Ferreira, J. J. New Treatments for Levodopa-Induced Motor Complications. *Mov. Disord.* **2015**, *30*, 1451–1460.

(133) Factor, S.; Mark, M. H.; Watts, R.; Struck, L.; Mori, A.; Ballerini, R.; Sussman, N. M. A Long-Term Study of Istradefylline in Subjects with Fluctuating Parkinson's Disease. *Park. Relat. Disord.* **2010**, *16*, 423–426.

(134) Micheli, F., Zúñiga-Ramírez, C. Preladenant: An Adenosine A2A Receptor Antagonist for Parkinson's Disease. *Future Neurol.* **2013**, *8*, 122–129.

(135) Hauser, R. A.; Cantillon, M.; Pourcher, E.; Micheli, F.; Mok, V.; Onofrj, M.; Huyck, S.; Wolski, K. Preladenant in Patients with Parkinson's Disease and Motor Fluctuations: A Phase 2, Double-Blind, Randomised Trial. *Lancet Neurol.* **2011**, *10*, 221–229.

(136) De Lera Ruiz, M.; Lim, Y.-H.; Zheng, J. Adenosine A 2A Receptor as a Drug Discovery Target. *J. Med. Chem.* **2014**, *57*, 3623–3650.

(137) Nazario, L. R.; da Silva, R. S.; Bonan, C. D. Targeting Adenosine Signaling in Parkinson's Disease: From Pharmacological to Non-Pharmacological Approaches. *Front. Neurosci.* **2017**, *11*, 1–12

(138) Postuma, R. B.; Lang, A. E.; Munhoz, R. P.; Charland, K.; Pelletier, A.; Moscovich, M.; Filla, L.; Zanatta, D.; Romenets, S. R.; Altman, R.; Chuang, R.; Shah, B. Caffeine for Treatment of Parkinson Disease: A Randomized Controlled Trial. *Neurology* **2012**, *79*, 651–658.

(139) Wills, A. A.; Eberly, S.; Tennis, M.; Lang, A. E.; Messing, S.; Togasaki, D.; Tanner, C. M.; Chen, J.; Oakes, D.; Mcdermott, M. P. Caffeine Consumption and Risk of Dyskinesia in CALM-PD. *Mov. Disord.* **2014**, *28*, 380–383.

(140) Mihara, T.; Mihara, K.; Yarimizu, J.; Mitani, Y.; Matsuda, R.; Yamamoto, H.; Aoki, S.; Akahane, A.; Iwashita, A.; Matsuoka, N. Pharmacological Characterization of a Novel , Potent Adenosine A1 and A2A Receptor Dual Antagonist , 5- [5-Amino- (ASP5854), in Models of Parkinson's Disease and Cognition. *J. Pharmacol. Exp. Ther.* **2007**, *323*, 708–719.

(141) Lazarus, M.; Shen, H. Y.; Cherasse, Y.; Qu, W.-M.; Huang, Z. L.; Bass, C. E.; Winsky-Sommerer, Raphaelle Semba, K.; Fredholm, B. B.; Boison, D.; Hayaishi, O.; Urade, Y.; Chen, J.-F. Arousal Effect of Caffeine Depends on Adenosine A2A Receptors in the Shell of the Nucleus Accumbens. *J. Neurosci.* **2011**, *27*, 10067–10075.

(142) Kelsey, J. E.; Langelier, N. A.; Oriel, B. S.; C., R. The Effects of Systemic, Intrastriatal, and Intrapallidal Injections of Caffeine and Systemic Injections of A2A and A1 Antagonists on Forepaw Stepping in the Unilateral 6-OHDA-Lesioned Rat. *Psychopharmacol.* **2009**, *201*, 529–539.

(143) Matsuya, T.; Takuma, K.; Sato, K.; Asai, M.; Murakami, Y.; Miyoshi, S.; Noda, A.; Nagai, T.; Mizoguchi, H.; Nishimura, S.; Yamada, K. Synergistic Effects of Adenosine A2A Antagonist and L-DOPA on Rotational Behaviors in 6-Hydroxydopamine-Induced Hemi-Parkinsonian Mouse Model. *J. Pharmacol. Sci.* **2007**, *103*, 329–332.

(144) Collins, L. E.; Galtieri, D. J.; Brennum, L. T.; Sager, T. N.; Hockemeyer, J.; Müller, C. E.; Hinman, J. R.; Chrobak, J. J.; Salamone, J. D. Oral Tremor Induced by the Muscarinic Agonist Pilocarpine Is Suppressed by the Adenosine A2A Antagonists MSX-3 and SCH58261, but Not the Adenosine A1 Antagonist DPCPX. *Pharmacol. Biochem. Behav.* **2010**, *94*, 561–569.

(145) Suzuki, K.; Miyamoto, M.; Miyamoto, T.; Uchiyama, T.; Watanabe, Y.; Suzuki, S.; Kadowaki, T.; Fujita, H.; Matsubara, T.; Sakuramoto, H.; Hirata, K. Istradefylline Improves Daytime Sleepiness in Patients with Parkinson's Disease: An Open-Label, 3-Month Study. *J. Neurol. Sci.* **2017**, *380*, 230–233.

(146) Basheer, R.; Strecker, R. E.; Thakkar, M. M.; Mccarley, R. W. Adenosine and Sleep – Wake Regulation. *Prog. Neurobiol.* **2004**, *73*, 379–396.

(147) Huang, Z.-L.; Urade, Y.; Hayaishi, O. The Role of Adenosine in the Regulation of Sleep. *Curr. Top. Med. Chem.* **2011**, *11*, 1047–1057.

(148) Atack, J. R.; Shook, B. C.; Rassnick, S.; Jackson, P. F.; Rhodes, K.; Drinkenburg, W. H.; Ahnaou, A.; Te Riele, P.; Langlois, X.; Hrupka, B.; De Haes, P.; Hendrickx, H.; Aerts, N.; Hens, K.; Wellens, A.; Vermeire, J.; Megens, A. A. H. P. JNJ-40255293, a Novel Adenosine A2A/A1 Antagonist with Efficacy in Preclinical Models of Parkinson's Disease. *ACS Chem. Neurosci.* **2014**, *5*, 1005–1019.

(149) Rebola, N., Pinheiro, P. C., Oliveira C. R., Malva J. O., Cuhna, R. A. Subcellular Localization of Adenosine A1 Receptors in Nerve Terminals and Synapses of the Rat Hippocampus. *Brain Res.* **2003**, *987*, 49–58.

(150) Maemoto, T.; Tada, M.; Mihara, T.; Ueyama, N.; Matsuoka, H.; Harada, K.; Yamaji, T.; Shirakawa, K.; Kuroda, S.; Akahane, A.; Iwashita, A.; Matsuoka, N.; Mutoh, S. Pharmacological Characterization of FR194921, a New Potent, Selective, and Orally Active Antagonist for Central Adenosine A1 Receptors. *J. Pharmacol. Sci.* **2004**, *96*, 42–52.

(151) Mihara, T.; Noda, A.; Arai, H.; Mihara, K.; Iwashita, A.; Murakami, Y.; Matsuya, T.; Miyoshi, S.; Nishimura, S.; Matsuoka, N. Brain Adenosine A2A Receptor Occupancy by a Novel A1/A2A Receptor Antagonist, ASP5854, in Rhesus Monkeys: Relationship to Anticataleptic Effect. *J. Nucl. Med.* **2008**, *49*, 1183–1188.

(152) Mihara, T.; Iwashita, A.; Matsuoka, N. A Novel Adenosine A1 and A2A Receptor Antagonist ASP5854 Ameliorates Motor Impairment in MPTP-Treated Marmosets: Comparison with Existing Anti-Parkinson's Disease Drugs. *Behav. Brain Res.* **2008**, *194*, 152–161.

(153) Bansal, Y.; Silakari, O. Multifunctional Compounds: Smart Molecules for Multifactorial Diseases. *Eur. J. Med. Chem.* **2014**, *76*, 31–42.

(154) Marzo, A.; Dal Bo, L.; Monti, N. C.; Crivelli, F.; Ismaili, S.; Caccia, C.; Cattaneo, C.; Fariello, R. G. Pharmacokinetics and Pharmacodynamics of Safinamide, a Neuroprotectant with Antiparkinsonian and Anticonvulsant Activity. *Pharmacol. Res.* **2004**, *50*, 77–85.

(155) Butini, S.; Nikolic, K.; Kassel, S.; Brückmann, H.; Filipic, S.; Agbaba, D.; Gemma, S.; Brogi, S.; Brindisi, M.; Campiani, G.; Stark, H. Polypharmacology of Dopamine Receptor Ligands. *Prog. Neurobiol.* **2016**, *142*, 68–103.

(156) Anighoro, A.; Bajorath, J.; Rastelli, G. Polypharmacology: Challenges and Opportunities in Drug Discovery. *J. Med. Chem.* **2014**, *57*, 7874–7887.

(157) Leon, R.; Garcia, A. G.; Marco-Contelles, J. Recent Advances in the Multitarget-Directed Ligands Approach for the Treatment of Alzheimer's Disease. *Med. Res. Rev.* **2013**, *33*, 139–189.

(158) Morphy, R.; Kay, C.; Rankovic, Z. From Magic Bullets to Designed Multiple Ligands. *Drug Discov. Today* **2004**, *9*, 641–651.

(159) Peters, J. U. Polypharmacology - Foe or Friend? *J. Med. Chem.* **2013**, *56*, 8955–8971.

(160) Ramsay, R. R.; Popovic-Nikolic, M. R.; Nikolic, K.; Uliassi, E.; Bolognesi, M. L. A Perspective on Multi-Target Drug Discovery and Design for Complex Diseases. *Clin. Transl. Med.* **2018**, *7*, 1–14.
(161) Decker, M. *Design of Hybrid Molecules for Drug Development*; Elsevier, 2017; pp 1-132.
(162) Khanfar, M. A.; Affini, A.; Lutsenko, K.; Nikolic, K.; Butini, S.; Stark, H. Multiple Targeting Approaches on Histamine H3 Receptor Antagonists. *Front. Neurosci.* **2016**, *10*, 1–17.
(163) Bautista-Aguilera, Ó. M.; Hagenow, S.; Palomino-Antolin, A.; Farré-Alins, V.; Ismaili, L.; Joffrin, P. L.; Jimeno, M. L.; Soukup, O.; Janočková, J.; Kalinowsky, L.; Proschak, E.; Iriepa, I.; Moraleda, I.; Schwed, J. S.; Romero Martínez, A.; López-Muñoz, F.; Chioua, M.; Egea, J.; Ramsay, R. R.; Marco-Contelles, J.; Stark, H. Multitarget-Directed Ligands Combining Cholinesterase and Monoamine Oxidase Inhibition with Histamine H3R Antagonism for Neurodegenerative Diseases. *Angew. Chemie* **2017**, *56*, 12765–12769.
(164) Petroianu, G.; Arafat, K.; Sasse, B. C.; Stark, H. Multiple Enzyme Inhibitions by Histamine H3 Receptor Antagonists as Potential Procognitive Agents. *Pharmazie* **2006**, *61*, 179–182.
(165) Apelt, J.; Ligneau, X.; Pertz, H. H.; Arrang, J.-M.; Ganellin, C. R.; Schwartz, J.-C.; Schunack, W.; Stark, H. Development of a New Class of Nonimidazole Histamine H(3) Receptor Ligands with Combined Inhibitory Histamine N-Methyltransferase Activity. *J. Med. Chem.* **2002**, *45*, 1128–1141.
(166) Huang, L., Lu, C., Sun, Y., Mao, F., Luo, Z., Su, T., Jiang, H., Shan, W., Li, X. Multitarget-Directed Benzylideneindanone Derivatives: Anti-β-Amyloid (Aβ) Aggregation, Antioxidant, Metal Chelation, and Monoamine Oxidase B (MAO-B) Inhibition Properties against Alzheimer's Disease. *J. Med. Chem.* **2012**, *55*, 8483–8492.
(167) Khan, N.; Saad, A.; Nurulain, S. M.; Darras, F. H.; Decker, M.; Sadek, B. The Dual-Acting H3 Receptor Antagonist and AChE Inhibitor UW-MD-71 Dose-Dependently Enhances Memory Retrieval and Reverses Dizocilpine-Induced Memory Impairment in Rats. *Behav. Brain Res.* **2016**, *297*, 155–164.
(168) Affini, A.; Hagenow, S.; Zivkovic, A.; Marco-Contelles, J.; Stark, H. Novel Indanone Derivatives as MAO B/H3R Dual-Targeting Ligands for Treatment of Parkinson's Disease. *Eur. J. Med. Chem.* **2018**, *148*, 487–497.
(169) Nel, M. S.; Petzer, A.; Petzer, J. P.; Legoabe, L. J. 2-Benzylidene-1-Indanone Derivatives as Inhibitors of Monoamine Oxidase. *Bioorganic Med. Chem. Lett.* **2016**, *26*, 4599–4605.
(170) Mostert, S.; Petzer, A.; Petzer, J. P. Indanones as High-Potency Reversible Inhibitors of Monoamine Oxidase. *ChemMedChem* **2015**, *10*, 862–873.
(171) Von Coburg, Y.; Kottke, T.; Weizel, L.; Ligneau, X.; Stark, H. Potential Utility of Histamine H3 Receptor Antagonist Pharmacophore in Antipsychotics. *Bioorg. Med. Chem. Lett.* **2009**, *19*, 538–542.
(172) Mikó, T.; Ligneau, X.; Pertz, H. H.; Arrang, J.-M.; Ganellin, C. R.; Schwartz, J.-C.; Schunack, W.; Stark, H. Structural Variations of 1-(4-(phenoxymethyl)benzyl)piperidines as Nonimidazole Histamine H3 Receptor Antagonists. *Bioorg. Med. Chem.* **2004**, *12*, 2727–2736.
(173) Matasi, J. J.; Caldwell, J. P.; Hao, J.; Neustadt, B.; Arik, L.; Foster, C. J.; Lachowicz, J.; Tulshian, D. B. The Discovery and Synthesis of Novel Adenosine Receptor (A2A) Antagonists. *Bioorganic Med. Chem. Lett.* **2005**, *15*, 1333–1336.
(174) Lim, H.; Chen, J.; Sensenhauser, C.; Cook, K.; Preston, R.; Thomas, T.; Shook, B.; Jackson, P. F.; Rassnick, S.; Rhodes, K.; Gopaul, V.; Salter, R.; Silva, J.; Evans, D. C. Overcoming the Genotoxicity of a Pyrrolidine Substituted Arylindenopyrimidine As a Potent Dual Adenosine A2A /A1 Antagonist by Minimizing Bioactivation to an Iminium Ion Reactive Intermediate. *Chem. Res. Toxicol.* **2011**, *24*, 1012–1030.

(175) Caccia, C.; Maj, R.; Calabresi, M.; Maestroni, S.; Faravelli, L.; Curatolo, L.; Salvati, P.; Fariello, R. G. Safinamide From Molecular Targets to a New Anti-Parkinson Drug. *Neurology* **2006**, *67*, S18–S23.

(176) Nel, M. S.; Petzer, A.; Petzer, J. P.; Legoabe, L. J. 2-Benzylidene-1-Indanone Derivatives as Inhibitors of Monoamine Oxidase. *Bioorg. Med. Chem. Lett.* **2016**, *26*, 4599–4605.

(177) Wingen, W., Stark, H. Scaffold Variations in Amine Warhead of Histamine H3 Receptor Antagonists. *Drug Discov. Today Technol.* **2013**, *10*, 483–489.

(178) Tomasch, M.; Schwed, J. S.; Weizel, L.; Stark, H. Novel Chalcone-Based Fluorescent Human Histamine H3 Receptor Ligands as Pharmacological Tools. *Front. Syst. Neurosci.* **2012**, *6*, 1–16.

(179) Sander, K.; Kottke, T.; Hoffend, C.; Walter, M.; Weizel, L.; Camelin, J. C.; Ligneau, X.; Schneider, E. H.; Seifert, R.; Schwartz, J. C.; Stark, H. First Metal-Containing Histamine H3 Receptor Ligands. *Org. Lett.* **2010**, *12*, 2578–2581.

(180) Finkelstein, H. Finkelstein Reaction. *Chem. Ber.* **1910**, *43*, 1528–1532.

(181) Stark, H. Convenient Procedures for Synthesis of Ciproxifan, a Histamine H3-Receptor Antagonist. *Arch. Pharm.* **2000**, *333*, 315–316.

(182) Morales-Camilo, N.; Salas, C. O.; Sanhueza, C.; Espinosa-Bustos, C.; Sepúlveda-Boza, S.; Reyes-Parada, M.; Gonzalez-Nilo, F.; Caroli-Rezende, M.; Fierro, A. Synthesis, Biological Evaluation, and Molecular Simulation of Chalcones and Aurones as Selective MAO-B Inhibitors. *Chem. Biol. Drug Des.* **2015**, *85*, 685–695.

(183) Böhme, A.; Thaens, D.; Schramm, F.; Paschke, A.; Schüürmann, G. Thiol Reactivity and Its Impact on the Ciliate Toxicity of α,β-Unsaturated Aldehydes, Ketones, and Esters. *Chem. Res. Toxicol.* **2010**, *23*, 1905–1912.

(184) Park, B. K.; Boobis, A.; Clarke, S.; Goldring, C. E. P.; Jones, D.; Kenna, J. G.; Lambert, C.; Laverty, H. G.; Naisbitt, D. J.; Nelson, S.; Nicoll-Griffith, D. A.; Obach, R. S.; Routledge, P.; Smith, D. A.; Tweedie, D. J.; Vermeulen, N.; Williams, D. P.; Wilson, I. D.; Baillie, T. A. Managing the Challenge of Chemically Reactive Metabolites in Drug Development. *Nat. Rev. Drug Discov.* **2011**, *10*, 292–306.

(185) Mulliner, D.; Wondrousch, D.; Schüürmann, G. Predicting Michael-Acceptor Reactivity and Toxicity through Quantum Chemical Transition-State Calculations. *Org. Biomol. Chem.* **2011**, *9*, 8400–8412.

(186) Slawik, C.; Rickmeyer, C.; Brehm, M.; Böhme, A.; Schüürmann, G. Glutathione Adduct Patterns of Michael-Acceptor Carbonyls. *Environ. Sci. Technol.* **2017**, *51*, 4018–4026.

(187) Huang, L.; Miao, H.; Sun, Y.; Meng, F.; Li, X. Discovery of Indanone Derivatives as Multi-Target-Directed Ligands against Alzheimer's Disease. *Eur. J. Med. Chem.* **2014**, *87*, 429–439.

(188) Bansal, R.; Narang, G.; Zimmer, C.; Hartmann, R. W. Synthesis of Some Imidazolyl-Substituted 2-Benzylidene Indanone Derivatives as Potent Aromatase Inhibitors for Breast Cancer Therapy. *Med. Chem. Res.* **2011**, *20*, 661–669.

(189) Abdel-Magid, A. F.; Mehrman, S. J. A Review on the Use of Sodium Triacetoxyborohydride in the Reductive Amination of Ketones and Aldehydes. *Org. Process Res. Dev.* **2006**, *10*, 971–1031.

(190) Abdel-Magid, A. F.; Carson, K. G.; Harris, B. D.; Maryanoff, C. A.; Shah, R. D. Reductive Amination of Aldehydes and Ketones with Sodium Triacetoxyborohydride. Studies on Direct and Indirect Reductive Amination Procedures. *J. Org. Chem.* **1996**, *61*, 3849–3862.

(191) Pereira, C.; Salgado, S.; Rizzo-Aguiar, F.; Garcia-Mera, X.; Rodríguez-Borges, J. Synthesis of New Propargylated 1-Pyrindane Derivatives as Rasagiline Analogues. *Synlett* **2013**, *24*, 837–838.

(192) Herzig, Y.; Lerman, L.; Goldenberg, W.; Lerner, D.; Gottlieb, H. E.; Nudelman, A. Hydroxy-1-Aminoindans and Derivatives: Preparation, Stability, and Reactivity. *J. Org. Chem.* **2006**, *71*, 4130–4140.

(193) Dong, L.; Aleem, S.; Fink, C. A. Microwave-Accelerated Reductive Amination between Ketones and Ammonium Acetate. *Tetrahedron Lett.* **2010**, *51*, 5210–5212.

(194) Patil, P. O.; Bari, S. B.; Firke, S. D.; Deshmukh, P. K.; Donda, S. T.; Patil, D. A. Bioorganic & Medicinal Chemistry A Comprehensive Review on Synthesis and Designing Aspects of Coumarin Derivatives as Monoamine Oxidase Inhibitors for Depression and Alzheimer ' S Disease. *Bioorg. Med. Chem.* **2013**, *21*, 2434–2450.

(195) Llàcer, E.; Romea, P.; Urpí, F. Studies on the Hydrogenolysis of Benzyl Ethers. *Tetrahedron Lett.* **2006**, *47*, 5815–5818.

(196) Weissman, S. A.; Zewge, D. Recent Advances in Ether Dealkylation. *Tetrahedron* **2005**, *61*, 7833–7863.

(197) Fang, Z.; Zhou, G. C.; Zheng, S. L.; He, G. L.; Li, J. L.; He, L.; Bei, D. Lithium Chloride-Catalyzed Selective Demethylation of Aryl Methyl Ethers under Microwave Irradiation. *J. Mol. Catal.* **2007**, *274*, 16–23.

(198) Pettit, G. R.; Hoffmann, H.; Herald, D. L.; McNulty, J.; Murphy, A.; Higgs, K. C.; Hamel, E.; Lewin, N. E.; Pearce, L. V.; Blumberg, P. M.; Pettit, R. K.; Knight, J. C. Antineoplastic Agents 491.1 Synthetic Conversion of Aaptamine to Isoaaptamine, 9-Demethylaaptamine, and 4-Methylaaptamine. *J. Org. Chem.* **2004**, *69*, 2251–2256.

(199) Tomasch, M.; Schwed, J. S.; Paulke, A.; Stark, H. Bodilisant - A Novel Fluorescent, Highly Affine Histamine H3 Receptor Ligand. *ACS Med. Chem. Lett.* **2013**, *4*, 269–273.

(200) Diveshkumar, K. V.; Sakrikar, S.; Harikrishna, S.; Dhamodharan, V.; Pradeepkumar, P. I. Targeting Promoter G-Quadruplex DNAs by Indenopyrimidine-Based Ligands. *ChemMedChem* **2014**, *9*, 2754–2765.

(201) Krohn, K. A.; Link, J. M. Interpreting Enzyme and Receptor Kinetics: Keeping It Simple, but Not Too Simple. *Nucl. Med. Biol.* **2003**, *30*, 819–826.

(202) Kenakin, T.; Williams, M. Defining and Characterizing Drug/compound Function. *Biochem. Pharmacol.* **2014**, *87*, 40–63.

(203) Moss GP. Queen Mary, U. of L. Glossary of terms used in Medicinal Chemistry www.chem.qmul.ac.uk/iupac/medchem/index.html.

(204) Schneider, E. H.; Schneider, E. H.; Schnell, D.; Schnell, D.; Papa, D.; Papa, D.; Seifert, R.; Seifert, R. High Constitutive Activity and a G-Protein-Independent High-Affinity State of the Human Histamine H4-Receptor. *Biochemistry* **2009**, *48*, 1424–1438.

(205) Cheng, Y. C.; Prusoff, W. H. Relationship between the Inhibition Constant (Ki) and the Concentration of Inhibitor Which Causes 50 per Cent Inhibition (I50) of an Enzymatic Reaction. *Biochem. Pharmacol.* **1973**, *22*, 3099–3108.

(206) Smit, M. J.; Timmerman, H.; Hijzelendoorn, J. C.; Fukui, H.; Leurs, R. Regulation of the Human Histamine H1 Receptor Stably Expressed in Chinese Hamster Ovary Cells. *Br. J. Pharmacol.* **1996**, *117*, 1071–1080.

(207) Kottke, T.; Sander, K.; Weizel, L.; Schneider, E. H.; Seifert, R.; Stark, H. Receptor-Specific Functional Efficacies of Alkyl Imidazoles as Dual Histamine H3/H4 Receptor Ligands. *Eur. J. Pharmacol.* **2011**, *654*, 200–208.

(208) Ligneau, X.; Garbarg, M.; Vizuete, M. L.; Diaz, J.; Purand, K.; Stark, H.; Schunack, W.; Schwartz, J. C. [125I]iodoproxyfan, a New Antagonist to Label and Visualize Cerebral Histamine H3 Receptors. *J. Pharmacol. Exp. Ther.* **1994**, *271*, 452–459.

(209) Ligneau, X.; Morisset, S.; Tardivel-Lacombe, J.; Gbahou, F.; Ganellin, C. R.; Stark, H.; Schunack, W.; Schwartz, J. C.; Arrang, J. M. Distinct Pharmacology of Rat and Human Histamine H(3) Receptors: Role of Two Amino Acids in the Third Transmembrane Domain. *Br. J. Pharmacol.* **2000**, *131*, 1247–1250.

(210) Ligneau, X.; Perrin, D.; Landais, L.; Camelin, J.; Calmels, T. P. G.; Lecomte, J.; Parmentier, R.; Anaclet, C.; Lin, J.; Rochelle, C. D.; Aniello, F.; Rouleau, A.; Gbahou, F.; Arrang, J.; Ganellin, C. R.; Stark, H.; Schunack, W.; Schwartz, J.; Kingdom, C. R. G. BF2.649 [1-{3-[3-(4-Chlorophenyl)propoxy]propyl}piperidine, Hydrochloride], a Nonimidazole Inverse Agonist/Antagonist at the Human Histamine H3 Receptor: Preclinical Pharmacology. *J. Pharmacol. Exp. Ther.* **2007**, *320*, 365–375.

(211) Sander, K.; Kottke, T.; Tanrikulu, Y.; Proschak, E.; Weizel, L.; Schneider, E. H.; Seifert, R.; Schneider, G.; Stark, H. 2,4-Diaminopyrimidines as Histamine H4 Receptor Ligands-Scaffold Optimization and Pharmacological Characterization. *Bioorg. Med. Chem.* **2009**, *17*, 7186–7196.

(212) Decker, M.; Lehmann, J. Dopamine Receptor Ligands. Part VII [1]: Novel 3-Substituted 5-Phenyl-1, 2, 3, 4, 5, 6-Hexahydro-Azepino-[4, 5-B]indoles as Ligands for the Dopamine Receptors. *Arch. Pharm.* **2003**, *336*, 466–476.

(213) Sasse, B. C.; Mach, U. R.; Leppaenen, J.; Calmels, T.; Stark, H. Hybrid Approach for the Design of Highly Affine and Selective Dopamine D3 Receptor Ligands Using Privileged Scaffolds of Biogenic Amine GPCR Ligands. *Bioorganic Med. Chem.* **2007**, *15*, 7258–7273.

(214) Klotz, N. K.; Lohse, M. J.; Schwabe, U.; Cristalli, G.; Vittori, S.; Grifantini, M. 2-Chloro-N6-[3H]cyclopentyladenosine ([3H]CCPA) a High Affinity Agonist Radioligand for A1 Adenosine Receptors. *Naunyn. Schmiedebergs. Arch. Pharmacol.* **1989**, *6*, 679–683.

(215) Mueller, C. E.; Maurinsh, J.; Sauer, R. Binding of [3H]MSX-2 (3-(3-Hydroxypropyl)-7-Methyl-8-(m-Methoxystyryl)-1-Propargylxanthine) to Rat Striatal Membranes--a New, Selective Antagonist Radioligand for A(2A) Adenosine Receptors. *Eur. J. Pharm. Sci.* **2000**, *10*, 259–265.

(216) Mueller, C. E.; Diekmann, M.; Thorand, M.; Ozola, V. [3H]8-Ethyl-4-Methyl-2-Phenyl-(8R)-4,5,7,8-Tetrahydro-1H-Imidazo [2,1-I]-Purin-5-One ([3H]PSB-11), a Novel High-Affinity Antagonist Radioligand for Human A3 Adenosine Receptors. *Bioorganic Med. Chem. Lett.* **2002**, *12*, 501–503.

(217) Ji, X.; Jacobson, K. A. Use of the Triazolotriazine [3H]ZM 241385 as a Radioligand at Recombinant Human A2B Adenosine Receptors. *Drug Des Discov.* **1999**, *16*, 217–226.

(218) Bylund, DB, Deupree, JD, Toews, M. Radioligand-Binding Methods for Membrane Preparations and Intact Cells. *Methods Mol. Biol.* **2004**, *259*, 1–28.

(219) Mendel, CM, Mendel, D. Non-Specific Binding. The Problem, and a Solution. *Biochem. J.* **1985**, *228*, 269–272.

(220) Meiring, L.; Petzer, J. P.; Petzer, A. Inhibition of Monoamine Oxidase by 3,4-Dihydro-2(1H)-Quinolinone Derivatives. *Bioorg. Med. Chem. Lett.* **2013**, *23*, 5498–5502.

(221) Tieu, K. A Guide to Neurotoxic Animal Models of Parkinson's Disease. *Cold Spring Harb. Perspect. Med.* **2011**, *1*, 1–20.

(222) Luthman, J.; Fredriksson, A.; Sundström, E.; Jonsson, G.; Archer, T. Selective Lesion of Central Dopamine or Noradrenaline Neuron Systems in the Neonatal Rat: Motor Behavior and Monoamine Alterations at Adult Stage. *Behav. Brain Res.* **1989**, *33*, 267–277.

(223) Mazzio, E. A.; Soliman, K. F. A. Effects of Enhancing Mitochondrial Oxidative Phosphorylation with Reducing Equivalents and Ubiquinone on 1-Methyl-4-Phenylpyridinium Toxicity and Complex I-IV Damage in Neuroblastoma Cells. *Biochem. Pharmacol.* **2004**, *67*, 1167–1184.

(224) Cenci, M. A.; Lee, C. S.; Björklund, A. L-DOPA-Induced Dyskinesia in the Rat Is Associated with Striatal Overexpression of Prodynorphin- and Glutamic Acid Decarboxylase mRNA. *Eur. J. Neurosci.* **1998**, *10*, 2694–2706.
(225) Pinna, A.; Ko, W. K. D.; Costa, G.; Tronci, E.; Fidalgo, C.; Simola, N.; Li, Q.; Tabrizi, M. A.; Bezard, E.; Carta, M.; Morelli, M. Antidyskinetic Effect of A2A and 5HT1A/1B Receptor Ligands in Two Animal Models of Parkinson's Disease. *Mov. Disord.* **2016**, *31*, 501–511.
(226) Keserü, G. M.; Makara, G. M. The Influence of Lead Discovery Strategies on the Properties of Drug Candidates. *Nat. Rev. Drug Discov.* **2009**, *8*, 203–212.
(227) Hopkins, A. L.; Keserü, G. M.; Leeson, P. D.; Rees, D. C.; Reynolds, C. H. The Role of Ligand Efficiency Metrics in Drug Discovery. *Nat. Rev. Drug Discov.* **2014**, *13*, 105–121.
(228) Desideri, N.; Bolasco, A.; Fioravanti, R.; Proietti Monaco, L.; Orallo, F.; Yáñez, M.; Ortuso, F.; Alcaro, S. Homoisoflavonoids: Natural Scaffolds with Potent and Selective Monoamine Oxidase-B Inhibition Properties. *J. Med. Chem.* **2011**, *54*, 2155–2164.
(229) Desideri, N.; Proietti Monaco, L.; Fioravanti, R.; Biava, M.; Yáñez, M.; Alcaro, S.; Ortuso, F. (E)-3-Heteroarylidenechroman-4-Ones as Potent and Selective Monoamine Oxidase-B Inhibitors. *Eur. J. Med. Chem.* **2016**, *117*, 292–300.
(230) Huang, M.; Xie, S.; Jiang, N.; Lan, J.; Kong, L.; Wang, X. Multitarget-Directed Benzylideneindanone Derivatives: Anti-β-Amyloid (Aβ) Aggregation, Antioxidant, Metal Chelation, and Monoamine Oxidase B (MAO-B) Inhibition Properties against Alzheimer's Disease. *Bioorg. Med. Chem. Lett.* **2015**, *25*, 508–513.
(231) Lan, J.-S.; Xie, S.-S.; Huang, M.; Hu, Y.-J.; Kong, L.-Y.; Wang, X.-B. Chromanones: Selective and Reversible Monoamine Oxidase B Inhibitors with Nanomolar Potency. *Medchemcomm* **2015**, *6*, 1293–1302.
(232) Veber, D. F.; Johnson, S. R.; Cheng, H. Y.; Smith, B. R.; Ward, K. W.; Kopple, K. D. Molecular Properties That Influence the Oral Bioavailability of Drug Candidates. *J. Med. Chem.* **2002**, *45*, 2615–2623.
(233) G. R., R.; G. V., P.; J., B.; S., M.; A. L., D. Quantifying the Chemical Beauty of Drugs. *Nat Chem* **2012**, *4*, 90–98.
(234) Johnson, D. S.; Weerapana, E.; Cravatt, B. F. Strategies for Discovering and Derisking Covalent, Irreversible Enzyme Inhibitors. *Future Med. Chem.* **2010**, *2*, 949–964.
(235) Petroianu, G.; Arafat, K.; Sasse, B. C.; Stark, H. Multiple Enzyme Inhibitions by Histamine H3 Receptor Antagonists as Potential Procognitive Agents. *Pharmazie* **2006**, *61*, 179–182.
(236) Burbiel, J. C.; Ghattas, W.; Küppers, P.; Köse, M.; Lacher, S.; Herzner, A. M.; Kombu, R. S.; Akkinepally, R. R.; Hockemeyer, J.; Müller, C. E. 2-Amino[1,2,4]triazolo[1,5-C]quinazolines and Derived Novel Heterocycles: Syntheses and Structure-Activity Relationships of Potent Adenosine Receptor Antagonists. *ChemMedChem* **2016**, *11*, 2272–2286.
(237) Sun, Y.; Huang, P. Adenosine A2B Receptor: From Cell Biology to Human Diseases. *Front. Chem.* **2016**, *4*, 1–11.
(238) Millan, M. J.; Seguin, L.; Gobert, A.; Cussac, D.; Brocco, M. The Role of Dopamine D3 Compared with D2 Receptors in the Control of Locomotor Activity: A Combined Behavioural and Neurochemical Analysis with Novel, Selective Antagonists in Rats. *Psychopharmac.* **2004**, *174*, 341–357.
(239) Hisahara, S.; Shimohama, S. Dopamine Receptors and Parkinson's Disease. *Int. J. Med. Chem.* **2010**, *2011*, 1–16.
(240) Das, B.; Modi, G.; Dutta, A. Dopamine D3 Agonists in the Treatment of Parkinson's Disease. *Curr. Top. Med. Chem.* **2015**, *15*, 908–926.

(241) Ryoo, H. L.; Dylan, B. S.; Bs, P.; Joyce, J. N. Dopamine D3 Receptor Is Decreased and D2 Receptor Is Elevated in the Striatum of Parkinson ' S Disease. *Mov. Disord.* **1998**, *13*, 788–797.
(242) Hackling, A. E.; Stark, H. Dopamine D3 Receptor Ligands with Antagonist Properties. *Chembiochem* **2002**, *3*, 946–961.
(243) Reilly, S. W.; Griffin, S.; Taylor, M.; Sahlholm, K.; Weng, C. C.; Xu, K.; Jacome, D. A.; Luedtke, R. R.; Mach, R. H. Highly Selective Dopamine D3 Receptor Antagonists with Arylated Diazaspiro Alkane Cores. *J. Med. Chem.* **2017**, *60*, 9905–9910.
(244) Maramai, S.; Gemma, S.; Brogi, S.; Campiani, G.; Butini, S.; Stark, H.; Brindisi, M. Dopamine D3 Receptor Antagonists as Potential Therapeutics for the Treatment of Neurological Diseases. *Front. Neurosci.* **2016**, *10*, 1–16.
(245) Micheli, F. Novel, Selective, and Developable Dopamine D3 Antagonists with a Modified 'Amino' Region. *ChemMedChem* **2017**, *12*, 1254–1260.
(246) Lipinski, C. A.; Lombardo, F.; Dominy, B. W.; Feeney, P. J. Experimental and Computational Approaches to Estimate Solubility and Permeability in Drug Discovery and Develop Ment Settings. *Adv. Drug Deliv. Rev.* **1997**, *23*, 3–25.
(247) Duffy, E. M.; Jorgensen, W. L. Prediction of Properties from Simulations: Free Energies of Solvation in Hexadecane, Octanol, and Water. *J. Am. Chem. Soc.* **2000**, *122*, 2878–2888.
(248) Duroux, R.; Renault, N.; Cuelho, J. E.; Agouridas, L.; Blum, D.; Lopes, L. V.; Melnyk, P.; Yous, S. Design, Synthesis and Evaluation of 2-Aryl Benzoxazoles as Promising Hit for the A2A Receptor. *J. Enz. Inhib. Med. Chem.* **2017**, *32*, 850–864.
(249) Wang, W.-W.; Zhang, M.-M.; Zhang, X.-R.; Zhang, Z.-R.; Chen, J.; Feng, L.; Xie, C.-L. A Meta-Analysis of Adenosine A2A Receptor Antagonists on Levodopa-Induced Dyskinesia In Vivo. *Front. Neurol.* **2017**, *8*, 1–9.
(250) Xiao, D.; Cassin, J. J.; Healy, B.; Burdett, T. C.; Chen, J. F.; Fredholm, B. B.; Schwarzschild, M. A. Deletion of Adenosine A1 or A2A Receptors Reduces L-3, 4- Of, Dihydroxyphenylalanine-Induced Dyskinesia in a Model Parkinson's Disease. *Brain Res.* **2011**, *1367*, 310–318.
(251) Morini, G.; Comini, M.; Rivara, M.; Rivara, S.; Bordi, F.; Plazzi, P. V.; Flammini, L.; Saccani, F.; Bertoni, S.; Ballabeni, V.; Barocelli, E.; Mor, M. Synthesis and Structure-Activity Relationships for Biphenyl H3 Receptor Antagonists with Moderate Anti-Cholinesterase Activity. *Bioorg. Med. Chem.* **2008**, *16*, 9911–9924.
(252) Duty, S.; Jenner, P. Animal Models of Parkinson's Disease: A Source of Novel Treatments and Clues to the Cause of the Disease. *Br. J. Pharmacol.* **2011**, *164*, 1357–1391.
(253) Guigoni, C.; Aubert, I.; Li, Q.; Gurevich, V. V.; Benovic, J. L.; Ferry, S.; Mach, U.; Stark, H.; Leriche, L.; Håkansson, K.; Bioulac, B. H.; Gross, C. E.; Sokoloff, P.; Fisone, G.; Gurevich, E. V.; Bloch, B.; Bezard, E. Pathogenesis of Levodopa-Induced Dyskinesia: Focus on D1 and D3 Dopamine Receptors. *Park. Relat. Disord.* **2005**, *11*, 25–29.
(254) Bézard, E.; Ferry, S.; Mach, U.; Stark, H.; Leriche, L.; Boraud, T.; Gross, C.; Sokoloff, P. Attenuation of Levodopa-Induced Dyskinesia by Normalizing Dopamine D 3 Receptor Function. *Nat. Med.* **2003**, *9*, 762–767.
(255) Solís, O.; Garcia-Montes, J. R.; González-Granillo, A.; Xu, M.; Moratalla, R. Dopamine D3 Receptor Modulates L-DOPA-Induced Dyskinesia by Targeting D1 Receptor-Mediated Striatal Signaling. *Cereb. Cortex* **2017**, *27*, 435–446.
(256) Visanji, N. P.; Fox, S. H.; Johnston, T.; Reyes, G.; Millan, M. J.; Brotchiea, J. M. Dopamine D3 Receptor Stimulation Underlies the Development of L-DOPA-Induced Dyskinesia in Animal Models of Parkinson's Disease. *Neurobiol. Dis.* **2009**, *35*, 184–192.
(257) Beauregard, C.; Schwartz, J. The Histamine H3 Receptor : From Discovery to Clinical Trials with Pitolisant. *Br. J. Pharmacol.* **2011**, *163*, 713–721.

(258) Parmentier, R.; Anaclet, C.; Guhennec, C.; Brousseau, E.; Bricout, D.; Giboulot, T.; Bozyczko-Coyne, D.; Spiegel, K.; Ohtsu, H.; Williams, M.; Lin, J. S. The Brain H3-Receptor as a Novel Therapeutic Target for Vigilance and Sleep-Wake Disorders. *Biochem. Pharmacol.* **2007**, *73*, 1157–1171.

(259) Huang, Z.-L.; Qu, W.-M.; Eguchi, N.; Chen, J.-F.; Schwarzschild, M. A.; Fredholm, B. B.; Urade, Y.; Hayaishi, O. Adenosine A2A, but Not A1, Receptors Mediate the Arousal Effect of Caffeine. *Nat. Neurosci.* **2005**, *8*, 858–859.

(260) Gomtsyan, A.; Bayburt, E. K.; Schmidt, R. G.; Surowy, C. S.; Honore, P.; Marsh, K. C.; Hannick, S. M.; Mcdonald, H. A.; Wetter, J. M.; Sullivan, J. P.; Jarvis, M. F.; Faltynek, C. R.; Lee, C.; Laboratories, A.; Road, A. P. Identification of (R) -1- (5-Tert-Butyl-2 , 3-Dihy- (ABT-102) as a Potent TRPV1 Antagonist for Pain Management. *J. Med. Chem.* **2008**, *51*, 392–395.

(261) Woo, L. W. L.; Howarth, N. M.; Purohit, A.; Hejaz, H. A. M.; Reed, M. J.; Potter, B. V. L. Steroidal and Nonsteroidal Sulfamates as Potent Inhibitors of Steroid Sulfatase. *J. Med. Chem.* **1998**, *41*, 1068–1083.

(262) Hang, Z.; Vandenbossche, C. P.; Koenig, S. G.; Singh, S. P.; Bakale, R. P. An Efficient Synthesis of Enamides from Ketones. *Org. Lett.* **2008**, *10*, 505–507.

(263) Mueller, C. E.; Thorand, M.; Qurishi, R.; Diekmann, M.; Jacobson, K. a.; Padgett, W. L.; Daly, J. W. Imidazo[2,1- I]purin-5-Ones and Related Tricyclic Water-Soluble Purine Derivatives: Potent A2A - and A3 -Adenosine Receptor Antagonists. *J. Med. Chem.* **2002**, *45*, 3440–3450.

(264) Drabczyńska, A.; Mueller, C. E.; Karolak-Wojciechowska, J.; Schumacher, B.; Schiedel, A.; Yuzlenko, O.; Kieć-Kononowicz, K. N9-Benzyl-Substituted 1,3-Dimethyl- and 1,3-Dipropyl-pyrimido[2,1-F]purinediones: Synthesis and Structure-Activity Relationships at Adenosine A1 and A2A Receptors. *Bioorg, Med. Chem.* **2007**, *15*, 5003–5017.

(265) Takahashi, K.; Lin, J.-S.; Sakai, K. Neuronal Activity of Histaminergic Tuberomammillary Neurons During Wake-Sleep States in the Mouse. *J. Neurosci.* **2006**, *26*, 10292–10298.

Curriculum Vitae

PROFESSIONAL EXPERIENCES

Oct. 2013 – present

Researcher and Teaching Assistant

Institute of Pharmaceutical und Medicinal Chemistry, Heinrich-Heine Düsseldorf University

- Practical courses for students (Inorganic Chemistry) Faculty of Pharmacy, Düsseldorf University

Apr. 2015 – June 2015

Visiting Researcher-Expertise in multi-targets synthesis

Institute of General Organic Chemistry, Madrid Spanish National Research Council

Mar. 2012 – Nov. 2012

Research Intern

Fraunhofer Institute of Chemical Technology, Department of Energetic Materials, Karlsruhe and Institute of Organic Chemistry, Parma University, Italy.

- Master Thesis: "*Study of Reactions in Continuous Flow and in Batch Using MOFs as Catalysts*"

EDUCATION

Oct. 2013 – present

PhD Fellow in Pharmacy

Institute of Pharmaceutical and Medical Chemistry,

Heinrich-Heine Düsseldorf University

Expected graduation time – March 2018

Oct. 2010 – Apr. 2013

Master of Organic Chemistry

Institute of Organic Chemistry, Parma University, Italy

Oct. 2007 – Sept. 2010

Bachelor of Science in Chemical Technology

Institute of Chemistry, Parma University, Italy

Sept. 2003 – July 2007

High School in Science and Mathematics

Liceo Scientifico Belfiore, Mantova, Italy

CONTINUOUS PROFESSIONAL DEVELOPMENT

Soft-skills	"Good scientific practice and communications"; "Preparing for potential conflicts"; "Carrier planning: How to shape your future"; "Get into teaching"
Languages	Italian – native English – fluent in written and spoken German – intermediate Spanish – Basic knowledge

PUBLICATIONS

1. **Affini A.**; Hagenow S.; Zivkovic A.; Contelles J.M.; Stark H. Novel Indanone Derivatives as MAO B/H3R Dual-Targeting Ligands for the Treatment of Parkinson's Disease. Eur. J. Med. Chem. 2018, 148, 487-497.

2. Khanfar M. A.; **Affini A.**; Lutsenko K.; Nikolic K.; Butini S.; Stark H. Multiple Targeting Approaches on Histamine H3 Receptor Antagonists. Front. Neurosci. 2016, 10, 201.

3. Calogero P. G.; Schwarzer M.; Herrmann M.; **Affini A.**; Pelegatti P.; Maestri G.; Maggi R.; Loebbecke S. Batch Versus Flow Acetalization of Benzaldehyde with HKUST-1: Diffusion Pathways and Performance Comparison. Chem. Cat. Chem., 2016, 8, 1293-1297.

SCIENTIFIC AND TECHNICAL SKILLS

- Experience in organic/inorganic synthesis, automated column chromatography, microwave reactor, light, temperature and air sensitive reactions.
- Expertise in using ^{1}H, ^{13}C, NOESY NMR as well as mass spectroscopy and HPLC to identify organic compounds.
- Competent in using literature search software, like SciFinder and Reaxys.
- Pharmacological characterization of multi-target drugs: biological evaluations, background in studying neurodegenerative diseases with special interest in utilizing animal models for Parkinson's disease.
- Skilled at communicating scientific works in the form of posters, presentations and written reports

Eigenständigkeitserklärung

Ich versichere an Eides Statt, dass die Dissertation „Histamine H_3 receptor antagonists in combination with monoamine oxidase B and adenosine A_1/A_{2A} receptor ligands as multi-target approach for the treatment of Parkinson's disease" von mir selbständig und ohne unzulässige fremde Hilfe unter Beachtung der "Grundsätze zur Sicherung guter wissenschaftlicher Praxis an der Heinrich-Heine-Universität Düsseldorf" erstellt worden ist. Außerdem versichere ich, dass die vorgelegte elektronische mit der schriftlichen Version der Dissertation übereinstimmt und die Abhandlung in dieser oder ähnlicher Form noch nicht anderweitig als Promotionsleistung vorgelegt und bewertet wurde.

List of Publications and Contribution

Parts of this thesis have already been published in peer-reviewed journals:

ORIGINAL MANUSCRIPTS:

Affini A.; Hagenow S.; Zivkovic A.; Contelles J.M.; Stark H. Novel Indanone Derivatives as MAO B/H3R Dual-Targeting Ligands for the Treatment of Parkinson's Disease. Eur. J. Med. Chem. 2018, 148, 487-497.

Khanfar M. A.; **Affini A.**; Lutsenko K.; Nikolic K.; Butini S.; Stark H. Multiple Targeting Approaches on Histamine H3 Receptor Antagonists. Front. Neurosci. 2016, 10, 201.

Affini A.; Hagenow S.; Pioli E.P.; Porras G.; Namasivayam V.; Müller C. E.; Lin J.-S.; Bezard E.; Stark H. Adenosine $A_{2A}R/A_1R$ antagonists enabling additional H_3R antagonism for the treatment of Parkinson's disease, in preparation.

OTHER PUBLICATIONS (NOT IN THIS THESIS):

Calogero P. G.; Schwarzer M.; Herrmann M.; **Affini A.**; Pelegatti P.; Maestri G.; Maggi R.; Loebbecke S. Batch Versus Flow Acetalization of Benzaldehyde with HKUST-1: Diffusion Pathways and Performance Comparison. Chem. Cat. Chem., 2016, 8, 1293-1297.